DEDICATION

TO MY WIFE AWATIF

AND TWO SONS

SARMAD AND AHMED

The University of Aston in Birmingham

THE APPLICATION OF FINITE ELEMENT ANALYSIS TO FRACTURE MECHANICS

by

MOHAMMED BASSIM AHMED YOUNIS

For the degree of
Master of Philosophy
1984

Summary

The work described in this thesis is concerned with the application of the finite element method related to fracture mechanics, for Mode I, mixed-mode, I and II, plane stress/strain problems, and Mode I axisymmetric bodies under axisymmetric loading.

Numerical examples are presented to demonstrate the validity of the fracture program packages, which has been translated from its existing Algol format to Basic, during the course of this work, in order to suit the HP 9845 desk-top computer. These programs include Mode I and mixed-mode I and II plane crack problems, and Mode I axisymmetric bodies under axisymmetric loading.

An improvement to the accuracy of the values of stresses calculated using the already, available standard plane stress/strain finite element method has been achieved, by the application of a smoothing technique. Numerical examples are given in details describing the technique and its application. All examples are run on the HP 9845 desk-top computer.

All the above mentioned programs are run in conjunction with the automatic mesh generation package available in the Department of Mechanical Engineering of the University of Aston, except that of the Mode I axisymmetric program which deploy a semi automatic mesh generation method.

A preview of the most useful methods for the determination of the stress intensity factors has been presented in a short concise form.

Key Words

STRESS INTENSITY FACTOR, FRACTURE MECHANICS
FINITE ELEMENT METHOD, PLANE STRESS/STRAIN, AXISYMMETRIC

ACKNOWLEDGEMENTS

The author wishes to express his sincere gratitude to his supervisor, Mr. T. H. Richards, for his advice and encouragement throughout this work.

The author is grateful to the University of Mosul in Iraq for providing time of leave and some financial help.

Finally, the author would like to express his thanks to Mrs. H. M. Turner for the typing of this thesis.

CONTENTS

	Page
SUMMARY	
DEDICATION	
ACKNOWLEDGEMENTS	
CONTENTS	(i)
LIST OF FIGURES	(vi)
LIST OF TABLES	(xi)
SYMBOLS	(xii)
CHAPTER 1 - INTRODUCTION	1
CHAPTER 2 - THE FINITE ELEMENT METHOD	4
2.1 INTRODUCTION	4
2.2 BRIEF HISTORICAL BACKGROUND	5
2.3 GENERAL DESCRIPTION OF THE FINITE ELEMENT METHOD	6
2.4 GENERAL PROCEDURE OF THE FINITE ELEMENT METHOD	6
2.4.1 Definition of the Finite Element Method	7
(i) Type of Elements	8
(ii) Size of Elements	9
(iii) Number of Elements	9
(iv) Symmetrical Configuration	9
(v) Node Numbering Scheme	10
2.4.2 (a) Selection of Displacement Function	11
(b) Generation of Polynomial Shape Functions	12
2.4.3 Derivation of Element Characteristic Matrix and Vectors	16

Page

2.4.4 Assemblage of All Element Characteristic Matrices and Vectors to Provide the System Matrices and Vectors 19

2.4.5 Solution of System Equations 21

(i) Frontal Solution Method 22

(ii) Choloski Reduction Sequence 22

2.4.6 Computation of Nodal and Element Stresses and Strains 24

CHAPTER 3 - NUMERICAL EXAMPLES FOR THE APPLICATION OF PLANE STRESS/STRAIN PROBLEMS 27

3.1 INTRODUCTION 27

3.2 BASIS OF THE SCHEME 28

3.3 THE GENERAL PROGRAM 33

3.4 EXAMPLE 1 - A CANTILEVER UNDER AN END LOAD 35

3.5 EXAMPLE 2 - THICK CYLINDER UNDER INTERNAL PRESSURE 43

3.6 EXAMPLE 3 - A PLATE WITH A SMALL CIRCULAR HOLE IN ITS MIDDLE UNDER TENSION 49

3.7 EXAMPLE 4 57

3.8 SMOOTHING OF STRESSES 69

CHAPTER 4 - REVIEW OF STUDIES IN FRACTURE MECHANICS 81

4.1 INTRODUCTION 81

4.2 GRIFFITH THEORY 86

4.3 ROLE OF PLASTICITY 91

4.4 STRESS INTENSITY FACTOR AND FRACTURE TOUGHNESS 92

4.5 RELATION BETWEEN THE GRIFFITH THEORY AND IRWIN APPROACHES 98

4.6 PLASTICITY CORRECTION 101

4.7 THE STRAIN-ENERGY-DENSITY FACTOR 104

Page

4.8 THE STRESS INTENSITY FACTOR AND FRACTURE MECHANICS 108

CHAPTER 5 - METHODS FOR THE DETERMINATION OF STRESS INTENSITY FACTORS 110

5.1 INTRODUCTION 110

5.2 METHODS OF EVALUATION OF STRESS INTENSITY FACTORS 111

5.2.1 Experimental Methods 111

(1) Compliance 112

(2) Photoelasticity 113

(3) Fatigue Crack Growth Rate 115

(4) Interferometry and Holography 116

5.2.2 Analytical Methods 117

(1) Westergaard Stress Function 118

(2) Complex Stress Function 119

5.2.3 Approximate Methods 121

(1) Boundary Collocation 121

(i) William's Stress Function 122

(ii) Complex Stress Function 122

(2) Conformal Mapping 123

(3) Stress Concentration Factors 124

(4) Green's Functions 125

(5) Integral Transform and Dislocation Models 126

(6) Force-Displacement Matching 127

(7) Alternating Methods 128

(8) Finite Element Methods 128

(i) Crack Tip Stress and Displacement Methods 129

Page

(a) Crack Tip Stress 129

(b) Crack Tip Displacement 130

(ii) Energy Methods 131

(a) The Strain Energy Method 131

(b) Line Integral Method 133

(c) Crack Closure Method 135

(iii) The Singularity Function Formulation 135

(a) Elements Employing Distorted Shape Functions 135

(b) Elements Employing Standard Shape Functions 140

(c) Elements Based on Analytical Solutions 145

(d) Superposition Method 153

(e) Mixed and Hybrid Methods 154

(9) Boundary Element Methods 156

5.3 FINAL REMARKS 158

CHAPTER 6 - THE FINITE ELEMENT METHOD RELATED TO FRACTURE MECHANICS 160

CHAPTER 7 - NUMERICAL EXAMPLES FOR THE CRACK PROBLEMS 172

7.1 INTRODUCTION 172

7.2 TRANSITION ELEMENTS 174

7.3 EXAMPLE 1 - A PLATE WITH A 90° SINGLE-EDGE-CRACK IN TENSION - MODE I 177

7.4 EXAMPLE 2 - A PLATE WITH A 90° SINGLE-EDGE-CRACK IN TENSION - MIXED MODE I AND II 190

Page

7.5 EXAMPLE 3 - A SQUARE PLATE IN UNIFORM TENSION CONTAINING A 45° CENTRAL CRACK 194

7.6 EXAMPLE 4 - A ROUND BAR WITH A CIRCUMFERENTIAL NORMAL-EDGE-CRACK IN TENSION 199

CHAPTER 8 207

8.1 DISCUSSION 207

8.2 POSSIBLE IMPROVEMENTS AND SUGGESTED FUTURE WORK 212

8.3 CONCLUSIONS 214

CHAPTER 9 - APPENDICES 216

9.1 APPENDIX (A)
USER GUIDE FOR THE MESH GENERATION PROGRAM 216

9.2 APPENDIX (B)
MANUAL INPUT DATA PREPARATION FOR AXISYMMETRIC CRACK PROBLEMS 233

CHAPTER 10 - REFERENCES 236

LIST OF FIGURES

		Page
Figure (2.1)	General quadrilateral element	14
Figure (3.1)	Isoparametric quadrilateral element	29
Figure (3.2)	A disc in compression	32
Figure (3.3)	A Cantilever under end load	36
Figure (3.4)	Values of shear stress for Cantilever	40
Figure (3.5)	Thick cylinder under internal pressure	46
Figure (3.6)	Final structure for mesh of thick cylinder	47
Figure (3.7)	Element array showing element and nodal numbering for mesh of thick cylinder	47
Figure (3.8)	A plate with a centre hole, in tension.	50
Figure (3.9)	The quadrant of the plate above	50
Figure (3.10)	Distorted zone diagram and standard generated section for plate example	51
Figure (3.11)	Key diagrams for zone and element arrays	52
Figure (3.12a)	Final structure of plate example	53
Figure (3.12b)	Final structure of plate showing boundary constraints at the nodes and loading.	53
Figure (3.13)	Graph of nodal stress along x=0	54
Figure (3.14)	Details of component considered	60
Figures (3.15) - (3.18)	Equivalent of loading Example 4 using analytical method	61 -62
Figure (3.19)	Key diagrams for zone arrays	64
Figure (3.20)	Key diagrams for element arrays	65

		Page
Figure (3.21)	A graph of displacement against crack length	68
Figure (3.22)	Theoretical, smoothed and unsmoothed shear stress values	77
Figure (3.23a)	Comparison of smoothed and unsmoothed tangential stresses	78
Figure (3.23b)	Comparison of smoothed and unsmoothed radial stresses	79
Figure (3.24)	Smoothed and unsmoothed stress distributions for 1-D isoparametric element	80
Figure (4.1)	An infinite sheet containing a circular hole, in tension	84
Figure (4.2)	An infinite sheet containing ellipitcal hole, in tension	84
Figure (4.3)	An infinite sheet containing a crack	85
Figure (4.4)	An infinite sheet containing a crack, showing plastic enclaves at the crack tips.	85
Figure (4.5)	Local co-ordinate system at a crack tip	94
Figure (4.6)	Modes of fracture	95
Figure (4.7)	Plastic enclave at a crack tip	103
Figure (4.8)	Crack tip region of radius r	107
Figure (4.9)	Crack tip region with mechanical defects around it	107
Figure (5.1)	Path of integration for determining the J-integral	133

		Page
Figure (5.2)	Crack tip enclosed by triangular crack tip elements	137
Figure (5.3)	Near crack tip elements mapped into a square	137
Figure (5.4)	A quadrilateral finite element with a singular point at node (1)	143
Figure (5.5)	Finite element definition of side cracked panel	144
Figure (5.6)	Centrally notched plate under axial Mode I loading	147
Figure (5.7)	One quarter of centrally notched plate under axial Mode I loading	148
Figure (6.1)	A plate with 90° single-edge-crack, in tension, where a core region is identified surrounding the crack tip	164
Figure (6.2)	Partitioning of stiffness matrix, $\|K\|$	171
Figure (6.3)	Construction of stiffness matrix, $\|\overset{*}{K}\|$	171
Figure (7.1)	A plate with a 90° single-edge-crack in tension	179
Figure (7.2)	Distorted zone array showing zone numbers and super nodes of half the plate containing a 90° single-edge-crack	180
Figure (7.3)	Distorted element array showing element and nodal number of half the plate containing a 90° single-edge-crack, using quadrilateral element.	181

Page

Figure (7.4) Key diagrams for zone and element arrays 182

Figure (7.5) Crack tip core region arrangement, using isoparametric quadrilateral elements 183

Figure (7.6) Crack tip core region arrangement, using isoparametric triangular element 184

Figure (7.7) Distorted element array showing element and nodal number of half the plate containing a 90° single-dege-crack, using triangular element 185

Figure (7.8) Final structural idealisation diagram for Mode I crack problem in Example 1, of a plate in tension with a 90° single-edge-crack, employing the isoparametric quadrilateral element around the core 186

Figure (7.9) Final structural idealisation diagram for Mode I crack problem in Example 1, of a plate in tension with a 90° single-edge-crack, employing the isoparametric triangular element around the core. 187

Figure (7.10) Key diagrams for zone and element arrays for the mixed-mode fracture problem of Example 2 191

Figure (7.11) Final structural idealisation diagram for mixed-mode crack problem in Example 2, of a plate in tension with a 90° 192

Page

single-edge-crack, employing the isoparametric quadrilateral element around the core

Figure (7.12) Final structural idealisation diagram for mixed-mode crack problem in Example 3, employing the isoparametric quadrilateral element around the core region at the tips of the central slanted crack. 198

Figure (7.13) Round bar with a circumferential normal edge-crack in tension, of Example 4 for axisymmetric Mode I fracture problem 202

Figure (7.14) A diagram for the core region where three bands of triangular elements are used round the core element, where element and nodal numbering is shown for Example 4. 203

Figure (7.15) Final structural idealisation of a round bar with a circumferential normal edge-crack of Example 4 204

LIST OF TABLES

		Page
Table (1)	Comparison of the values of shear along the neutral axis of the Cantilever calculated theoretically, and by means of F.E.M. employing two meshes	39
Table (2)	Values of displacements corresponding to crack length	67
Table (3)	Values of compliance and stress intensity factor K_I	67
Table (4)	Comparison of the values of shear along the neutral axis of the Cantilever, calculated theoretically, and by means of F.E.M., smoothed and unsmoothed for mesh 1.	75
Table (5)	Values of radial and tangential stresses of a thick cylinder along its vertical axis through the thickness of the wall, obtained by theory of elasticity, smoothed and unsmoothed F.E.M. showing % of error in the last two cases	76
Table (7.1)	Tabulated values of K_I for Example 4	205

LIST OF SYMBOLS

u, v	Components of displacement
$\{u\}_o^e$	Element nodal displacement
$\{u\}^e$	Displacement field within the element
$\{q\}$	Generalised co-ordinates vector
r, θ	Polar co-ordinates with origin at crack tip
x_n, y_n	Nodal Cartesian co-ordinates
k	$= (3-4\nu)$ for plane strain
	$= (3-\nu)/(1+\nu)$ for plane stress
E, G, ν	Elastic constant
ξ, η	Natural co-ordinates
$[D]$	Elasticity matrix
σ_{ij}	Components of stress
ε_{ij}	Components of strain
$\{\sigma\}$	Vector of stresses
$\{\varepsilon\}$	Vector of strains
V	Total potential energy
Ω	Potential energy of applied loads
U_e	Element strain energy
U	Total strain energy
U_c	Core strain energy
$[K]_e$	Element stiffness matrix
$[K]$	Overall stiffness matrix
$[\bar{K}]$	Unconnected stiffness matrix
$[B]$	Strain displacement matrix
$[C]$	The connection compatibility matrix
$[J]$	Jacobian matrix

$[N]$	Shape functions matrix
G	Strain energy release rate
K_I, K_{II}, K_{III}	Stress intensity factors
$K_{Ic}, K_{IIc}, K_{III_c}$	Fracture toughness values
δ	Strain energy density factor
δ_c	Critical strain energy density factor
C	Compliance
a	Crack length
m	Mode of fracture, i.e. I, II, or III.
h	Thickness
N_1	Number of nodes on finite element mesh/core interface
R_c	Core radius
J	Rice's path independent integral
$\bar{T}$	Traction vector
$\bar{n}$	Vector outward normal
$\phi(z)$, $\psi(z)$	Complex stress functions

CHAPTER 1

INTRODUCTION

Fracture mechanics is a procedure by means of which the existence of the crack like defect in the engineering structure will lead to failure, at average stresses well below the yield strength. This problem arises in all kinds of metals.

One approach to the prediction, and hence the prevention of such failures, is based on the determination of stress intensity factors, which defines the magnitude of the singularities in the stress field near the crack tip. A knowledge of the crack tip "stress intensity factor" as a function of applied load and geometry of the structure is necessary. This information combined with the experimentally determined critical stress intensity factors and crack growth rates for the structural material make such predictions possible. A review of studies in fracture mechanics is in Chapter 4.

Numerous methods are available for the evaluation of the stress intensity factors. These have been described in Chapter 5. Among these methods is the finite element method. Its application to fracture mechanics without catering for the singularities near the crack tip requires a very fine mesh in that region. This is time consuming in

data preparation and very expensive regarding computer time. Also due to the availability and increasing trend to use desk-top computers with a limited capacity, the number of degrees of freedom employed in the solution is restricted. A method which modify the standard finite element formulation to allow for the singularities is the Hilton and Hutchinson[50] method is used in the work of this thesis. This method has been adopted and developed by Richards and Robertson[62] and is briefly described in Chapter 6.

Due to the fast development of desk-top computers, and the ease of their availability at a reasonable cost, the original programs were translated from ALGOL language to BASIC language and are implemented on the HP 9845 desk-top computer available in the Mechanical Engineering Department at Aston University. Chapter 3 reviews some numerical examples for the application of plane stress/strain problems. In this chapter a smoothing technique was adopted, as part of the work during the preparation of this thesis, and used to overcome the erratic behaviour of the calculated values of the shear stresses. This has been successfully achieved.

Chapter 7 describes some numerical examples for the application of Mode I and mixed-mode plane stress/strain fracture problems, and also Mode I axisymmetric fracture problems. The programs used are those of Robertson[67], Wood[15] and Al-Sharqi[68]. They are translated to BASIC from ALGOL as part of the work carried out during the

preparation of this thesis, and have been implemented successfully on the HP 9845 desk-top computer, although there were some limitations due to the capacity of this particular computer.

Discussion of the results and possible further improvements on prgrams used throughout this thesis with suggested future work are in Chapter 8, together with drawn conclusions.

CHAPTER 2

THE FINITE ELEMENT METHOD

2.1 INTRODUCTION

The finite element method is essentially a process through which a continuum, with infinite degrees of freedom, can be approximated by an asssemblage of sub-regions each with a specified but now finite number of degrees of freedom. The behaviour of each sub-region or element is described by a set of assumed functions are usually of a polynomial form and by using sufficient number of elements, an acceptable representation of the overall real situation is obtained. The process is analogous to a piece-wise Rayleigh-Ritz method, where integrations required to define the appropriate functional must be evaluated for each element in turn and the total contribution obtained by summation.

The finite element method is one of the powerful methods of numerical stress analysis presently available. In the past two decades, the developments and refinements in the field of analysis have been very impressive. By means of the finite element method approximate solutions can be calculated for a wide range of structures of complex properties.

The method has been applied to three dimensional bodies, plane bodies, axi-symmetric bodies, plates, shells, etc.

Linear and non-linear materials, time independent and time dependent materials, and non-homogenous and anisotropic bodies can be analysed with most equal ease.

Of the general finite element methods, for the solution of continuum mechanics problems, the "stiffness method" with displacements as primary unknowns, is the one more commonly used since it is the most well developed approach.

All the work and numerical examples in this thesis will be based on this method.

2.2 BRIEF HISTORICAL BACKGROUND

The finite element method, essentially as known today, was introduced in 1956 by Turner, Clough, Martin and Topp[54,55]. Their paper was concerned with the application of simple finite elements (pin-jointed bar and triangular plate with inplane loads) for the analysis of aircraft structures and is considered as one of the key contributions in the development of the finite element method. Subsequent wider applications of variational principles and, more recently still, methods of weighted residuals have broadened the regions of applications beyond the field of structural mechanics.

The development of high speed digital computers made this numerical method very attractive, and the use of the finite element method has found a wide range for its application to different mathematical and engineering problems.

2.3 GENERAL DESCRIPTION OF THE FINITE ELEMENT METHOD

In the finite element method, the actual continuum is represented as an assemblage of sub-regions called the finite elements. These elements are considered to be interconnected at specified points which are called nodes or nodal points. The nodes usually lie on the element boundaries when adjacent elements are connected. The variation of the field variable inside the continuum is not known and it can be approximated over an element by means of simple functions which are defined in terms of the values of the field variable at the nodes. Derivations of the element stiffness matrices and load vectors are based upon a variational principle and an assembly of the element equations is carried to obtain the overall equilibrium equations, in matrix form. These equations are solved for the unknown nodal displacements and if required the values of nodal and element stress and strain throughout the continuum are computed.

2.4 GENERAL PROCEDURE OF THE FINITE ELEMENT METHOD

The basic steps involved in the finite element analysis could be summarised as follows:

(i) Discretization of the structure or domain.

(ii) Selection of an appropriate polynomial model to represent the variation of the field variable over a typical element (in the case of the approach used

here, this is the displacement).

(iii) Derivation of element characteristic matrices and vectors.

(iv) Assemblage of all element characteristic matrices and vectors to obtain the overall equilibrium equations.

(v) Solution of the system equations to find the nodal values of the field variable, (in this case the displacements).

(vi) Computation of nodal and element stresses and strains.

2.4.1 Definition of the Finite Element Mesh

The continuum is subdivided into sub-regions or elements, whose form depend on the problem at hand. This is equivalent to replacing the domain having an infinite number of degrees of freedom by a system having a finite number of degrees of freedom. The shape, size, number and configurations of the elements have to be chosen carefully in order to represent the Domain correctly and as closely to the actual structure as is adequate, without increasing the computational effort needed for the solution of the problem.

It is appropriate to discretise the continuum either into one-dimensional (line), two-dimensional or three-dimensional sub-regions. The elements used are straight lines or curves in the one-dimensional case, straight sided or curvilinear triangles and quadrilaterials in the two-

dimensional plane stress and plane strain situations. The general three-dimensional solid may be divided up into the tetrahedran element, rectangular prisms, etc. If the solid enjoys axial symmetry in its geometry, then ring type elements are used.

In every case each element is connected to the next, through node points on its boundary, and the nodes are numbered and referenced to a coordinate origin. The elements are defined by a series of node numbers (element nodal connections) and from this information an element stiffness matrix relation may be determined between nodal forces and displacements.

Various considerations are to be taken into account in the discretization process:

(i) Type of Elements:

The type of problem at hand will usually give an indication of the type of element needed. If the structure under consideration is a truss, then the element used is the one-dimensional bar or line element, or in case of short beams, a three-dimensional element may be used. However, in some cases, there is a choice in selecting the type of element and that may depend on different things, like the number of degrees of freedom needed, the expected accuracy and the care with which the necessary equations can be derived. In certain problems two or more type of elements

are used for idealisation.

(ii) Size of Elements:

The size of the element influence the convergence of the solution directly and hence it has to be chosen with care. If the size of elements is small, the final solution is expected to be more accurate. However, smaller size elements means more of them and more computational time. Usually elements of different sizes are required in the discretization of a continuum; usually elements have to be very small in the regions where steep gradients of the field variable exits. The aspect ratio of the element is important, this ratio is that of largest dimension of the element to the smallest dimension. For a two-dimensional element, the aspect ratio of unity generally yield best results.

(iii) Number of Elements:

The number of elements chosen for idealization depends on the required accuracy of the solution, and will dictate the total number of degrees of freedom involved. Although the increase in the number of elements generally means more accurate results, there will be a limit beyond which the accuracy of the solution can not be improved to any significant amount, and the cost will be high.

(iv) Symmetrical Configuration:

If the configuration of the body as well as the external

conditions are symmetrical, only half or a quarter of the body need be considered, this of course makes the problem easier and the time required for the solution much shorter for a given accuracy.

(v) Node Numbering Scheme:

The finite element analysis of practical problems leads to matrix equations in which matrices involved will be banded. A matrix is "banded" if all non-zero coefficients are clustered about the leading diagonal. Banding is a simple way to exploit matrix sparsity because zeros outside the band need neither be stored nor processed.

The number of non-zero coefficients in the stiffness matrix is independent of how nodes are numbered. But changing the node numbers changes their arrangement.

The bandwidth of the overall or global characteristic matrix depends on the node numbering scheme and the number of degrees of freedom considered per node. Since the number of degrees of freedom per node is fixed for any given type of problem, the bandwidth can be minimised by using a proper node numbering scheme. Furthermore, since most of the matrices involved are symmetric, the demands on the computer storage can be substantially reduced by storing only the elements involved in half band width instead of storing the whole matrix.

The bandwidth could be defined as:

Bandwidth (B) = (D + 1).f

where D is the maximum largest difference in the node numbers occurring for all elements of the assemblage. f is the number of degrees of freedom at each node.

2.4.2 (a) Selection of Displacement Function

The assumed element behaviour is governed by its displacement function which is chosen to define the displacement field within the element in terms of its nodal displacements. Usually the same form of function is used in all the elements of the discretization, but it is not essentially to do so. If different types of elements are used, it will be clear that these functions will need to be different in the different types of elements. If a polynomial function is used, then it will be appreciated that the degree of the polynomial will govern the ability of the element to approximate the true displacement field.

The functions chosen to describe the assumed displacement pattern within a given element must satisfy FOUR requirements:

(i) The function must be continuous within the element.

(ii) The displacement must be continuous between adjacent elements, i.e. no interelement gaps are overlaps must be implied.

(iii) The state of constant strain must be included in the displacement function.

(iv) Rigid body displacements must be represented in the displacement function.

(b) Generation of Polynomial Shape Functions

Finite elements can be classified into three categories according to the order of the polynomial used in the interpolation function, these categories are simplex, complex and multiplex[54]. The simplex elements are those in which the approximating polynomial consists of constant and linear terms. In the two-dimensional anlaysis the simplex elements are the triangular or rectangular element defined by three and four corner nodes respectively. These two elements present the lowest possible forms of approximation and are of limited accuracy.

The complex elements are those for which the approximating polynomial consists of quadratic, cubic and higher order terms, according to the need, in addition to the constant and linear terms. The complex elements may have the same shape as the simplex elements, but will have additional boundary nodes and some times, internal nodes.

For the two-dimensional analysis a triangular or rectangular element may be used for which an obvious improvement which is the addition of a number of nodal

points along the sides of these elements in addition to those at the corners. These are the Isoparametric elements where both the geometry and the displacement of the element are described in terms of the same parameter and are of the same order, their shape functions yield a quadratic displacement function. In the case of axi-symmetric solids, a ring element is used in the descretization which can have any cross-sectional shape as above.

Finally, the multiplex elements are those whose boundaries are parallel to the coordinate axes to achieve interelement continuity and whose approximating polynomials contain higher order terms. As an example of a multiplex element in two dimensions, is the rectangular element. Here it can be noted that the boundaries of the simplex and complex elements need not be parallel to the coordinate axes.

In all cases suitable polynomials which satisfy the four conditions in section 2.4.2 can be written by introducing only terms which give the appropriate variation along the sides of the element.

As an example, an 8-node isoparametric quadrilateral element can be defined in terms of the local coordinates ξ and η, as shown in Fig.(2.1). The relationship between the cartesian coordinates and the local coordinates could be written in the following general form,

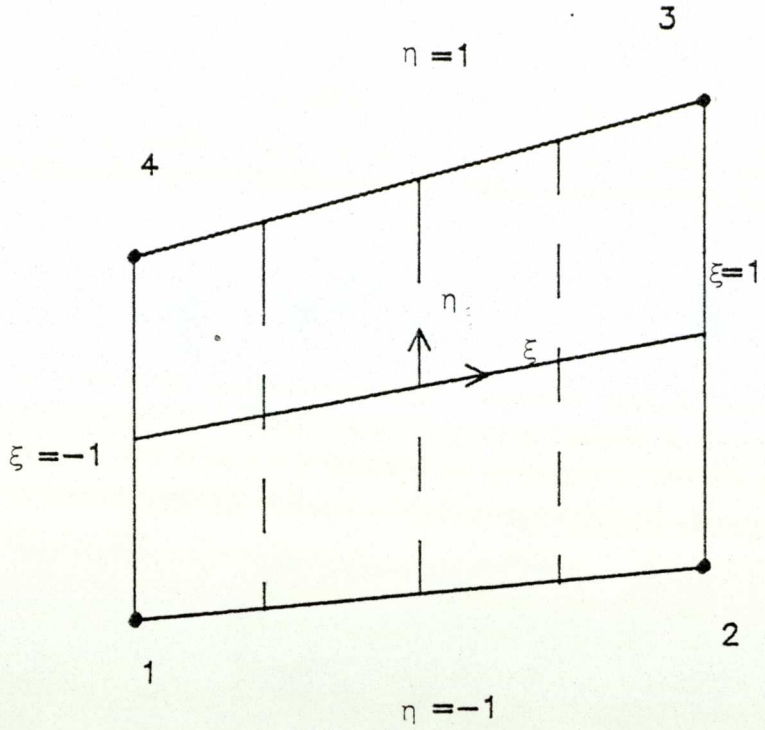

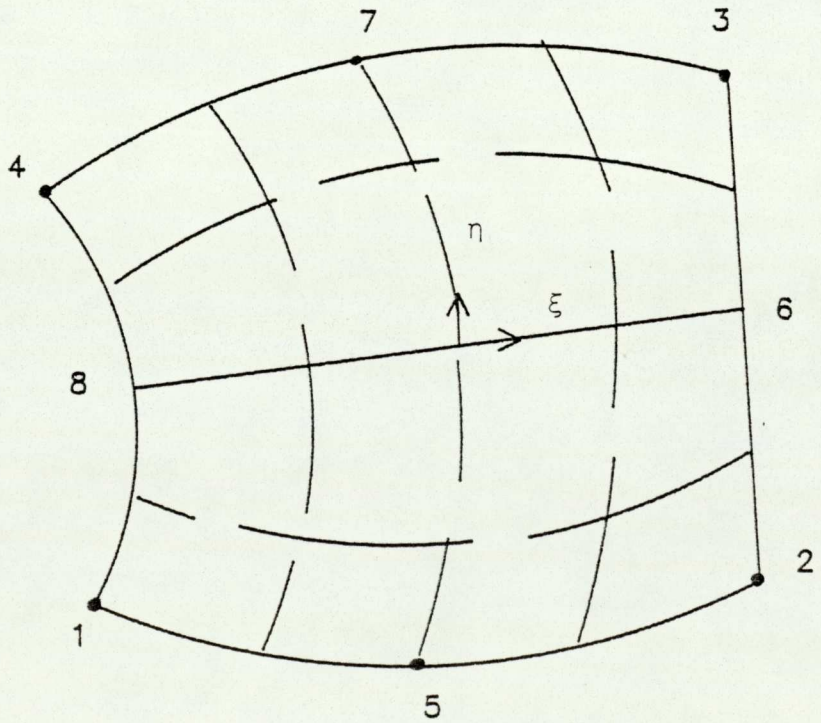

FIGURE(2.1) GENERAL QUADRILATERAL ELEMENT

$$X = N_1X_1 + N_2X_2 + N_3X_3 + ... = [N]\{X_n\} \quad (2.1)$$

$$Y = N_1Y_1 + N_2Y_2 + N_3Y_3 + ... = [N]\{Y_n\} \quad (2.2)$$

in which $\{X_n\}$ and $\{Y_n\}$ list the nodal coordinates X and Y and N_1 and N_2..... etc. are functions of ξ and η. For any value of ξ and η, the X and Y coordinates can be found once the functions N are known.

In the isoparametric formulation, the same functions, i.e. $N_1, N_2, \ldots$ etc. are used to define the variation of displacement components u and v as well as the geometry.

$$u(\xi,\eta) = N_1u_1 + N_2u_2 + \ldots = [N]\{u_n\} \quad (2.3)$$

$$v(\xi,\eta) = N_1v_1 + N_2v_2 + \ldots = [N]\{v_n\} \quad (2.4)$$

To find the shape functions

$$X = a_1+a_2\xi+a_3\eta+a_4\xi\eta+a_5\xi^2+a_6\eta^2+a_7\xi^2\eta+a_8\xi\eta^2 \quad (2.5)$$

$$X = [1 \quad \xi \quad \eta \quad \xi\eta \quad \xi^2 \quad \eta^2 \quad \xi^2\eta \quad \xi\eta^2]\{a_n\} \quad (2.6)$$

by substituting the appropriate nodal values in

$X = X_1 \qquad \eta = -1 \qquad \xi = -1$

$X = X_2 \qquad \eta = -1 \qquad \xi = -1$

etc.

yields eight equations of type

$$\{X_n\} = [A]\{a_n\}$$

$$\{a_n\} = [A]^{-1}\{X_n\}$$

and the shape functions follows as

$$[N_1 \quad N_2 \quad N_3 \quad N_4 \quad N_5 \ldots N_8] = [1 \quad \xi \quad \eta \quad \xi\eta \quad \xi^2 \quad \eta^2 \quad \xi^2\eta \quad \xi\eta^2][A]^{-1}$$

This can be cumbersome. It is possible to use a more direct approach by interpolation.

For corner nodes

$$N_i = \frac{1}{4}(1+\xi_o)(1+\eta_o)(\xi_o+\eta_o-1)$$

For mid-side nodes

$$N_i = \frac{1}{2}(1-\xi^2)(1+\eta_o) \qquad \text{at} \quad \xi_i = 0$$

$$N_i = \frac{1}{2}(1+\xi_o)(1-\eta^2) \qquad \text{at} \quad \eta_i = 0$$

where

$$\xi_o = \xi\xi_i$$

$$\eta_o = \eta\eta_i.$$

2.4.3 Derivation of Element Characteristic Matrix and Vectors

The strain energy stored in the element may be computed from the expression[62]

$$U_e = \frac{1}{2}\int_e \{\varepsilon\}^t [D]\{\varepsilon\} \quad dvol \qquad (2.7)$$

where

U_e is the element strain energy.

$\{\varepsilon\}$ is the vector of strains.

$[D]$ is the elasticity matrix defined by

$$\{\sigma\} = [D]\{\varepsilon\} \tag{2.8}$$

where $\{\sigma\}$ is the vector of stresses.

The displacement field within the element is assumed to be

$$\{u\}^e = [N]\{u\}_o^e \tag{2.9}$$

where

$[N]$ is the element shape function.

$\{u\}_o^e$ is the element nodal displacements.

Differentiating equation (2.9)

$$\{\varepsilon\} = [B]\{u\}_o^e \tag{2.10}$$

where

$$[B] = [\partial][N] \tag{2.11}$$

with $[\partial]$ an appropriate differential operator matrix.

Using equation (2.10) into equation (2.7)

$$U_e = \frac{1}{2}\{u\}_o^{e^t}\left(\int [B]^t [D][B]\ dvol\right)\{u\}_o^e \tag{2.12}$$

$$U_e = \frac{1}{2} \{u\}_o^{e^t} [K]_e \{u\}_o^e \tag{2.13}$$

where $[K]_e$ is called the element stiffness matrix, i.e.

$$[K]_e = \int [B]^t [D] [B] \, dvol \tag{2.14}$$

The forces on an element arise from three sources, firstly due to body forces, secondly due to external nodal forces and thirdly due to surface traction, i.e. the total potential energy of the element

$$V_e = U_e + \Omega_e \tag{2.15}$$

where U_e is as defined in equation (2.13) and

$$\Omega = -(U_F + U_R + U_S) \tag{2.16}$$

$$U_F = \int_{vol} \{\ddot{u}\}^t \{F\} \, dvol \tag{2.17}$$

where

$\{F\}$ is the body forces of the system

$\{\ddot{u}\}$ is the general displacement function.

$$U_R = \{u\}_o^{e^t} \{R\} \tag{2.18}$$

where

$\{u\}_o^e$ is the nodal displacement.

$\{R\}$ is the external nodal loads.

$$U_S = \int_{area} \{u\}^t \{S\}\, dA \tag{2.19}$$

where $\{S\}$ is the surface tractions.

Since $\{u\} = [N]\{u\}_o^e$ (2.20)

$$\{u\}^t = \{u\}_o^{e\,t} [N]^t \tag{2.21}$$

$$\therefore \quad \Omega = -\left(\int_{vol} \{u\}_o^{e\,t} [N]^t \{F\} dvol + \{u\}_o^{e\,t} \{R\} + \int_{area} \{u\}_o^{e\,t} [N]^t \{S\} dA\right) \tag{2.22}$$

Since the nodal displacements $\{u\}_o^e$ are independent of the general coordinates X and Y, therefore it can be taken out of the integrals of equation (2.22).

i.e.
$$\Omega = -\{u\}_o^{e\,t} \left(\int_{vol} [N]^t \{F\} dvol + \{R\} \int_{area} [N]^t \{S\} dA\right) \tag{2.23}$$

And the terms in Brackets in the above equation represent the total loading system on the element, Q, so that

$$\Omega = -\{u\}_o^{e\,t} \{Q\} \tag{2.24}$$

2.4.4 Assemblage of All Element Characteristic Matrices and Vectors to Provide the System Matrices and Vectors

Summing U_e over all the elements yields the total strain energy stored in the solid

$$U = \sum_{e=1}^{n} U_e \tag{2.25}$$

Now for compatibility the element nodal displacements may be written in terms of the generalised coordinates $\{q\}$ of the discretized system in the form

$$\{\tilde{u}\} = [C]\{q\} \tag{2.26}$$

So that

$$U = \frac{1}{2} \{\tilde{u}\}^t [\bar{K}] \{\tilde{u}\} \tag{2.27}$$

where

$\{\tilde{u}\}$ is the array of unconnected displacement of elements.

$[\bar{K}]$ is the unconnected stiffness matrix.

$[C]$ is the connection compatibility matrix.

i.e.

$$U = \frac{1}{2} \{q\}^t [C]^t [\bar{K}] [C] \{q\} \tag{2.28}$$

$$U = \frac{1}{2} \{q\}^t [K] \{q\} \tag{2.29}$$

where $[K]$ is the assembly stiffness matrix given formally by $[C]^t [\bar{K}] [C]$.

The externally applied loads will have a potential energy function Ω. If these loads are expressed in terms of the generalised forces Q, applied at the generalised coordinates q, then

$$\Omega = -\{q\}^t\{Q\} \tag{2.30}$$

and the total potential energy of the system can be written as

$$V = U + \Omega = \frac{1}{2}\{q\}^t[K]\{q\} - \{q\}^t\{Q\} \tag{2.31}$$

For equilibrium, V must be stationary so that

$$\delta V = 0 = \{\delta q\}^t([K]\{q\} - \{Q\}) \tag{2.32}$$

Since the variations of $\{\delta q\}$ are arbitrary, equation (2.32) yields the usual stiffness equilibrium equation

$$[K]\{q\} = \{Q\} \tag{2.33}$$

After imposing the displacement boundary conditions equation (2.33) may be solved for the q's and the element strains and stresses may subsequently be found.

For the non-linear situation, the same procedure will lead to non-linear algebraic equations.

2.4.5 Solution of System Equations

Numerous routines are available for the solution of the stiffness equations[54]. These are usually based on the Gaussian elimination or Cholesky decomposition processes. Efficient routines take account of the symmetric banded nature of the stiffness matrix in order to reduce the storage requirements demanded of the computer.

(i) Frontal Solution Method

In recent years the "frontal solution method" has been adopted and used effectively. Usually an element by element frontal assembly and elimination procedure is employed. Such procedure can utilize a relatively small memory. The efficiency of "frontal" methods is independent of node numbers and is dependent on the element processing order.

The frontal method stores only equations that are currently active. Equations that have received all of their element (and constant) contributions are eliminated to provide storage for equations that may become active with the next element.

Since in this method the equations are assembled in the order of the elements, an effective ordering of the elements is necessary.

An advantage of this method is that at any one time only the equations that are currently needed are assembled in the high-speed storage[74].

(ii) Cholesky Reduction Sequence

The Cholesky triangular factorisation method is well suited to large problems. Expressing the simultaneous equations in matrix form, we have,

$$[K]\{X\} = \{b\} \tag{2.34}$$

where $[K]$ is a symmetric positive-definite matrix using Cholesky factorization, $[K]$ can be written as

$$[L][L]^t = [K] \tag{2.35}$$

where $[L]$ is a lower triangular matrix with positive diagonal terms.

To obtain the displacement vector $\{X\}$, by substituting equation (2.34) into (2.35),then

$$[L][L]^t\{X\} = \{b\} \tag{2.36}$$

or

$$[L][Y] = \{b\} \tag{2.37}$$

where

$$[Y] = [L]^t \{X\} \tag{2.38}$$

The last two equations can easily be solved by forward and backward substitution. Equation (2.37) and (2.38) are solved with vector $\{Y\}$ overwriting vector $\{b\}$ and vector $\{X\}$ overwriting vector $\{Y\}$. The matrix $[L]$ will overwrite matrix $[K]$ in the solving routine by using the recursive relationships.

$$\ell ij = (Kij - \sum_{z=1}^{j-1} \ell iz\ell jz)/\ell jj \qquad \text{for } j<i \tag{2.39}$$

and

$$\ell ii = \sqrt{Kii - \sum_{z=1}^{i-1} (\ell iz)^2} \tag{2.40}$$

2.4.6 Computation of Nodal and Element Stresses and Strains

In the standard formulation of plane stress and plane strain, the stiffness matrix is given by

$$[K]_e = \iint [B]^t [D] [B] \, dx \, dy \tag{2.41}$$

in which $[B]$ is the matrix defining the strains in terms of the nodal displacements and $[D]$ is the elasticity matrix which relates the stress to the strain.

For plane problems, the strain displacement matrix is given by

$$\{\varepsilon\} = \begin{Bmatrix} \frac{\partial u}{\partial x} \\ \frac{dv}{dy} \\ \frac{\partial u}{\partial y} + \frac{\partial v}{\partial x} \end{Bmatrix} = [B]\{u\}_o^e \tag{2.42}$$

In which $[B] = [B_1, B_2, \ldots\ldots]$ (2.43)

with

$$Bi = \begin{bmatrix} \frac{\partial N_i}{\partial x} & 0 \\ 0 & \frac{\partial N_i}{\partial y} \\ \frac{\partial N_i}{\partial y} & \frac{\partial N_i}{\partial x} \end{bmatrix} \tag{2.44}$$

as N_i is defined in terms of ξ and η, it is necessary to change the derivatives to $\frac{\partial}{\partial x}$ and $\frac{\partial}{\partial y}$, noting that

$$\begin{Bmatrix} \frac{\partial N_i}{\partial \xi} \\ \frac{\partial N_i}{\partial \eta} \end{Bmatrix} = \begin{bmatrix} \frac{\partial x}{\partial \xi} & \frac{\partial y}{\partial \xi} \\ \frac{\partial x}{\partial \eta} & \frac{\partial y}{\partial \eta} \end{bmatrix} \begin{Bmatrix} \frac{\partial N_i}{\partial x} \\ \frac{\partial N_i}{\partial y} \end{Bmatrix} = [J] \begin{Bmatrix} \frac{\partial N_i}{\partial x} \\ \frac{\partial N_i}{\partial y} \end{Bmatrix} \tag{2.45}$$

where $[J]$ is the Jacobian matrix, can be evaluated by a numerical process, noting that

$$[J] = \begin{bmatrix} \frac{\partial N_1}{\partial \xi} & \frac{\partial N_2}{\partial \xi} & \frac{\partial N_3}{\partial \xi} & \cdots \\ \frac{\partial N_1}{\partial \eta} & \frac{\partial N_2}{\partial \eta} & \frac{\partial N_3}{\partial \eta} & \cdots \end{bmatrix} \begin{bmatrix} X_1 & Y_1 \\ X_2 & Y_2 \\ \cdot & \cdot \\ \cdot & \cdot \\ \cdot & \cdot \\ \cdot & \cdot \end{bmatrix} \tag{2.46}$$

where

$$\frac{\partial x}{\partial \xi} = \frac{\partial x}{\partial N_i} \cdot \frac{\partial N_i}{\partial \xi} \tag{2.47}$$

and

$$\frac{\partial x}{\partial N_i} = x_i \tag{2.48}$$

So

$$\frac{\partial N_i}{\partial x} = [1,0][J]^{-1} \begin{Bmatrix} \frac{\partial N_i}{\partial \xi} \\ \frac{\partial N_i}{\partial \eta} \end{Bmatrix} \tag{2.49}$$

$$\frac{\partial N_i}{\partial y} = [0,1][J]^{-1} \begin{Bmatrix} \frac{\partial N_i}{\partial \xi} \\ \frac{\partial N_i}{\partial \eta} \end{Bmatrix} \tag{2.50}$$

and hence $[B_i]$ can be formulated.

The only further change which is required to be done is to replace the element area in equation (2.41) as

$$\partial x \, \partial y = \det[J] \, \partial \eta \, \partial \xi$$

The limits of integration are -1 and 1 in both integrals in equation (2.41).

Hence element strains are obtained, and the stresses too, since

$$\{\sigma\} = [D] \{\varepsilon\} \tag{2.51}$$

where $[D]$ is the elasticity matrix.

CHAPTER 3

NUMERICAL EXAMPLES FOR THE APPLICATION OF PLANE STRESS/STRAIN PROBLEMS

3.1 INTRODUCTION

Although the computer use for the application of the finite element method has provided the engineer with a powerful means to analyse problems of a considerable complexity, there is still the tedious preparation and checking of the large number of input data needed for the computer in order to solve the problems at hand which is time consuming and more liable to produce human error when feeding this information into the computer prior to solving the problem.

Research students[67, 68] have attempted to improve upon data input routine when solving a problem, but still there was no single complete package to define the mesh generation for different types of problems. Wood[15] adopted the technique outlined by Zienkiewicz and Phillips[69], where a computer orientated method is presented which generates meshes of triangular elements in plane and curved surfaces. In addition Wood[15] also used the quadrilateral isoparametric element as well as the original triangular element suggested by Zienkiewicz et al[69]. Depending on the geometrical and material variations, the

region to be discretised is divided into a number of four sided zones. By using curvi-linear co-ordinate systems, nodes within and on the boundary of each zone are automatically positioned and referred to global cartesian co-ordinate system. Elements are automatically assembled from these nodes. Input data is required to specify the positions and material properties of each zone and how they are connected.

The program has been developed by Wood[15] to deal with different types of problems using the finite element method. The programs were written in ALGOL Language. It was run at Aston University and Manchester University computer centres.

It was decided to run the mesh generation program coupled with different finite element programs on the HP-9845 Desk-Top computer available in the department. So the mesh generation program together with the plane stress/strain and the axisymmetric programs were transferred to BASIC from ALGOL, by the department. Crack problem programs were still in ALGOL Language and needed to be translated to BASIC to implement them on the HP-9845 computer. Chapter 7 deals with crack problems.

3.2 BASIS OF THE SCHEME

This scheme is fully described by Reference (15). The basis of the scheme is the use of the "isoparametric"

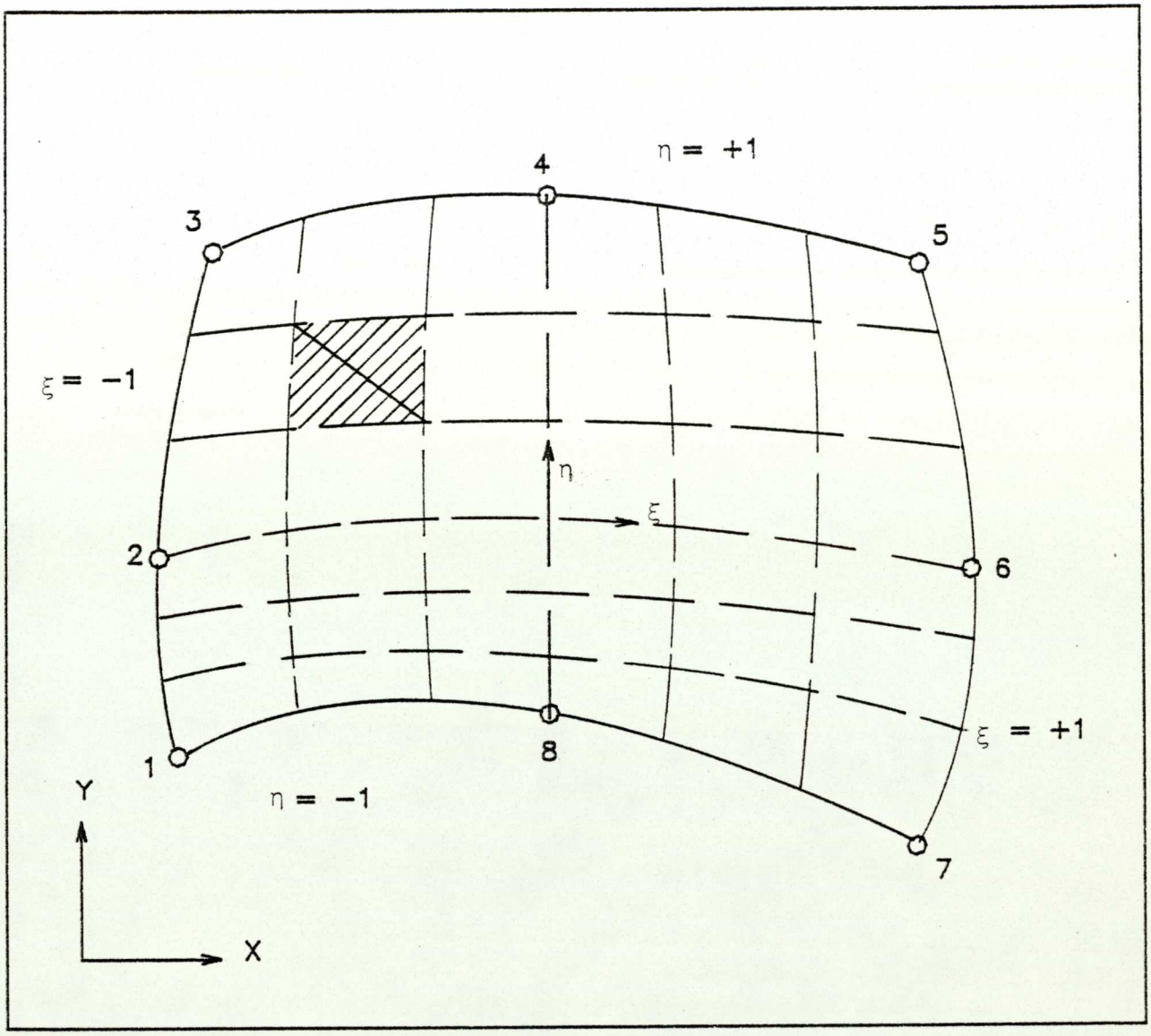

FIGURE (3.1) ISOPARAMETRIC QUADRILATERAL ELEMENT.

curvilinear mapping of quadrilaterals. This allows a unique co-ordinate mapping of curvilinear and cartesian co-ordinates. Having discretised the whole structure into a number of four sided zones, curvilinear co-ordinate system can be used to position nodes on the boundary and within each zone, and reference them to a global cartesian co-ordinate system. Elements are automatically assembled from these nodes. The term "isoparametric" is derived from using the same interpolation functions to define the element shape and displacements within the elements.

Considering the particular case of a two-dimensional isoparametric quadrilateral with 8 nodes as shown in Fig. (3.1), in which X and Y co-ordinates of eight nodes are known and can be written as

$$\left.\begin{aligned} X &= \sum_{i=1}^{8} N_i X_i \\ Y &= \sum_{i=1}^{8} N_i Y_i \end{aligned}\right\} \qquad (3.1)$$

where N_i is the shape function associated with each node i, and defined in terms of curvi-linear co-ordinate system (ξ and η) which has values ranging from +1 to -1 on opposite sides of the quadrilateral.

For this particular element, the shape functions for corner nodes are:

$$N_i = \frac{1}{4}(1+\xi_o)(1+\eta_o)(\xi_o+\eta_o-1)$$

and mid-side nodes

$$\text{for } \xi_i = 0, \quad N_i = \frac{1}{2}(1-\xi^2)(1+\eta_o)$$

$$\eta_i = 0, \quad N_i = \frac{1}{2}(1+\xi_o)(1-\eta^2) \qquad (3.2)$$

$$\xi_o = \xi\xi_i$$

$$\eta_o = \eta\eta_i$$

Typical shape functions are given in general form for a variety of elements in reference (70).

If the co-ordinates of the nodal points are known, the cartesian co-ordinates of any specified point ξ,η can be simply found by equation (3.1).

A mesh of any refinement could be automatically generated inside a region if the later could be described adequately by a quadrilateral of the shape in Fig. (3.1) by specifying:-

(1) Co-ordinates of eight "nodal" points.

(2) The number of required subdivisions in ξ and η directions.

In the scheme the nodal points of the mesh are created and numbered from the lower left-hand corner, vertically and from column to column, in equal ξ and η increments. The element nodal connections can be established using an

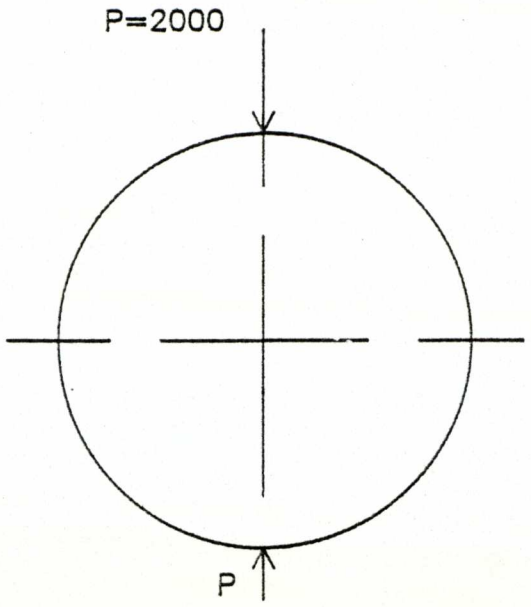

a) ACTUAL DISC

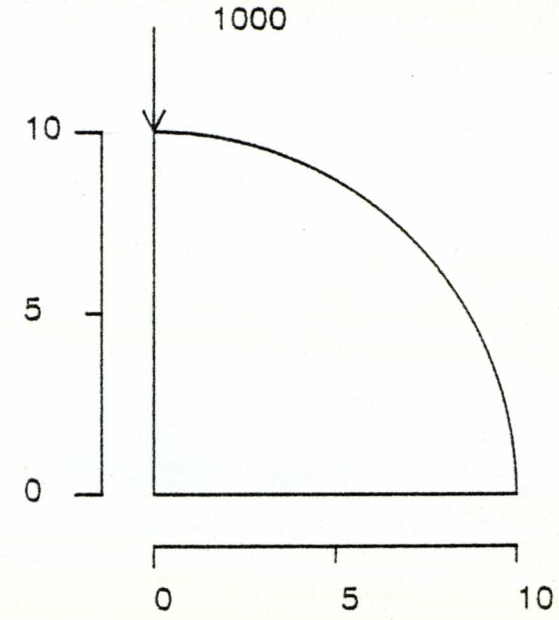

b) A QUARTER OF THE DISC.

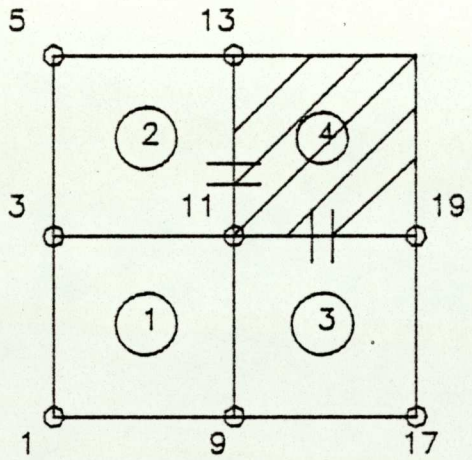

c) ZONE ARRAY WITH ZONE AND SUPER NODE NUMBERING,SHOWING ZONE 4 AS VOID, AND CLOSING FACES.

NOTE THAT NUMBERING SCHEME IS CONTINOUS EVEN WITH VOID PRESENT.

(·) ZONE NUMBER

O SUPER NODE

NUMBER OF ZONES = 3
NUMBER OF ELEMENTS= 24
NUMBER OF NODES = 61

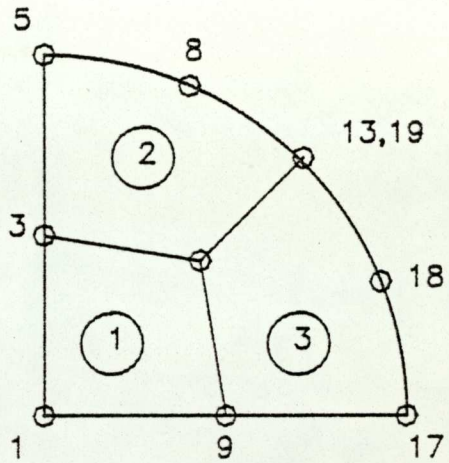

d) DISTORTED ZONE DIAGRAM.

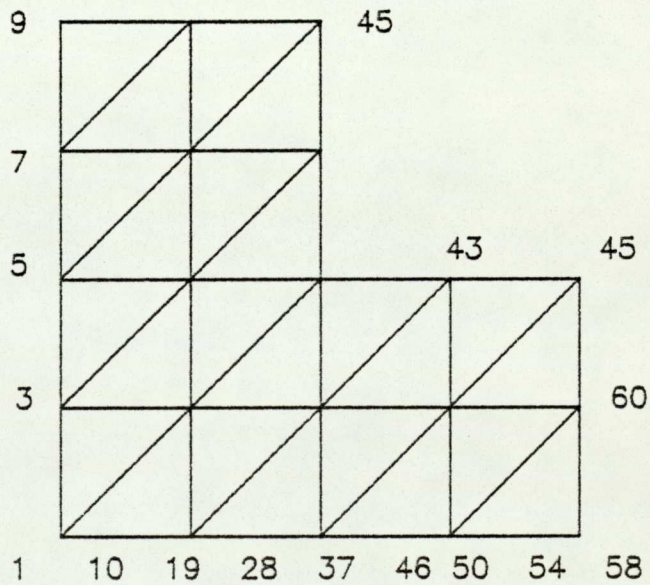

e) ELEMENT ARRAY SHOWING NODAL NUMBERING.
NOTICE NODAL NUMBERING DUE TO CLOSING FACES.

FIGURE (3.2) A DISC IN COMPRESSION.

appropriate rule. Figure (3.1) shows how the elementary quadrilaterals are formed, and the shaded area shows how this region is divided. By selecting the shorter diagonal in the quadrilateral, two triangular elements are obtained. In choosing the shorter diagonal in the quadrilateral a better shape conditioning is obtained.

3.3 THE GENERAL PROGRAM

For complete generality the scheme is extended by dividing the whole region into a "chequer board" pattern of quadrilateral elements used as the basis of the mapping scheme which is termed a "zone". Each of these may define a material with a single property, and if such property is specified zero, a void is achieved, allowing multiply connected zones to be mapped.

In this program, for simplicity the full rectangular "chequer board" pattern is always established using, when necessary, void zones as seen from Fig. (3.2).

The zones are usually described by an 8-nodal co-ordinates called "super nodes". If the zone boundaries are straight, then the co-ordinates of the mid-side nodes can be omitted from the input data, and this information can be determined by interpolation.

A proper node numbering scheme is used to minimize the "bandwidth" of the stiffness matrix as already been described in section (2.1.5), where the matrix bandwidth

is proportional to the difference in adjacent element node numbers. If an inadequate node numbering system is chosen then one would expect the storage space of the stiffness matrix in the computer to increase. In this scheme the element nodal points are numbered from left-hand corner of the zone array, moving vertically and from column to column in equal ξ and η increments as can be seen in Fig. (3.2).

The final stage of the mesh generation scheme is to determine the element nodal co-ordinates. This is achieved by using zone subdivision, and in order to distinguish between zone "super nodes" and element nodes, it is preferable to construct two zone arrays. One containing the "super nodes" numbering and zone numbers, and the second containing the element numbers and element node numbers. The first is required to generate the mesh and the second would be useful as a means to check the total number of elements and total number of nodes in the whole mesh.

Material properties, geometric boundary conditions and load conditions can be applied using the element node numbers concerned.

The above described mesh generation scheme is implemented on the HP 9845 Desk-Top Computer using the BASIC language. All the numerical examples described in this chapter are implemented on the HP 9845 Desk-Top Computer, using the above mentioned program to obtain the structural idealization of the problem and then using the finite element program to

find out the displacements, stresses and strains throughout the body under consideration.

A user guide for the mesh generation program is in Appendix (A).

3.4 EXAMPLE (1) - A CANTILEVER UNDER AN END LOAD

Considering the simple problem of a cantilever under an end load of (1000). The problem is of plane stress. An 8-node quadrilateral element is chosen to describe the structure. (Figure (3.3)).

Material properties are:

$E = 3 \times 10^7$

$\nu = 0.3$

$G = 1.2 \times 10^7$

The loading is in a parabolic manner as shown in Fig. (3.3c).

The first step is to establish a zone pattern. The structure is represented by one single zone as a rectangle. Zone node numbering - super nodes - starts from the bottom left-hand corner and working upwards, and then column by column. In this particular problem, no need for mid-side super nodes, because there are no curved boundaries. The zone array is shown in Fig. (3.3b).

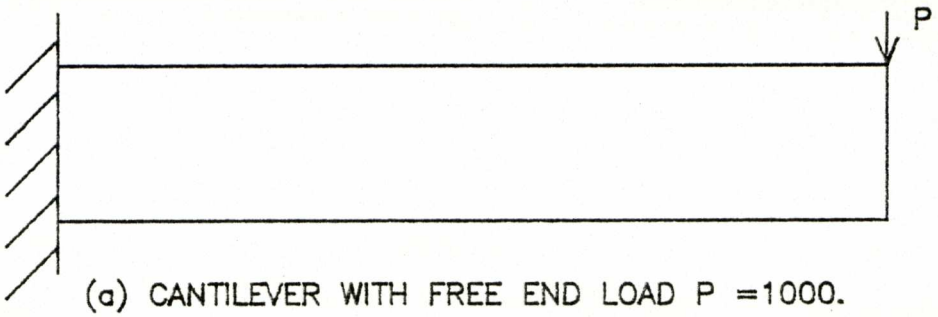

(a) CANTILEVER WITH FREE END LOAD P =1000.

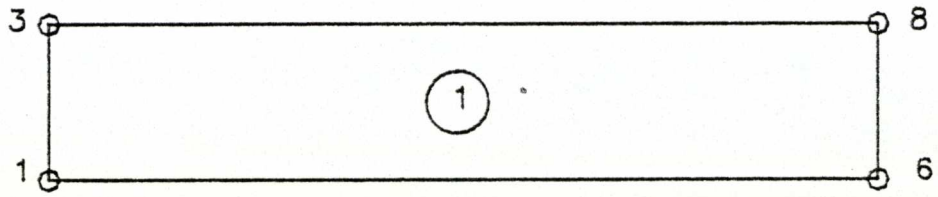

(b) ZONE DIAGRAM SHOWING SUPER NODE NUMBERING.

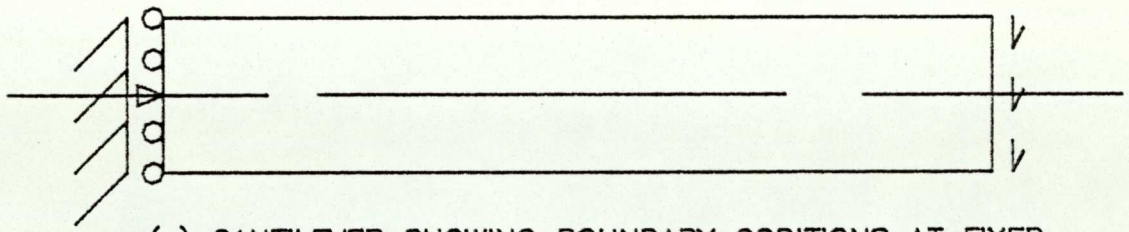

(c) CANTILEVER SHOWING BOUNDARY CODITIONS AT FIXED END AND EQUIVALENT PARABOLIC LOAD AT FREE END.

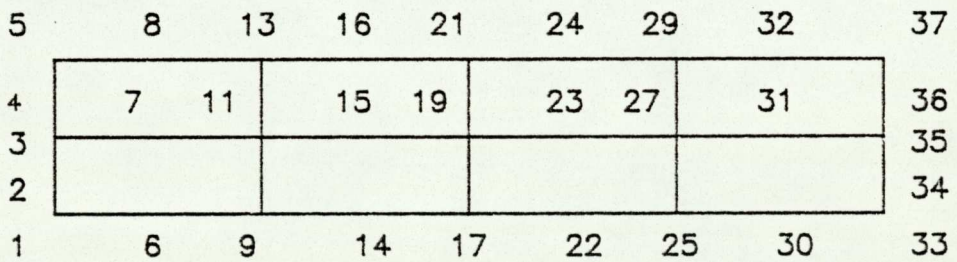

d) ELEMENT ARRAY SHOWING FINITE ELEMENT IDEALIZATION AND NODAL NUMBERING FOR MESH NO. 1.

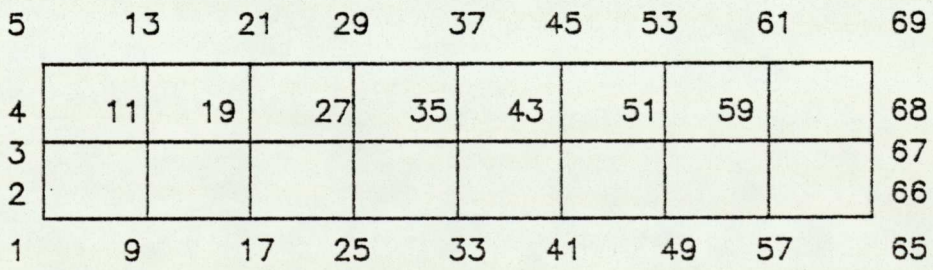

e) ELEMENT ARRAY SHOWING FINITE ELEMENT IDEALIZATION AND NODAL NUMBERING FOR MESH NO. 2.

FIGURE (3.3) A CANTILEVER UNDER END LOAD.

Having established the zone array, a mesh pattern of any refinement can be chosen. In this particular example two meshes are selected, one of an 8-element mesh and the second is a 16-element mesh.

Data input for the two meshes are given in the same order as that described in the user guide for mesh generation program (see Appendix (A)). The first mesh has 37 nodes, and the second mesh has 69 nodes.

Nodal numbering for the element array start from the bottom left-hand corner working upwards, and from column to column, (this way a minimum band-width for the K matrix is achieved).

Boundary conditions and loading are imposed on the structure. At the fixed end of the cantilever, the middle node is considered fixed, while the other nodes are only fixed in the X-direction. The loading at the free end is in a parabolic manner. From the theory of elasticity[5]:

$$\sigma_x = - \frac{pxy}{I} \qquad (3.3a)$$

where p is the point load

$$I = \frac{bd^3}{12}$$

$$\sigma_y = 0 \qquad (3.3b)$$

$$\sigma_{xy} = - \frac{p}{I} \cdot \frac{1}{2}(c^2 - y^2) \qquad (3.3c)$$

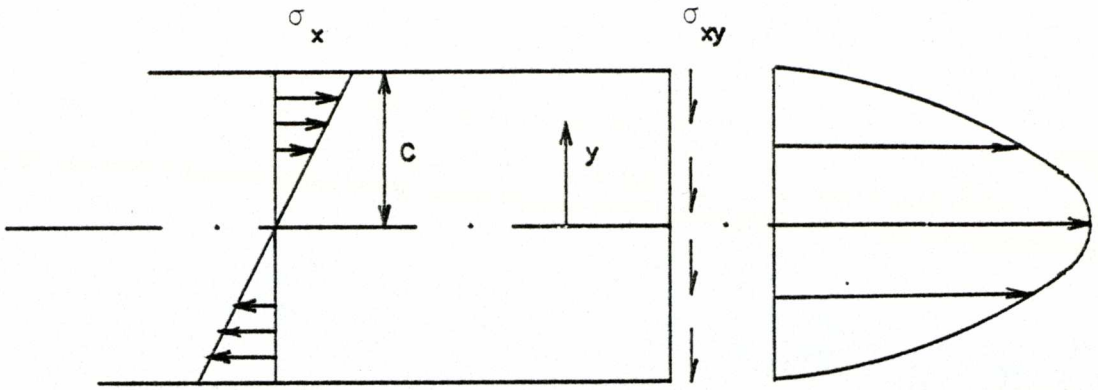

It was shown from equation (3.3) that the load distribution applied at the free end of the cantilever for both meshes are as follows:

Load	Node Number (Mesh (1))	Node Number (Mesh (2))
0	33	65
-1125	34	66
-1500	35	67
-1125	36	68
0	37	69

MESH NO 1		MESH NO.2	
NODE NO.	SHEAR STRESS (−ve)	NODE NO.	SHEAR STRESS (−ve)
3	3421.2	3	2684.6
		7	1440.7
7	708.33	11	2079.4
		15	1609.6
11	3450.7	19	2029.7
		23	1523.3
15	993.94	27	2107.7
		31	1527.2
19	3268.4	35	2111.5
		39	1521.2
23	898.53	43	2118.2
		47	1520
27	3295.9	51	2118.9
		55	1521.0
31	966.64	59	2120.2
		63	1517.9
35	3221.3	67	2117.4

THEORETICAL VALUE OF STRESS : −1500

TABLE (1) : COMPARISON OF THE VALUES OF SHEAR STRESS ALONG THE NUETRAL AXIS OF THE CANTILEVER , CALCULATED THEORETICALLY , & BY MEANS OF F. E. M . EMPLOYING TWO MESHES.

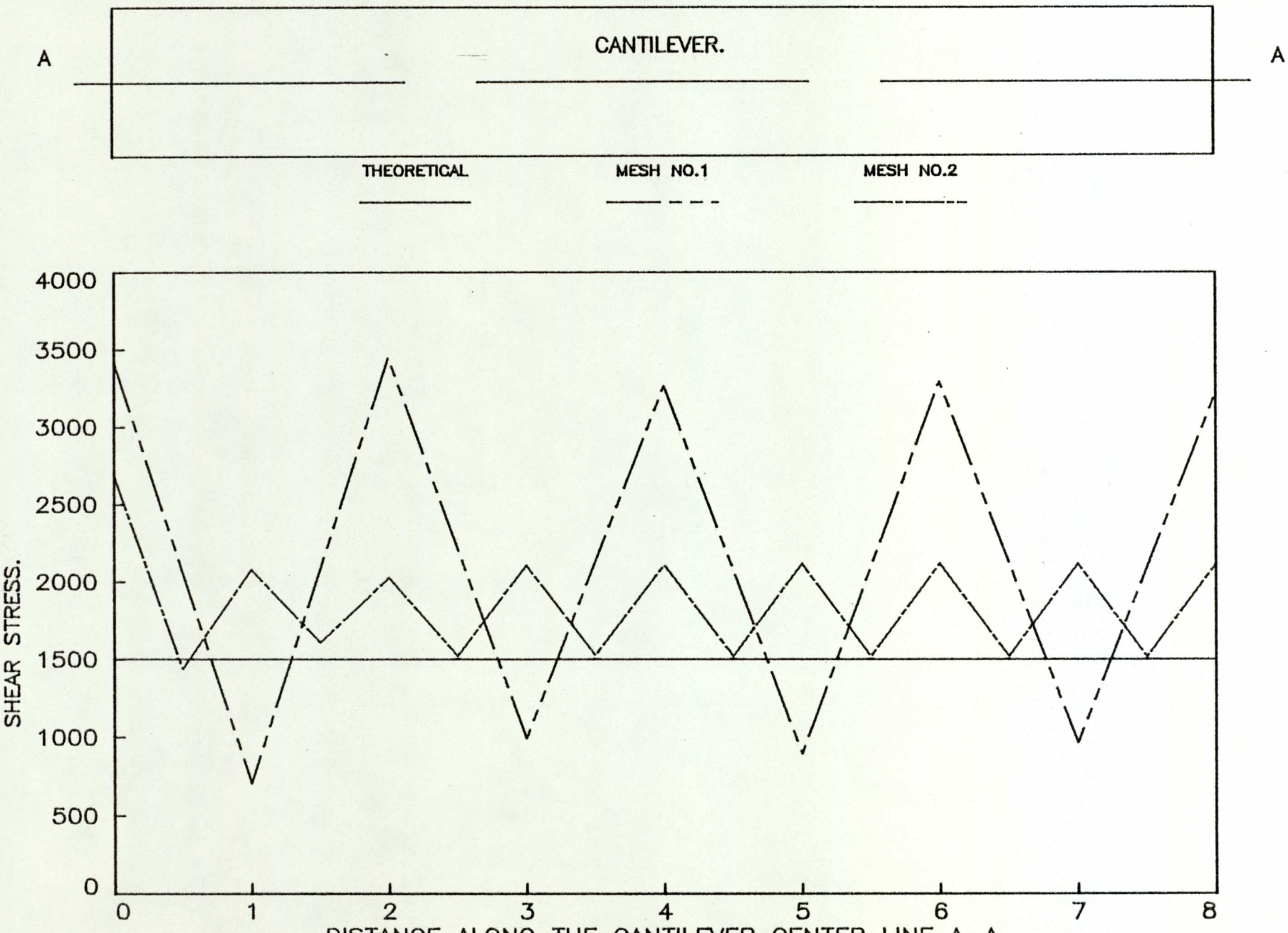

FIGURE (3.1) VALUES OF SHEAR STRESS FOR CANTILEVER

DATA INPUT FOR MESH NUMBER 1.

DATAFILE #1 : CANTD1

DATAFILE #2 : CANTD2

A) Initial control variables

1, 1, 1, 8, 37, 1, 3, 0, 0, 1, 1, 1

B) Control variables

4, 1, 1, 1, 1

C) Standard geometries

0, 0

D) Specific points, super nodes

1, 0, 0, 1 1, 0, 1, 3

1, 8, 0, 6 1, 8, 1, 8

E) Zone specification

1, 1, 4, 2, 1

F) Closing faces

0

G) Boundary conditions, material properties

5

4, 1, 0, 0, 1, 2, 4, 5

1, 3, 0, 0

0, 0, 1

3E7, .3, 1.2E7, 3E7, .3

Distributed loading

2, 33, 0, 0, 34, 0, −1125, 35, 0, −1500

35, 0, −1500, 36, 0, −1125, 37, 0, 0

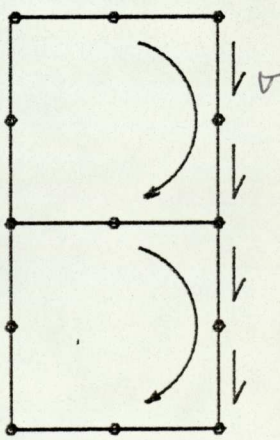

DATA INPUT FOR MESH NUMBER 2.

DATAFILE #1 : CANTR1

DATAFILE #2 : CANTR2

A) 1, 1, 1, 16, 69, 1, 3, 0, 0, 1, 1, 1

B) 4, 1 ,1, 1, 1

C) 0, 0

D) 1, 0, 0, 1 1, 0, 1, 3

1, 8, 0, 6 1, 8, 1, 8

E) 1, 1, 8, 2, 1

F) 0

G) 5

4, 1, 0, 0, 1, 2, 4, 5

1, 3, 0, 0

3, 0, 0, 1

3E7, .3, 1.2E7, 3E7, .3

Distributed loading

2, 65, 0, 0, 66, 0, −1125, 67, 0, −1500, 67, 0, −1500

67, 0, −1500, 68, 0, 0, −1125, 69, 0, 0

The stresses obtained by running the plane stress program, is compared with that calculated by means of equations (3.3). It is found that the values of σ_x obtained by the F.E. method using Mesh (2) is more close to the theoretical values than that obtained by using Mesh (1), and the maximum error is of the order of 0.75%, i.e., there is a convergence as the number of nodes increases. In other words, a finer mesh produces better results. σ_y has a negligible small value compared to the zero theoretical value, again Mesh (2) gives better approximation.

It is when the values of the shear stress are considered that the discrepancies happen. The values taken across the neutral axis of the beam at the nodes along this axis is found to be erratic in manner. Comparing mesh (1) and mesh (2), the values obtained generating mesh (2) which is the finer mesh, are better than values from mesh (1). Better values could be obtained for the shear stress using the smoothing technique. This will be discussed in section (3.8). Graphs of the values of the shear stress for both mesh (1) and mesh (2) are seen in Fig. (3.4), together with the theoretical values.

3.5 EXAMPLE 2 - THICK CYLINDER UNDER INTERNAL PRESSURE

Figure (3.5) shows a thick cylinder under internal pressure. The problem is of plane strain. Only one quarter of the cylinder is used in the analysis due to symmetry.

Quadrilateral element is used in the mesh. The internal pressure is $p_1 = 200$. Material properties are:

$E = 3 \times 10^7$ lbf/in^2

$\nu = 0.3$

$G = 1.2 \times 10^7$. lbf/in^2

As in example 1, the first step is to establish a zone pattern. The structure is represented by one single zone as a rectangle. In this example upper and lower sides of the zone, require mid-side nodes because they represent curved boundaries. Having established the zone array, a mesh of 9 elements is constructed (Figs. (3.6) and (3.7)). Data input for this mesh is written down. For guidance see Appendix (A).

Nodal numbering is arranged in the same manner as that of example 1.

As a check for the stress values obtained using the F.E.M., values of the radial and tangential stresses are calculated[5] across the thickness of the cylinder through the vertical axis.

Theoretically

$$\sigma_r = \frac{a^2b^2(p_o-p_i)}{b^2-a^2}\ \frac{1}{r^2} + \frac{p_ia^2 - p_ob^2}{b^2-a^2} \qquad (3.4a)$$

$$\sigma_\theta = -\frac{a^2b^2(p_o-p_i)}{b^2-a^2}\ \frac{1}{r^2} + \frac{p_ia^2 - p_ob^2}{b^2-a^2}$$

$$\sigma_{r\theta} = 0$$

where (see Fig. (3.5a))

a is the inner radius of cylinder

b is the outer radius of cylinder

p_i is the internal pressure

p_o is the external pressure

r is the distance from the vertical axis through the centre.

If p_o is zero then:

$$\sigma_r = \frac{a^2 p_i}{b^2 - a^2}\left(1 - \frac{b^2}{r^2}\right)$$

$$\sigma_\theta = \frac{a^2 p_i}{b^2 - a^2}\left(1 + \frac{b^2}{r^2}\right) \qquad (3.4b)$$

$$\sigma_{r\theta} = 0$$

These values are compared with values obtained by the F.E.M., and a graph of these values is shown in Figures (3.23a) and (3.23b). Where the values of the smoothed stresses are also shown on the same figures. The latter are discussed in section (3.8) of this chapter. Table 5 shows the theoretical values of the tangential and radial stress, and that obtained by means of the F.E.M. with % error in comparison with the theoretical values.

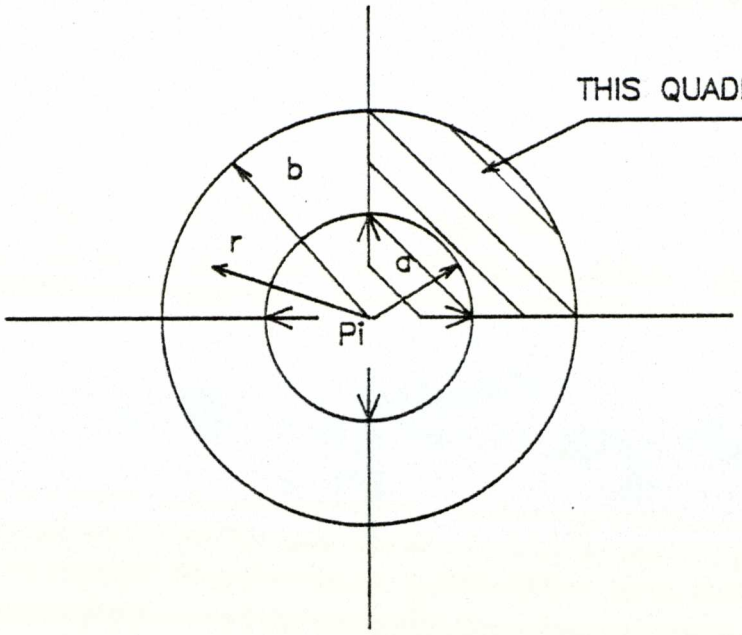

a) THE COMPLETE STRUCTURE.

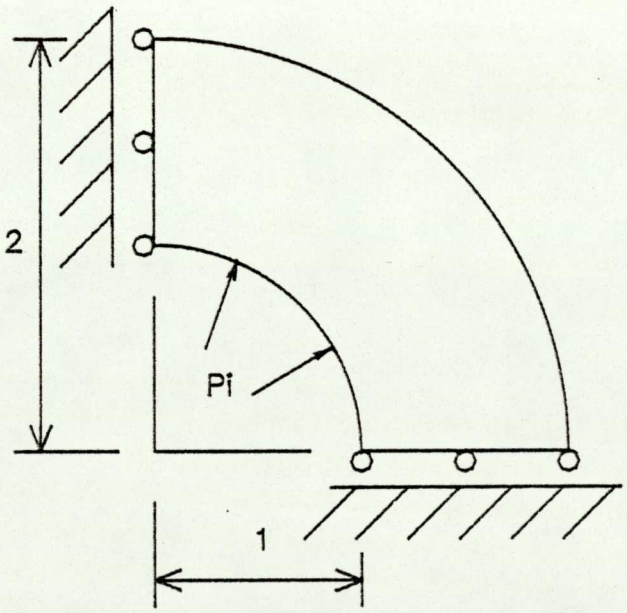

b) QUADRANT OF THE THICK CYLINDER SHOWING LOADING, AND BOUNDARY CONDITIONS.

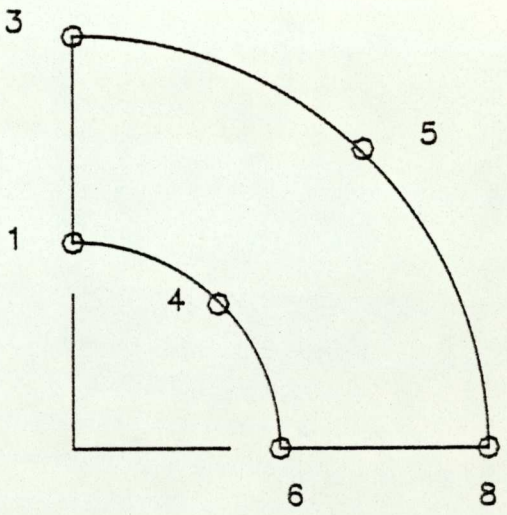

c) DISTORTED ZONE ARRAY

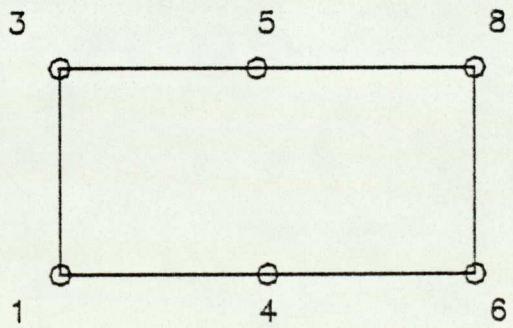

d) ZONE ARRAY.

FIGURE (3.5) THICK CYLINDER UNDER INTERNAL PRESSURE.

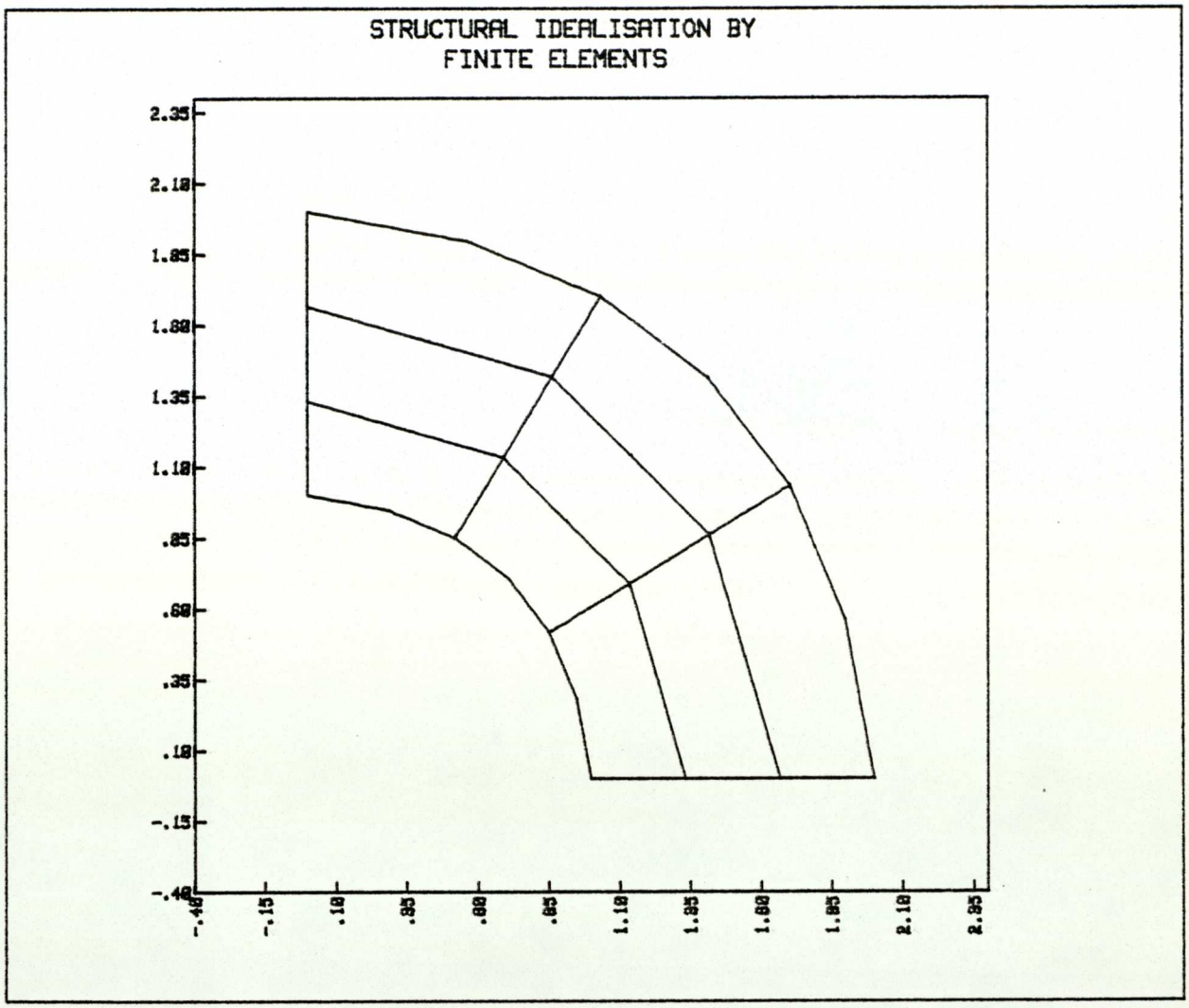

FIGURE (3.6) FINAL STRUCTURE FOR MESH OF THICK CYLINDER .

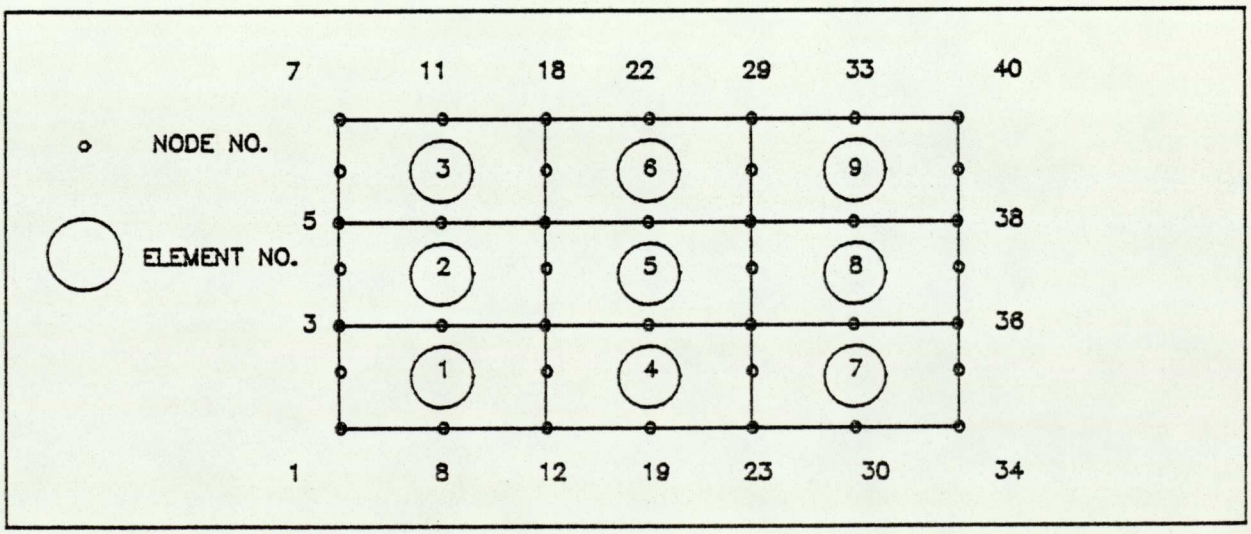

FIGURE (3.7) ELEMENT ARRAY SHOWING ELEMENT, AND NODAL NUMBERING FOR MESH OF THICK CYLINDER.

DATA INPUT FOR EXAMPLE NUMBER 2.

DATAFILE #1 : THCYL5

DATAFILE #2 : THCYL6

A) 1, 1, 1, 9, 40, 1, 3, 0, 0, 1, 1, 1

B) 6, 1, 1, 1, 1

C) 0, 0

D) 1, 0, 1, 1 1, 0, 2, 3 1, 1, 0, 6 1, 2, 0, 8

1, .7071067, .7071067, 4 1, 1.4142135, 1.4142135, 5

E) 1, 1, 3, 3, 1

F) 0

G) 14

7, 1, 0, 0, 1, 2, 3, 4, 5, 6, 7

7, 2, 0, 0, 34, 35, 36, 37, 38, 39, 40

1, 0, 1

3E7, .3, 1.2E7, 3E7, .3

Distributed loading

3

1, 200, 0, 8, 200, 0, 12, 200, 0, 12, 200, 0, 19, 200, 0

23, 200, 0, 23, 200, 0, 30, 200, 0, 34, 200, 0

3.6 EXAMPLE 3 - A PLATE WITH A SMALL CIRCULAR HOLE IN ITS MIDDLE UNDER TENSION

The tensile load applied is of the value p = 1200/unit length, the problem is one of plane stress. The element used in the mesh is the 8-node quadrilateral element. (Figs. (3.8) to (3.13)). Thickness of plate = 1. Material properties are:-

$E = 3 \times 10^7$

$\nu = 0.3$

$G = 1.2 \times 10^7$.

In this example the symmetry is exploited and only one quadrant of the plate is used in the solution. The mesh is generated automatically round the core (circular hole) without putting extra data input for standard generated zones. The structure is divided into 6 four-sided regions, Fig. (3.10a). No voids are required to complete the key diagrams. Zones 1 and 2 are generated by means of a sub-program "STDGEN", (see Figure (3.10b)). Super nodes belonging to these zones are omitted and will not be considered, (Figures (3.11a) and (3.11b)). Figure (3.11c) shows the element array chosen with element and nodal numbering. The structural idealization by the F.E.M. is shown in Figures (3.12a) and (3.12b).

In this example, where the quadrilateral isoparametric element is used, the value of the stress concentration factor at the edge of the cicular hole is found to be 3.0247. The

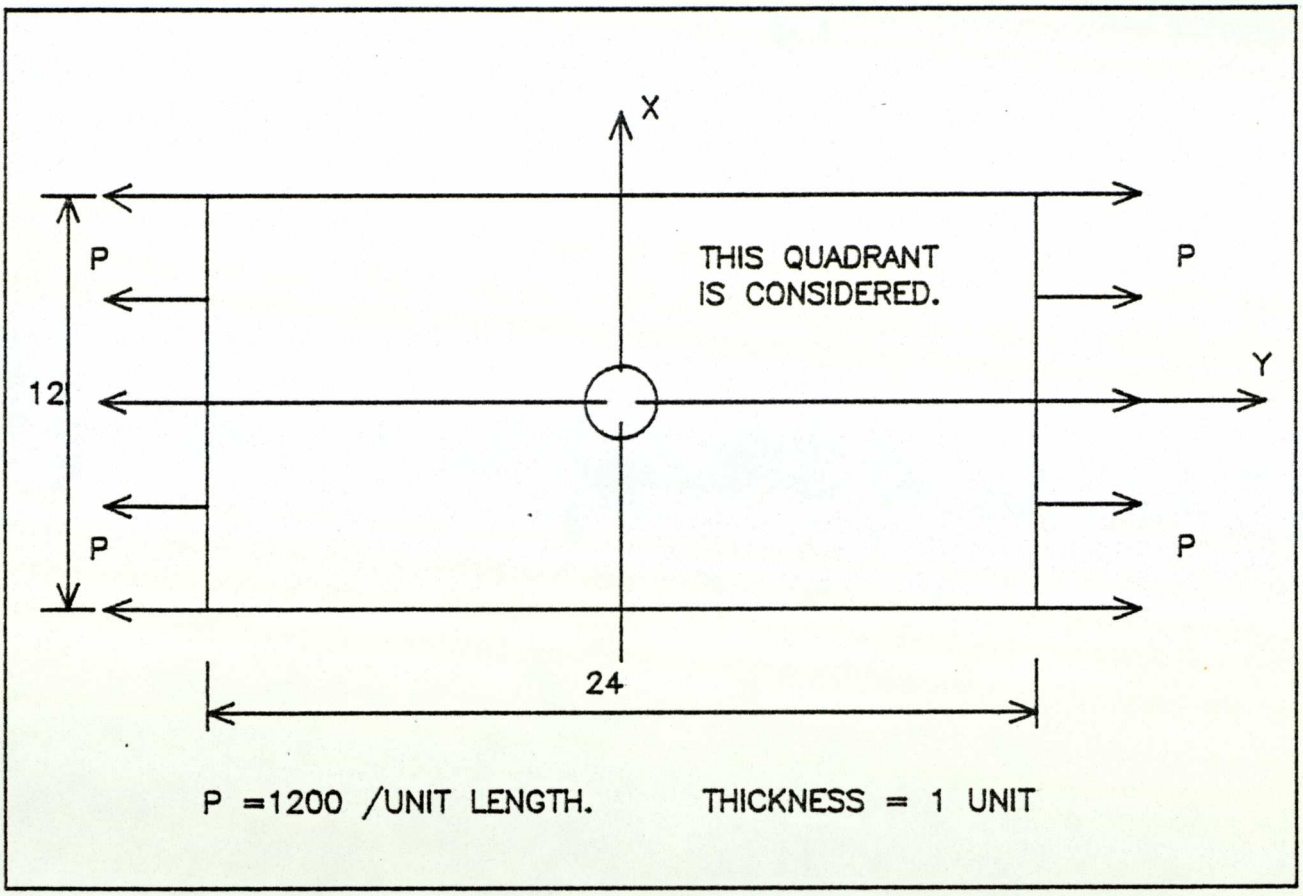

FIGURE (3.8) A PLATE WITH A CENTER HOLE, IN TENSION.

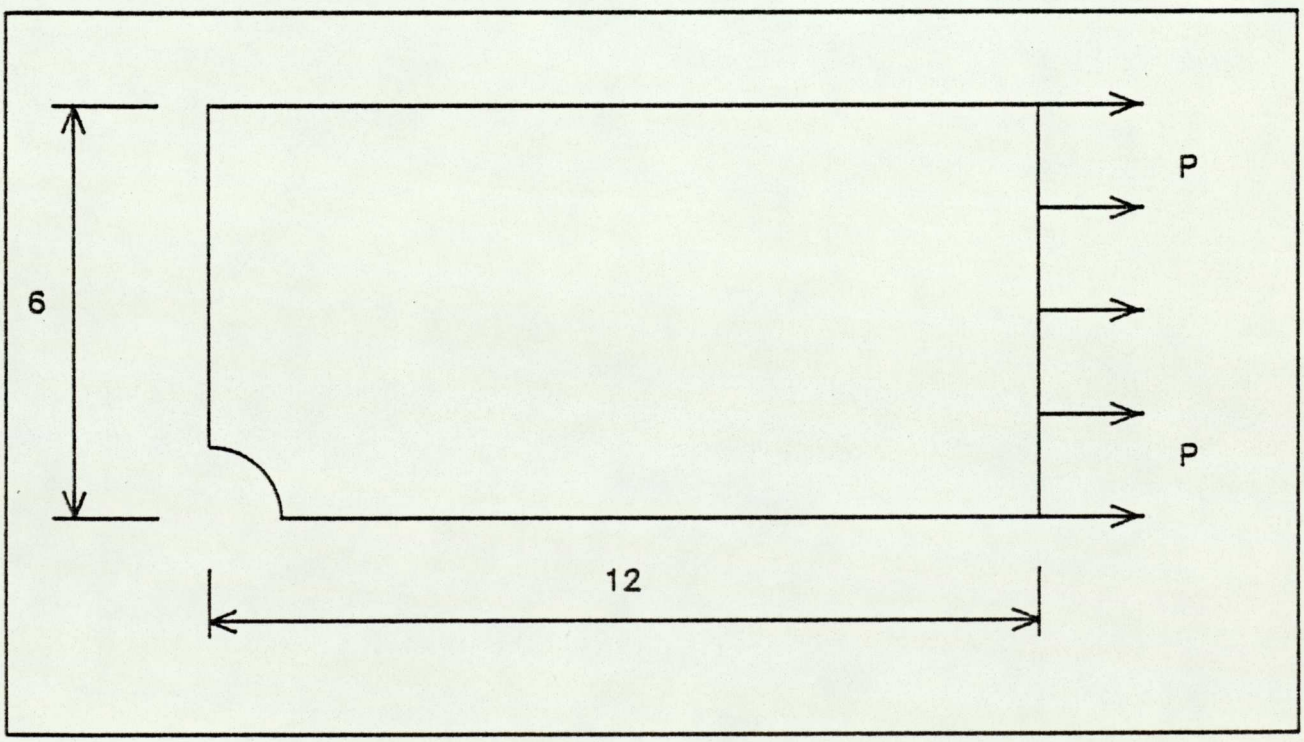

FIGURE (3.9) THE QUADRANT OF THE PLATE ABOVE.

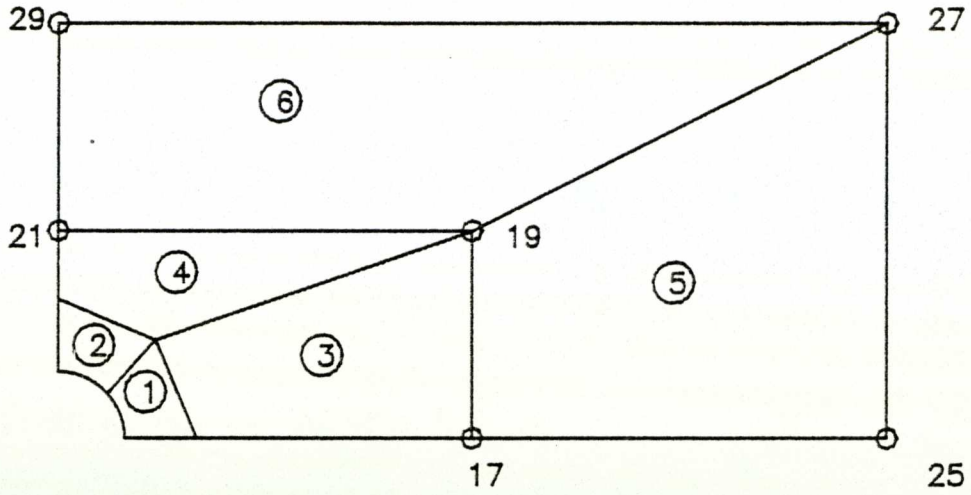

a) DISTORTED ZONE DIAGRAM SHOWING ZONES, AND SUPER NODES.

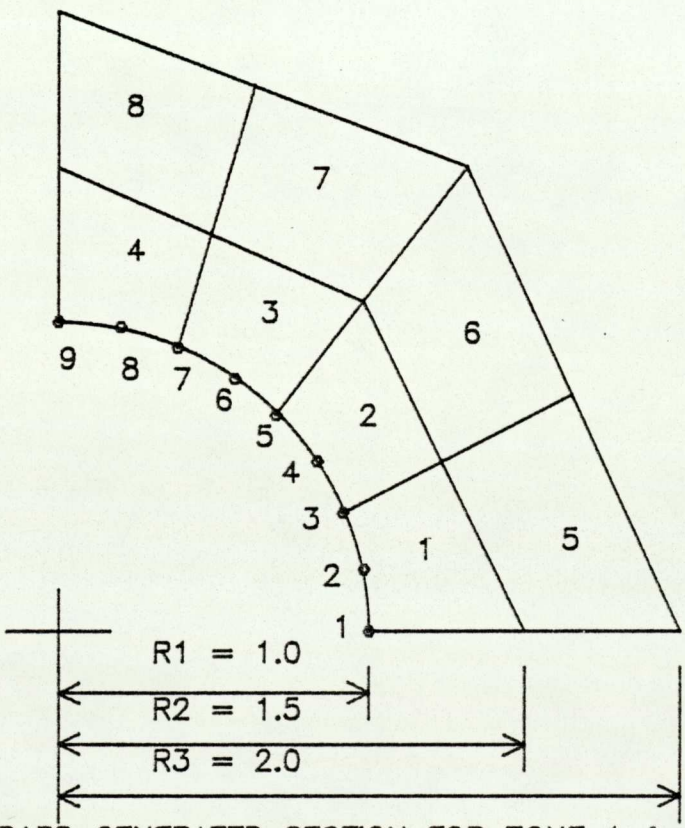

b)THE STANDARD GENERATED SECTION FOR ZONE 1 & 2 SHOWING ZONES SUB–DIVISION & ELEMENT NO.

FIGURE (3.10) DISTORTED ZONE DIAGRAM AND STANDARD GENERATED SECTION FOR PLATE EXAMPLE.

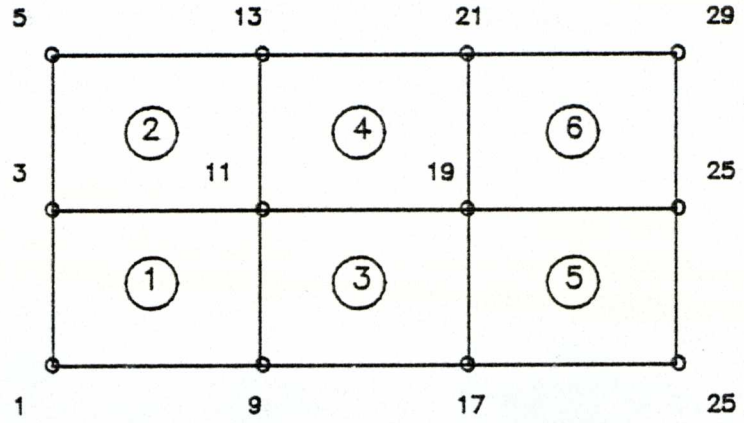

a) ZONE ARRAY DIAGRAM SHOWING SUPER NODES INCLUDING STANDARD GENERATED NODES.

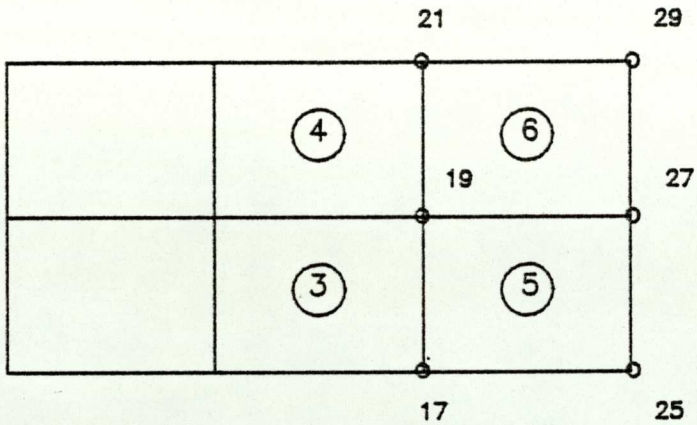

b) ZONE ARRAY DIAGRAM WITH EXTRA SUPER NODES DELETED DUE TO THE USE OF STANDARD GENERATED SECTION.

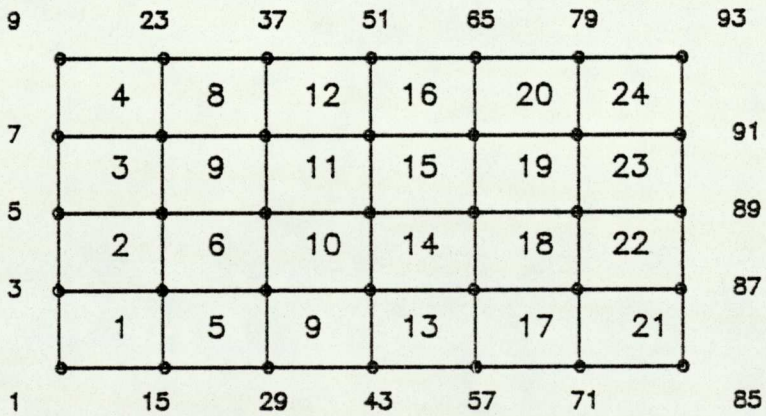

c) ELEMENT ARRAY DIAGRAM SHOWING ELEMENT NUMBERING, AND NODAL NUMBERING.

NUMBER OF ELEMENTS = 24
NUMBER OF NODES = 93

FIGURE (3.11) KEY DIAGRAMS FOR ZONE AND ELEMENT ARRAYS.

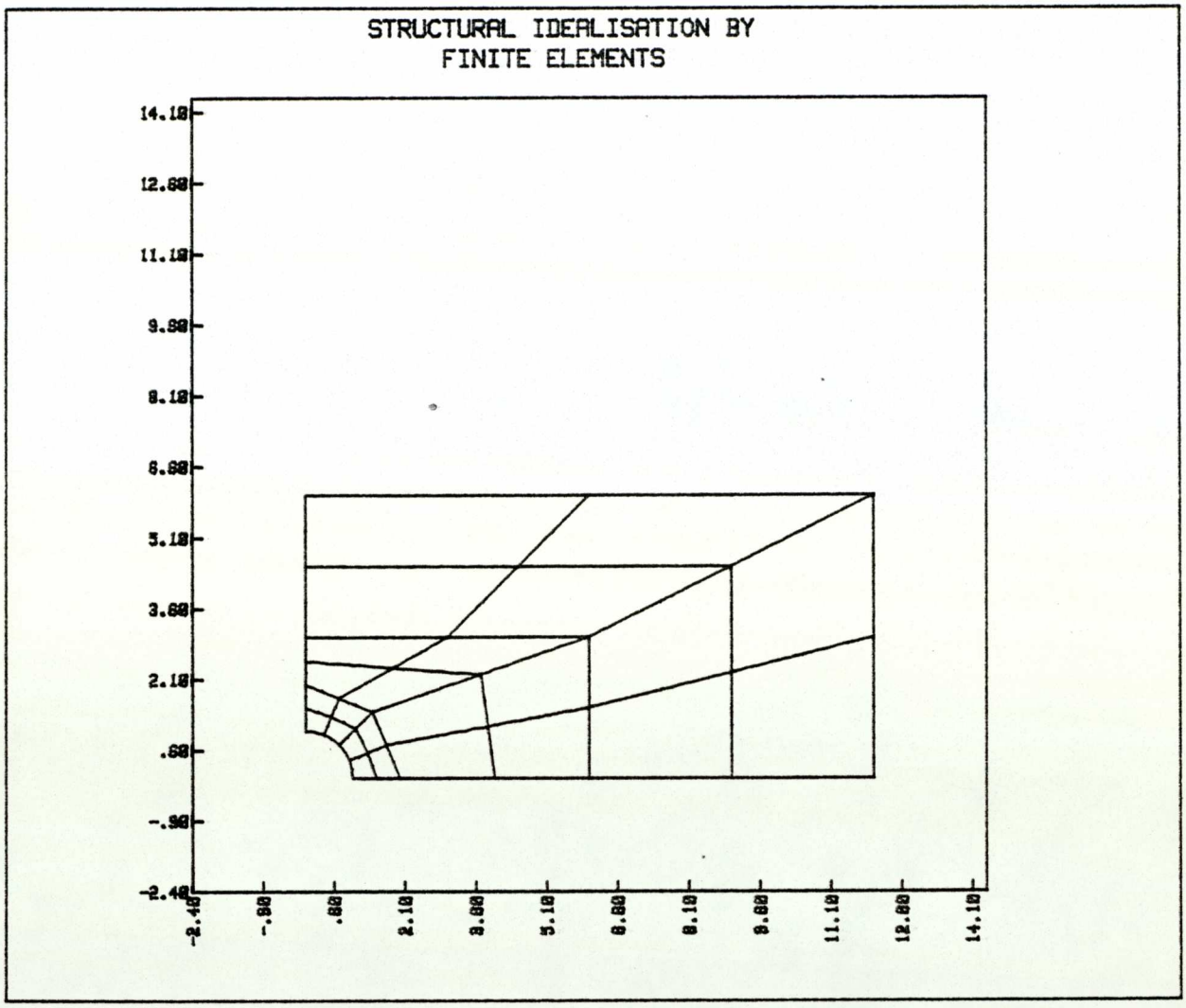

FIGURE (3.12a) FINAL STRUCTURE OF PLATE EXAMPLE.

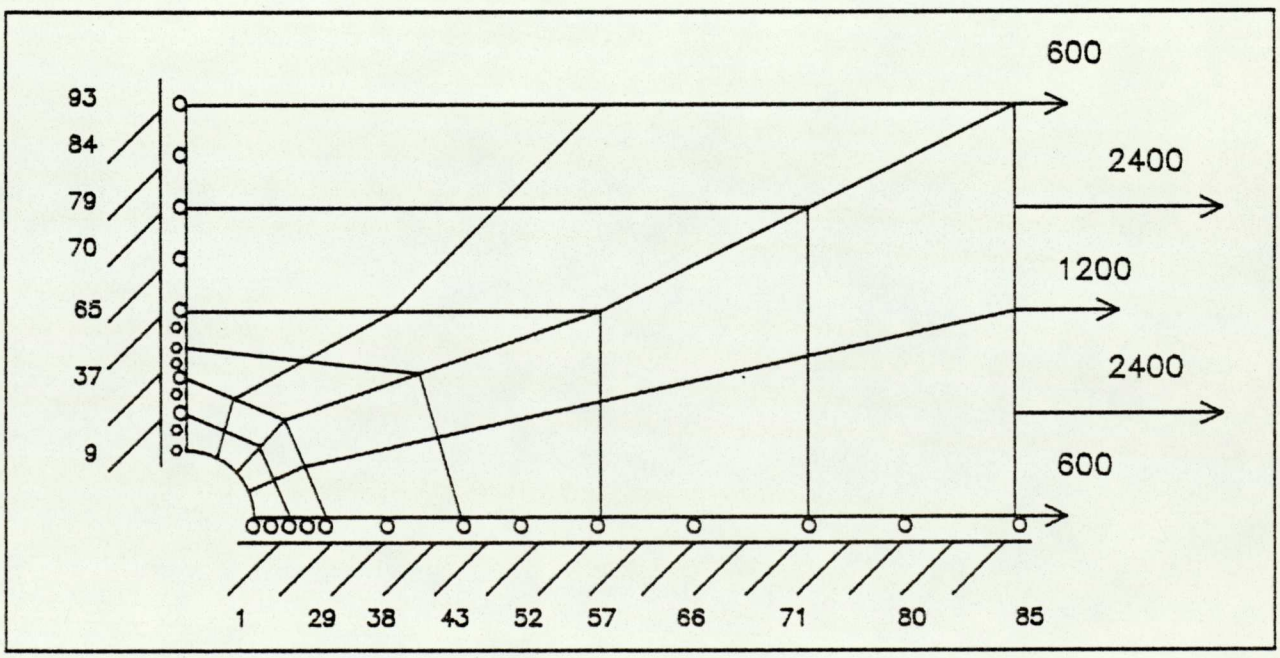

FIGURE (3.12b) FINAL STRUCTERE OF PLATE SHOWING BOUNDARY CONSTRAINTS AT THE NODES &, LOADING

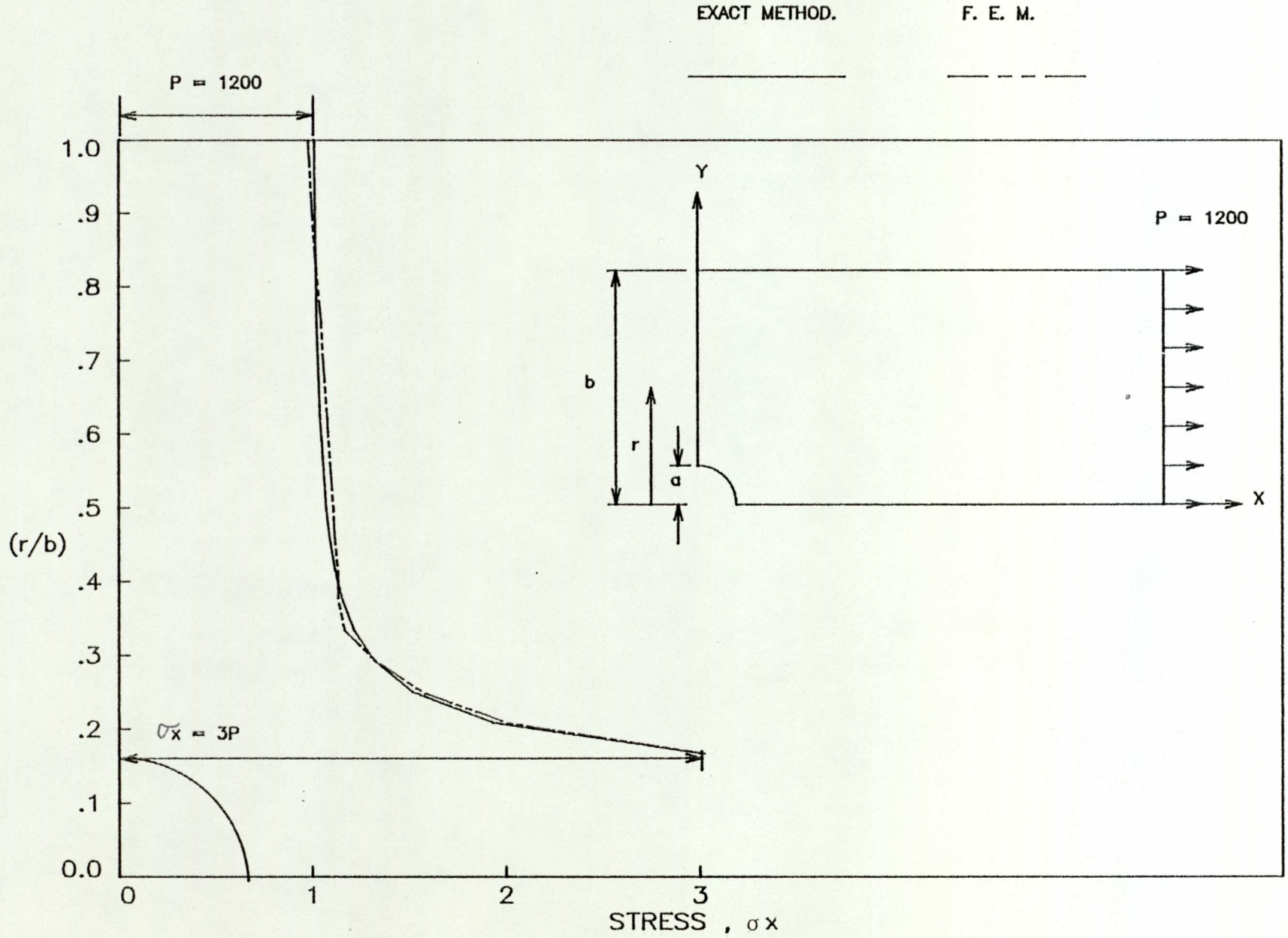

FIGURE (3.13) GRAPH OF NODAL STRESS ALONG X = 0

DATA INPUT FOR EXAMPLE NUMBER 3.

DATAFILE #1 : PLATE1

DATAFILE #2 : PLATE2

A) 1, 1, 1, 24, 93, 1, 3, 0, 0, 1, 1, 1

B) 6, 4, 2, 3, 1

C) 0, 1

1, 1, 5, 0, 0, 1, 1, 5, 2, 0, 22.5, 2, 2

D) 1, 6, 0, 17 1, 6, 3, 19 1, 0, 3, 21

1, 12, 0, 25 1, 12, 6, 27 1, 0, 6, 29

E) 4, 1, 2, 2, 3, 4, 5, 6

F) 0

G) 30

13, 1, 0, 0, 9, 14, 23, 28, 37, 42, 51, 56, 65, 70, 79, 84, 93

12, 2, 0, 0, 1, 10, 15, 24, 29, 38, 43, 52, 57, 66, 71, 80

1, 2, +600, 0, 85 1, 0, +600, 0, 89

1, 0, +1200, 0, 87 2, 0, +2400, 0, 86, 88

0, 0, 1

3E7, .3, 1.2E7, 3E7, .3, 0

Section C above deals with the generated section and input parameters for this section are as follows :

Note:– See also user guide in appendix A .

Number of crack tips Ntip = 0

Super number of generated section Ngm = 1

Super node number starting the core	Nstart	= 1
Zone number starting the core	Zns	= 1
Number of super nodes on the core face	N1	= 5
Co–ordinates of centre of semi circle are	X1, Y1	= 0,0
Radii	R1, R2, R3=	1, 1.5,2.0
Start angle	A	= 0°
Incremental angle	Al	= 22.5°
Zone's sub–divisions in X and Y direction are	Dx, Dy	= 2, 2

infinite plate solution given by Timoshenko and Goodier[5] gives a value of 3.0, i.e. an error of 0.82% is present in the F.E.M. solution compared to the exact method.

Mirza and Olson[73] used the mixed finite element formulation, employing the 6-node triangular element, for a square plate with a circular hole in the middle, loaded by a uniform uniaxial stress. They calculated the stress concentration factor at the edge of the hole to be 3.263 i.e. an error of 8.76% is present in their solution. They have used a total of 106 elements compared to the 24 elements used in the present method which proves beyond doubt that the present method is far superior to theirs.

3.7 EXAMPLE 4

In this example, the problem is to find the relationship between the displacement at the point of load application and the crack length extending through the groove at the centre of the component which is shown in Fig. (3.14). The load applied is 1000 Kg, and the thickness of the component is considered to be one unit.

A structural idealization by finite element method is prepared (see Figs. (3.19) and (3.20)). Only half of the component is considered since it is symmetrical about the horizontal central line (Fig. (3.14)). The structural idealization is obtained by discretising the component into sub-regions. The element employed is the quadrilateral

isoparametric element. Void regions are used in this example (Figs. (3.19) and (3.20)).

Preparing the necessary data and using the mesh generation program, a new file is compiled with the necessary information to solve the problem. F.E.M. computer program 1,which deals with plane problems with the help of the file compiled, is used on the 9845 HP Computer and results of displacements at the nodes of the elements are obtained, including that at the point of load application which is found to be 63.8105×10^{-3} mm in the first run where there is no crack extending from the groove.

To verify the results obtained by the finite element method, a solution of the problem by means of analytical method is carried out using the super-position method as shown in Figs (3.15) to (3.18). The value of the displacement at the point of the load application is found to be 46.5025×10^{-3} mm. The difference between the two results is 27%, which is acceptable since there is an approximation in using the super-position method.

Once it was clear that the results were verified, further runs were carried out increasing the crack length in each case and the corresponding displacement at the point of load application is obtained. Table 2 displays the values of these displacements corresponding to crack length. Figures (3.20a) and (3.20b) show location of these constraints. One can deduce from them the crack

length starting at the groove.

A graph of displacement at the point of load application versus crack length is plotted as shown in Figure (3.21). The values of dC/dA are calculated from this graph.

Values of stress intensity factor (K_I) are obtained in $N/(cm)^{3/2}$, using the following formula.

Where N is Newton

$$K_I = Q \left[\frac{E}{2} \cdot \frac{dC}{dA}\right]^{\frac{1}{2}} \qquad (3.5)$$

where

K_I = stress intensity factor, mode I.

Q = Applied load

E = Young's Modulus of elasticity

$\frac{dC}{dA}$ = Rate of change of compliance to rate of change of crack area.

Table 3 shows the corresponding values of dC/dA and K_I related to crack length. A sample calculation for the value of K_I is shown below:

Calculation of K_I

For a crack of length 3.75 cm

From Graph 3.22,

$$\frac{dC}{dA} = \frac{0.0095 \times 10^{-1}}{5.6 \times 9810} = 1.729 \times 10^{-8}$$

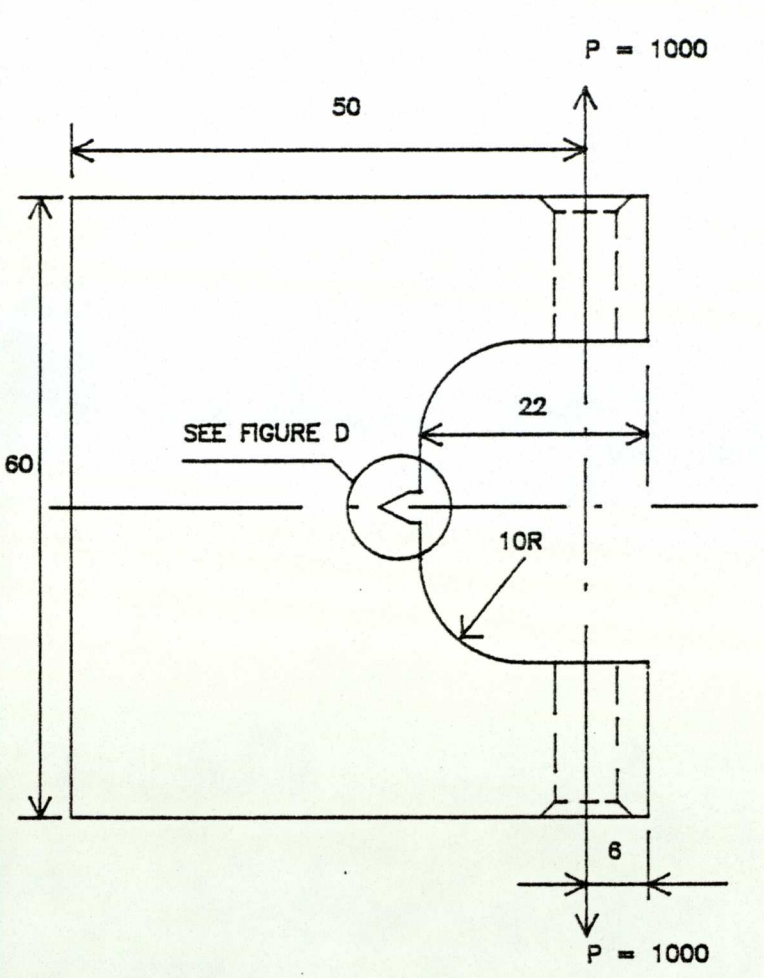

a) ORIGINAL STRUCTURE.

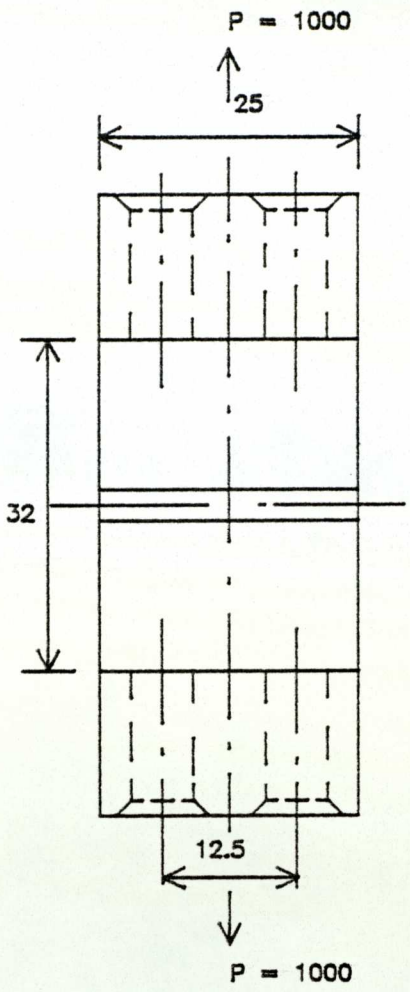

B) SIDE VIEW.

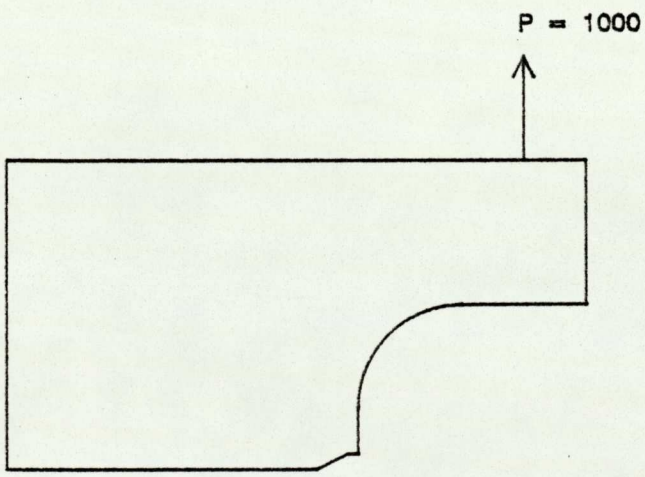

C) HALF THE STRUCTURE ABOVE.
SYMMETRY IS EXPLOITED.

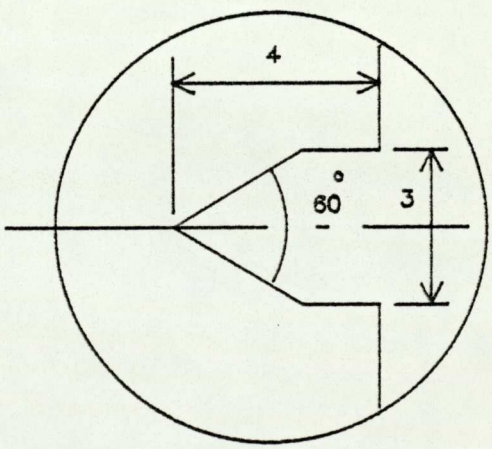

D) THE ENCIRCLED GROOVE
IN FIGURE a.

FIGURE (3.14) DETAILS OF COMPONENT CONSIDERED.

$E = 2.07 \times 7 \ N/cm^2$

$G = 0.796 \times 7 \ N/cm^2$

$\nu = 0.3$

$P = 1000 \ KG.$

$= 9810 \ N.$

THICKNESS= 1 cm.

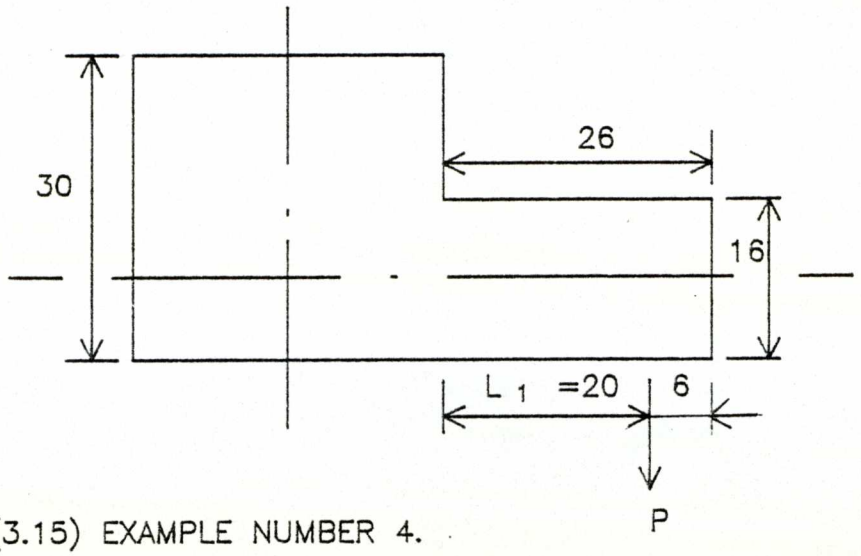

FIGURE (3.15) EXAMPLE NUMBER 4.

SIMPLIFY PROBLEM – BY MEANS OF SUPERPOSITION.

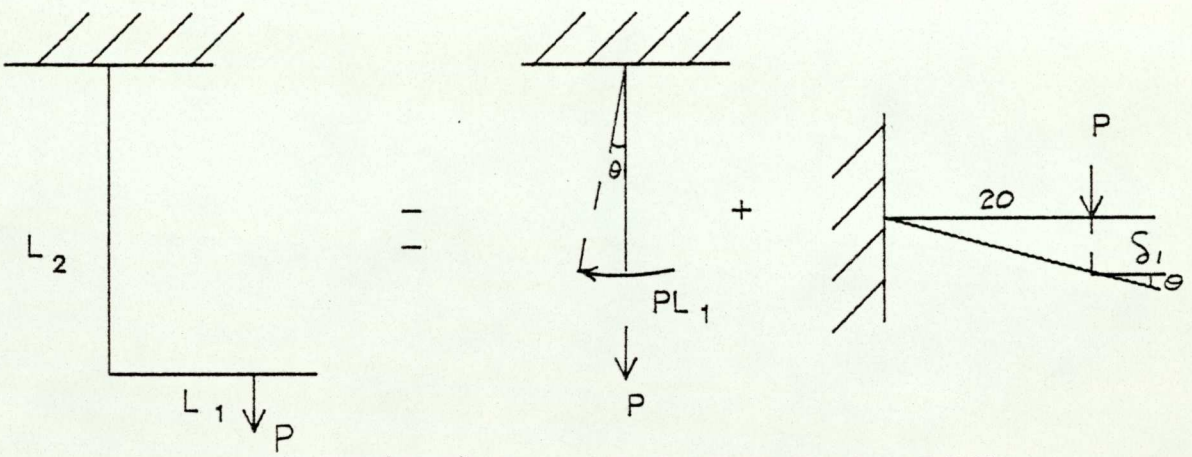

FIGURE (3.16) EQUIVALENT OF PROBLEM ABOVE.

TOTAL DISPLACEMENT AT POINT OF LOADING = $T\delta$

$$T\delta = PL_1^3 / 3EI + L_1\theta + e$$

$T\delta$ DUE TO : CANTILEVER + COUPLE + DIRECT EXTENSION.

FOR THE FIRST TERM DUE TO CANTILEVER –INCLUDING NOTCH

$$\delta_1 = PL_1^3/3EI$$

$$I = 2(C)/3 = 2x(8)^3/3 = 341.333$$

$$\delta_1 = (1000 \times 9.81 \times 20^3) / (3 \times 2.07 \times 10^7 \times 341.333)$$

$$\therefore \delta_1 = 37.014 \times 10^{-3} \ mm.$$

FOR THE SECOND TERM :

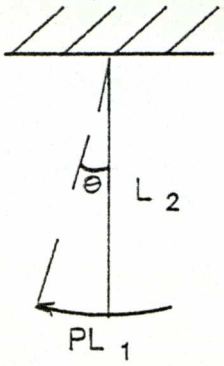

$L_1 = 15$

$I = 2(C)^3/3 = 2x(15)^3/3$

$I = 2250$

$\theta = 9810x(15)^2/(2x2.07x10^7x2250)$

$\theta = 2.3696x10^{-5}$

$\theta L_1 = 2.3696x10x20^{-5}$

$= 4.739x10^{-4}$ cm

$= 4.739x10^{-3}$ mm

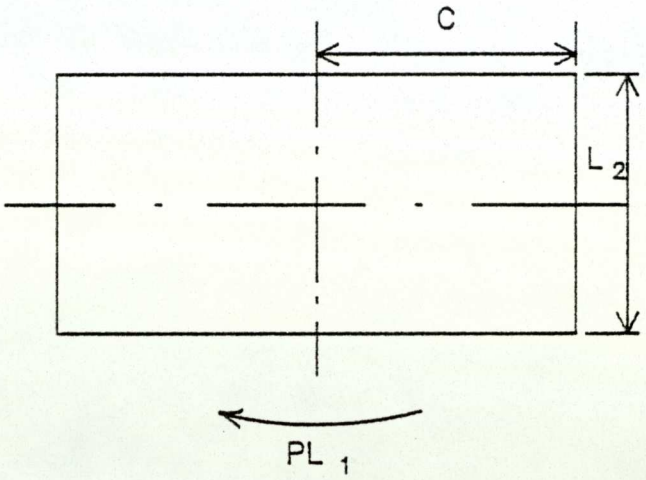

FIGURE (3.17)

THIRD TERM DUE TO EXTENSION :

$E = (P/A)/(e/L)$

$E = (1000x9.81/30)/(30x2.07x10^7)$

$e = 4.739x10^{-4}$ cm

$e = 4.739x10^{-3}$ mm

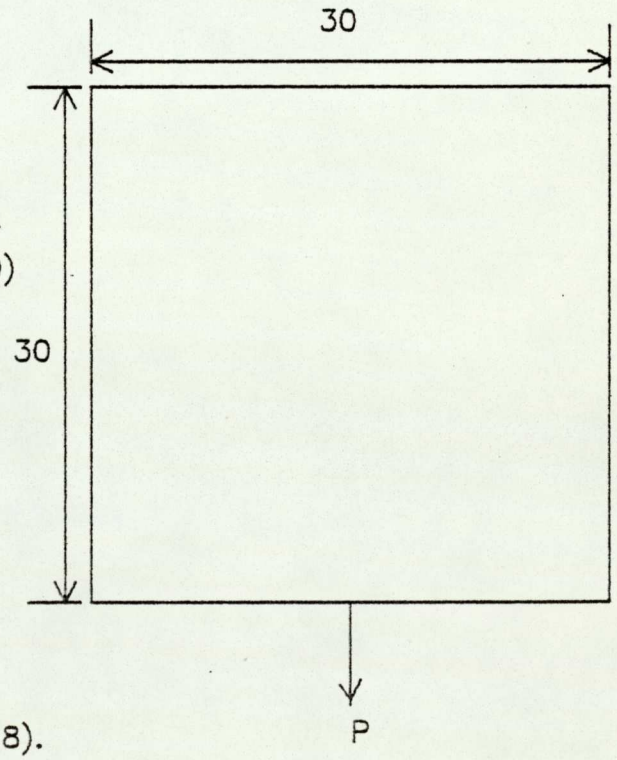

FIGURE (3.18).

$T\delta = 37.024x10^{-3} + 4.739x10^{-3} + 4.739x10^{-3}$

$= \underline{46.503x10^{-3}}$ mm

To compare results of displacements at point of load application using theoretical calculation and the finite element method :

Displacement at node 71 = 63.8105×10^{-3} mm.

% Error = $(63.8105 \times 10^{-3} - 46.5025 \times 10^{-3}) / (63.8105 \times 10^{-3})$

= 27.1

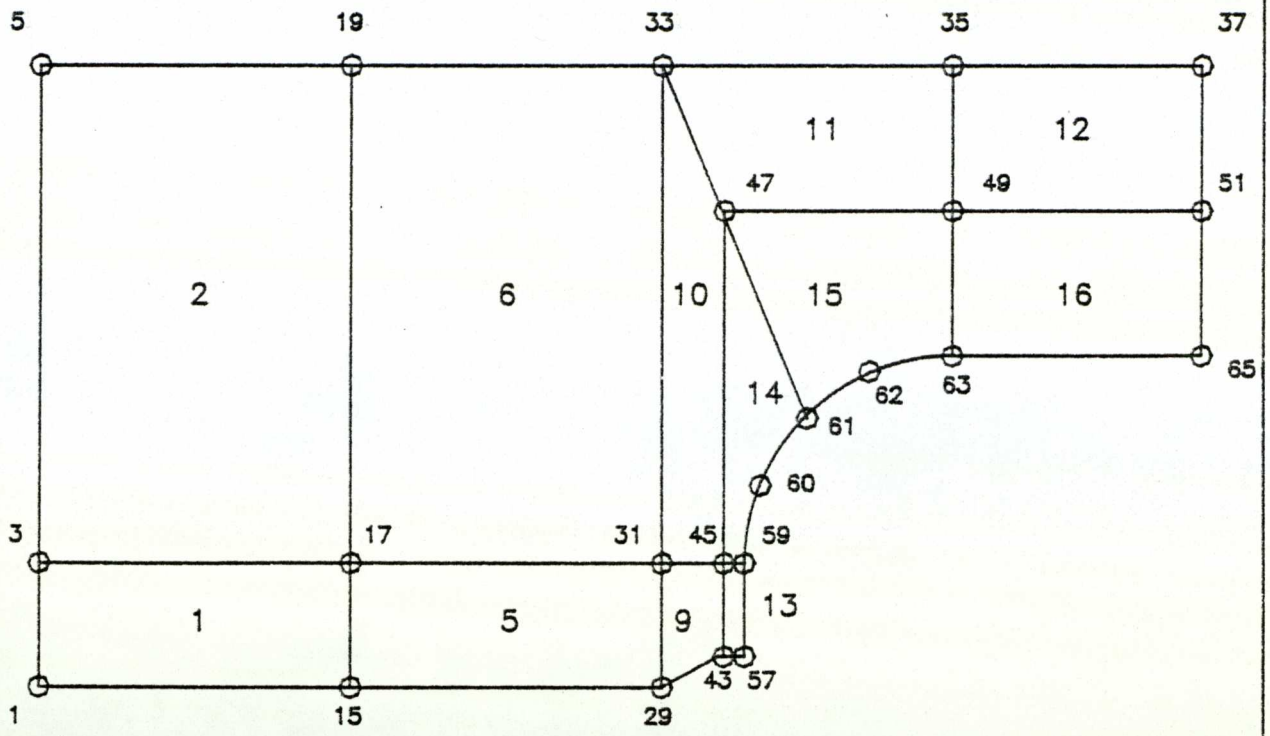

a) DISTORTED ZONE ARRAY SHOWING ZONE NUMBERS AND SUPER NODES.

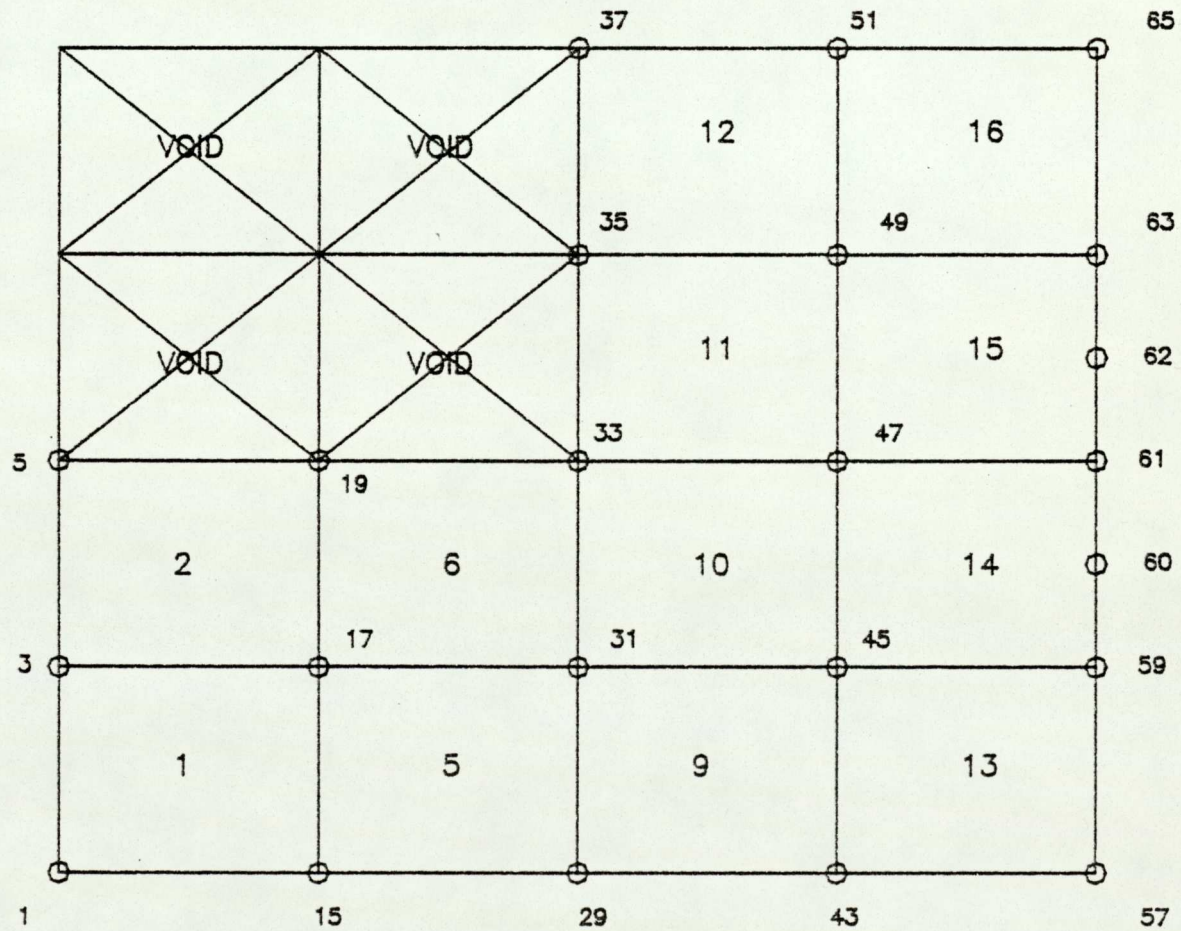

b) ZONE ARRAY SHOWING ZONE & SUPER NODE NUMBERS.
NOTICE VOID ZONES NUMBER 3,4,7,&8.
NUMBER OF ZONES = 12 NUMBER OF SUPER NODES = 23

FIGURE (3.19) KEY DIAGRAMS FOR ZONE ARRAYS.

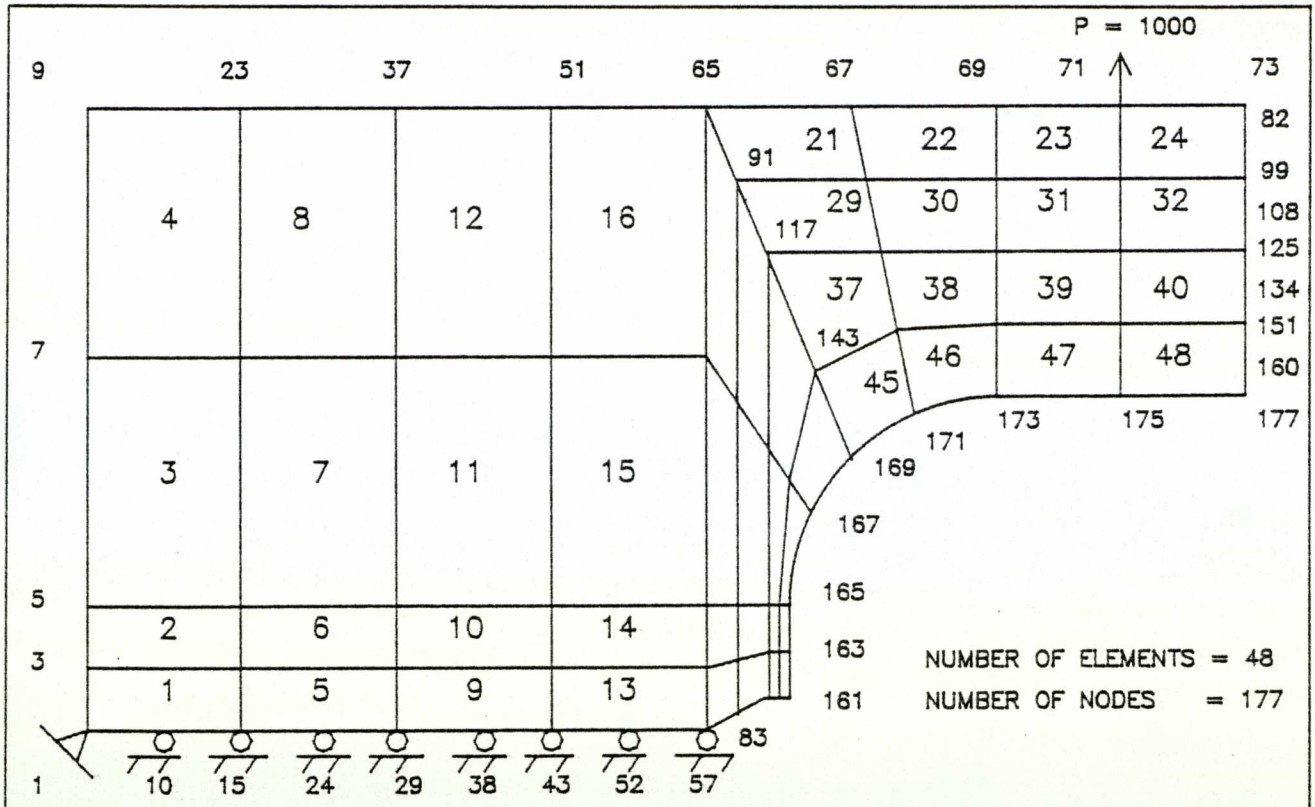

a) DISTORTED ELEMENT ARRAY SHOWING ELEMENT & NODAL NUMBERING , AND NODAL CONSTRAINTS.

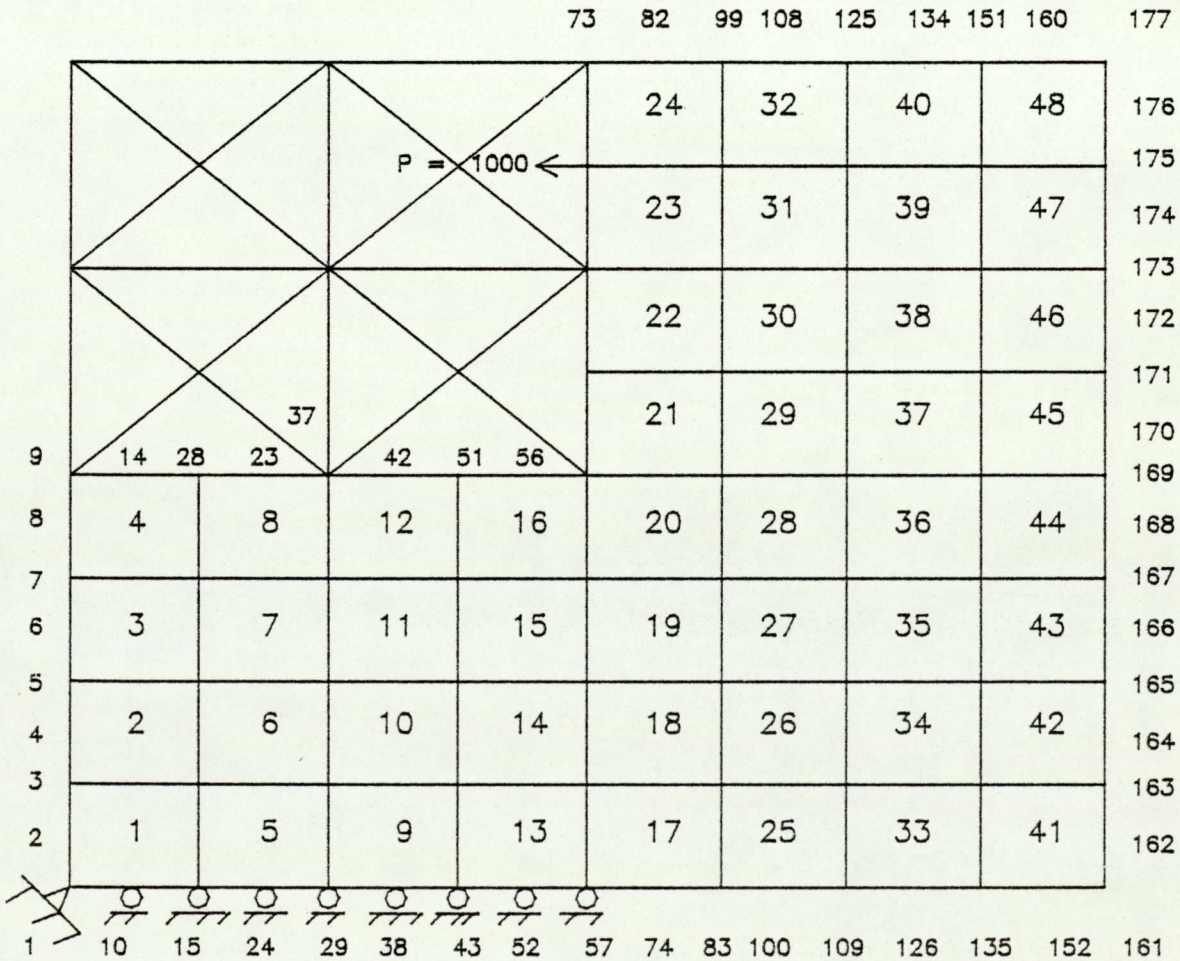

b) ELEMENT ARRAY SHOWING ELEMENT & NODAL NUMBERING , & NODAL CONSTRAINTS.

FIGURE (3.20) KEY DIAGRAMS FOR ELEMENT ARRAYS.

DATA INPUT FOR EXAMPLE NUMBER 4.

DATAFILE #1 : JOB11

DATAFILE #2 : JOB12

A) 1, 1, 1, 48, 177, 1, 3, 0, 0, 1, 1, 1

B) 23, 12, 4, 4, 1

C) 0, 0

D) 1, 0, 0, 1 1, 0, 6, 3 1, 0, 30, 5

1, 15, 0, 15 1, 15, 6, 17 1, 15, 30, 19

1, 30, 0, 29 1, 30, 6, 31 1, 30, 30, 33

1, 32.6, 1.5, 43 1, 32.6, 6, 45 1, 32.6, 23, 47

1, 34, 1.5, 57 1, 34, 6, 59 1, 34.7612, 9.826, 60

1, 36.929, 13.071, 61 1, 40.174, 15.239, 62 1, 44, 16, 63

1, 44, 23, 49 1, 44, 30, 35 1, 56, 30, 37

1, 56, 23, 51 1, 56, 16, 65

E) 12, 1, 2, 2, 1, 2, 5, 6, 9, 10, 11, 12, 13, 14, 15, 16

F) 0

G) 10

1, 3, 0, 0, 1

8, 2, 0, 0, 10, 15, 24, 29, 38, 43, 52, 57

1, 1, 0, 9.81E3, 71

0, 0, 1

2.07E7, .3, .796E7, 2.07E7, .3, 0

NUMBER OF CONSTRAINTS	CRACK LENGTH cm	VALUE OF DISPLACEMENT AT THE NODE OF LOAD APPLICATION .mm	DIFFERENCE WITH PREVIOUS CONDITION 1N %	DIFFERENCE WITH FIRST CONDITION IN %
10	0	63.810×10^{-3}		
9	3.75	67.487×10^{-3}	+6.94	+ 6.94
8	7.50	77.520×10^{-3}	+14.86	+22.84
7	11.25	85.915×10^{-3}	+13.23	+36.14
6	15.00	101.750×10^{-3}	+18.43	+60.3

TABLE (2) :VALUES OF DISPLACEMENTS CORRESPONDING TO CRACK LENGTH.

CRACK LENGTH cm.	dC/dA 1/(N.cm)	KI $N/(cm)^{3/2}$
3.75	1.729×10^{-8}	4150
7.50	2.73×10^{-8}	5215
11.25	3.276×10^{-8}	5712
15.00	4.096×10^{-8}	6387

TABLE (3) : VALUES OF COMPLIANCE & STRESS INTENSITY FACTOR KI.

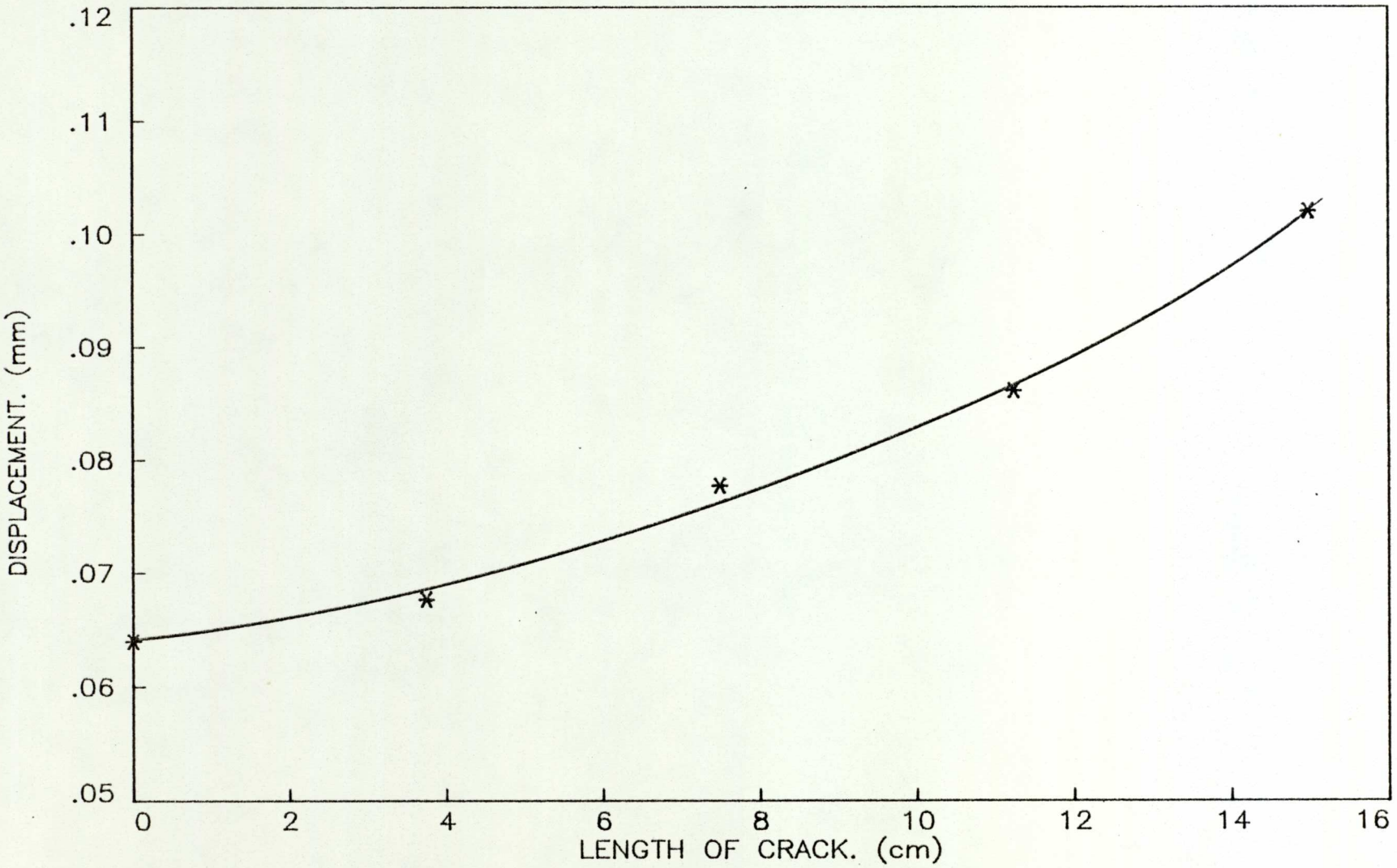

FIGURE (3.21) A GRAPH OF DISPLACEMENT AGAINST CRACK LENGTH.

$$K_I = Q \left[\frac{E}{2} \frac{dC}{dA}\right]^{\frac{1}{2}}$$

$$Q = 9810N$$

$$E = 2.07 \times 10^7 \quad N/cm^2$$

$$K_I = 9810\left[\frac{2.07\times10^7}{2} \times 1.729\times10^{-8}\right]^{\frac{1}{2}}$$

$$K_I = 9810\left[0.423\right]^{\frac{1}{2}} = 4150.$$

3.8 SMOOTHING OF STRESSES

Finite element analysis generally involves the minimization of some functional defined in terms of piecewise functions. These functions are generally required to have a certain degree of inter-element continuity depending on terms in the functional.

In many finite element problems, the quantities of primary engineering interest involve the function derivatives, and in many cases, especially with lower order elements. These derivatives do not possess inter-element continuity.

In the displacement method, the stresses are discontinuous between elements because of the nature of the assumed displacement variation. In analysis involving numerically integrated elements such as isoparametric elements, the integration points are the best stress sampling points. The nodes, which are the most useful output locations for

stresses, appear to be the worst sampling points. Reasons for this phenomenon are not immediately apparent; however it is well known that interpolation functions tend to behave badly near the extremities of the interpolation region. It is therefore reascnable to expect that shape function derivatives (and hence stresses) sampled in the interior of elements would be more accurate than those sampled at the element periphery.

The least square smoothing procedure may be carried out over the whole of the finite element domain and this is referred to as "global smoothing". Or it may be performed over each individual element separately in the finite element domain, and this method is called the Local Function Smoothing[71].

Hinton and Ricketts[72] formed a readily usable form method, for locally smoothing stresses, using quadrilateral isoparametric elements. Stresses sampled at the 4-point Gaussian integration sampling locations are multiplied by a smoothing matrix to give smoothed values at the nodes of the element. Smoothed values from adjacent elements are then averaged at the same element nodes.

Local Smoothing Matrices

Consider a typical stress $\sigma(\xi)$ which varies parabolically over the 1-D element as shown in Fig. (3.24). The straight line representing the smoothed stresses $\hat{\sigma}(\xi) = a_1 + a\xi$ is defined

uniquely by the values of the stress $\sigma(\xi)$ at the two Gaussian points. The smoothed stresses may be written as

$$\hat{\sigma}(\xi) = [1, \xi] \begin{Bmatrix} a_1 \\ a_2 \end{Bmatrix} \tag{3.6a}$$

$$\hat{\sigma} = [p]\{a\} \tag{3.6b}$$

Since $\sigma(\xi) = \hat{\sigma}(\xi)$ at the two Gaussian points

$$\begin{Bmatrix} \sigma_1 \\ \sigma_{II} \end{Bmatrix} = \begin{Bmatrix} \sigma(-\frac{1}{\sqrt{3}}) \\ \sigma(+\frac{1}{\sqrt{3}}) \end{Bmatrix} = \begin{bmatrix} 1 - \frac{1}{\sqrt{3}} \\ 1 + \frac{1}{\sqrt{3}} \end{bmatrix} \begin{Bmatrix} a_1 \\ a_2 \end{Bmatrix} \tag{3.7}$$

Hence

$$\{a\} = [p]^{-1}\{\sigma\} \tag{3.8}$$

The smoothed nodal values at the corners of the element may now be calculated by substituting equation (3.8) into (3.6). Thus

$$\begin{Bmatrix} \hat{\sigma}_I \\ \hat{\sigma}_2 \end{Bmatrix} = \begin{Bmatrix} \hat{\sigma}(-1) \\ \hat{\sigma}(+1) \end{Bmatrix} = \begin{bmatrix} 1 & -1 \\ 1 & 1 \end{bmatrix} \begin{bmatrix} \frac{1}{2} & \frac{1}{2} \\ -\frac{\sqrt{3}}{2} & \frac{\sqrt{3}}{2} \end{bmatrix} \begin{Bmatrix} \sigma_I \\ \sigma_{II} \end{Bmatrix} \tag{3.9}$$

or

$$\{\hat{\sigma}\} = [A]\{\sigma\} \tag{3.10}$$

where

$$[A] = \begin{bmatrix} \frac{1+\sqrt{3}}{2} & \frac{1-\sqrt{3}}{2} \\ \frac{1-\sqrt{3}}{2} & \frac{1+\sqrt{3}}{2} \end{bmatrix} \tag{3.11}$$

For two-dimensional problems, the smoothed stresses are assumed to have a bilinear variation over the element as given by the expression

$$\hat{\sigma}(\xi,\eta) = [1, \xi, \eta, \xi\eta] \begin{Bmatrix} a_1 \\ a_2 \\ a_3 \\ a_4 \end{Bmatrix} \tag{3.12}$$

Using the same procedure as for one-dimensional element, the smoothed stresses at the nodes may be calculated from the expression

$$\begin{Bmatrix} \hat{\sigma}_1 \\ \hat{\sigma}_2 \\ \hat{\sigma}_3 \\ \hat{\sigma}_4 \end{Bmatrix} = \begin{bmatrix} a & b & c & b \\ b & a & b & c \\ c & b & a & b \\ d & c & b & a \end{bmatrix} \begin{Bmatrix} \sigma_I \\ \sigma_{II} \\ \sigma_{III} \\ \sigma_{IV} \end{Bmatrix} \tag{3.13}$$

or

$$\{\hat{\sigma}\} = [A]\{\sigma\} \tag{3.14}$$

where

$$a = 1 + \frac{\sqrt{3}}{2}, \qquad b = -\frac{1}{2}, \qquad c = 1 - \frac{\sqrt{3}}{2}$$

Smoothed stresses at mid-side nodes can be found simply by averaging between corner node values.

This method can be extended to three-dimensional problems by considering the 8-Gaussian points in the element[72].

The smoothing technique has been included in the present plane stress/strain finite element computer program and examples 1 and 3 are presented to illustrate the application of this technique.

Example 1, a cantilever under an end load have been considered. In mesh (1), the number of elements used are 8, and the total number of degrees of freedom are 74 (refer to Fig. (3.3)). Results of the values of the shear stress along the neutral axis of the cantilever are calculated using the smoothing technique and without using the smoothing technique. It is found that the values of the shear stress when not using the smoothing technique to be erratic and inconsistent, and errors of more than 100% are present in the solution. While those obtained using the smoothing technique are more stable and much more accurate, their errors do not exceed 20%. Figure (3.22) illustrates these facts where graphs of the theoretical, smoothed and unsmoothed shear stress values are shown.

Example 2 of the thick cylinder under internal pressure (Fig. (3.5)). A mesh of 9 elements is constructed with a

total number of 80 degrees of freedom. Stresses are calculated by the computer program using the finite element method, with and without smoothing. Values of the radial stresses and tangential stresses at the nodes at X=0, are plotted for both the smoothed and unsmoothed conditions. These values are compared with the theoretical values obtained using equation (3.4), as shown in Figures (3.23a) and (3.23b).

It is found that the values of the smoothed stresses are far superior than those which are not smoothed. Table 5 shows these values together with the percentage error in comparison to values calculated by means of the theory of elasticity.

Merits of the Technique

(1) The use of the smoothing technique improves the values of the stresses output in situations in which averaged conventional stresses are poor as it has been demonstrated in the last two examples.

(2) Implementation is extremely easy involving only a small subroutine for matrix multiplication.

(3) For the same accuracy of results obtained without smoothing, a smaller mesh can be used when implementing this technique, hence saving time and money.

NODE NO.	VALUES OF SMOOTHED STRESSES. (−ve)	VALUES OF UNSMOOTHED STRESSES. (−ve)
3	1788.6	3421.2
7	1810.1	708.33
11	1831.5	3450.7
15	1751.8	993.94
19	1672.2	3268.4
23	1694.1	898.53
27	1716.1	3295.9
31	1682.1	966.64
35	1648.1	3221.3

THEORETICAL VALUE OF STRESS: −1500

TABLE (4) : COMPARISON OF THE VALUES OF SHEAR STRESS ALONG THE NUETRAL AXIS OF THE CANTILEVER , CALCULATED THEORETICALLY , & BY MEANS OF F. E. M , SMOOTHED & UNSMOOTHED FOR MESH NO.1.

NODE NO.	r	THEORY OF EALSTICITY		SMOOTHED F.E.		% ERROR		UNSMOOTHED F.E.		% ERROR	
		T.S	R.S	T.S	R.S	T.S	R.S	T.S	R.S	T.S	R.S
1	1.0000	333.333	−200.000	348.43	−212.41	4.53	6.20	357.80	−148.020	7.34	26.00
2	1.1667	262.585	−129.252	288.53	−156.69	9.89	21.22	297.23	−106.41	13.2	17.67
3	1.3333	216.667	− 83.333	228.62	−100.96	5.52	21.15	255.51	− 56.513	17.92	32.18
4	1.5000	185.185	− 51.852	201.90	− 69.41	9.03	33.87	218.08	− 33.875	17.76	34.67
5	1.6667	162.667	− 29.333	175.18	− 37.86	7.70	29.07	194.35	− 8.92	19.47	69.59
6	1.8333	146.005	− 12.672	156.10	− 19.85	6.91	56.64	160.00	− 1.098	9.58	91.33
7	2.0000	133.333	0.0	137.02	− 1.84	2.76		143.54	+ 17.727	7.6	

T.S :− TANGENTIAL STRESS. R.S :− RADIAL STRESS.

TABLE (5) VALUES OF RADIAL & TANGENTIAL STRESSES OF A THICK CYLINDER ALONG ITS VERTICAL AXIS THROUGH THE THICKNESS OF THE WALL , OBTAINED BY THEORY OF ELASTICITY , SMOOTHED & UNSMOOTHED F.E.M , SHOWING % OF ERROR IN THE LAST TWO CASES.

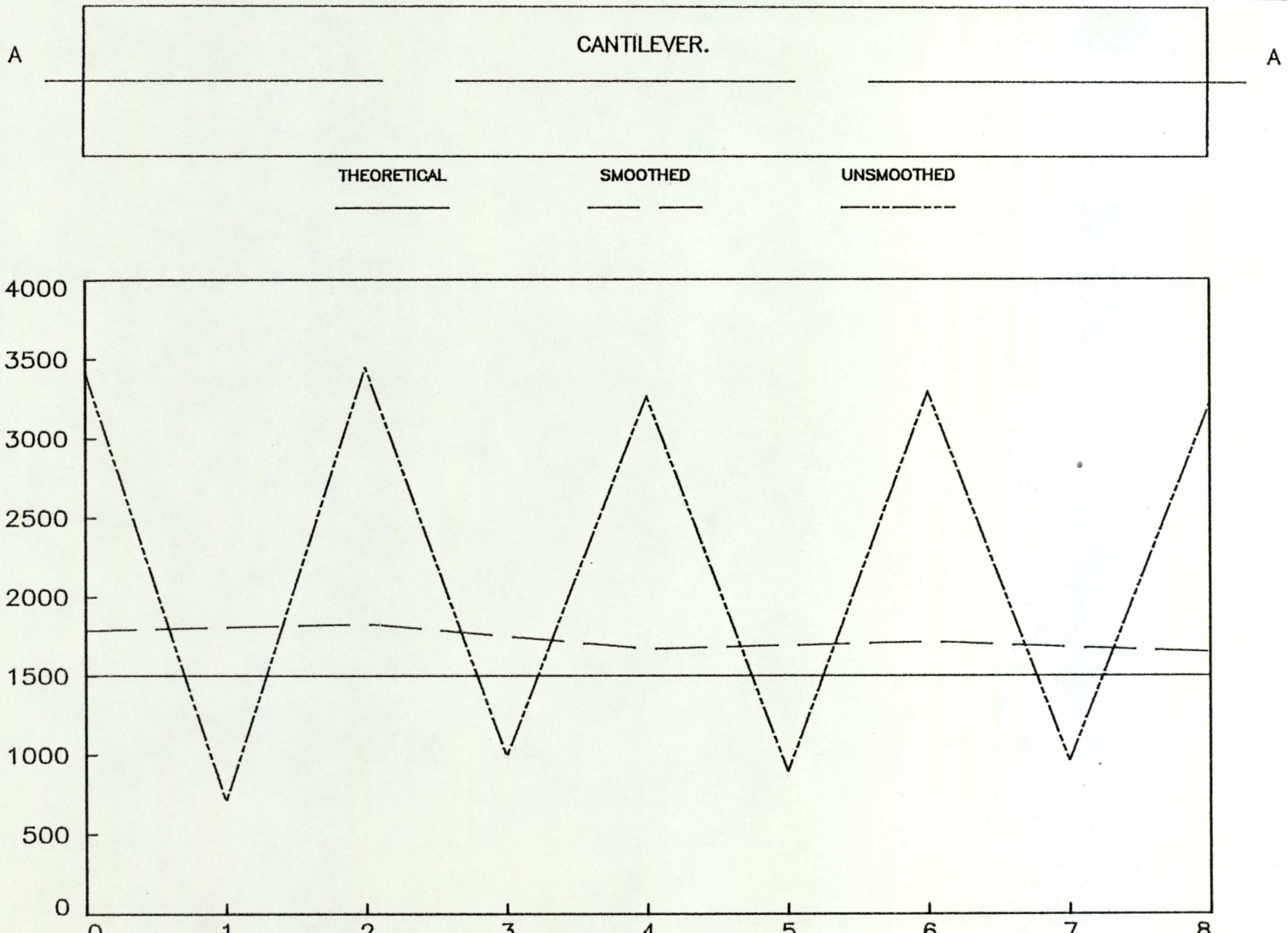

FIGURE (3.22) THEORETICAL, SMOOTHED & UNSMOOTHED SHEAR STRESS VALUES.

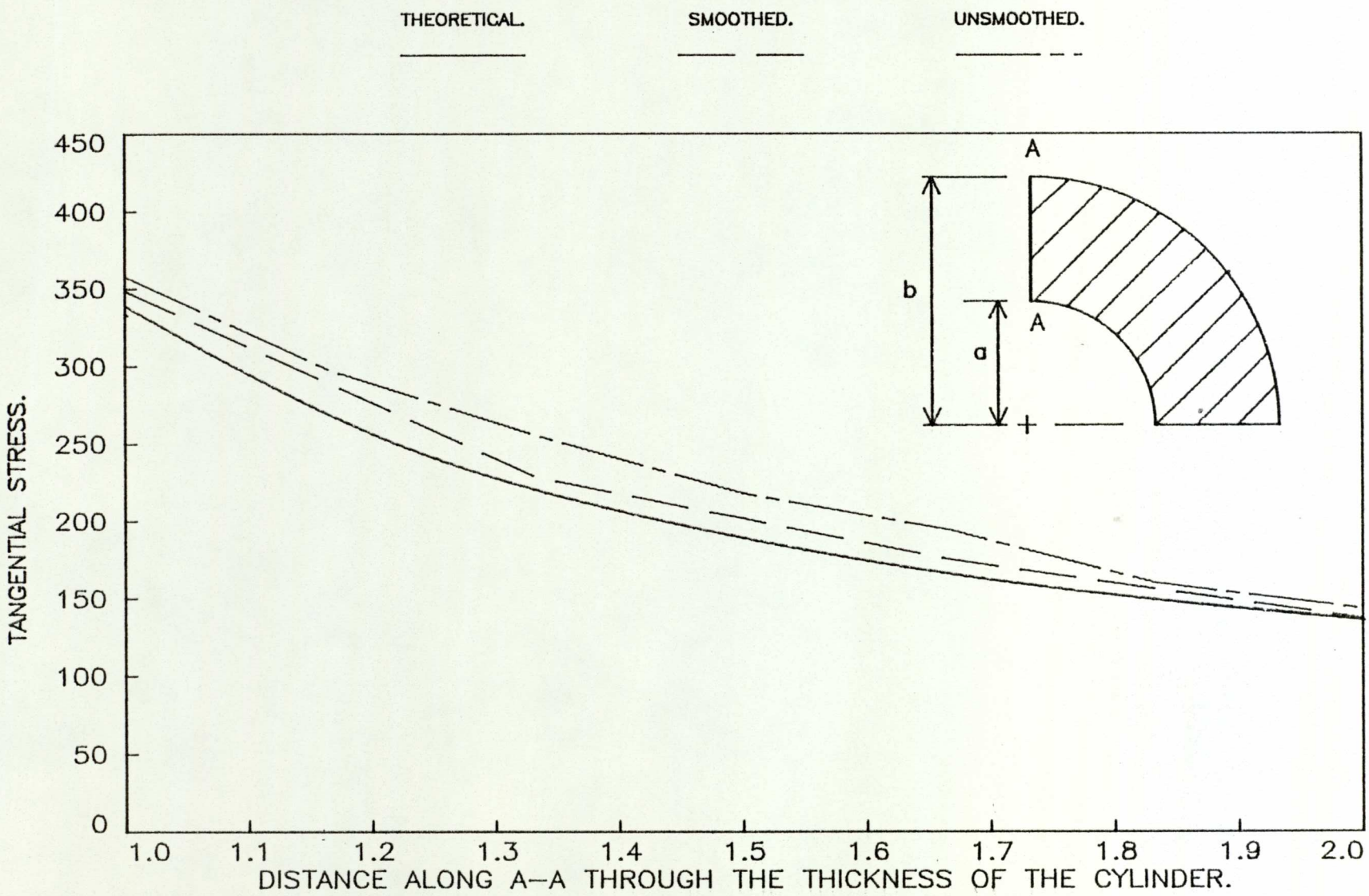

FIGURE (3.23a) COMPARISON OF SMOOTHED & UNSMOOTHED TANGENTIAL STRESSES

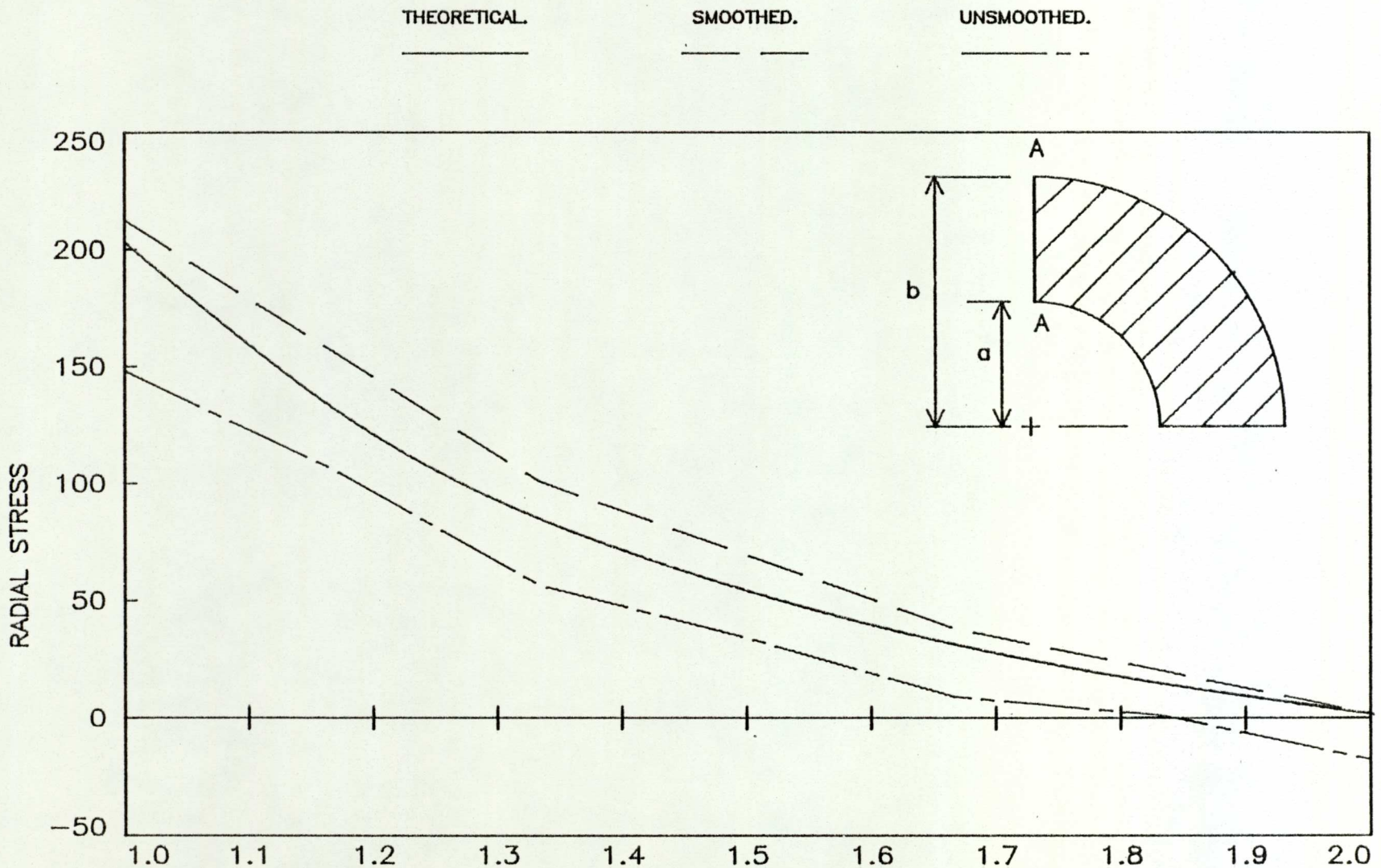

FIGURE (3.23b) COMPARISON OF SMOOTHED & UNSMOOTHED RADIAL STRESSES.

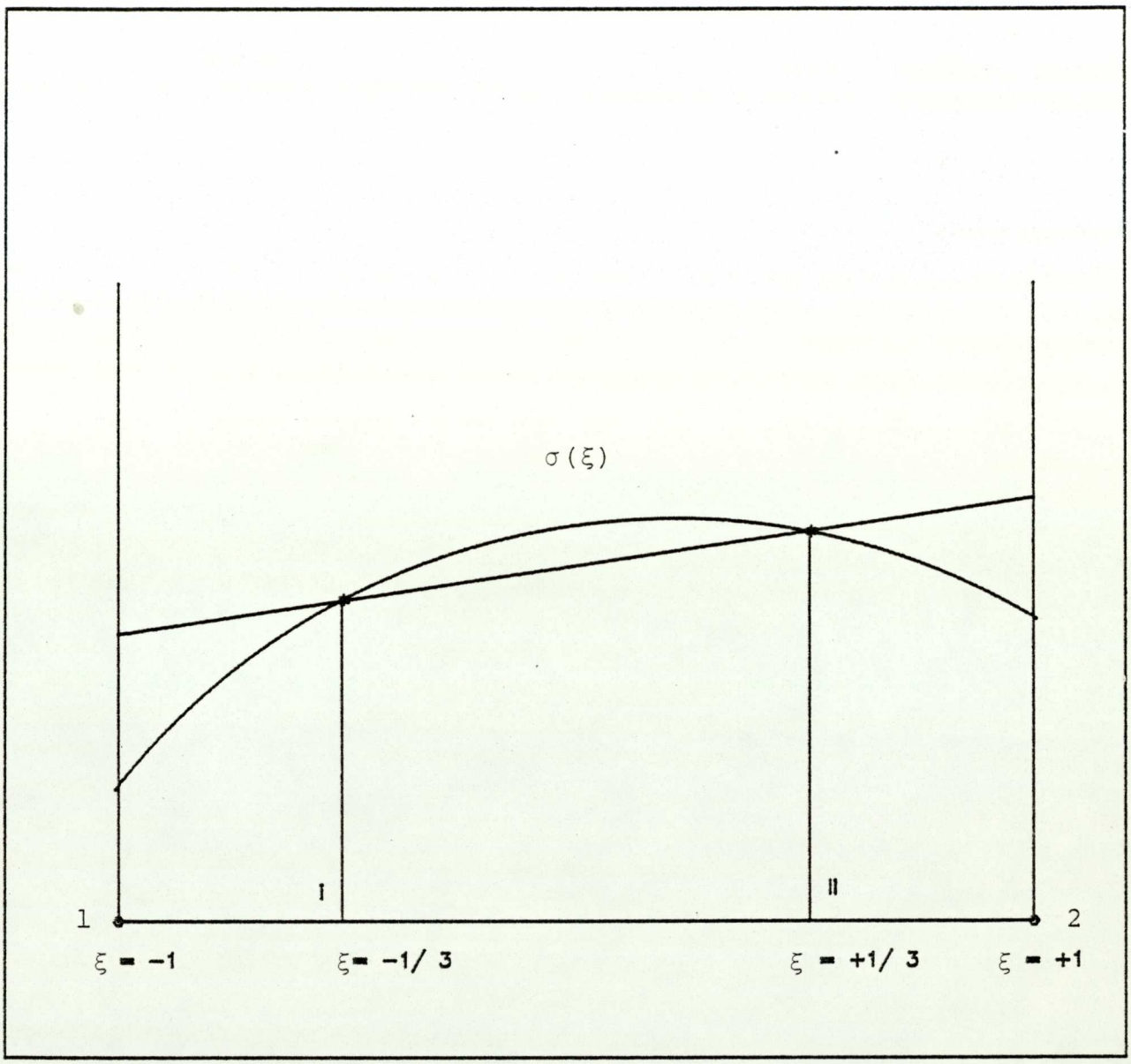

FIGURE (3.24) SMOOTHED AND UNSMOOTHED STRESS DISTRIBUTIONS FOR 1−D ISOPARAMETRIC ELEMENT.

CHAPTER 4

REVIEW OF STUDIES IN FRACTURE MECHANICS

4.1 INTRODUCTION

The essence of fracture is that it is a failure mechanism which involves the unstable propagation of a crack in a structure. Once the crack has started to move, the loading system is such that it produces accelerating growth[1]. Fracture occurs when failure happens at a stress below that of a yield stress for that particular material. It could happen in thick sections as well as thin plates.

The process involved in the fracture of solids are so complicated and varied that no single formula or criterion can be expected realistically to describe all of the observed fracture phenomena[2]. Despite this, a sizeable body of useful knowledge concerning certain aspects of fracture does currently exist, having been obtained from extensive theoretical and experimental research efforts.

The objective of this chapter is to present a somewhat technical review of fracture mechanics, highlighting its strengths as well as its current limitations. The lack of a comprehensive understanding of the failure process in structural materials has resulted in the catastrophic failure, over the past sixty years, of a variety of engineering structures[3,4].

Analysis of the failed components of such structures as pressure vessels, storage tanks, welded ship structures, aircraft parts, bridges, pipelines, turbine blades and housing, rocket motor casings and various heavy machine parts have shown that cracks or flow induced brittle fracture has often been responsible for the failures.

The trend towards use of exceptionally high yield strength materials, such as is available in certain steel, aluminium and titanium alloys, present the designer with an unfortunate dilema. The advantages of higher strength materials that the designer now has at his disposal for structural applications are offset by a significant reduction in ductility, a factor that tends to enhance the possibility of failure by unstable fracture.

The effects of the stress concentrations due to holes or cutouts in otherwise continuous structural members were first recognised during the latter part of the nineteenth century. Figures 4.1 and 4.2 illustrate the variation of the stress components parallel to the direction of the uniform tension applied to an infinite sheet containing a circular or elliptical hole, according to the theory of elasticity[5]. The presence of a circular hole raises the stress level at the edge of the hole to three times the applied stress level in a large plate. While for an elliptic hole, the stress level at the edge with the smaller radius of curvature increases with the slenderness

ratio of the ellipse, i.e. to the ratio of the major to minor axes. When the major axis is twice the minor axis, the stress concentration is five. These results approximate quite accurately the situation for finite sheets with holes when similarly loaded, provided that the major dimension of the hole is very much smaller than the dimensions of the sheet. Hence their practical significance is immediately apparent.

A crack or flaw of finite proportion, can be thought of as the limiting case of an elliptic hole as the ratio b/a approaches zero, as illustrated in Fig. 4.3. According to the theory of elasticity, the maximum stress parallel to the direction of the applied load at the edge of the crack increases in this case without limit. This behaviour explains why cracks oriented transversely to the direction of the applied tensile loads tend to grow or spread. However, the material at the edge of a sharp crack obviously cannot support infinitely large stresses. In real metals a state of pastic yield develops over a small region bordering the edge of the crack, Fig. 4.4. The plastic enclaves which develop at the borders of a stationary crack, however small, tend to inhibit potential crack growth through blunting of the curvature of the crack tip. Hence any set of circumstances which inhibits the free development of plastic yield at the crack borders, e.g., low temperature, fast rate of load application, high degree of triaxiality in the crack region, tends to promote

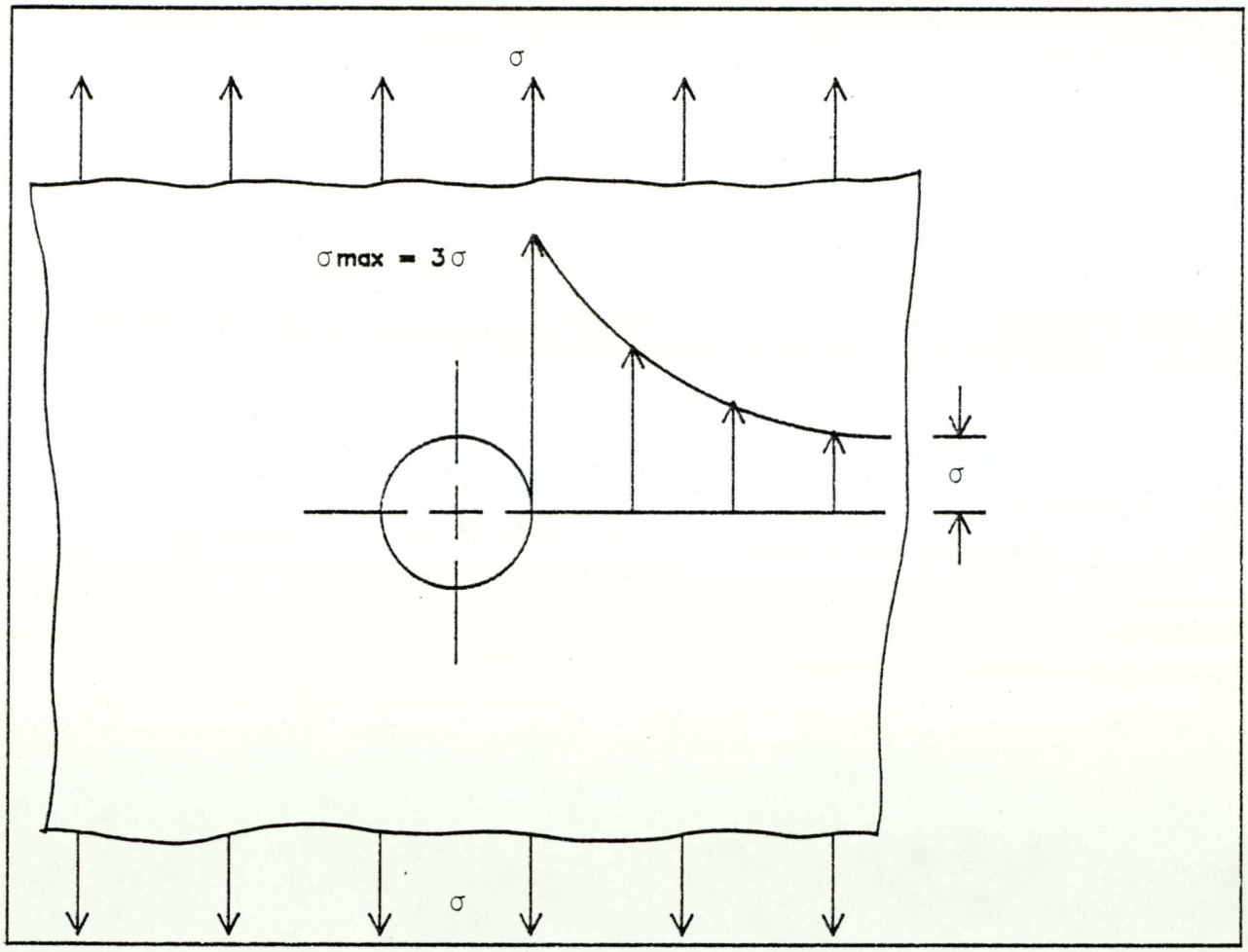

FIGURE (4.1)

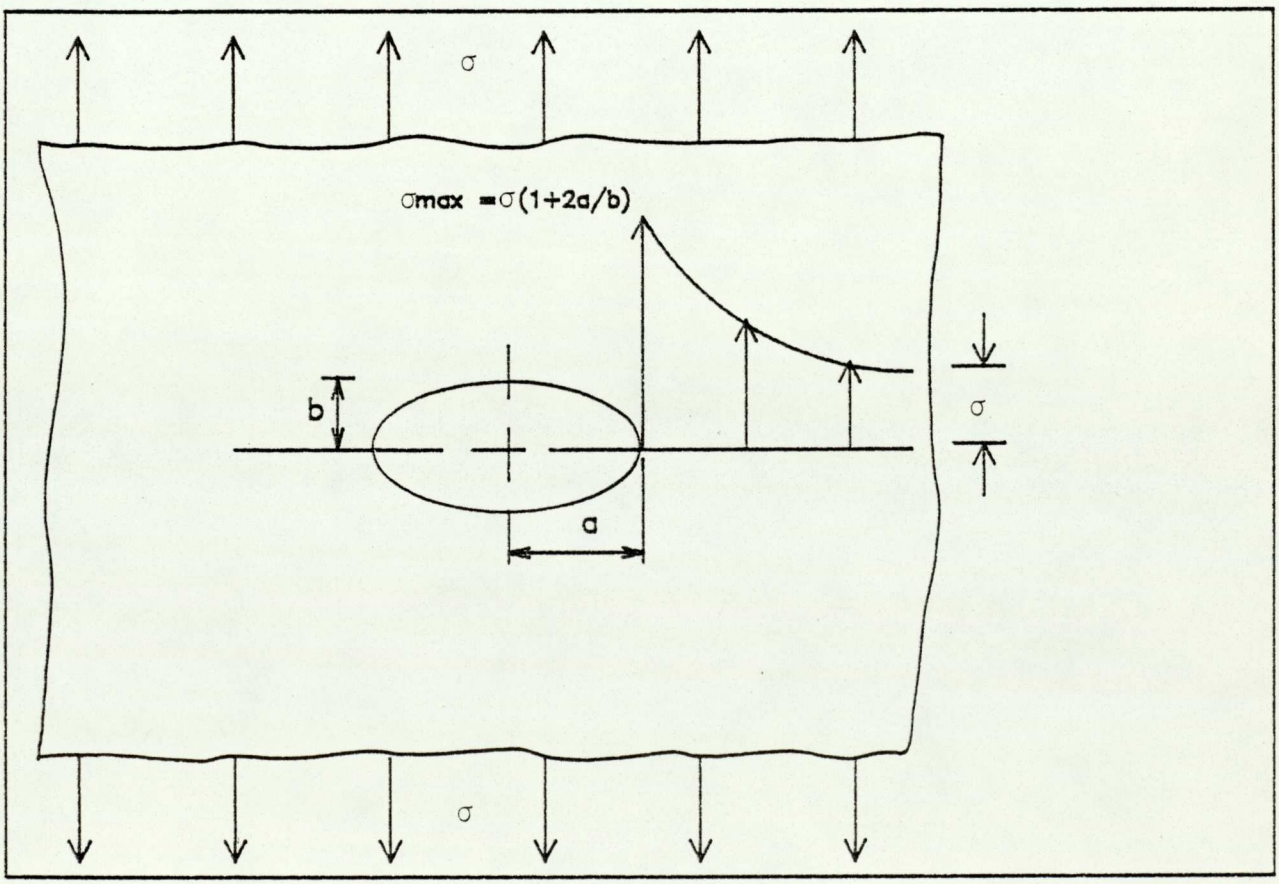

FIGURE (4.2)

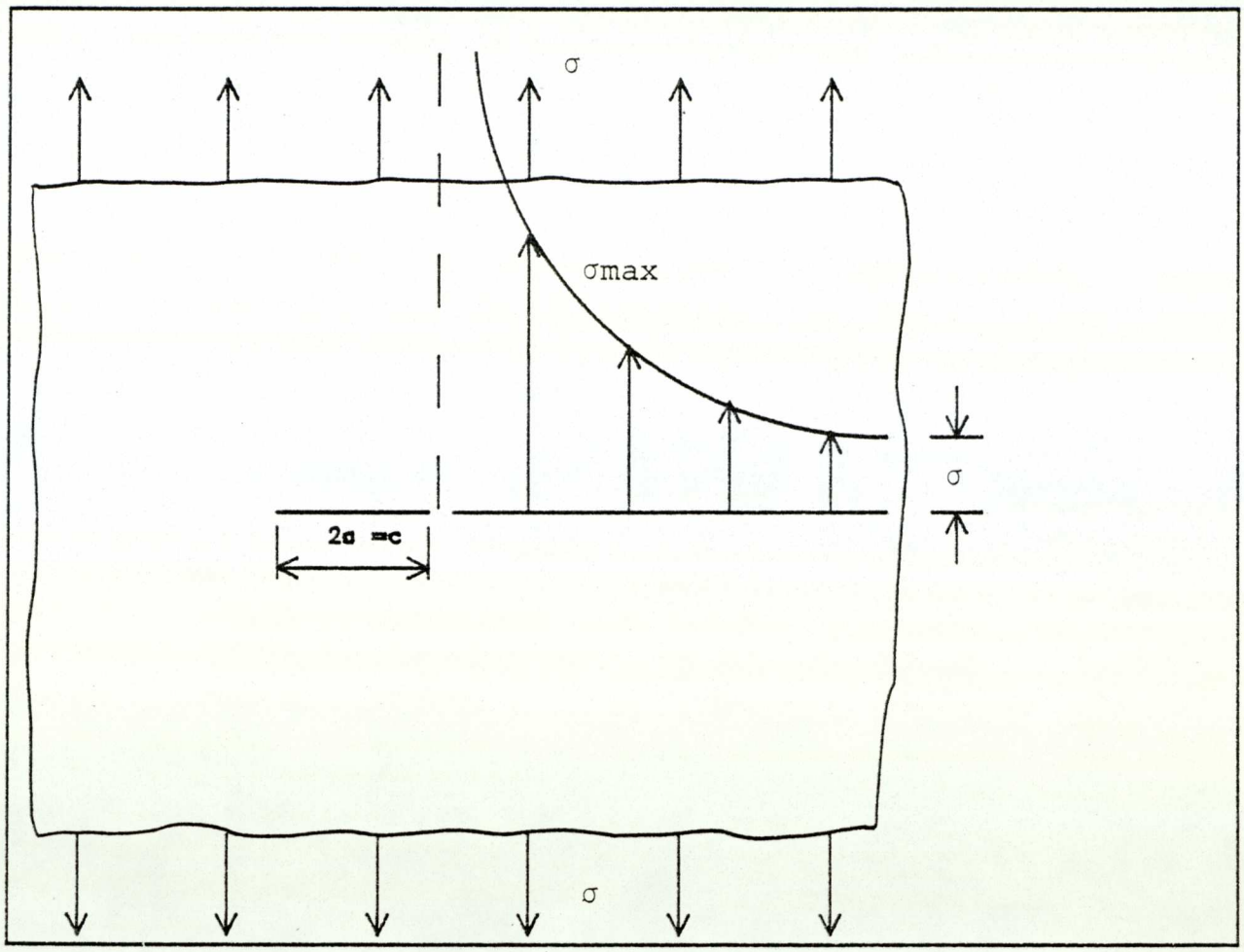

FIGURE (4.3)

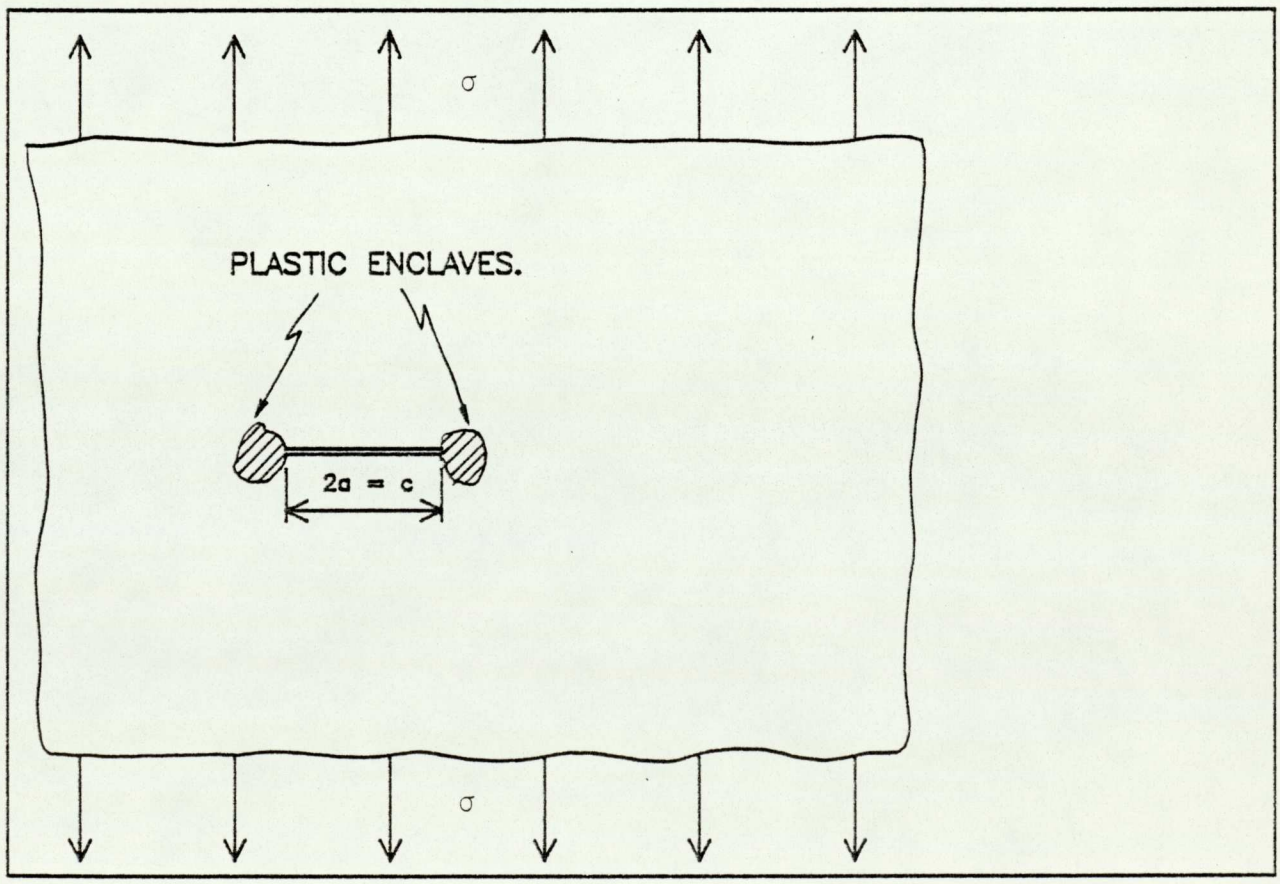

FIGURE (4.4)

easy crack expansion, or brittle fracture. For any given enclave development generally requires greater net section stresses for initiating crack extension.

In the design of engineering structures there are two important items to be considered:

The first to be considered is a stress analysis of the problem so that the magnitude and direction of the stresses and strains at various points of the structure are known.

The second item is to select a criterion of failure which determine the type of material to be used for each component in the structure. We now consider criteria for fracture type failures.

4.2 GRIFFITH THEORY[7]

The traditional method is to design the cross-sectional area of the structure such that the applied stresses are kept below the yield strength of the ductile material. Such an approach is adequate for low and medium strength material. But for high strength materials which are particularly sensitive to the presence of flaws or defects, this approach is inadequate.

The first attempt to put forth a rational theory of fracture mechanics was put by Griffith in 1921, who laid down the conditions under which a small crack in a solid

becomes unstable. This analytical model is based on elasticity solution of an elongated cavity in the form of an ellipse, the idea is to focus attention on the redistribution of stresses around such a cavity.

Referring to Fig. 4.2, the maximum stress σ_m occurs at the apex of the major axis of the cavity and is given by:

$$\sigma_m = \sigma(1 + 2a/b) \qquad (4.1)$$

where

σ is the applied stress.

a and b are the semi-major and semi-minor axis of the ellipse.

Equation (4.1) shows that the magnitude of the stress at the loading edge of the cavity becomes increasingly large as the ellipse is flattened out.

For a narrow crack having a very small radius of curvature ρ at the tip $\rho = \frac{b^2}{a}$, equation (4.1) becomes,

$$\sigma_m = \sigma\left(1 + 2\sqrt{\frac{a}{\rho}}\right) \simeq 2\sigma\sqrt{\frac{a}{\rho}} \quad \text{since} \quad \rho << a \qquad (4.2)$$

As ρ becomes very small σ_m becomes exceedingly large and in the limit as $\rho \to$ zero, σ_m becomes infinite and this cannot be a suitable criteria of fracture.

The basic concept of Griffith theory is to evaluate

the decrease of elastic energy when a crack of length 2a is formed.

Referring to Fig. 4.3, let U_o represent the total elastic strain energy in an uncracked infinite sheet of unit thickness loaded as shown. Suppose that a crack of length 2a = C is introduced slowly enough such that all dynamic effects are negligibly small, while the load boundary is held fixed. Since the plane dimensions of the sheet are infinite while the crack size is finite, the applied stress will remain at the same level σ as the crack is inserted. Let U designate the strain energy of the cracked sheet. With the loaded boundary held fixed, the applied load can do no work as the crack appears. Consequently, the strain energy in the body can only decrease by virtue of the relaxation of the stresses over the surface, which define the crack. Thus $U<U_o$. The creation of new surfaces which total area 2C, assuming the crack to extend through the unit thickness of the sheet, requires an expenditure of energy which Griffith assumed to be linearly proportional to the crack surface area, $\gamma_s.2C$. Where γ_s is a fracture surface energy density. The surface energy density is presumed to be determinable by experiment for any given solid at any given temperature. The quantity $2\gamma_s.C$ can be interpreted as the work done by the relaxing stress as the new internal surface (crack) is introduced, i.e. $2\gamma_s C$ represents the energy expended in overcoming the inherent cohesion of the solid across the plane crack surface.

Using the plane strain linear elastic solution for the elliptic hole of Fig. 4.2. In the limit as 2b approaches zero, Griffith deduced that insertion of a crack 2a, subject to the given circumstances, changes the elastic strain energy by $\pi\sigma^2C^2(1-\nu^2)/4E$,[7], where $C = 2a$, E being Young's modulus and ν Poisson's ratio.

The strain energy of the cracked body with a stationary crack C is thus

$$U = U_o - \frac{\pi\sigma^2C^2(1-\nu^2)}{4E} \tag{4.3}$$

while the total energy is

$$\begin{aligned}\psi &= U + 2\gamma_s C \\ &= U_o - \frac{\pi\sigma^2C^2(1-\nu^2)}{4E} + 2\gamma_s C\end{aligned} \tag{4.4}$$

Griffith postulated that the crack is in a state of unstable or critical equilibrium, that is, at a point of incipient growth, when the free energy attains a stationary (in this case maximum) value. Analytically this means the parameters which determine the critical crack equilibrium state are obtained from the condition

$$\frac{d\psi}{dC} \;/\; \text{fixed boundary} = 0 \tag{4.5}$$

which from equation (4.4) leads to the requirement that

$$-\frac{dU}{dC} = 2\gamma_s \tag{4.6}$$

or

$$\sigma^2 C = \frac{4E\gamma_s}{\pi(1-\nu^2)} \tag{4.7}$$

For a given applied load σ the critical equilibrium crack size is thus:

$$C = 2a = \frac{4E\gamma_s}{\pi(1-\nu^2)} \frac{1}{\sigma^2} \tag{4.8}$$

Alternatively, for a given crack size 2a = C, equation (4.8) can be viewed as determining the applied stress level which is necessary to bring on a state of incipient crack growth or

$$\sigma_c = \sqrt{\frac{4E\gamma_s}{\pi C(1-\nu^2)}} \tag{4.9}$$

where σ_c is the critical tensile stress.

This is Griffith'S formula. It can be interpreted as a brittle fracture criterion for the plane infinite sheet described in Fig. 4.1. (For condition of plane stress, the factor $(1-\nu^2)$ is replaced by unity.) i.e.

$$\sigma_c = \sqrt{\frac{4E\gamma_s}{\pi C}} \tag{4.10}$$

Since γ_s is the specific energy which is constant for a material and E is material constant

$$\sigma_c\sqrt{C} = \sqrt{\frac{4E\gamma_c}{\pi}} = \text{constant} \tag{4.11}$$

The applied critical stress σ_c and flaw size C can be measured experimentally, and by introducing line cracks of different length 2a in a given material, Griffith has shown that in a given material $\sigma_c\sqrt{C}$ remained essentially constant[8,9].

4.3 ROLE OF PLASTICITY

Erwin and Orowan[13,14] proposed independently that a plastic work term γ_p be added to the fracture surface energy γ_s in equation (4.10), in order to account for any plastic deformation associated with the separation process. Thus:

$$\sigma = \sqrt{\frac{4E(\gamma_s+\gamma_p)}{\pi C(1-\nu^2)}} \qquad (4.12)$$

was proposed as a possible generalisation of Griffith's formula to instances of semi-brittle fracture. For structural metals, experimental data requires that the plastic work factor γ_p be 10^3 to 10^6 times larger than the surface energy γ_s.

It should be pointed out that for equation (4.12) it is necessary to assume that the plastic enclaves be confined to very narrow strip-like regions on each side of the crack plane as the crack extends. In practice[11], it is more common to find plastic regions which extend away from

the crack plane, as in Fig. 4.4. Thus it appears that the Irwin-Orowan modification of the Griffith formula is inadequate to deal with fracture in circumstances in which front plasticity is readily observable.

Griffith's formula applies vigorously only to the artificial case of an elastic solution for a plane infinite body. Thus, apart from the error associated with the omission of possible plasticity effects, additional error will arise when the theory is applied to cracked bodies of finite size.

4.4 STRESS INTENSITY FACTOR AND FRACTURE TOUGHNESS

In Griffith's theory of brittle fracture a critical stress-crack size relation is derived from an energy postulate, while the treatment by Irwin leads to stress-crack size relations by focusing attention on the elastic stresses very close to the tip of the crack[12]. For analytical purposes imagine an existing flaw or opening in a body to be, ideally, a plane sharp-ended crack. The solid is assumed to be homogeneous and isotropic, with the crack extending through the thickness of the body. Referring to Fig. 4.5, a local coordinate system is chosen so that the Z-axis is collinear with the leading edge of the crack, assumed to have a straight front, the Y direction is perpendicular to the plane of the crack while the X direction points in the direction of expected crack extension.

Loadings on the boundaries of the solid are taken to be applied symmetrically with respect to either the X-Y plane or the X-Z plane. If the Z-dimension of the body is large a condition of plane strain will exist throughout the body. At the other extreme, if the Z-dimension of the solid is small relative to the X and Y dimension, as in a thin plate, a plane stress situation will exist. Both of these situations are idealised cases. More realistically, in all but very thin plate-like specimens a mixed state of plane stress, plane strain will exist across the Z-dimension, varying from plane stress at and very near the X-Y plane surfaces to plane strain over the central portion. Any plastic deformation which may occur at the crack borders is neglected in a first approximation. Plasticity effects, provided they are small, are subsequently treated as a minor correction to the elastic anlaysis.

Three basic modes of crack surface displacements which can lead to crack extension are shown in Fig. 4.6. In the opening mode the crack surfaces move apart symmetrically with respect to the X-Z plane. In the sliding mode, when a shear stress is applied and the crack is said to be under the action of in-plane shear. The final mode is the tearing mode which is known as the antiplane shear mode.

Corresponding to the opening conditions outlined above, the stresses and displacements at points close to the crack border can be shown to have the form[13].

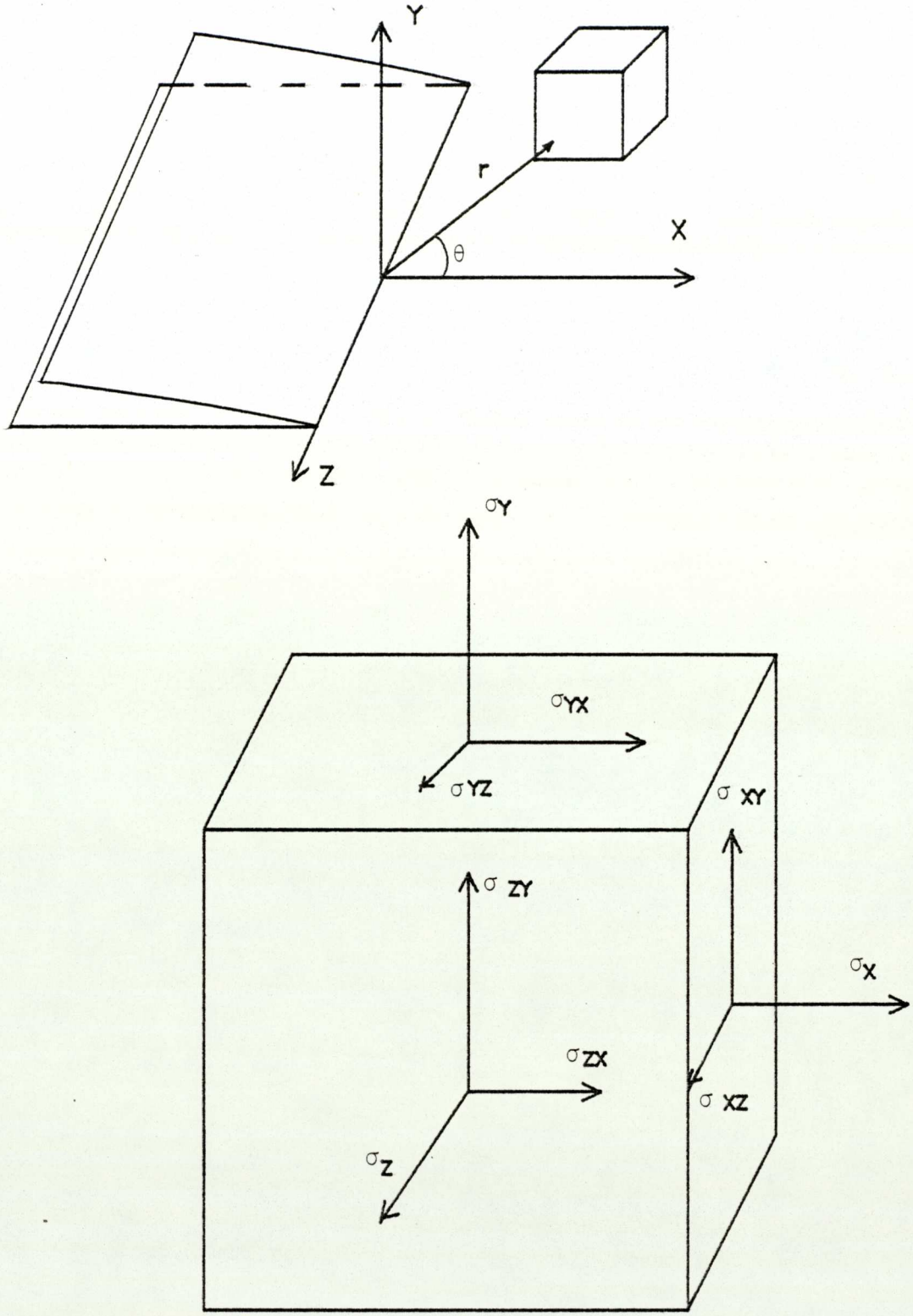

FIGURE(4.5)

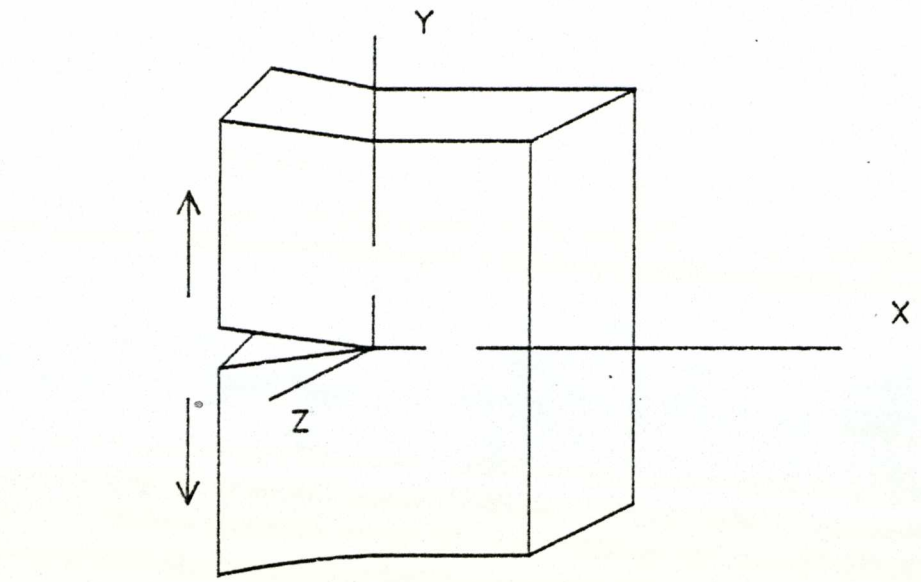

(a) OPENING—MODE I

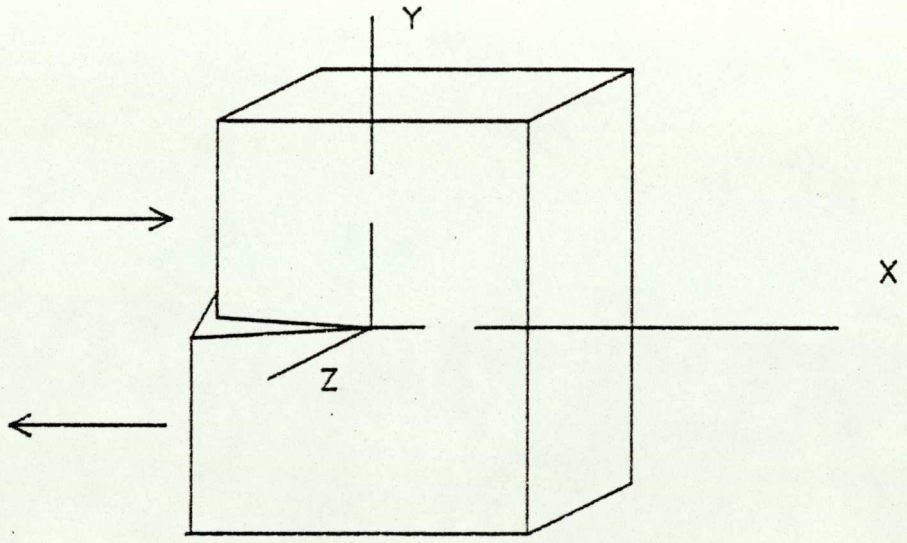

(b) EDGE SLIDING —MODEII

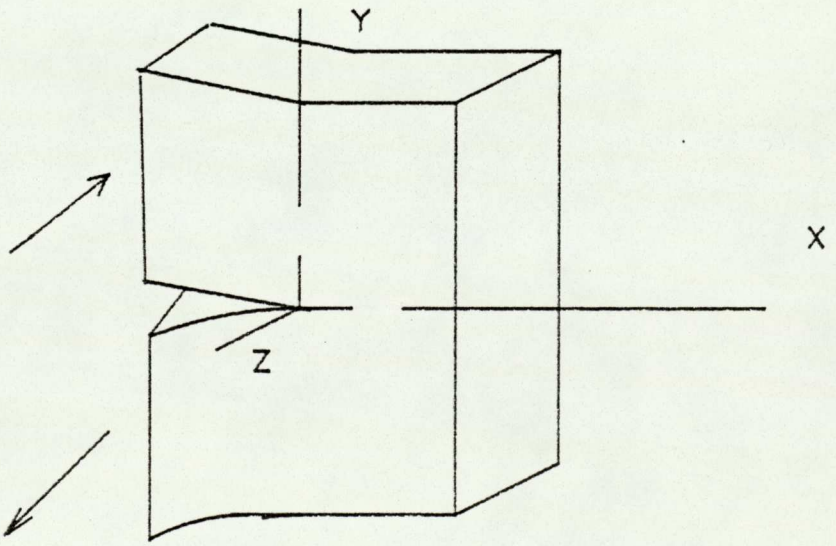

(c) TEARING —MODE III

FIGURE(4.6) MODES OF FRACTURE.

$$\sigma_X = \frac{K_I}{\sqrt{2\pi r}} \cos\theta/2\left[1-\sin\theta/2 \sin 3\theta/2\right] + \ldots \quad (4.13)$$

$$\sigma_Y = \frac{K_I}{\sqrt{2\pi r}} \cos \theta/2\left[1+ \sin\theta/2 \sin 3\theta/2\right] + \ldots \quad (4.14)$$

$$\tau_{XY} = \frac{K_I}{\sqrt{2\pi r}} \sin\theta/2 \cos\theta/2 \cos 3\theta/2 + \ldots \quad (4.15)$$

$$\sigma_Z = \begin{cases} 0 & \text{plane stress} \\ \nu(\sigma_X+\sigma_Y) & \text{plane strain} \end{cases} \quad (4.16)$$

$$\sigma_{XZ} = \sigma_{YZ} = 0 \quad (4.17)$$

$$U_X = \frac{K_I}{2G}\sqrt{\frac{r}{2\pi}} \{\cos\theta/2\left[K-1+2\sin^2\theta/2\right]\} + \ldots \quad (4.18)$$

$$U_Y = \frac{K_I}{2G}\sqrt{\frac{r}{2\pi}}\left[\sin\theta/2\left[K+1-2\cos^2\theta/2\right]\right] + \ldots \quad (4.19)$$

where

$K = 3-4\nu$ for plane strain

$K = \frac{3-\nu}{1+\nu}$ for plane stress

$G = \frac{E}{2(1+\nu)}$

$U_Z = 0$ (plane strain)

In these expressions only the first term of a series expansion is shown. The omitted terms involve increasing half powers of the ratio of r divided by the crack length, and consequently, are important only at large distances from

the crack tip[14]. Very near the crack tip the first term in each of these series dominates especially for the stresses, since they are porportional to $\sqrt{\frac{1}{r}}$. Thus over a region for which r is very small compared to the plane dimension of the body, e.g., the crack length or the specimen width, the above expressions specify the tip region elastic stresses and displacements to an acceptable degree of accuracy. The K term in these equations is independent of r and θ, and serves only as a positive multiplying factor which can be shown to depend on the applied boundary, load and the crack size. Its explicit functional form in any given situation depends on the geometry of the cracked body and the location of the crack. In fracture mechanics terminology, K is referred to as the "stress intensity factor".

The significance of the above expressions (4.13 - 4.19) is due to their generality, since they hold for all stationary plane cracks, regardless of the configuration of the body or the location of the crack. What changes in these equations, in going from one configuration to another, is only the functional form of K. Thus the state of elastic stress and displacement in the immediate region bordering a plane crack is, in effect, entirely characterized by the stress intensity factor K.

Expressions similar to (4.13-4.19) have been developed for the sliding and the tearing modes of crack surface separation[13].

The general expression for equations (4.13 - 4.19) which were developed by Irwin and corresponds to the first terms in a series expansion and describe the situation in the near tip field, could be interpreted in the following form[60].

$$ {}_m\sigma_{ij} = K_m r^{-\frac{1}{2}} {}_mf_{ij}(\theta) \qquad (4.20) $$

$$ {}_mu_i = K_m \frac{r^{\frac{1}{2}}}{G} {}_mg_i(\nu,\theta) \qquad (4.21) $$

where

$i,j = 1,2$

m = I, II, III, i.e. the mode

K_m = stress intensity factor of the mth mode

${}_mf_{ij}(\theta)$ and ${}_mg_i(\nu,\theta)$ are known functions.

4.5 RELATION BETWEEN THE GRIFFITH AND IRWIN APPROACHES

Irwing has shown by use of equations (4.13 - 4.19), that the work done per unit area by the stress field in slowly extending both ends of a crack in a sheet of unit thickness (in plane strain), while the outer boundary is held fixed, is simply $2K^2(1-\nu^2)/E$. It follows that this work represents twice the rate at which energy disappears from the strain energy field as the crack extends, i.e., the elastic strain energy release rate traditionally designated by the symbol G. Thus:

$$G = - \frac{dU}{dC} \tag{4.22}$$

and for opening mode crack surface displacements in plane strain.

$$G_I = \frac{K_I^2 \ (1-\nu^2)}{E} \tag{4.23}$$

For plane stress a similar calculation yields

$$G = \frac{K^2}{E} \tag{4.24}$$

K_I and G_I represent the stress intensity factor and the elastic strain energy release rate in plane strain, while K and G denote these same quantities for plane stress.

At the onset of fast crack propagation a subscript (c) is used to designate critical values.

Thus K_{IC} and G_{IC} represent critical values in plane strain and K_C and K_C specify critical values for plane stress.

Experiments conducted on a variety of high strength structural metals indicate that each material has a characteristic K_{IC} value which is basically the same regardless of the design of the specimens used for the tests. It is possible to interpret the K_{IC} value as a fracture resistance material property which, under certain conditions can be used to estimate the load that a structural member containing a crack of specified dimensions

can be expected to sustain without fracture. For a plane infinite sheet loaded as shown in Fig. 4.3, the stress intensity factor

$$K = \sigma\sqrt{\pi a} \tag{4.25}$$

At the onset of crack propagation

$$G_{IC} = \frac{K_I^2 (1-\nu^2)}{E} = \frac{\pi\sigma^2 C(1-\nu^2)}{2E} \tag{4.26}$$

where it is understood that σ and C are the load, and crack size which are observed at the critical condition.

In Griffith's theory the state of critical and unstable equilibrium is attained when equation (4.3) or equation (4.4) is satisfied. From equations (4.3) and (4.6) this leads to the requirement that

$$\frac{\pi\sigma^2 C(1-\nu^2)}{2E} = 2\gamma_s \tag{4.27}$$

From equations (4.24) and (4.25), it is seen that the onset of crack propagation in Irwin's theory corresponds to unstable equilibrium in Griffith's theory when the elastic strain energy release rate has the critical value

$$G_{IC} = 2\gamma_s \tag{4.28}$$

or when

$$\sigma = \sqrt{\frac{2E\, G_{IC}}{\pi C(1-\nu^2)}} \tag{4.29}$$

The surface energy in the Griffith theory must be determined by experiment for any given material. Irwin's theory likewise must rely on experimental determination of the critical value of G_{IC} or K_{IC} for a given material.

Criteria for the onset of a fracture mode of failure are thus available for design so that critical sizes may be estimated for given loading, etc.

4.6 PLASTICITY CORRECTION

From equations (4.22 - 4.28), it is seen that K is related to the rate of change with crack size of the total elastic strain energy in the body. If the crack tip region over which plastic deformation takes place is relatively small, then the contribution of such a region to the total elastic strain energy rate of the body will also be comparatively small. Thus elastically calculated K formulas will be substantially correct, i.e. will be affected only to a minor degree by the existence of small crack front yield zones.

A somewhat rational method for correcting for small scale plastic yield effects at the crack border has been proposed by Irwin[79], based on the following argument. The presence of a plastic zone at the crack front tends to elevate the elastic stress level in the elastic region between the boundary of the plastic enclave and the free edge of the cracked body as a consequence of the

redistribution of stress caused by the plastic deformation. To compensate for this increase, the actual half crack length can be imagined to be increased by an amount r_Y, which represents a measure of the plastic enclave dimension along the plane of the crack under conditions of small-scale yielding, as in Fig. 4.7., i.e., the actual stress in the elastic-plastic solid corresponding to a half crack length, a, is imagined to be equivalent to the stress that would arise from an "effective" half crack length.

$$a_e = a + r_Y \tag{4.30}$$

in a perfectly elastic material.

A precise, realistic calculation of the shape (and therefore the size) of the crack-tip plastic enclave is currently not possible because of the mathematical difficulties associated with the required elastic-strain hardening plastic analysis[58]. However, elastic-perfectly plastic analyis for the tearing mode problem (mode III) indicates a circular plastic zone with radius proportional to K^2 divided by the square of the yield stress in simple shear[79]. A result similar in form, mathematically, is obtained for the opening mode from equation (4.14). If, along the plane of the crack, $\theta=0$, the Y-direction stress is set equal to the uniaxial yield stress of the material σ_Y at some distance $r = r_Y$ from the crack tip. These considerations prompted Irwin to propose as a rough measure

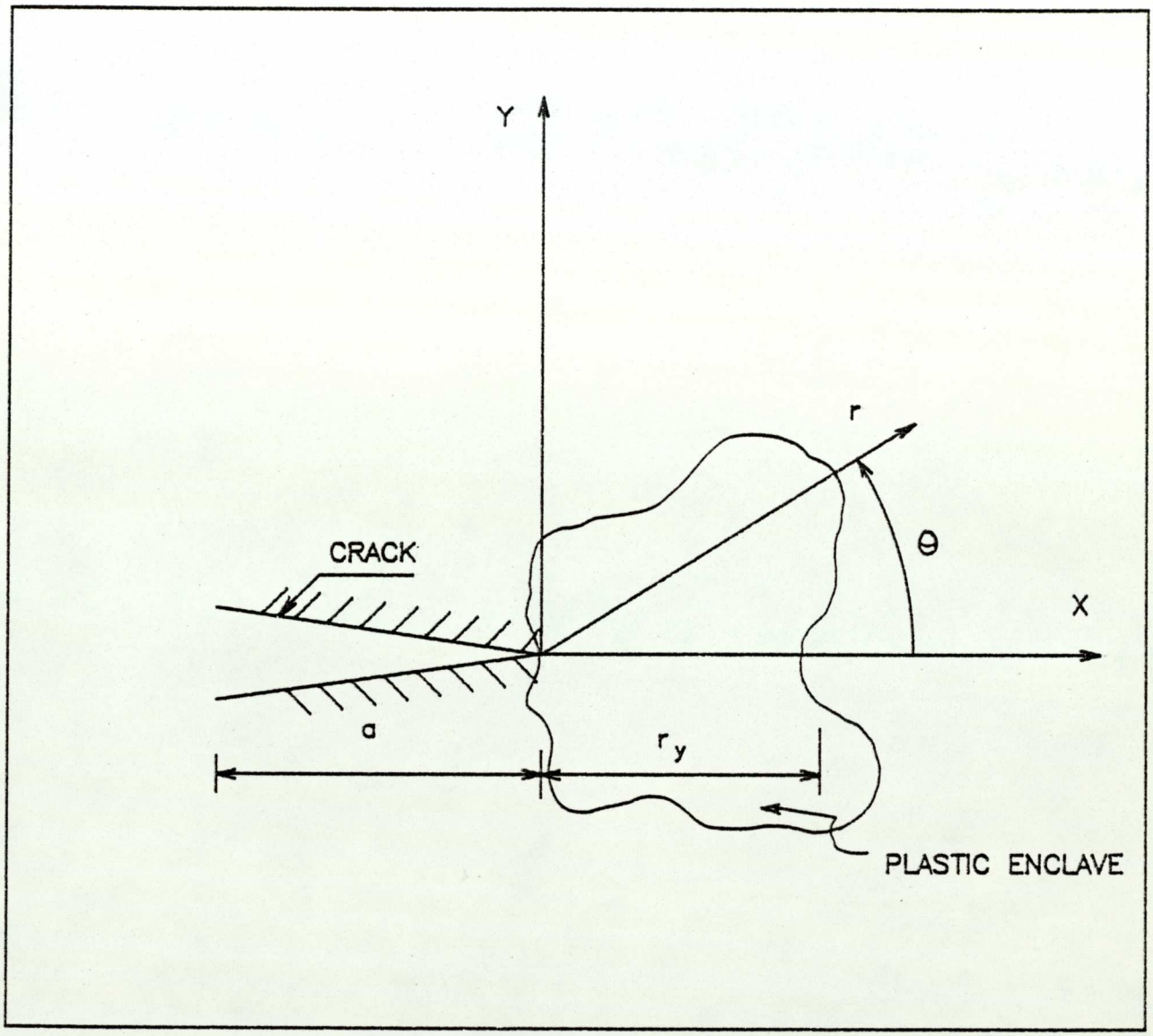

FIGURE (4.7)

of the plastic zone size

$$r_Y = \frac{1}{2\pi} \left(\frac{K}{\sigma_Y}\right)^2 \tag{4.31}$$

for plane stress

and

$$r_Y = \frac{1}{6\pi} \left(\frac{K}{\sigma_Y}\right)^2 \tag{4.32}$$

for plane strain.

The plane strain plastic zone size measure is reduced by a factor of one-third in order to account for the constraining effect of the lateral σ_Z stress, which is zero in plane stress.

If the K formulas are corrected for small scale plastic yield effects according to equations (4.30 - 4.32) for centre cracked sheets in plane stress, equation (4.25) becomes

$$K^2 = \sigma^2 \left[\pi a + \frac{1}{2} \left(\frac{K}{\sigma_Y}\right)^2\right] \tag{4.33}$$

4.7 THE STRAIN-ENERGY-DENSITY FACTOR

The critical stress intensity factor approach in fracture mechanics is analogous to the maximum stress criterion applied to a simple tension specimen and cannot be used in combined loading situations[15, 57] and since in most of the structural components the cracks are seldom aligned perpendicular to the direction of loading, the

criterion of fracture requires a combination of K_I and K_{II} and or K_{III} reaching some critical value, i.e.

$$f(K_I, K_{II}, K_{III}) = f_C \tag{4.34}$$

An alternative interpretation of fracture phenomena was presented by Sih[8,9]. His basic concept is that the material in the immediate vicinity of the crack tip, marked as the core region in Fig. 4.8, is free from defects of the same order of magnitude as the crack tip radius. Otherwise the crack tip would have advanced to and connected up with the nearest defect. These defects are assumed to be uniformly distributed outside the core region of radius r_o.

The amount of energy stored in one of these defects[57], occupying an incremental area of $\Delta A = r\Delta\theta\Delta r$ as could be shown in Fig. 4.9, and can be computed from

$$\frac{dW}{dA} = \frac{1}{r}(a_{11}K_I^2+2a_{12}K_IK_{II}+a_{22}K_{II}^2+a_{33}K_{III}^2) \tag{4.35}$$

in which the coefficients for plane strain are given by

$$\begin{aligned}
a_{11} &= \frac{1}{16\mu}\left[(3-4\nu-\cos\theta)(1+\cos\theta)\right] \\
a_{12} &= \frac{1}{16\mu}\left[(2\sin\theta)(\cos\theta-(1-2\nu)\right] \\
a_{22} &= \frac{1}{16\mu}\left[4(1-\nu)(1-\cos\theta)+(1+\cos\theta)(3\cos\theta-1)\right] \\
a_{33} &= \frac{1}{4\mu}
\end{aligned} \tag{4.36}$$

where

ν being the Poisson's ratio

μ is the shear modulus of elasticity

$\frac{dW}{dA}$ is the local strain-energy-density function and is inversely proportional to the radial distance r measured from the crack tip.

This factor describes the variation of the local energy density around the region since it depends on θ, marking the position of ΔA, through the coefficients a_{11}, a_{12}, a_{22} and a_{33}.

The fundamental hypotheses on unstable crack growth in the Sih theory[8,9,57] are as follows:

(1) The initial crack growth takes place in the direction along which the strain-energy-density factor possesses a stationary (minimum) value, i.e.

$$\frac{\partial S}{\partial \theta} = 0 \quad \text{at which } \theta = \theta_o$$

where θ_o is between $-\pi$ and π, i.e. $-\pi < \theta_o < \pi$.

(2) Crack extension occurs when the strain-energy-density factor reaches a critical value i.e.

$$S_c = S(K_I, K_{II}, K_{III}) \quad \text{for } \theta = \theta_o$$

where θ_o is the angle of crack extension.

The difference between S and S_c is analogous to the difference between K and K_c, and so S_c is also a measure of the resistance of a material against fracture.

where

ν being the Poisson's ratio

μ is the shear modulus of elasticity

$\frac{dW}{dA}$ is the local strain-energy-density function and is inversely proportional to the radial distance r measured from the crack tip.

This factor describes the variation of the local energy density around the region since it depends on θ, marking the position of ΔA, through the coefficients a_{11}, a_{12}, a_{22} and a_{33}.

The fundamental hypotheses on unstable crack growth in the Sih theory[8,9,57] are as follows:

(1) The initial crack growth takes place in the direction along which the strain-energy-density factor possesses a stationary (minimum) value, i.e.

$\frac{\partial S}{\partial \theta} = 0$ at which $\theta = \theta_o$

where θ_o is between $-\pi$ and π, i.e. $-\pi < \theta_o < \pi$.

(2) Crack extension occurs when the strain-energy-density factor reaches a critical value i.e.

$S_c = S(K_I, K_{II}, K_{III})$ for $\theta = \theta_o$

where θ_o is the angle of crack extension.

The difference between S and S_c is analogous to the difference between K and K_c, and so S_c is also a measure of the resistance of a material against fracture.

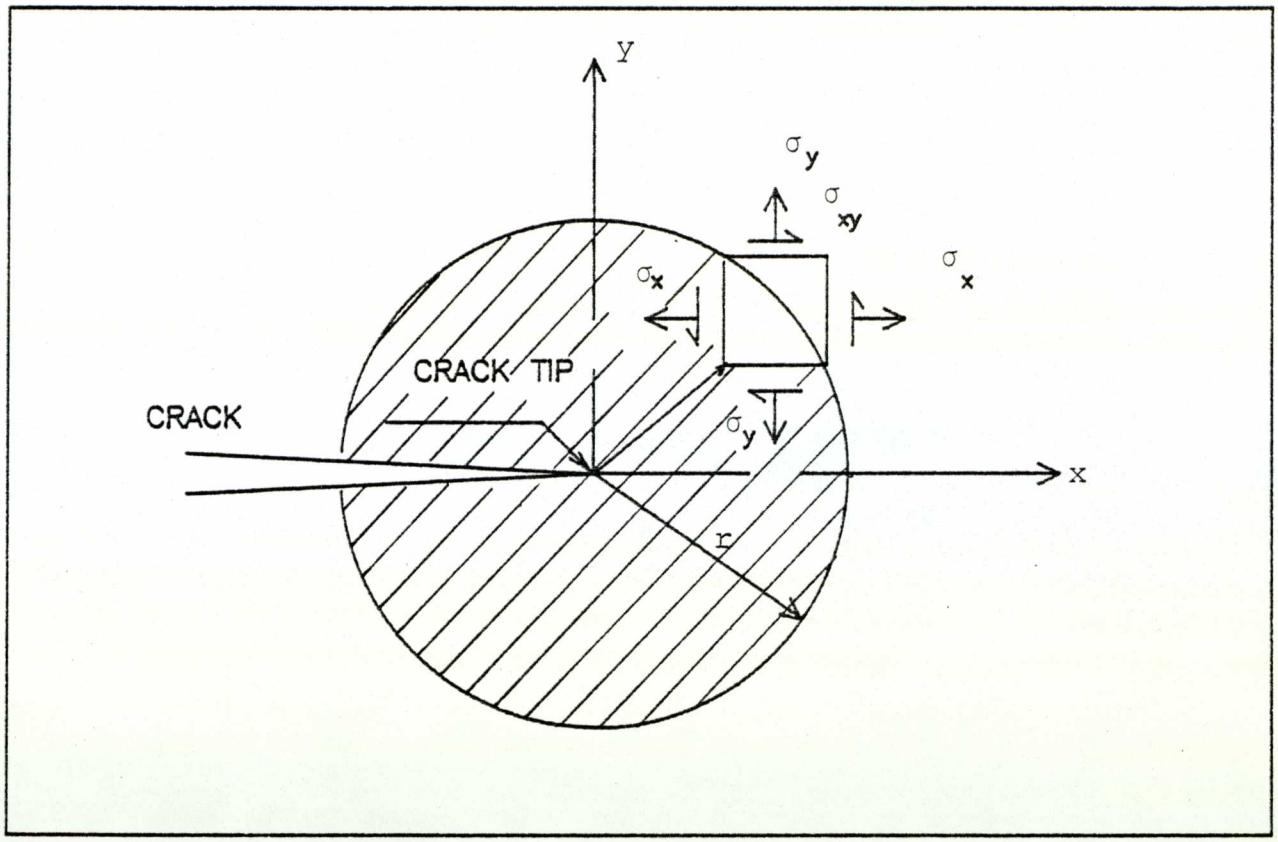

FIGURE (4.8) CRACK TIP REGION OF RADIUS r.

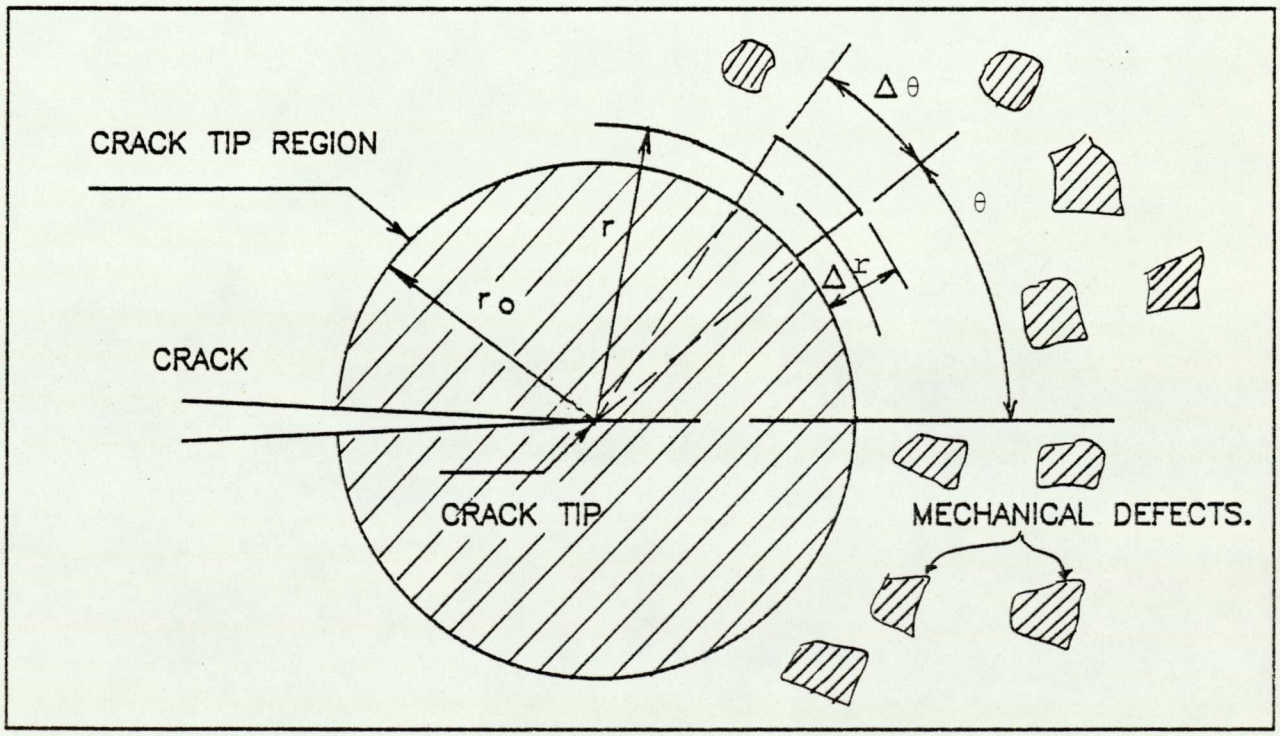

FIGURE (4.9) CRACK TIP REGION WITH MECHANICAL DEFECTS AROUND IT.

The validity of the theory can be checked by imposing different loading conditions on the cracked specimens made of the same material[9,57] and show that δ_c indeed remain constant and to be independent of the crack geometry and loading and hence it can be used as a material parameter for measuring the resistance against fracture.

4.8 THE STRESS INTENSITY FACTOR AND FRACTURE MECHANICS

Fracture mechanics technology is based on an analytical procedure that relates the stress-field magnitude and distribution in the vicinity of a crack tip to the nominal stress applied to the structure, to the shape, size and orientation of the crack discontinuity, and to material properties.

The fundamental principle of fracture mechanics is that the stress field ahead of a sharp crack in a structural member can be characterised in terms of a single parameter, K, the stress intensity factor, that has units of stress $\times$ $\sqrt{\text{Length}}$. This parameter, K, is related to both the nominal stress level in the member and the size of the crack present. Thus all structural members, or test specimens, that have flaws can be loaded to various levels of K.

A number of authors have collected solutions of crack problems into compendiums, Rooke and Cartwright[37] have classified solutions in their compendium into five structural

groups: flat sheets, stiffened sheets, discs, tubes and bars; also three dimensions where the cracks have curved boundaries and the stress intensity factors can vary with position on the crack front. Also in the same compendium, solutions of plates and shells are classified too.

In the next chapter, methods for the determination of the stress intensity factor is explained, some briefly, others in detail. Method employing the finite element is of particular interest to find the K values.

CHAPTER 5

METHODS FOR THE DETERMINATION OF STRESS INTENSITY FACTORS

5.1 INTRODUCTION

A parameter which can be used to distinguish between different cracks and measure the severity of a crack can be obtained from an examination of the stress field near the crack tip. The stress σ_{ij} at a small distance r ahead of the crack tip is given by:

$$\sigma_{ij} \simeq \frac{K_m}{\sqrt{2\pi r}} \tag{5.1}$$

that is, as r approaches zero, the stress near the tip of a crack approaches infinity as $r^{-\frac{1}{2}}$. The constant of proportionality K_m which is different for different cracks is called the 'stress intensity factor' and can be written as

$$K_m = Y\sigma\sqrt{\pi a} \tag{5.2}$$

where m = I, II or III indicates the relative movement of the crack faces, i.e. the mode of crack.

σ is a stress determined by the loading.

a is a crack length.

Y is a geometrical factor which accounts for such things as proximity effect of boundary surfaces or other cracks, orientation of the crack and the shape of the crack.

For the simple case of a crack of length 2a in a large sheet subjected to a uniform stress σ remote from and perpendicular to the crack, Y = 1, and the stress intensity factor is given by

$$K_I = \sigma\sqrt{\pi a} \qquad (5.3)$$

The power of the stress intensity factor method of analysis lies in the assumption that the behaviour of a sharp crack is determined by the stress field at the tip; it is thus necessary to determine the stress intensity factor only.

Some of the more useful methods of evaluating stress intensity factors are presented in the next section[17].

5.2 METHODS OF EVALUATION OF STRESS INTENSITY FACTORS

The methods for determining the stress intensity factors may be divided broadly into the following[17]

(a) Experimental Methods

(b) Analytical Methods

(c) Numerical Methods.

5.2.1 Experimental Methods

In this section some experimental methods of determining stress intensity factors are described. Experimental methods may either use a known relationship between a measurable

quantity (e.g. compliance or fatigue crack growth rate) and the stress intensity factor, or involve direct measurements on a model (e.g. by photoelasticity).

(1) Compliance

Irwin and Kies[16] showed that the strain energy release rate G could be written in terms of the applied load Q and the change in compliance C with respect to crack area A in the form

$$G = \frac{Q^2}{2} \frac{dC}{dA} \tag{5.4}$$

From which the stress intensity factor for plane stress is given by

$$K_I = Q\left[\frac{E}{2} \frac{dC}{dA}\right]^{\frac{1}{2}} \tag{5.5}$$

The determination of K_I from equation (5.5) involves measuring the compliance C for a range of crack lengths. Calculating the derivative of the compliance vs. crack length curve then enables K_I to be found. The experimental method needs considerable care if satisfactory results are to be obtained[59]. The method has been used for many problems, more details of the technique can be found in reviews by Cartwright and Rooke[63].

This method is applied when a body is subjected only to a single point load. It is most useful for relatively small test specimens which can have precise measurements

made on them in the laboratory under constant load. It cannot be used for the large structures.

(2) Photoelasticity

Of the optical methods for determining stress intensity factors, photoelasticity has been most used. The technique has several advantages. It is a well-known method for which experimental equipment and birefringent materials are readily available. By using the frozen stress technique photoelastic analysis may be extended to three-dimensional configuration; an assessment of this technique in relation to crack tip stress fields has been made in reference (19).

Two methods, which involve measurements of the stress near to a simulated crack, are based on the equation for the maximum shear stress τ_m, given by:

$$\tau_m = \frac{1}{2\sqrt{2\pi r}} \left[(K_I \sin\theta + 2K_{II}\cos\theta)^2 + (K_{II}\sin\theta)^2 \right]^{\frac{1}{2}} \qquad (5.6)$$

where (r,θ) are polar co-ordinates centred at the crack tip. In the first method used by Emery et al.[20], the stress intensity factors were evaluated from the maximum shear stress τ_m on lines perpendicular to and through the crack tip given by:

$$\tau_m = \frac{(K_I^2 + K_{II}^2)^{\frac{1}{2}}}{2\sqrt{2\pi r}} \qquad (5.7)$$

and on a line outside and collinear with the crack given by

$$\tau_m = \frac{K_{II}}{\sqrt{2\pi r}} \tag{5.8}$$

Evaluation of τ_m close to the tip at points above (or below) and ahead of the notch allows both K_I and K_{II} to be determined from equations (5.7) and (5.8).

In the second method, used by Smith and Smith[21], equation (5.6) is used together with the condition $\frac{\partial \tau_m}{d\theta} = 0$, that is the condition

$$\left(\frac{K_{II}}{K_I}\right)^2 - \frac{4}{3}\left(\frac{K_{II}}{K_I}\right) \cot 2\theta_m - \frac{1}{3} = 0 \tag{5.9}$$

The angle θ_m, is that at which a tangent to the isochromatic fringes is perpendicular to the radius r. The angle is measured from the isochromatic fringe pattern near the tip, the ratio $\frac{K_{II}}{K_I}$ is determined from equation (5.9) and hence K_I and K_{II} can be found using a known value of τ_m in equation (5.6).

Both of these methods have the advantage that τ_m may be obtained directly from the isochromatic fringe pattern, and so avoid the need for stress separation.

The advantage of these methods is that it is well established methods in stress analysis, the equipments and materials used are readily available. Its disadvantage

is that the analysis is tedious. Difficult and careful preparation of specimens are necessary.

(3) Fatigue Crack Growth Rate

Paris[22] proposed that the growth rate of a crack extending under fatigue loading could be characterised by the stress intensity range

$$\frac{da}{dN} = f(\Delta K) \tag{5.10}$$

where $\frac{da}{dN}$ is the crack growth rate with respect to number of cycles, and ΔK is the stress intensity factor range, i.e.

$$\Delta K = K_{max} - K_{min} \tag{5.11}$$

To determine the stress intensity factor for a new configuration, it is necessary to conduct a fatigue test on that configuration and record both the length and the rate of growth of the crack over the range of crack lengths required. A fatigue test must then be performed under identical conditions on a specimen of the same material, for which the stress intensity factor is known as a function of stress and crack length. The data from the two tests are then compared on the basis of equivalent crack growth rates. James et al.[23] have applied this method to the case of a thick walled, internally pressurized cylinder containing a longitudinal crack.

It is easy to conduct the fatigue test on the specimen

in question and record the crack growth rate. But, it should be noted that, ideally, the same thickness of material should be used in the tests to generate the $\frac{da}{dN}$ vs. ΔK data as will be used in the specimen since there appears to be some effect of thickness on the crack growth rate.

(4) Interferometry and Holography

Two optical methods based on measurements of interference fringes in transparent materials have been proposed. The method of Dudderar and Gorman[24] involves determining the opening mode stress intensity factor from measurements of the magnitude of the sum of the normal stresses at a series of points outside and collinear with the crack. A thin perspex sheet, containing a sharp notch is subjected to a tensile stress. The magnitude of $(\sigma_x+\sigma_y)$ is obtained for several loads from a series of interferograms. The magnitude of K_I is calculated from the slope of a plot of $(\sigma_x+\sigma_y)$ vs. $r^{-\frac{1}{2}}$ in a similar way to that used by Wilson[58] for photoelastic results.

The method, proposed by Sommer[25], involves measuring the relative displacement of the crack faces, by an interference technique in glass sheets under load. The relative displacement of the crack faces is determined at several positions along the crack and the opening mode stress intensity factor obtained using the known relationship

between the displacements and K_I.

For plane strain conditions

$$2v = \frac{4K_I}{E} (1 - \nu^2) \sqrt{\left(\frac{2r}{\pi}\right)}$$

where v is the crack opening displacement.

r is the distance from the crack tip along the crack opening

ν, E, and K_I are poisson ratio, Young's modulus of elasticity and the mode one stress intensity factor.

5.2.2 Analytical Methods

The methods considered here are those which satisfy the differential equations and all the boundary conditions exactly. Such methods have the advantage of leading to explicit expressions for stress intensity factors; but only certain classes of problems can be solved where the shape of the component considered is not too complex. In deriving the stress intensity factor, use is made of the formal definition

$$K_m = \lim_{r \to o} \sigma_m \sqrt{2\pi r} \qquad (5.12)$$

where σ_m is appropriate to the mode of cracking. For simplicity, all the methods are described for a crack of length 2a along the X-axis with the origin of the (x,y) co-ordinates at the crack centre.

(1) Westergaard Stress Function

Westergaard[26] formulated an Airy stress function F, which for mode I, with self-equilibriated forces on the crack, takes the form

$$F_I = \text{Re}\,[\bar{\bar{z}}_I] + Y_{Im}[\bar{z}_I] \tag{5.13}$$

where z_I is the Westergaard stress function.

$\bar{z}_I$ and $\bar{\bar{z}}_I$ are defined by

$$\frac{d\bar{\bar{z}}_I}{dz} = \bar{z}_I \quad \text{and} \quad \frac{d\bar{z}_I}{dz} = z_I \tag{5.14}$$

where

$$z = x + iy$$

The Cartesian components of stress, in terms of F_I, are

$$\sigma_x = \frac{\partial^2 F_I}{\partial y^2}, \quad \sigma_y = \frac{\partial^2 F_I}{\partial x^2}, \quad \tau_{xy} = \frac{\partial^2 F_I}{\partial x \partial y} \tag{5.15}$$

The simplest crack configuration studied by Westergaard was that of a crack in an infinite sheet subjected to uniform biaxial tension σ_∞ at infinity; the stress function is

$$z_I = \frac{\sigma_\infty z}{\sqrt{z^2 - a^2}} \tag{5.16}$$

Westergaard also studied a crack opened by wedge forces and an infinite series of collinear cracks under various loading conditions. The method can be extended to modes II

and III and comparison of the stress field in terms of the Westergaard stress function Z_m with equation (5.12) shows that the stress intensity factor is given by

$$K_m = \sqrt{2\pi} \lim_{z \to a} \{\sqrt{z-a} \quad Z_m\} \tag{5.17}$$

where

m = I, II, III, relating to the mode.

Several workers[27] have used Westergaards's method for solving crack problems.

(2) Complex Stress Functions

Mushkelishvillis complex stress function approach[17] enables the Airy stress function F to be written in terms of two complex functions $\phi(z)$ and $\psi(z)$, as

$$F = \mathrm{Re}\left[\bar{z}\phi(z) + \int \psi(z)\, dz \right] \tag{5.18}$$

which yields, from equation (5.15) with F_I replaced by F

$$\sigma_x + \sigma_y = 4\mathrm{Re}\left[\bar{\phi}(z)\right] \tag{5.19}$$

and

$$\sigma_x - \sigma_y + 2i\tau_{xy} = 2\left[\bar{z}\phi''(z) + \psi'(z)\right] \tag{5.20}$$

From equation (5.19) and the known properties of $\phi'(z)$ it can be shown that

$$K_I - iK_{II} = 2\sqrt{2\pi}\,\underset{z\to z_1}{\text{Lim}}\,\{\sqrt{z-z_1}\,\phi'(z)\} \qquad (5.21)$$

This method of determining stress intensity factors has an advantage over the Westergaard method since conformal mapping can be used to map cracks into holes.

This is important from a practical view point as many cracks initiate from areas of rapid stress change.

For a mapping function

$$z = \omega(\xi) \qquad (5.22)$$

and a crack tip at ξ in the ξ-plane, equation (5.21) becomes

$$K_I - iK_{II} = 2\sqrt{2\pi}\,\underset{\xi\to\xi_1}{\text{Lim}}\,\sqrt{\omega(\xi)-\omega(\xi_1)}\;\frac{\phi'(\xi)}{\omega'(\xi)} \qquad (5.23)$$

where

$$\phi(\xi) \equiv \phi(\omega(\xi)) \quad \text{and} \quad \phi'(\xi) = d\phi(\xi)/d\xi$$

A comparison of equations (5.17) and (5.23) shows that the Westergaard stress functions and the complex stress function are related by

$$z_I - iz_I = 2\phi' \qquad (5.23a)$$

For practical components, this technique is limited to certain idealised situations.

5.2.3 Approximate Methods

Several approximate numerical methods are available for calculating stress intensity factors. Suitable approximations have been applied in order to solve problems having more complex shapes than would be possible by analytical methods. The finite element method forms the basis of investigations described in this thesis, and its application to the determination of stress intensity factors is described here. Other methods are described briefly here.

(1) Boundary Collocation

In this method of boundary collocation the stress function is represented in series form and the determination of the stress intensity factor is reduced to the solution of a set of linear algebraic equations. The boundary conditions on the crack surface are built into the series chosen to represent the stress function and any remaining conditions around finite boundaries are then fitted approximately. The boundary points may be matched (collocated) exactly or fitted in a least square sense. Whilst convergence is not guaranteed, the boundary collocation method has contributed a considerable number of stress intensity factor solutions; accuracy of these solutions is assessed when possible by comparison with alternative solutions determined by analytical method. Application of boundary collocation to crack problems start either from the William's stress function or from series

representation of complex stress functions.

(i) William's Stress Function

The William's stress function[14] arises as a special case of the stress function for an infinite sector[17]. It is an Airy stress function which also satisfies the conditions that the normal and shearing stresses be zero along the crack surface. Considerable use has been made of boundary collocation of the William's stress function by Gross et al.[17] for condtions of geometry and loading which are symmetrical with respect to the plane of the crack. Boundary collocation of the William's stress function is suitable for singly connected configurations in two-dimensional problems.

The William's stress function as modified by Sih and Rice[35] has been used with boundary collocation to obtain stress intensity factors for finite bi-material plates. The method was used to analyse a centrally cracked bi-material plate and a partially debonded composite laminate.

(ii) Complex Stress Functions

Stress intensity factors in multiply connected two-dimensional bodies subjected to in-plane loading may be determined from a series representation of the complex functions $\phi(z)$ and $\psi(z)$ of Mushkelishvili.

The procedure has been employed extensively by Gross et al.[17] for edge cracks and in a modified form by Kobayashi et al.[28] for internal crack problems. There is no guarantee of numerical convergence, and accuracy is judged largely by insensitivity of result to the inclusion of more terms in the series. The selection of the number and distribution of the boundary points also plays an important role in the accuracy of the final solution[29].

(2) Conformal Mapping

Conformal mapping has been mentioned in Section 5.2.3 for complicated boundaries, e.g. radial cracks emanating from a circular hole[17], the exact form of mapping function equation (5.22), becomes multivalued and subsequent stress analysis is difficult. Bowie[30] has developed a technique for avoiding these difficulties by representing the mapping function as a polynomial, the coefficients of which are determined by comparison with the exact mapping function. This method is applicable to configurations for which an exact mapping is available; it has been applied by several workers to singly connected regions[17]. A method in which conformal mapping is combined with boundary collocation has been developed by Bowie and Neal[31]. This method avoids the difficulty of finding accurate polynomial mapping functions of the complete physical region. A simple form of mapping function is used to transform a crack and its exterior in the physical plane

into a circle and its exterior in the auxiliary plane. The remainder of the boundary in the physical plane corresponded to a directly calculable curve in the auxiliary plane. Collocation methods are used to satisfy conditions around this boundary. Bowie and Freese[32] have applied the modified mapping collocation technique to doubly connected regions in both isotropic and orthotropic sheets. Recently the method has been extended[33] to improve convergence in certain complicated configurations.

(3) Stress Concentration Factors

With reference to Figure (4.2) the stress at the apex of the major axis of the ellipse (σ_m) is given by:

$$\sigma_m = \sigma(1 + \frac{2a}{b}) \tag{5.24}$$

The crack configuration may be approximated to a narrow elliptical cavity having a radius of curvature

$$\rho = \frac{b^2}{a} \quad , \qquad \rho << a \tag{5.25}$$

Equation (5.24) may be rewritten as:

$$\sigma_m = \sigma(1 + 2\sqrt{\frac{a}{\rho}}) \simeq 2\sigma\sqrt{\frac{a}{\rho}} \tag{5.26}$$

or

$$\sigma\sqrt{a} = \frac{1}{2}\,\sigma_m\sqrt{\rho} \tag{5.27}$$

The stress intensity factors may be obtained from the limiting values of maximum stresses at the base of a notch

whose radius of curvature is allowed to vanish

$$K_I = \frac{\sqrt{\pi}}{2} \lim_{\rho \to o} (\sigma_m \sqrt{\rho}) \tag{5.28}$$

If τ_m is the maximum value of τ_{xy} then:

$$K_{II} = \sqrt{\pi} \lim_{\rho \to o} (\tau_m \sqrt{\rho}) \tag{5.29}$$

and if τ'_m is the maximum value of τ_{zy} then:

$$K_{III} = \sqrt{\pi} \lim_{\rho \to o} (\tau'_m \sqrt{\rho}) \tag{5.30}$$

Although the relationship between K_m and σ_{max} or (τ_{max}) or (τ'_{max}) is exact the actual expressions for the maximum stresses may be known only approximately. The values of σ_m for a variety of notches can be found in the work of Neuber[34].

(4) Green's Functions

Certain solutions[17] are particularly useful in that they may be used to construct Green's functions for determining stress intensity factors for cracks in arbitrary stress fields[13]. The stress intensity factor, for the tip at x = a due to a pair of point forces Q perpendicular to the crack surface ($-a<x<a$, $Y=o$), where the crack length is 2a, and at a distance x from the origin, is given by

$$K_I = Q \left[\frac{1}{\pi a}\left(\frac{a+x}{a-x}\right)\right]^{\frac{1}{2}} \tag{5.31}$$

where $\left[\frac{a+x}{a-x}\right]^{\frac{1}{2}}$ is a Green's function for this situation.

If $\sigma_y(x,o)$ is the stress along the crack site in the absence of the crack, then writing $Q = \sigma_y(x,o)\,dx$ and integrating over the crack length gives the contribution of all the forces distributed along the crack line, i.e.

$$K_I = \frac{1}{\sqrt{\pi a}} \int_{-a}^{+a} \left[\frac{a+x}{a-x}\right]^{\frac{1}{2}} \sigma_y(x,o)\,dx \qquad (5.32)$$

$\sigma_y(x,o)$ may be measured experimentally in the uncracked solid or determined theoretically. Equation (5.32) then enables the stress intensity factor to be determined; equivalent forms exist for modes II and III[13,36]. Graphical and analytical Green's functions have been determined by several workers[37,38] and applications to several problems of practical interest can be found in the work of Chell[17].

In order to apply the method, it is necessary to know the appropriate Green's function and the distribution of stress along the crack site in the uncracked solid. The technique will give exact results providing that the exact Green's function is used. Often this may not be available and it is then necessary to make an approximation[65].

(5) Integral Transforms and Dislocation Models

In this method the elastic problem is considered as a mixed boundary value problem and solved using standard transform techniques. Many solutions using various transforms

have been collected by Sneddon and Lowengrub[17]. These methods usually reduce to the solution of an integral equation which takes the form

$$\int_{-a}^{a} K(s,x)q(s)ds = L(x) \tag{5.33}$$

where $L(x)$ is a function of the known stress along the crack site in the uncracked body, $K(s,x)$ is the known kernel, and $q(s)$ is the unknown function. The function $q(x)$ is proportional to the derivative of the relative displacement $v(x,o)$ of the crack faces, i.e.

$$\frac{E}{2(1-\nu^2)} \frac{\partial v(x,o)}{\partial x} = q(x) \tag{5.34}$$

where E is Young's modulus, and

ν is Poisson's ratio.

A knowledge of q enables the stress intensity factor to be determined from the relationship

$$K_a = \lim_{x \to a} \left[\sqrt{2\pi(a-x)} \frac{E}{2(1-\nu^2)} \frac{\partial v(x,o)}{\partial x} \right] \tag{5.35}$$

A method based on continuous dislocation arrays also leads to integral equation similar to (5.33) for references see reference (17).

(6) Force-Displacement Matching

This method is applicable to configurations in which there are boundaries between different materials; it involves

matching the forces and displacements in the region over which the materials are joined. The method has been used mainly for determining stress intensity factors for cracks in stiffened sheets[39] where the stiffener is represented as a distribution of point forces. The distribution is determined by satisfying compatibility of displacements and equilibrium of forces at each attachment point between the sheet and the stiffener.

(7) Alternating Methods

This method has been useful in determining stress intensity factors for a number of two-dimensional and three-dimensional crack problems and many applications have been viewed by Hortranft and Sih[38,Ch.4]. This method uses existing solutions of simple crack problems to construct approximate ones to a more complicated range. This is done by superimposing the known solutions of component problems, each satisfying boundary conditions on a portion of the boundary. Its application to three-dimensional problems has been made in reference (40).

(8) Finite Element Methods

The use of finite element methods to analyse fracture problems is complicated by the stress field singularity which exists at the crack tip. The methods for determining stress intensity factors using finite elements[17] fall into three categories. The first of these three methods

allow stress intensity factors to be determined directly, this method requires small elements in the vicinity of the crack tip. The other two methods are the most successful methods of approach and would appear to be the so-called energy technique, and the singularity function formulation. In the latter the necessity for extremely fine meshes in the crack tip region can be overcome by the use of special elements which incorporate the required stress singularity in their formulation. These elements are based on the eight node quadrilateral isoparametric element; this being the most popular element in general use. Such crack tip elements may be readily incorporated into a mesh of standard isoparametric elements permitting numerical fracture studies to be undertaken without extensive mesh generation or refinement. In particular elements based on the use of distorted shape functions, standard shape functions, analytic soluctions, a superposition process and a hybrid technique are considered.

(i) Crack Tip Stress and Displacement Methods (direct methods)

(a) Crack Tip Stress

The stress method correlates the stresses at the nodal points of the finite element mesh with those at the crack tip which are given by equation (4.20)

$$m\sigma_{ij} = K_m \, r^{-\frac{1}{2}} \, mf_{ij}(\theta) \qquad (5.36)$$

where m = I, II or III, i.e. the mode.

For the opening mode (m=I) equation (5.36) can be written as

$$K_I = \sigma_y \sqrt{2r}/f(\theta) \qquad (5.37)$$

Hence K_I may be determined from σ_y at some small distance r from the crack tip. This method has been used by Chan et al[41]. It was concluded that the results were not as accurate as those obtained by correlating the displacements of the finite element nodal points as described next.

(b) Crack Tip Displacement

In this method the displacements are the primary unknowns to be determined. This method has been used by many workers[42,43] for a variety of problems. It seemed that better results may be achieved by using the displacements obtained from the finite elements method. The relevant stress intensity factor may be obtained by substituting the appropriate displacement components (u_i) and angle θ in equation (4.21):

$$mu_i = K_m(r^{\frac{1}{2}}/G)\ mf_{ij}(\nu,\theta) \qquad (5.38)$$

Since no provision is made for the crack tip singularity, several values of the stress intensity factors are evaluated at a number of points close to the crack tip and are plotted

versus their distance from the tip of the crack. Such a curve becomes linear some distance away from the crack tip, and by extrapolating the linear portion to the tip point, a better estimate of the stress intensity factor is obtained.

(ii) Energy Methods

These methods do not need such small elements in the vicinity of the crack tip. Since they do not rely on the accuracy of the localised crack tip stresses, strains, or displacements obtained from a finite element program. Consequently, for the same accuracy, the energy methods allow coarser grids to be used than were admissable for the first method.

There are three main energy methods:

(a) The Strain Energy Method

The crack tip stress intensity factor can be related to the strain energy release rate G, by the following relations[13]. For plane strain,

$$G = \frac{(1-\nu^2)}{E}(K_I^2 + K_{II}^2) + \frac{(1+\nu)}{E} K_{III}^2 \qquad (5.39)$$

and plane stress

$$G = \frac{1}{E}(K_I^2 + K_{II}^2 + K_{III}^2) \qquad (5.40)$$

and for mode I loading condition as in equations (4.23) and (4.24)

$$G = (1-\nu^2)\frac{K_I^2}{E} \quad \text{(for plane strain)} \tag{5.41}$$

or

$$G = \frac{K_I^2}{E} \quad \text{(for plane stress)} \tag{5.42}$$

The strain energy release rate is the amount of energy made available at the crack tip for the crack extension process per unit area extension of the crack. As shown in equation (4.22)

$$G = -\frac{dU}{dA} \quad \text{for a fixed displacement condition} \tag{5.43}$$

where U is the elastic strain energy of the body containing the crack.

A is the crack area.

By obtaining finite element solutions for the cracked structure of interest at two or more slightly different crack lengths, G and subsequently the crack tip stress intensity factor, can be estimated by means of equation (5.43). The strain energy stored in the body for each solution is determined by summing over the elements and G is calculated by a finite difference representation of equation (5.43).

The above method has been developed and used by Watwood[44], and Anderson et al[42].

It was shown by Paris and Sih[13] that the energy release rate can also be related to the rate of change of compliance C, the inverse spring constant, with crack

extension by the equation

$$G = \frac{Q^2}{2} \frac{dc}{dA} \qquad (5.44)$$

where Q is the applied load.

Dixon and Pook[45] calculated the compliance of a cracked structure for a number of different crack lengths by the finite element technique and then, by means of equation (5.44), calculated the energy release rate.

(b) Line Integral Method

Rice[46] has shown that the value of the line integral

$$J = \int_{\Gamma} (U dy - T.\frac{\partial u}{\partial x} ds) \qquad (5.45)$$

is proportional to the square of the crack tip stress intensity factor for plane linear elastic bodies free from body forces; Γ is an arbitrary contour surrounding the crack tip. U is the strain energy density, along Γ, T is the traction vector along the outward normal to the contour. u is the displacement vector on an arc element ds along the arc s.

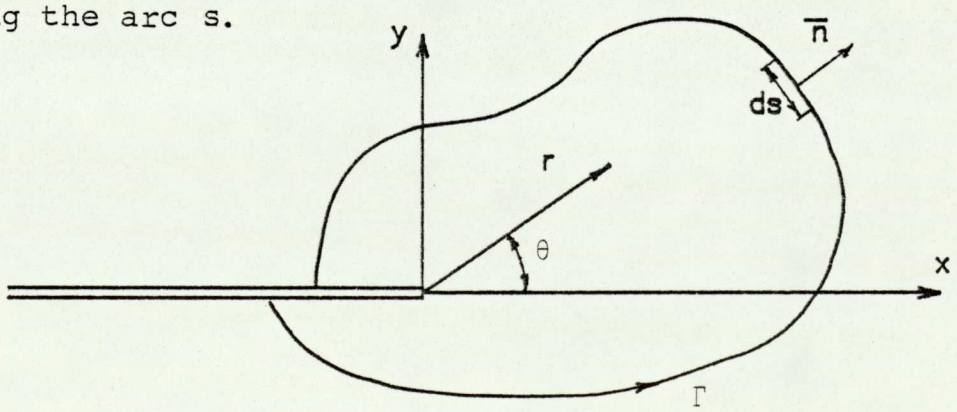

Fig. (5.1) (Path of integration for determining the J-integral)

The crack surface must also be traction free between the crack tip and the contour intercepts.

For a mode I condition the relationship is

$$J = (1-\nu^2)\frac{\pi K_I^2}{E} \quad \text{(plane strain)} \tag{5.46}$$

$$J = \frac{\pi K_I^2}{E} \quad \text{(plane stress)} \tag{5.47}$$

The line integral is evaluated in a counter-clockwise sense starting from the lower crack surface and continuing along the path Γ to the upper flat surface and ds is an element of arc length along Γ.

By numerically evaluating the J-integral for the finite element solution over a path surrounding the crack tip, an estimate of the crack tip stress intensity factor can be made by use of equations (5.46) and (5.47).

For a crack tip subject to combined modes I and II loading the relation between J and the stress intensity factors is

$$J = \frac{\pi(1-\nu^2)}{E}\left[K_I^2 + K_{II}^2\right] \quad \text{(plane strain)} \tag{5.48}$$

$$J = \frac{\pi}{E}\left[K_I^2 + K_{II}^2\right] \quad \text{(plane stress)} \tag{5.49}$$

An estimate of the sum of the squares of the stress intensity factors can be made. The magnitude of the separate intensity factors cannot be made.

In general, the J-integral method is somewhat more accurate than the displacement and stress method for the same mesh. Its accuracy is not as dependent on mesh refinement at the crack tip as are the other two methods.

(c) Crack Closure Method

This method calculates the amount of work required to close successive nodal intervals along a crack[47]. The displacement of the first nodal point along the crack face from the tip is calculated with all the boundary conditions applied. By applying unit loads to this node, the work required to close the crack over nodal intervals can be calculated. A graph of the closure work done versus crack area is plotted and the strain energy release rate (G) is determined from its slope. The (K_I) value is then determined from (G) as in the method described in section (a).

(iii) The Singularity Function Formulation

The formulation is based on the isoparametric element. Singularity elements can be either coupled to, or replaced, standard elements in a structural mesh to represent the appearance of the crack.

(a) Elements Employing Distorted Shape Functions

Element shape functions can be modified to produce displacements proportional to the crack tip singularity function. Tracy[48] employed this technique which is based

on isoparametric quadrilateral elements, for the calculation of mode I stress intensity factors. Two types of elements were employed, the crack tip is surrounded by triangular elements (Fig. (5.2)) which are basically quadrilateral elements with two of the nodes made to coincide at the crack tip, so to form a triangular element. The second type of elements employed in the mesh are the conventional quadrilateral isoparametric elements which surrounds the special elements.

The isoparametric type of elements in the form of a general quadrilateral ABCD, Figure (5.3), has the displacement function specified in the form:

$$u(\xi,\eta) = \alpha_1 + \alpha_2\xi + \alpha_3\eta + \alpha_4\xi\eta \tag{5.50}$$

$$v(\xi,\eta) = \alpha_5 + \alpha_6\xi + \alpha_7\eta + \alpha_8\xi\eta \tag{5.51}$$

Such isoparametric elements can be joined with the singular elements in such a way that there is no displacement incompatibility along the element boundary.

In an application of the technique, values for the element stresses and nodal point displacements are obtained from a finite element program adopted to include these elements. Stress intensity factors may be computed from these stresses and displacements using the direct methods previously described.

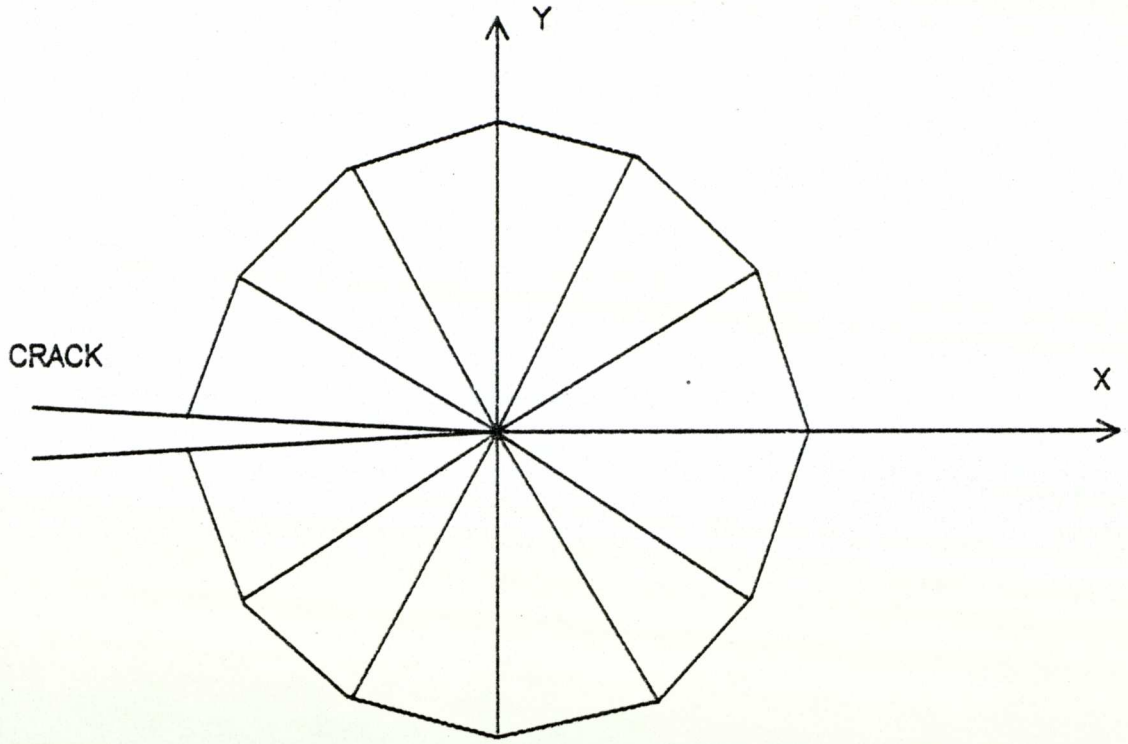

FIGURE(5.2) CRACK TIP ENCLOSED BY TRIANGULAR CRACK TIP ELEMENT.

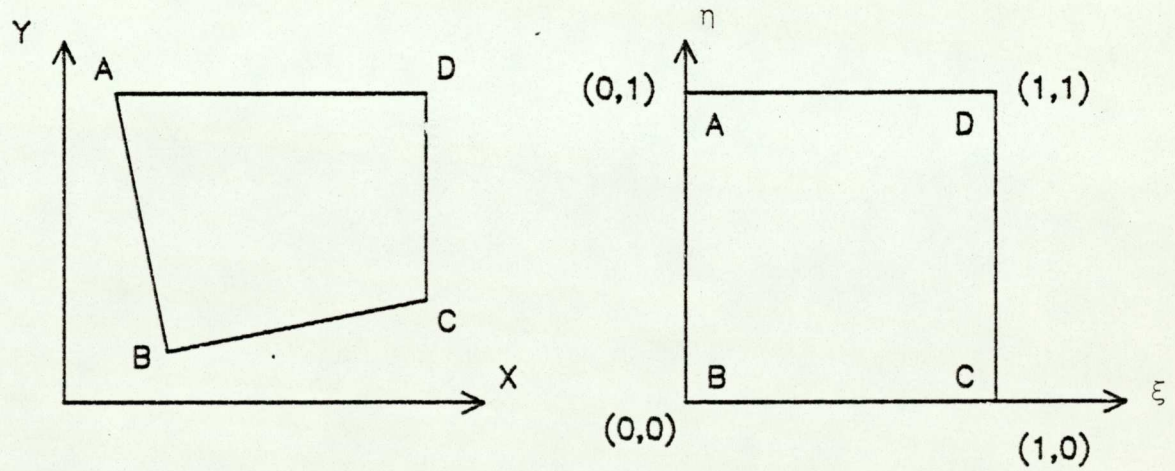

QUADRILATERAL ELEMENT MAPPED INTO A SQUARE

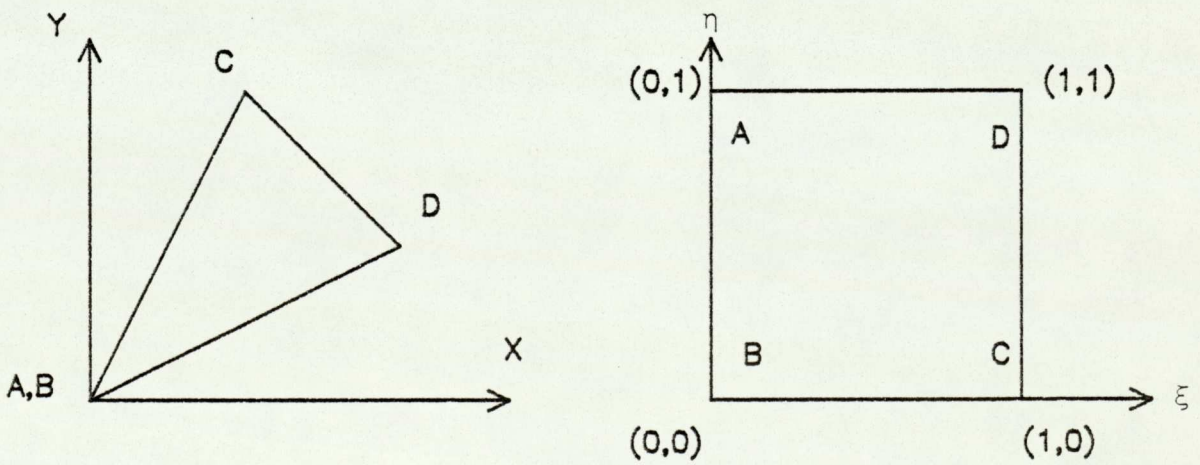

FIGURE (5.3) NEAR CRACK TIP TRIANGULAR ELEMENT MAPPED INTO A SQUARE.

The problem of a double notched edge plate under tension was solved by Tracey[48] using this method. He arranged the values obtained for (K_I) from the displacements of the first ring of nodes surrounding the crack tip, and the results were within (4%) of the exact value for (248) degrees of freedom and (2.9%) for (548) degrees of freedom.

Blackburn[61] eliminated the requirement for mapping a rectangular into a triangular element by developing additional triangular functions proportional to $\sqrt{r}$ for both linear and parabolic edge displacements.

$$u(\xi,\eta) = b_1 + \frac{(b_2\xi+b_3\eta)}{\sqrt{\xi+\eta}} \tag{5.52}$$

which is equivalent to a constant strain triangular element and

$$u(\xi,\eta) = \frac{c_1+c_2\xi+c_3\eta+c_4\xi\eta}{\sqrt{\xi+\eta}} \tag{5.53}$$

which is equivalent to a linear strain one where ξ and η are area coordinates[49] and simplified the procedure by moving the mid-side nodes in a parabolic isoparametric element to positions one quarter of the side length away from the corner node representing the crack tip. This automatically produces a stress singularity proportional to $1/\sqrt{r}$ without any special shape functions or numerical integration formulae.

The element formulations evolved by Blackburn and Henshell and Shaw were tested by Fawkes et al.[61] for several load and geometric conditions. The stress intensity factor, K, could be calculated by extrapolating either the stresses or displacements back to the crack tip region, where the singularity effect was not accurately modelled. This SIF values based on displacements were far more consistent than those based on stresses.

A test computation was run for size-edge-crack plate[61] for a crack running from a=0.1 to 0.9W, where a is the crack length and W is the plate width. The stress intensity factor obtained by use of both the Blackburn and Henshell and Shaw elements were in excellent agreement with the A.S.T.M. results over the range of published a/w ratios 0.1 - 0.6. The two finite element solutions were also in good agreement even at a/w = 0.9. The tests were then repeated for the case of pure bending and again excellent comparison with the A.S.T.M. was evident[61]. The case of pure shear was also considered by Fawkes et al. in which both stress and displacement field are Skew-symmetric. The only non-zero stress intensity factor, K_2, was calculated. Values obtained by Blackburn and Henshell elements consistently underestimate the Wilson[22] result by 10%.

While these tests show that both the Blackburn and Henshell elements perform equally well in single mode fracture,

it is found that for mixed mode problems and at the higher range of a/w, the results diverge dramatically from Wilson's results, and that the results of the Blackburn and Henshell elements no longer coincide but give widely differing results in some cases. It was also found that[61] the Henshell and Shaw element was more accurate than Blackburn's, but both were capable of yielding highly significant differences from analytical results for particular loadings.

(b) Elements Employing Standard Shape Functions

This method employs the development of a general, arbitrary quadrilateral finite element (Fig. 5.4) with a singular corner node. The element formulation is generalised such that any singularity may be treated by including the proper near-field terms, Benzley[51] was the first to use this modelling technique. He employed Linear rectangular elements to model the crack tip geometry and introduced a $\sqrt{r}$ singularity by superposition, utilising the normal element shape functions for the purpose. Benzley obtained good results for certain simple test problems and therefore it was decided to extend this technique to the case of parabolic isoparametric elements. If the elements containing the singularity function are connected to standard elements, as is the case at the boundary of the chosen singularity zone of the influence, the two types of elements no longer conform. This incompatibility can be corrected by

specifying that the singularity displacement function must have zero contribution at the boundary of its zone of influence which can be achieved by the introduction of an appropriate product function.

Benzley[51] represented the arbitrary quadrilateral element with a singular point at node i' as shown in Fig. (5.4). The effects of the singularity are included in the element by enriching a bilinear element displacement assumption with terms that give the proper singularity at node i', i.e.

$$u_i = \alpha_{i_1} + \alpha_{i_2} a + \alpha_{i_3} b + \alpha_{i_4} ab + K_I Q_{1i}(\rho,\theta) + K_{II} Q_{2i}(\rho,\theta) \quad (5.54)$$

where

$i = 1,2$

u_i = displacement in 1 and 2 directions

α_{ij} = unknown coefficients

a,b= local, non-dimensional oblique co-ordinates

ρ,θ= polar co-ordinates with origin at the crack tip

K_I, K_{II} = intensities (unknown coefficients) of singular terms

Q_{1_i} = specific singular assumptions.

Solving equation (5.54) for the unknown coefficients α_{ij}'s in terms of the nodal displacements, $\bar{u}_{ik}$ where k = 1,2, 3,4, the displacement assumption may be written as

$$u_i = \sum_{k=1}^{4} f_k \bar{u}_{ik} + K_I (Q_{1i} - \sum_{k=1}^{4} f_k \bar{Q}_{1ik}) + K_{II} (Q_{2i} - \sum_{k=1}^{4} f_k \bar{Q}_{2ik}) \quad (5.55)$$

where

$\bar{Q}_{1ik}$ = the value of Q_{1i} evaluated at node k

$f_k = \frac{1}{4}(1-aa_k)(1-bb_k)$

a_k, b_k = the coordinates of node k(± 1).

The terms in the parentheses in equation (5.55) account for the singularity.

To remove the incompatibility mentioned earlier Benzley altered the displacement assumption of equation (5.55) to

$$u_i = \sum_{k=1}^{4} f_k u_{ik} + R(a,b)\{K_I (Q_{1i} - \sum_{k=1}^{4} f_k \bar{Q}_{1ik}) + K_{II} (Q_{2i} - \sum_{k=1}^{4} f_k Q_{2ik})\} \quad (5.56)$$

Here, R(a,b) is set equal to a function of $\frac{1}{2}(1-aa_k)$ and/or $\frac{1}{2}(1-bb_k)$, such that it equals 1 on boundaries adjacent to 'enriched' elements (i.e. type A elements) and equals zero on boundaries adjacent to 'bilinear' elements (i.e. type C elements). Elements with the displacement assumption given in equation (5.56) are referred to as type B elements (see Fig. (5.5)).

The most interesting feature of this type of element is that the stress intensity factors are treated as unknowns in the same way as nodal displacements. Therefore on

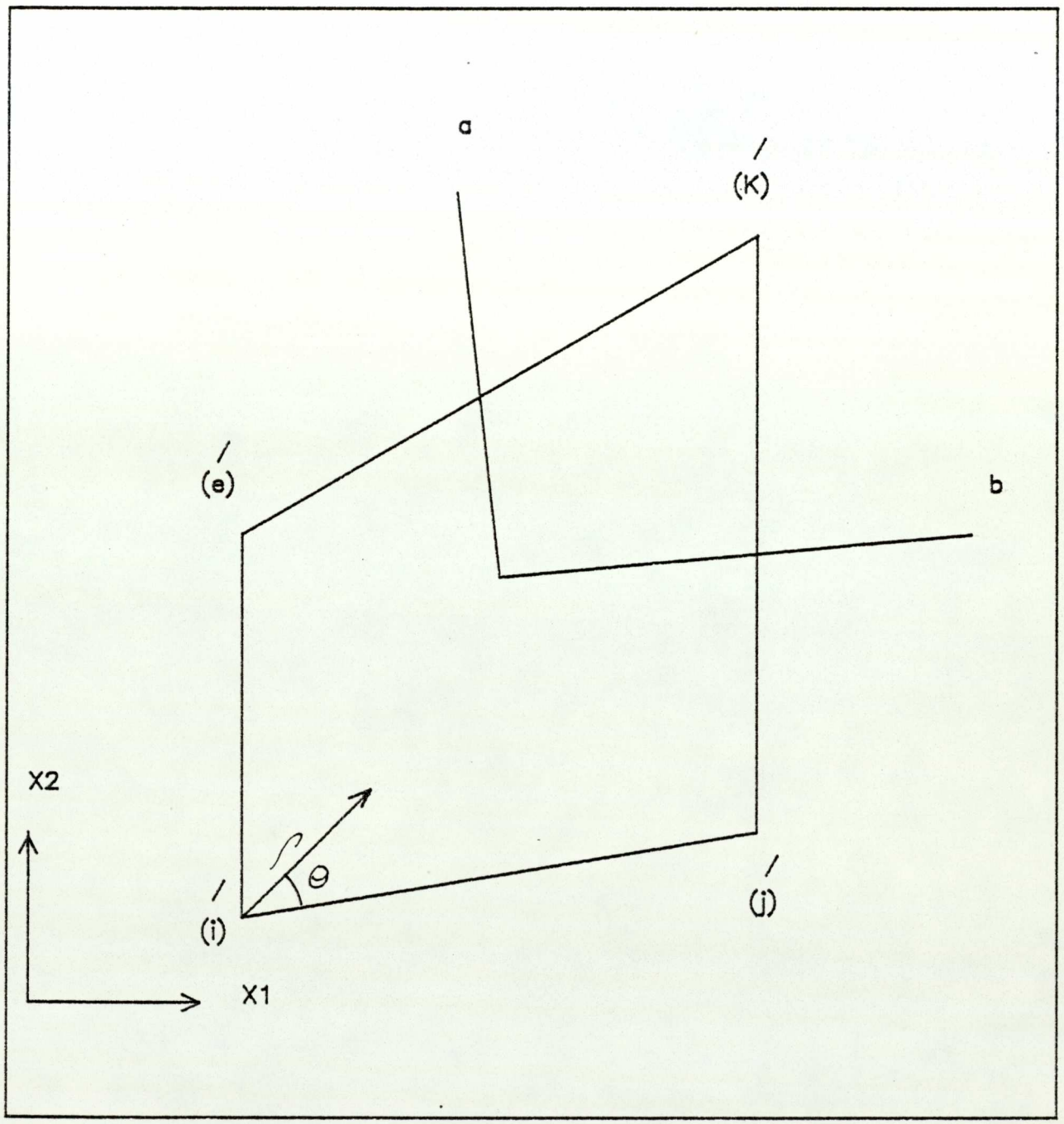

FIGURE (5.4) A QUADRILATERAL FINITE ELEMENT WITH A SINGULAR POINT AT NODE (i).

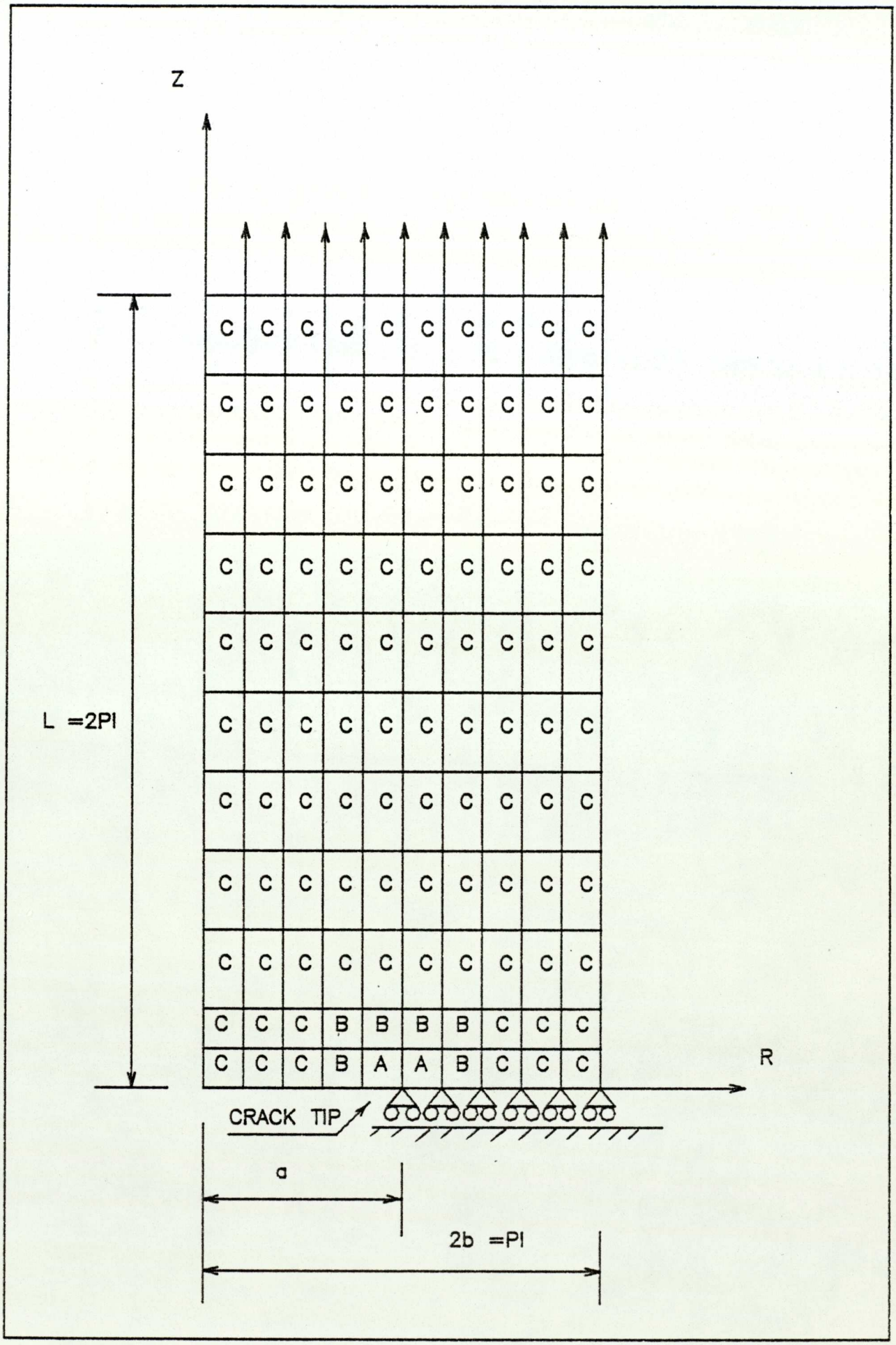

FIGURE (5.5) FINITE ELEMENT DEFINITION OF SIDE CRACKED PANEL.

solution the K values are printed out directly and no supplementary calculations and extrapolations are required.

(c) Elements Based on Analytical Solutions

In this approach the element is formulated so that the full crack field is represented and not just the crack tip singularity. This one element could then be used to model the crack affected zone in place of refined meshes at the crack tip. If this type of element truly represented the complete cracking field, it should be possible to specify the crack to anywhere within the element boundary. Crack extension could be permitted by merely redefining the crack tip position, so avoiding the generation of a new finite element mesh[61].

The element stiffness matrix is formulated using normal energy theorems but with the stress and displacement fields expressed in terms of mode I and II cracking coefficients which in turn can be related to the nodal displacements.

One obvious advantage of such an approach is that it combines the analytical solution, which is accurate near the crack tip but not remote from it, with the finite element solution, which is accurate remote from the crack tip but not, close to it.

The method was developed by Hilton and Hutchinson[50] to evaluate the elastic plastic stress intensity factors for mode I and III, and by Wilson[84] for elastic plastic

mode III. For the case of centrally cracked infinite plate under uniform applied tension, elastic mode I stress intensity factors were obtained with an accuracy of within 1% of the theoretical one.

Essentially the procedure involves the embedding of the singular solution into a finite element grid. As an example of the procedure, consider a centrally notched plate under axial mode I loading (Fig. (5.6)). By symmetry, only one quadrant of this plate is analysed, (Fig. (5.7)). A circular core of radius R_c is constructed around the crack tip together with the first ring of triangular or quadrilateral elements in position around the core.

The displacements within the core region are defined from equation

$$\left.\begin{aligned} u_x &= \frac{K_I}{4G}\left(\frac{r}{2}\right)^{\frac{1}{2}}\left[(2k-1)\cos\theta/2 - \cos 3\theta/2\right] + \delta x \\ u_y &= \frac{K_I}{4G}\left(\frac{r}{2}\right)^{\frac{1}{2}}\left[(2k+1)\sin\theta/2 - \sin 3\theta/2\right] \end{aligned}\right\} \qquad (5.57)$$

δx is the rigid body displacement of the core in the x-direction and constitutes one of the parameters to be determined from the solution of the problem.

In addition to specifying the displacement pattern within the core, equation (5.57) also represents constraints on those nodal points of the first ring of elements that fall on the circumference Γ_i.

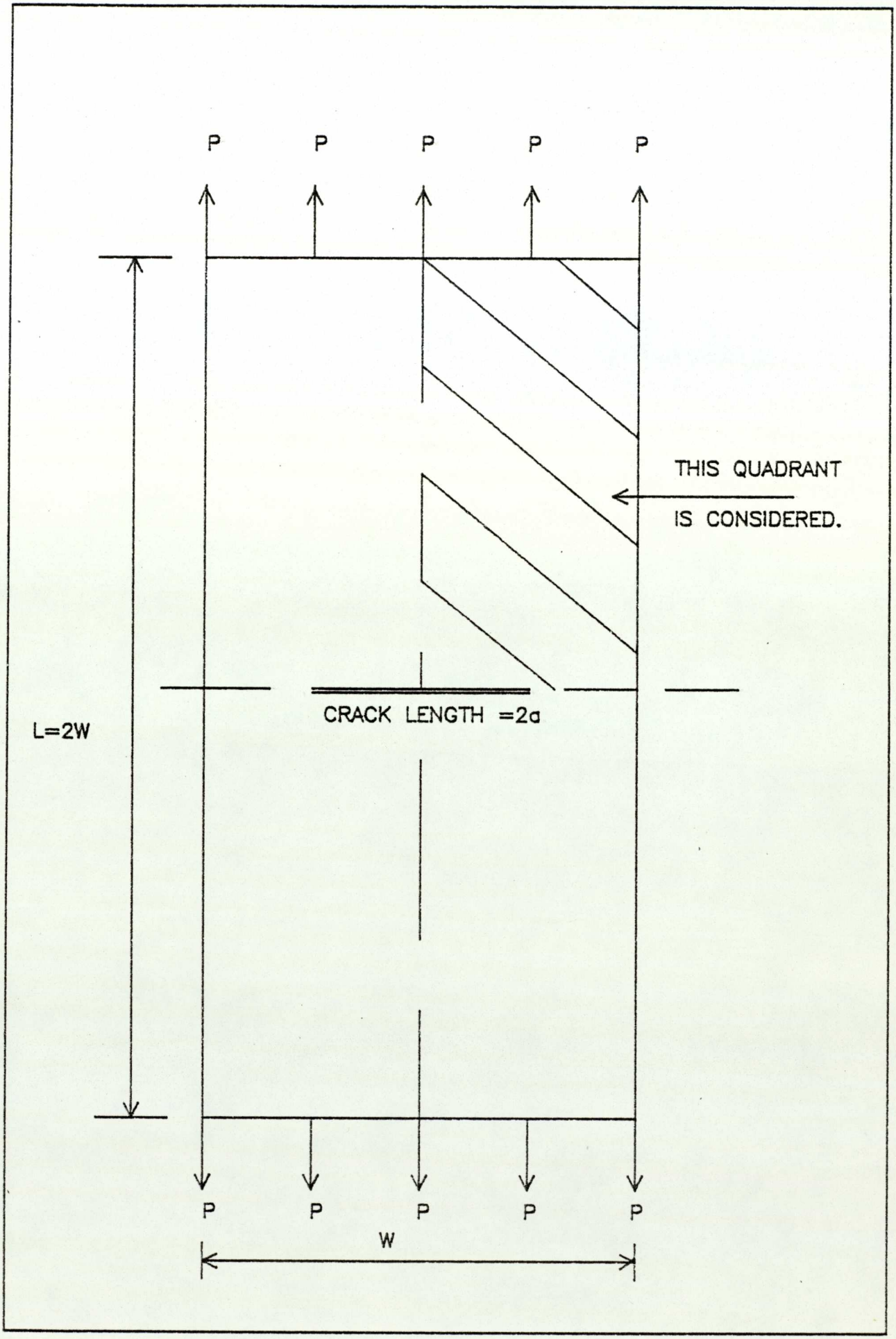

FIGURE (5.6) CENTRALLY NOTCHED PLATE UNDER AXIAL MODE I LOADING.

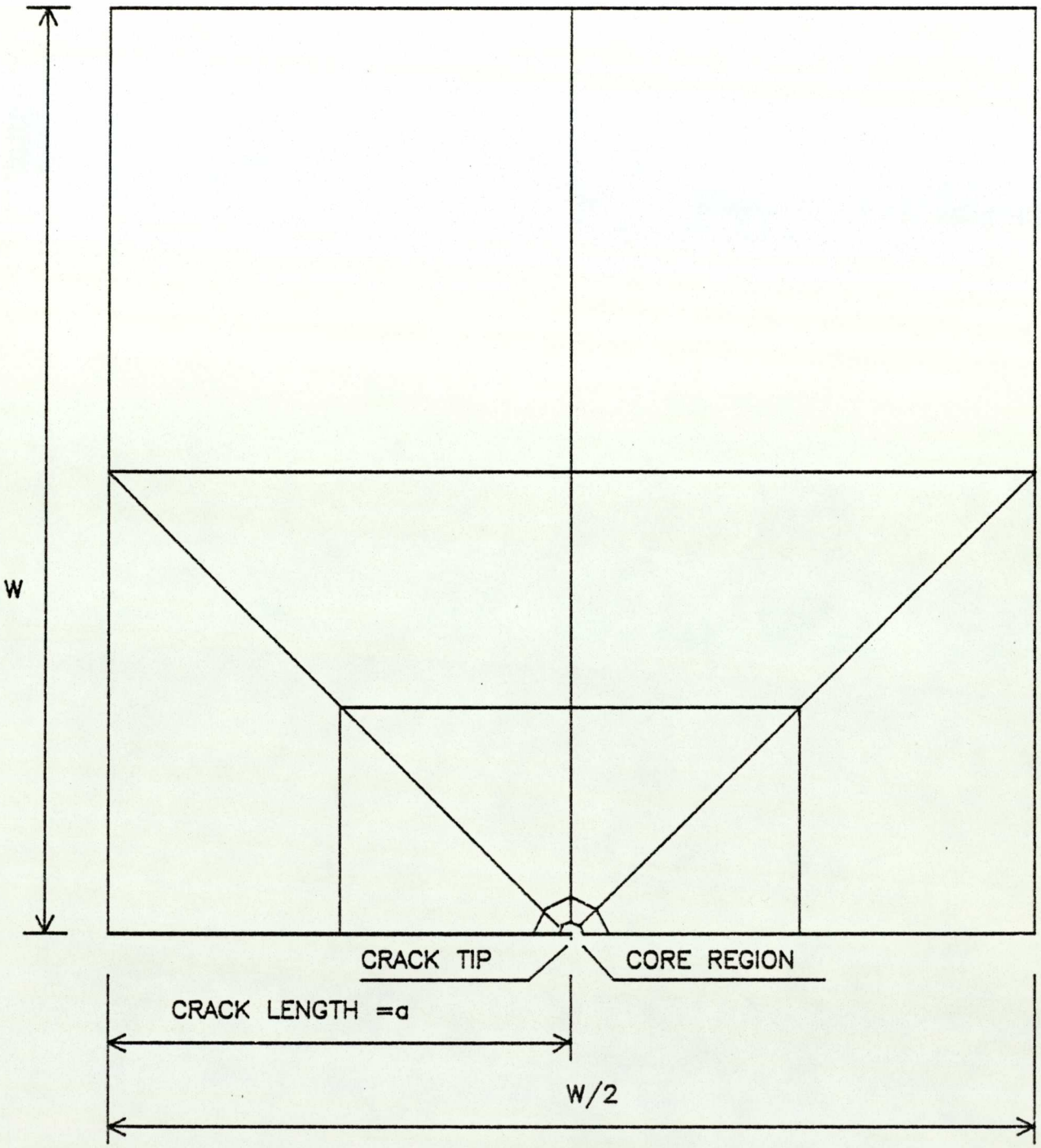

FIGURE (5.7) ONE QUARTER OF CENTRALLY NOTCHED PLATE UNDER AXIAL MODE I LOADING.

The potential energy of the quadrant is

$$pE = U_{core} + \sum_{el} SE - \int_{s} \bar{T}.\bar{u}\, ds \qquad (5.58)$$

where

U_{core} is the strain energy stored in the core

$\sum_{el} SE$ is the total strain energy stored in all the elements outside the core.

$\int \bar{T}.\bar{u} ds$ the work done by the surface traction vector $\bar{T}$ on the surface displacement vector $\bar{u}$.

The strain energy stored in the core

$$U_{core} = \int_{core} \frac{1}{2} \sigma_{ij} \varepsilon_{ij} \, dvol \qquad (5.59)$$

$$= \frac{K_I^2 R_c \pi}{32G} \qquad (5.60)$$

The stress intensity factor K_I and the rigid body displacement component δx therefore become generalised coordinates of the problem together with the nodal displacement u_i (at node i). The governing linear algebraic equations to be solved for u_i, K_I and δx are obtained by minimising the potential energy equation (5.58)

$$\left.\begin{aligned} &\frac{\partial(p\varepsilon)}{\partial K_I} = 0 \\ &\frac{\partial(p\varepsilon)}{\partial \delta x} = 0 \\ &\frac{\partial(p\varepsilon)}{\partial u_i} = 0 \qquad\qquad i = 1, 2, \ldots . N \end{aligned}\right| \qquad (5.61)$$

where N is the total number of unconstrained degrees of freedom. The nodes on the interface between the core and the first ring of elements are constrained by equation (5.57).

The continuity of displacement at the interface between the core and the neighbouring elements is not fully satisfied, compatibility is assumed only at the nodes, and hence monosonic convergence, to the exact solution cannot be expected. However, the number of nodes on the core-ring interface can be increased to reduce the discontinuity of displacements to an acceptable level.

The above procedure can be incorporated into a standard finite element program[15,67,68]. Modification of such program consists essentially of constraining the nodes on the first ring of elements surrounding the crack tip and adding equations which couple the stress intensity factors and rigid body modes of the core to the displacements of the second ring of elements, and thus through the remainder of the elements. The stress intensity factors are obtained

directly, together with the nodal displacements, as output from the program.

Richards and Robertson[62] developed this approach by using a 'circular core' region, surrounding the crack tip, embedded in an ordinary six node isoparametric triangle finite element mesh. Eight-node isoparametrix quadrilateral element was later used by Wood[15]. Within the core a displacement pattern, incorporating a rigid body mode and the usual near crack tip field, is assumed. Only minor changes to a standard finite element program are necessary. The values of the stress intensity factor are obtained directly along with the other finite element results.

The stress and displacement fields in the immediate neighbourhood of the crack tip are described by expressions of the type[60]

$$m\sigma_{ij} = K_m \, r^{-\frac{1}{2}} \, mf_{ij}(\theta) \qquad ij = 1, 2 \quad m = I, II, III$$

$$m\, u_i = K_m \frac{r^{\frac{1}{2}}}{G} \, mg_i(\nu,\theta) \qquad i = 1, 2 \quad m = I, II, III \tag{5.62}$$

where the $mf_{ij}(\theta)$ and $mg_i(\nu,\theta)$ are known functions and K_m is the stress intensity factors for the mth mode.

The functions $f_{ij}(\theta)$ and $mg_i(\nu,\theta)$ for mode I are:

$$If_{11} = \frac{1}{\sqrt{2}} \cos\theta/2(1-\sin\theta/2 - \sin 3\theta/2) \tag{5.63}$$

$$Ig_1 = \frac{\sqrt{2}}{8} |(2k-1)(\cos\theta/2 - \cos 3\theta/2)| \tag{5.64}$$

where

$k = 3-4\nu$ for plane strain

$k = 3-\nu/1+\nu$ for plane stress.

These equations correspond to the first term in a series expansion and describe the situation in the near tip field. Adequately to describe the situation further removed from this zone, it is necessary to retain more terms in the series[14]. A mixed mode situation may be described by a superposition of expressions of the form of equations (5.62).

The advantages of this method could be stated as the following

(1) The simplicity of incorporating the core element within a standard finite element program.

(2) The stress intensity factors K_I and K_{II} and K_{III} are obtained directly.

(3) Separation of K_I and K_{II} for combined mode analysis.

(4) Possibilities of extending this method to elastic-plastic, plastic cases, and other material properties.

(d) Superposition Method

This is one of the methods used to solve a problem with a singularity, by the linear combination of a classical solution for the singular fields, and a non-singular finite element analysis. In this case a solution for a crack in an infinite plate is chosen to represent a crack in a finite specimen. This analytic solution will not satisfy the boundary conditions existing on the periphery of finite region. These boundary discrepancies can be calculated from the correct boundary values, as given by the non-singular finite element analysis, and then applied as nodal forces in the reverse direction on the analytic solution to produce the final solution.

Since the elements formulated in the last method produce good results, and were formulated using analytical solutions, they are also used here as a superposition scheme. The zone of the singular function to be used in the superposition method can vary from one element only up to the entire finite element mesh. Further details of this method are found in reference (53).

The present formulation is limited to cracks occurring along the edge of elements, since standard isoparametric elements are incapable of representing cracks through their interior.

The superposition method is one of the most common

and simplest techniques in use for obtaining stress intensity factors. Complex configurations are considered to a combination of a number of separate simpler configurations with separate boundary conditions and which have known stress intensity factors. The stress intensity factors for the simple configuration are then added together to obtain the required solution[65].

(e) Mixed and Hybrid Elements

Most of the finite elements developed in the field of structural and solid mechanics are those which are based on the assumed displacement fields and the principle of minimum potential energy. In this formulation, the field variables are the element displacements. Similarly, the principle of minimum complementary energy based on the assumed stresses as field variables instead of the displacements in the minimum potential energy. In the equilibrium element models, the nodal values of stresses or forces are treated as the primary unknowns of the discretised structure. The stress field is selected such that internal equilibrium is satisfied with continuous stress transmission between elements. In the principle of stationary Reissner energy[54], both displacements and stresses are treated as field variables. The application of this principle results in finite element formulations known as 'mixed finite element models'.

The three basic variational principles mentioned above can be modified to derive additional finite element formulations with the aim of improving the accuracy and efficiency of the finite element discretisation. "Hybrid finite element models" are obtained if an addition to one field variable like displacements or stresses, Other variable like stress or displacement are introduced and the parameters that correspond to the additional variables are eliminated at the element stage before assembling the element equations[54].

RAO et al.[18] suggested a possibility to overcome difficulties of convergence by developing a hybrid technique combining continuum and finite element concepts. In such techniques, each region of stress concentration is covered by one large "primary element" whose description includes term(s) identifying the type and order of concentration, while the remaining structure is split into a few "secondary elements" which are conventional finite elements.

A special super-element was used by Pin Tong et al.[75] which was used jointly with conventional finite elements for the analysis of elastic stress intensity factors for plane cracks. This super-element has been developed for the crack tip region based on the assumed stress hybrid model. The singular terms included in such a development involve only those stress terms which are proportional to $\frac{1}{\sqrt{r}}$. The results obtained shows that by the use of such a

super-element, an accurate assessment of the stress intensity factor can be achieved by using much smaller number of degrees of freedom than using only conventional finite elements. Using conventional elements like that used by Anderson et al[42], with 1500 degrees of freedom, the error of their solutions for K_I is of the order of 5 per cent. Byskov [85] and Tracey [48] employed special elements at the crack tip to include the effect of the stress singularity. Yet, by using around 500 degrees of freedom, the errors of their solutions for K_I are still around 3 per cent. By using the assumed stress hybrid approach 5 per cent error was obtained using only 70 degrees of freedom, and when 194 degrees of freedom were used the error reduced to 0.5 per cent.

(9) The Boundary Element Method

The term 'Boundary Element' originated within the department of Civil Engineering at Southampton University. It is used to indicate the method whereby the external surface of a domain is divided into a series of elements over which the functions under consideration can vary in different ways, in much the same manner as in finite elements[56]. One of the interesting features of the method is the smaller system of equations and considerable reduction in the data required to run a problem, particularly in, two- and three-dimensional problems. This is because the n-dimensional mesh is used for (n+1) dimensional problems[55].

In the boundary element mehod, a trial function is chosen in such a manner, that the differential equations are satisfied throughout the domain. Only the boundary conditions have to be approximated[77].

Rudulphi[78] have used the method for crack problems where equations of the boundary element method and of a stressed semi-infinite crack in an infinite plane are combined to formulate the solution to the finite edge cracked plate. The coupled integral equations are solved numerically by the form of the boundary element method and by Gaussian quadrature.

Value for Mode I Stress Intensity Factor for a doubly edge cracked rectangular plate in tension, where the length of the edge crack is half the plate width, was 1.12% less than that obtained by Tada et al.[64] using the expression

$$F(a/b) = (1+0.22 \cos^4 \frac{\pi a}{2b}) \sqrt{\frac{2b}{\pi a} \tan \frac{\pi a}{2b}}$$

where $F(a/b) = K_I \sigma_o \sqrt{\pi a}$

where

a is the edge crack length

b is half the plate width.

Drawbacks of this method is its greater mathematical complexity and the necessity of having an analytical solution as a starting point[55].

5.3 FINAL REMARKS

The methods described in this chapter have been developed over the last thirty-five years. They contributed to the solutions of a large number of problems. Providing that a computer is available, the numerical methods for evaluating stress intensity factors are sufficiently well developed to enable most problems to be solved in two-dimensions. The finite element method shows the greatest potential for solving three-dimensional problems. It has the highest growth rate.

The choice of a means of evaluating the stress intensity factors will often depend on the following[65]:

(1) The time available.

(2) The required accuracy.

(3) The cost.

(4) The use (once or many times).

(5) How simply the real structure can be modelled.

For simple geometrical solutions, or where a complex structure can be simply modelled, it may be possible to use one of the reference books[57,37,64]. Many other solutions are available, for instance, in the series of special technical publications, published by A.S.T.M., in the series entitled'fracture', edited by Liebowitz[36], and the series entitled'Mechanics for fracture'edited by Sih[66]. The methods both experimental and theoretical have also been

reviewed by Cartwright and Rooke[17], Liebowitz, Vol. II of Reference (36), Sih, Vol. I of Reference (66).

Generally, the experimental techniques are less accurate. The finite element method may contain errors of up to 6% depending on the computational effort employed. These errors are obtained compared with analytical solutions available[63].

CHAPTER 6

THE FINITE ELEMENT METHOD RELATED TO FRACTURE MECHANICS

Fracture mechanics is concerned with the phenomenon of structural failure by catastrophic crack propagation at average stresses well below the yield strength.

One approach to the prediction, and hence prevention of such failures is based on stress intensity factors which define the magnitude of the singularities in the stress field which occur in a linear elastic analysis of a structural component with an infinitely sharp notch. Methods for the determination of the stress intensity factors are numerous as described in Chapter 5. The finite element method is among these methods, its use in fracture mechanics has been quite extensive both in the elastic and elastic-plastic range.

The finite element method of interest here is the Hilton and Hutchinson method[50] as it has been described in Chapter 5, was originally applied to the calculation of Mode I and Mode III plastic stress intensity factors and by Wilson[76] for problems of out of plane shear, Mode III.

Essentially the procedure involves the embedding of the singular solution into a finite element mesh. A 'core'

element is used, surrounding the crack tip region. The core is constrained to match the finite nodal displacements on its boundary. The method of Lagrange multipliers, as used by Richards[60], is employed to formulate the stiffness equations.

The purpose of this chapter is to illustrate the Richards/Robertson[63] formulation to accommodate the Hilton Hutchinson core, in the general finite element program developed by Robertson[67]. This program has been adopted in solving crack problems during this work. The program, including the modification, was done originally in Algol Language. It has been translated to Basic Language during the course of this work, to suit the HP9845 Desk-Top Computer available in the department.

A complete detail of the necessary modification and reconstruction of the stiffness matrix $[K]$, is to be found in Reference (15). It is felt that it is necessary to outline the important procedures in the formulation of this method as it has been executed by Richards/Robertson.[63]

In the stiffness finite element analysis of structural problems, a displacement field local to an element is assumed in the form

$$\{u\}^e = [N(x_i)]\ \{u\}_o^e \qquad (6.1)$$

where

$[N(x_i)]$ is an interpolation matrix, and

$\{u\}_o^e$ is a vector of nodal displacement.

Using the strain displacement relation equation (6.1) becomes

$$\{\varepsilon\}^e = [\partial][N]\{u\}_o^e = [B]\{u\}_o^e \tag{6.2}$$

The strain energy of an element may be written as

$$U_e = \frac{1}{2}\int \{\sigma\}^t\{\varepsilon\}\ \text{dvol} \tag{6.3}$$

where

$\{\sigma\}$ is the stress vector

$\{\varepsilon\}$ is the strain vector.

Using the stress-strain relation $\{\sigma\} = [D]\{\varepsilon\}$ (6.4)

equation (6.3) becomes

$$U_e = \frac{1}{2}\{u\}_o^{e^t}\left(\int [B]^t[D][B]\ \text{dvol}\right)\{u\}_o^e \tag{6.5}$$

which yields

$$U_e = \frac{1}{2}\{u\}_o^{e^t}[K]\{u\}_o^e \tag{6.6}$$

where

$$[K]_e = \int [B]^t[D][B]\text{dvol} \tag{6.7}$$

is the element stiffness matrix.

Summing up the contribution of all the elements surrounding the core in the discretised structure, the total strain energy becomes

$$U = \frac{1}{2} \{q\}^t [K]\{q\} \tag{6.8}$$

where

$\{q\}$ is the generalised coordinates replaces the local coordinates $\{u\}_o^e$, and $[K]$ is the stiffness matrix for the whole structure, except the core region.

In a cracked configuration such as that in Fig. (6.1) where a core region is identified surrounding the crack tip. The near tip displacement components can be described in the form

$$u_i = \Sigma\ K_m\ (r^{\frac{1}{2}}/G)_m g_i(\nu,\theta) + \bar{u}_i + \omega h_i(r,\theta) \tag{6.9}$$

where the displacements are augmented by rigid body translations and rotations $\bar{u}_i$, $\omega h_i(r,\theta)$.

The above may be expressed in a matrix form

$$\{u\}_c = [N]_c\{\alpha\} \tag{6.10}$$

where

$[N]_c$ comprises a shape function for the core and $\{\alpha\}$ is a vector of core generalised coordinates which include the stress intensity factors explicitly together with the rigid body modes.

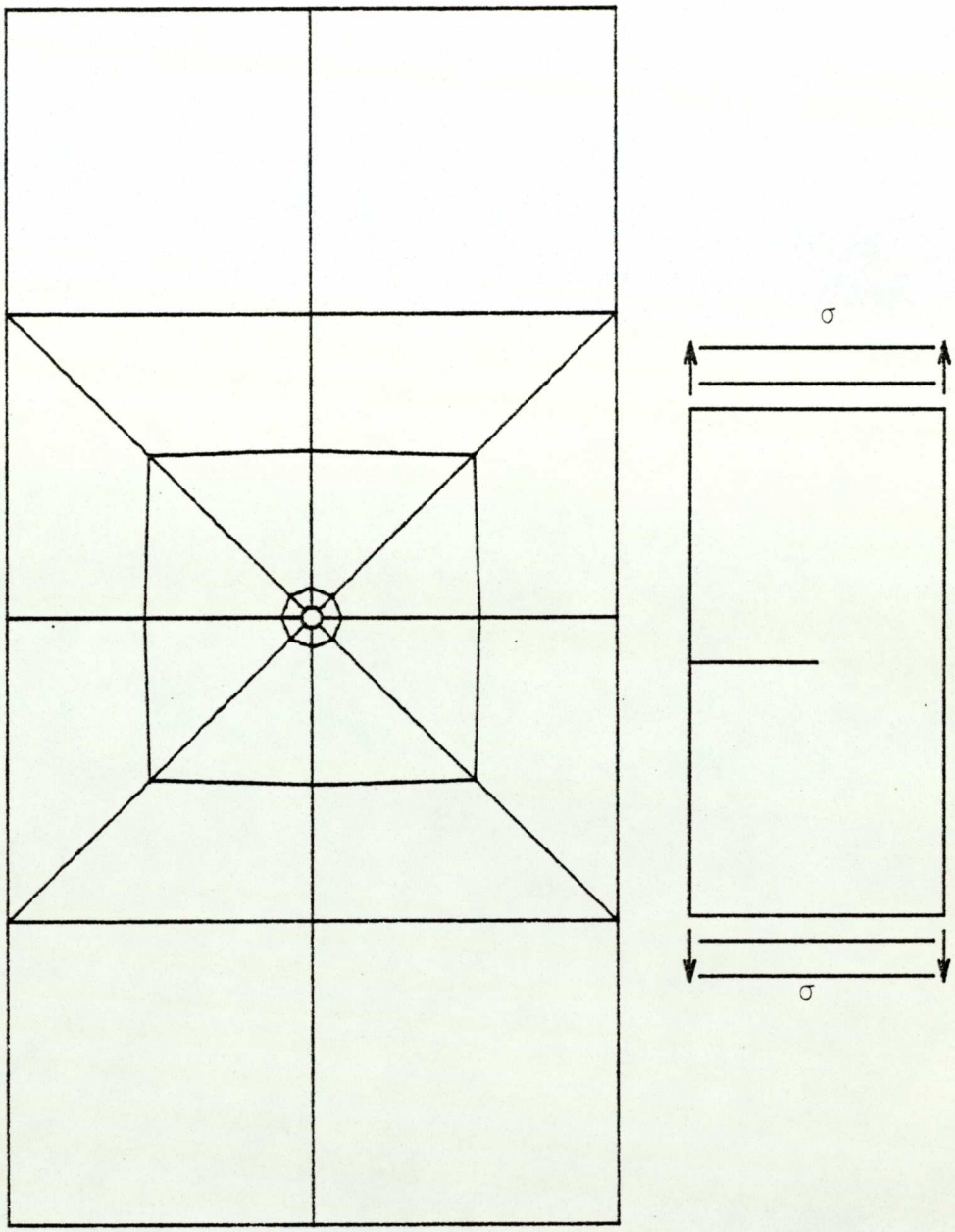

FIGURE (6.1) A PLATE WITH A 90° SINGLE–EDGE–CRACK, IN TENSION, WHERE A CORE REGION IS IDENTIFIED SURROUNDING THE CRACK TIP.

The strain energy of the core region may be written as

$$U_c = \frac{1}{2} \int_{core} \{\sigma\}^t \{\varepsilon\} \, dvol \tag{6.11}$$

again using the core stress-strain relation

$$\{\sigma\} = [D] \{\varepsilon\}$$

$$U_c = \frac{1}{2} \int \{\varepsilon\}^t [D] \{\varepsilon\} \, dvol \tag{6.12}$$

from equation (6.10)

$$\{\varepsilon\} = [B]_c \{\alpha\} \tag{6.13}$$

equation (6.12) becomes

$$U_c = \frac{1}{2}\{\alpha\}^t (\int [B]_c^t [D]_c [B]_c \, dvol) \{\alpha\} \tag{6.14}$$

$$U_c = \frac{1}{2}\{\alpha\}^t [K]_c \{\alpha\}$$

where

$$[K]_c = \int [B]_c^t [D]_c [B]_c \, dvol \tag{6.15}$$

The total potential energy of the plate i.e.

$$V = \frac{1}{2}\{\alpha\}^t [K]_c \{\alpha\} + \frac{1}{2}\{q\}^t [K] \{q\} - \{q\}^t \{Q\} \tag{6.16}$$

where $[K]$ is the stiffness matrix of the mesh surrounding the core, $\{q\}$ is the nodal displacement and $\{Q\}$ is the force vector.

The displacements of nodes on the mesh-core interface boundary can be expressed as a function of the unknown αs

$$\{u\}_c = \left\{ \begin{matrix} \{u_1\}_c \\ \{u_2\}_c \\ \cdot \\ \cdot \\ \cdot \\ \cdot \end{matrix} \right\} = \left| \begin{matrix} [N_1]_c & \{\alpha\} \\ [N_2]_c & \{\alpha\} \\ \cdot & \cdot \\ \cdot & \cdot \\ \cdot & \cdot \\ \cdot & \cdot \end{matrix} \right| = \bar{[A]} \{\alpha\} \qquad (6.17a)$$

where

$\{u_1\}_c$ refers to interface node 1, and

$\{u_2\}_c$ refers to interface node 2 , ... etc.

Partitioning $\{q\}$ into $\{q_1\}$ and $\{q_2\}$ corresponding to nodes on and outside the interface respectively, then for compatibility at the interface nodes

$$\{u\}_c = [\bar{A}] \{\alpha\} = [C]_{int} \{q_1\} \qquad (6.17b)$$

$$\{q_1\} = [C]^{-1}_{int} [\bar{A}] \{\alpha\} = [A] \{\alpha\} \qquad (6.18)$$

Using the Lagrange multiplier method to enforce continuity of displacement at the core and the finite elements, the modified potential energy $\bar{V}$ is given by

$$\bar{V} = \frac{1}{2}\{\alpha\}^t [K]_c \{\alpha\} + \frac{1}{2}\{q\}^t [K] \{q\} - \{q\}^t \{Q\} + (\{q_1\} - [A]\{\alpha\})^t \{\lambda\} \qquad (6.19)$$

Partitioning $\{Q\}$ and $[K]$ to correspond to q_1 and q_2

$$\{Q\} = \begin{Bmatrix} \{Q_1\} \\ \{Q_2\} \end{Bmatrix}$$

$$[K] = \begin{bmatrix} [K_{11}] & [K_{12}] \\ [K_{21}] & [K_{22}] \end{bmatrix} \qquad (6.20)$$

For equilibrium

$$\delta \bar{V} = 0$$

$$\delta\bar{V} = 0 = \{\delta\alpha\}^t[K]_c\{\alpha\} + \{\delta q\}^t[K]\{q\} - \{\delta q\}^t\{Q\}$$

$$+ (\{\delta q_1\} - [A]\{\delta\alpha\})^t \{\lambda\} \qquad (6.21)$$

The above equation may be written as:

$$\begin{aligned} 0 = {} & \{\delta\alpha\}^t([K]_c\{\alpha\} - [A]^t\{\lambda\}) \\ & + \{\delta q_1\}^t([K_{11}]\{q_1\} + [K_{12}]\{q_2\} - \{Q_1\} + \{\lambda\}) \\ & + \{\delta q_2\}([K_{21}]\{q_1\} + [K_{22}]\{q_2\} - \{Q_2\}) \end{aligned} \qquad (6.22)$$

Since $\{\delta\alpha\}$, $\{\delta q_1\}$ and $\{\delta q_2\}$ are arbitrary, equation (6.22) yields three simultaneous matrix equations of equilibrium

$$[K]_c\{\alpha\} - [A]^t\{\lambda\} = 0 \tag{6.23}$$

$$[K_{11}]\{q_1\} + [K_{12}]\{q_2\} - \{Q\} + \{\lambda\} = 0 \tag{6.24}$$

$$[K_{21}]\{q_1\} + [K_{22}]\{q_2\} - \{Q_2\} = 0 \tag{6.25}$$

multiplying equation (6.24) by $[A]^t$ and combining with equation (6.23), yields:

$$[A]^t[K_{11}]\{q_1\}+[A]^t[K_{12}]\{q_2\}+[K]_c\{\alpha\}-[A]^t\{Q_1\} = 0 \tag{6.26}$$

Replacing vector $\{q_1\}$, results in the final expressions

$$\begin{aligned} &([K]_c+[A]^t\,[K_{11}]\,[A])\{\alpha\}+[A]^t[K_{12}]\{q_2\}-[A]^t\{Q_1\} = 0 \\ &[K_{21}]\,[A]\;\{\alpha\} \qquad\qquad +[K_{22}]\{q_2\} \quad - \{Q_2\} \quad = 0 \end{aligned} \tag{6.27}$$

The above equations can be represented in one modified form

$$[\overset{*}{K}]\{\overset{*}{q}\} = \{\overset{*}{Q}\} \tag{6.28}$$

where

$$[\overset{*}{K}] = \begin{bmatrix} [\overset{*}{K}_{11}] & [\overset{*}{K}_{12}] \\ [\overset{*}{K}_{21}] & [\overset{*}{K}_{22}] \end{bmatrix} \tag{6.29}$$

$$\{\overset{*}{q}\} = \begin{Bmatrix} \{\overset{*}{q}_1\} \\ \\ \{\overset{*}{q}_2\} \end{Bmatrix} \tag{6.30}$$

$$\{\overset{*}{Q}\} = \begin{Bmatrix} \{\overset{*}{Q}_1\} \\ \\ \{\overset{*}{Q}_2\} \end{Bmatrix} \tag{6.31}$$

with

$$\begin{aligned} [\overset{*}{K}_{11}] &= [K_{22}] \\ [\overset{*}{K}_{12}] &= [\overset{*}{K}_{21}]^t = [K_{21}][A] \\ [\overset{*}{K}_{22}] &= [K]_c + [A]^t [K_{11}][A] \\ \{\overset{*}{Q}_1\} &= \{Q_2\} \\ \{\overset{*}{Q}_2\} &= [A]^t \{Q_1\} \end{aligned} \tag{6.32}$$

so that

$$[\overset{*}{K}] = \begin{bmatrix} [K_{22}] & [K_{21}][A] \\ \\ [A]^t [K_{12}] & [K]_c + [A]^t [K_{11}][A] \end{bmatrix} \tag{6.33}$$

and the generalised coordinates:

$$\{\overset{*}{q}\} = \begin{Bmatrix} \{q_2\} \\ \\ \{\alpha\} \end{Bmatrix} \tag{6.34}$$

and the force vector:

$$\{\overset{*}{Q}\} = \begin{Bmatrix} \{Q_2\} \\ \\ [A]^t\{Q_1\} \end{Bmatrix} \tag{6.35}$$

The partitioning of the original matrix equation and the construction of the modified stiffness equations are shown in Fig. (6.2) and Fig. (6.3) for Mode I case, give an indication of the manipulations required in combining the core and finite element system.

Once the modified stiffness matrix and load vector have been obtained, the solution of the simultaneous equations is carried out in the normal manner to give the values of $\{q_2\}$ throughout the mesh and the core variables $\{\alpha\}$.

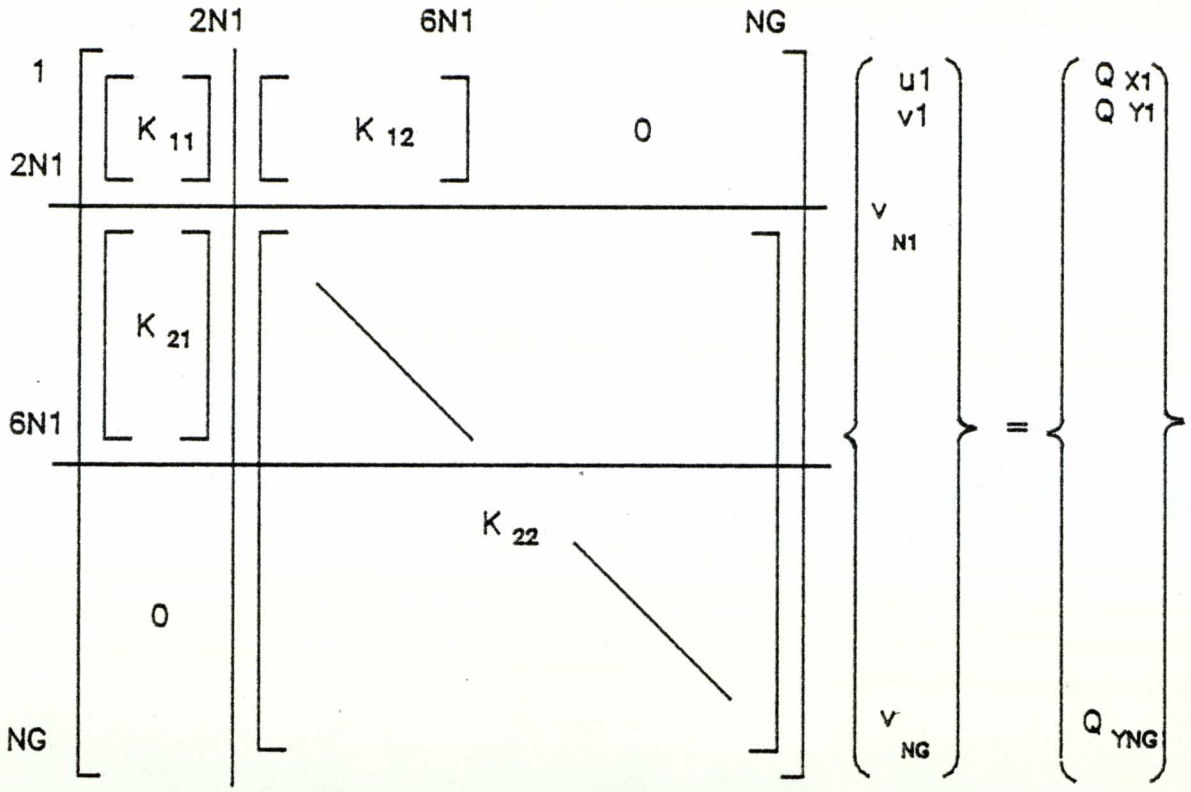

FIGURE (6.2) PARTITIONING OF STIFFNESS MATRIX,[K].

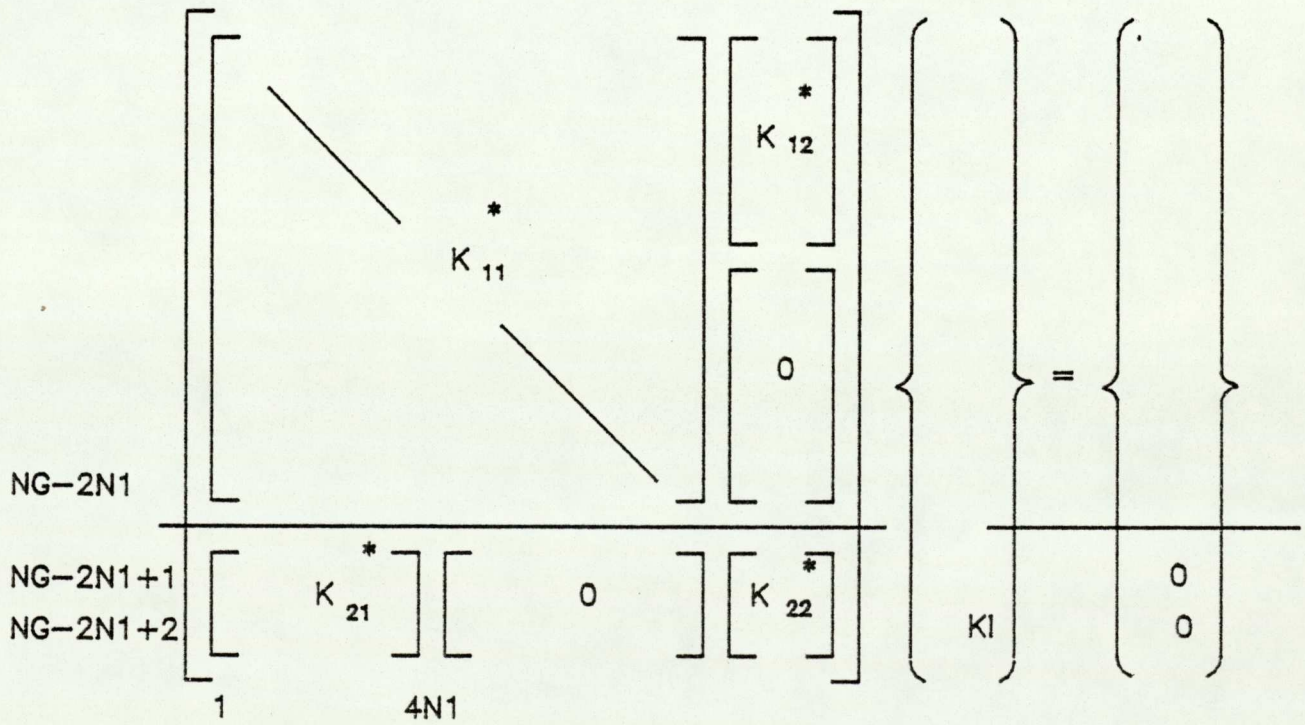

FIGURE (6.3) CONSTRUCTION OF STIFFNESS MATRIX,[K*].

CHAPTER 7

NUMERICAL EXAMPLES FOR THE CRACK PROBLEMS

7.1 INTRODUCTION

This chapter deals with the numerical examples regarding fracture mechanics. Applying different programs which fall under two categories. The first consists of programs concerned with Mode I and mixed-mode plane stress/strain fracture problems, which were originally developed by Robertson[67], and have been augmented by Wood[15]. The second consists of a program which deals with Mode I axisymmetric fracture problems, which has been developed by Al-Sharqi[68]. All these programs with their relevant procedures were written originally in ALGOL Language and run in the Computer Centre at Aston University by the forementioned research students.

The plane stress/strain Mode I and mixed-mode fracture programs employ the Hilton and Hutchinson element[50], and the crack tip as it has been described in Chapter 6, and Section 5.2.3 with a choice of either triangular or quadrilateral isoparametric element around the core element throughout the mesh. These programs with all the necessary procedures have been implemented on the HP 9845 Desk-Top Computer during the preparation of this thesis.

All the programs with the relevant procedures, for Mode I and mixed-mode fracture problems, are fully explained, and listed with their flow charts in references (15) and (67).

The mesh design adopted by Robertson[67] was forming a finely graded element distribution around the core, so that the rapid stress changes, in this region, can be accurately interpreted. A series of tests were carried out by Robertson[67] to find out the influence, of core radius/crack length ratio, and that of the number of nodes on the mesh/core interface, on the values of the stress intensity factors. He found that the core radius R_c within the limits $a/30<R_c<a/50$ gave the best results, also that a minimum number of core/mesh interface nodes to be 17 or 19 produced accurate results.

Wood[15] substituted using the finely graded element around the core by using one ring of special isoparametric elements, which is constructed to sense the crack tip singularity. These elements have been termed 'Transition' elements. They are described in Section 7.2.

Example 1 illustrates the application of Mode I fracture program 'FMODIA', by considering a plate with a 90^{o} single-edge-crack in uniform tension. In this example only half the plate is used due to symmetry. The value of K_I is found and compared with a known value for the same problem found in the literature.

Because of the problem of Integer Precision Overflow by the HP 9845 Desk-Top Computer during the execution of the mixed-mode program 'PCPOY' for example 3, which consists of a plate with a central crack inclined at 45^{o}, no solution was obtained. As a result, the sample problem used in example 1 is repeated in example 2, as a mixed-mode fracture problem, to demonstrate the working order of the mixed-mode fracture program 'PCPOY' and to check the accuracy of the value of K_I and K_{II}.

The axisymmetric Mode I fracture program, 'AXYMD1' with its procedures, were developed by Al-Sharqi[68], and have been translated to BASIC from ALGOL Language during the preparation of this thesis. In this case, the mesh generated by a semi-automatic data input as was originally developed. Example 4 of a round bar with circumferential crack was chosen to illustrate the application of the program 'AXYMD1', using two meshes. Values of calculated K_I compared to that of values available in the literature for the same configuration.

7.2 TRANSITION ELEMENTS

The 'transition' element has been adopted from the method proposed by Lynn and Ingraffea[83], where they have shown that, by variable placement of the side-node between quarter- and mid-point in an isoparametric element, the point of singularity sensed by the element can be controlled.

Considering a one-dimensional element which may form a side of an 8-noded isoparametric element, as shown in the diagram below:

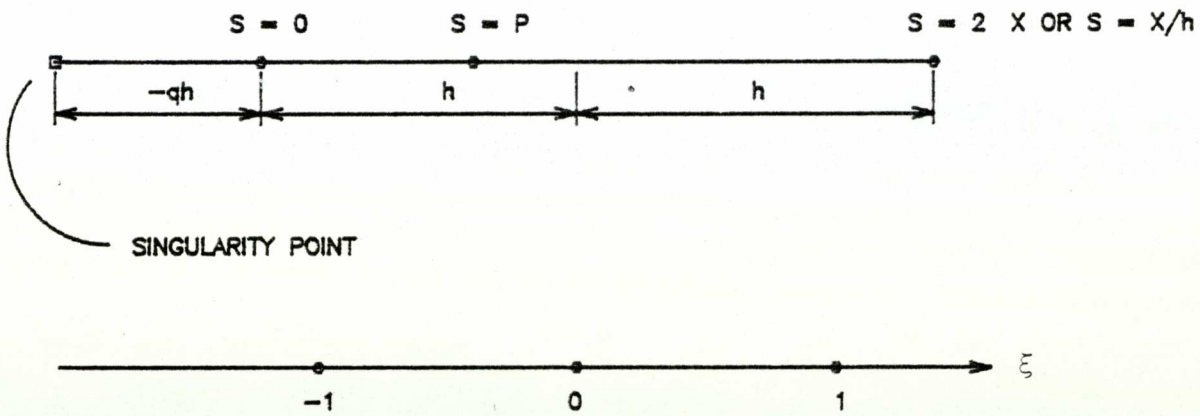

ELEMENT CO-ORDINATE MAPPING.

The three nodes of this element shown above, designated by the non-dimensional variable s = 0, p and 2, have been mapped to ξ = -1, 0 and +1 on the ξ scale respectively.

The transformation is accomplished in general by the following quadratic equation

$$s = c_1 + c_2\xi + c_3\xi^2 \qquad (7.1)$$

substitution of s and ξ nodal values into equation (7.1) gives three simultaneous equations from which c_1, c_2 and c_3 could be derived to be $c_1 = p$, $c_2 = 1$ and $c_3 = 1-p$.

Referring to equation (7.1) and solving for ξ then

$$\xi = \frac{-1+\sqrt{[1-4(1-p)(p-s)]}}{2(1-p)} \qquad (7.2)$$

and

$$\frac{d\xi}{ds} = \frac{1}{\sqrt{[1-4(1-p)(p-s)]}} \tag{7.3}$$

In the isoparametric element the displacement is represented in an analogous manner, using the form of equation (7.1) it has been shown[49] that the vanishing of the quantity under the radical sign of equation (7.3) is responsible for the stress singularity. So the desired singularity occurs when

$$s = p - \frac{1}{4(1-p)} \tag{7.4}$$

The singularity point may be located outside of the element, this depends on the position of the mid-side node. On setting $s = -q$ in equation (7.4) and solving for p, we find

$$p = \frac{(1-q) \pm \sqrt{q^2+2q}}{2} \tag{7.5}$$

Equation (7.5) relates the location, p, of the element side node to the point, q, outside the element domain, at which the singularity is sensed.

Lynn and Ingraffea[83] have found that the 'transition' elements produce an acceptable error bound of ±4 per cent whereas without these elements a larger error may be introduced.

7.3 EXAMPLE 1 - A PLATE WITH A 90° SINGLE-EDGE-CRACK IN TENSION

Dimensions of plate: As shown in Fig. (7.1)

$L = 10$, $w = 5$, $a = 2.5$, $a/w = 0.5$

Thickness of plate = 1

Applied Load $\sigma = 12000$ lbf/in^2

Core Radius $R_c = 0.083$

Number of nodes on the finite element mesh/core interface $N_1 = 9$

Material Properties:

$E = 3 \times 10^7$

$G = 1.2 \times 10^7$

$\nu = 0.3$

This is the simplest example of crack configuration, of a plate with a 90° single-edge-crack in uniform tension, Fig. (7.1). From symmetry, only one half of the plate is considered. A zone pattern is established as seen in Fig. (7.2) and Fig. (7.4a), also element sub-division is shown in Fig. (7.3) and Fig. (7.4b). The mesh is generated according to the user guide for mesh generation program in Appendix (A). As this program involves Mode I fracture, the program code used in the mesh generation is 2. Total number of zones used, not including the two void zones 9 and 12, and the standard generated zones around the core element, 1, 2, 3 and 4, are 6. In this example, the

procedure 'COREGEN' in the mesh generation program has been used, to construct the special 'Transition' elements around the core element. DATAFILE# 2 is generated as an output from the mesh generation program. This is used in the Mode I Fracture Program, 'FMODIA'. Full details of this program are found in Reference (67).

Because of symmetry, and since only one half of the plate is used, a core region configuration is used as that shown in Figs. (7.5a) and (7.6a).

The problem is of plane strain. In the first run, the element used is the 8-node isoparametric quadrilateral element with semi-circular core element surrounded by half a band of 'Transition' elements, as shown in Fig. (7.5a). The final structural idealization diagram of half the plate considered is shown in Fig. (7.8) as a graphic output using the 9872A x-y plotter in conjunction with the HP 9845 Desk-Top Computer, employing the mesh generation program.

In the second run for this problem, a different mesh is employed using the 6-node isoparametric triangular element. Although the structure is divided into the same number of zones, the element mesh is different to that of the first run. Core region construction is shown in Fig. (7.6a) and the final structural idealization diagram is shown in Fig. (7.9).

The total number of nodes used in run one using the 8-node quadrilateral element is 59, and the value of the

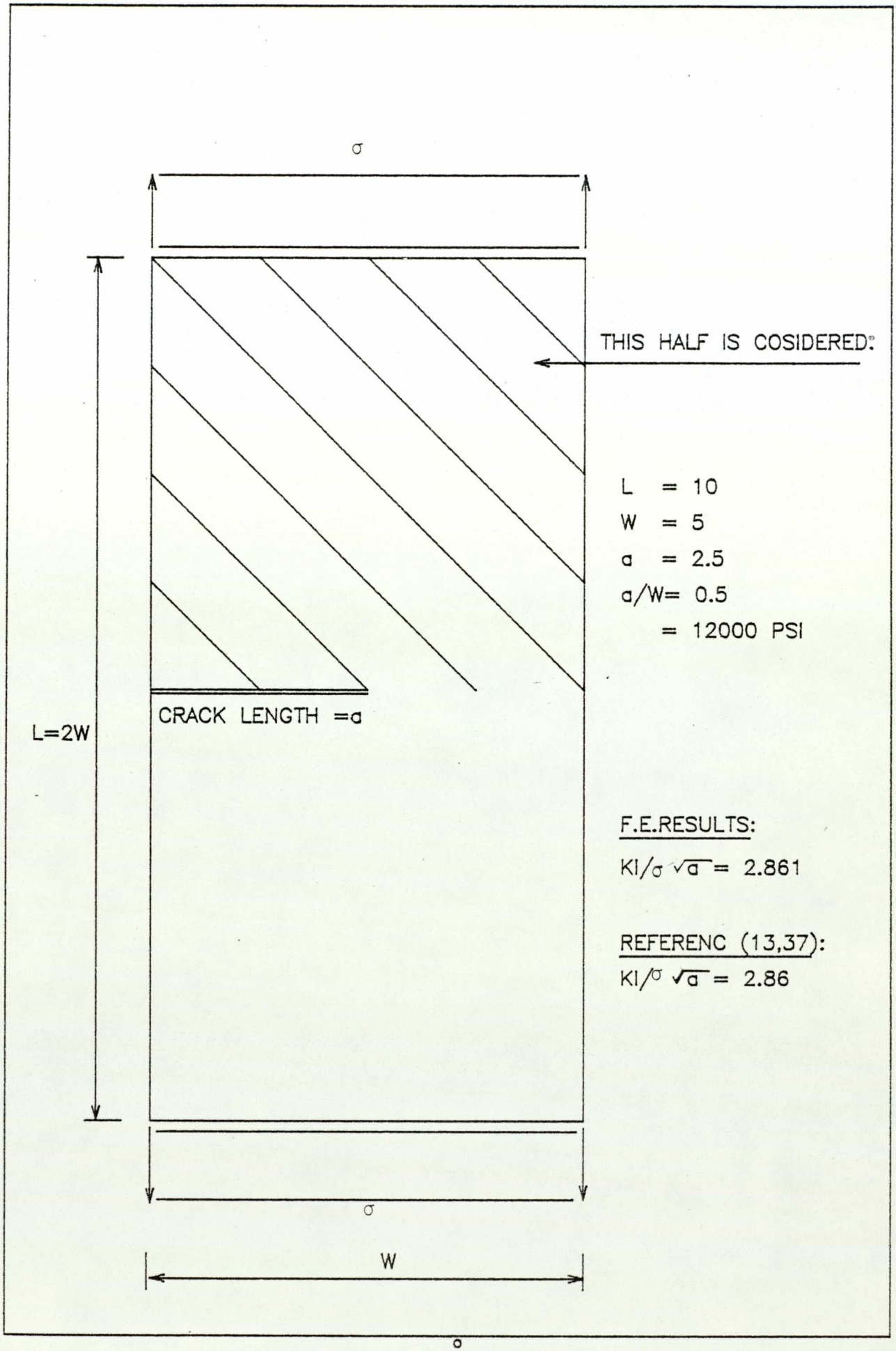

FIGURE (7.1) A PLATE WITH A 90° SINGLE-EDGE-CRACK IN TENSION.

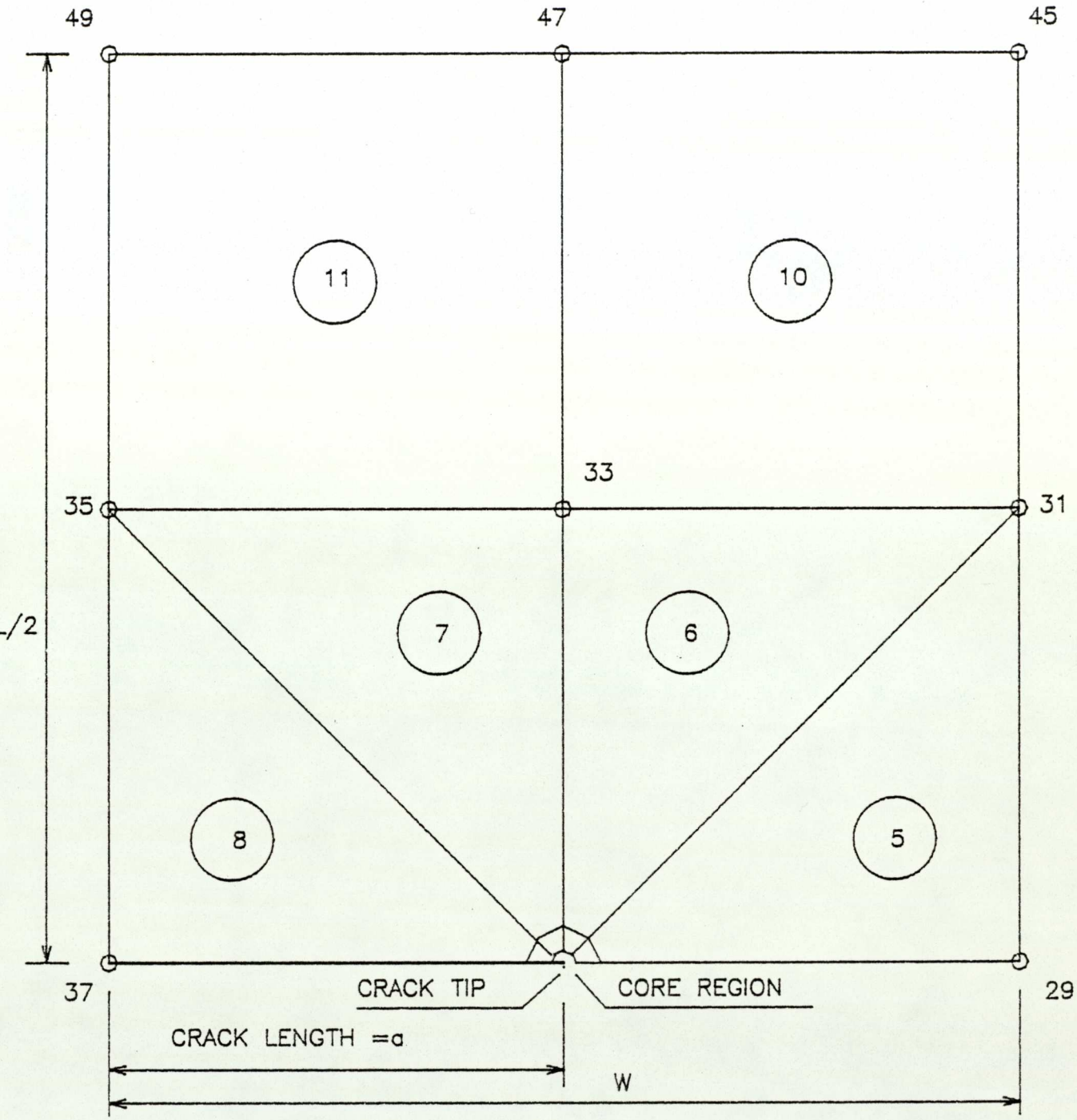

NUMBER OF ZONES = 10
NUMBER OF SUPER–NODES = 8

FIGURE (7.2) DISTORTED ZONE ARRAY SHOWING ZONE NUMBERS AND SUPER NODES OF HALF THE PLATE CONTAINING A 90° SINGLE–EDGE–CRACK,(SYMMETRY EXPLOITED).

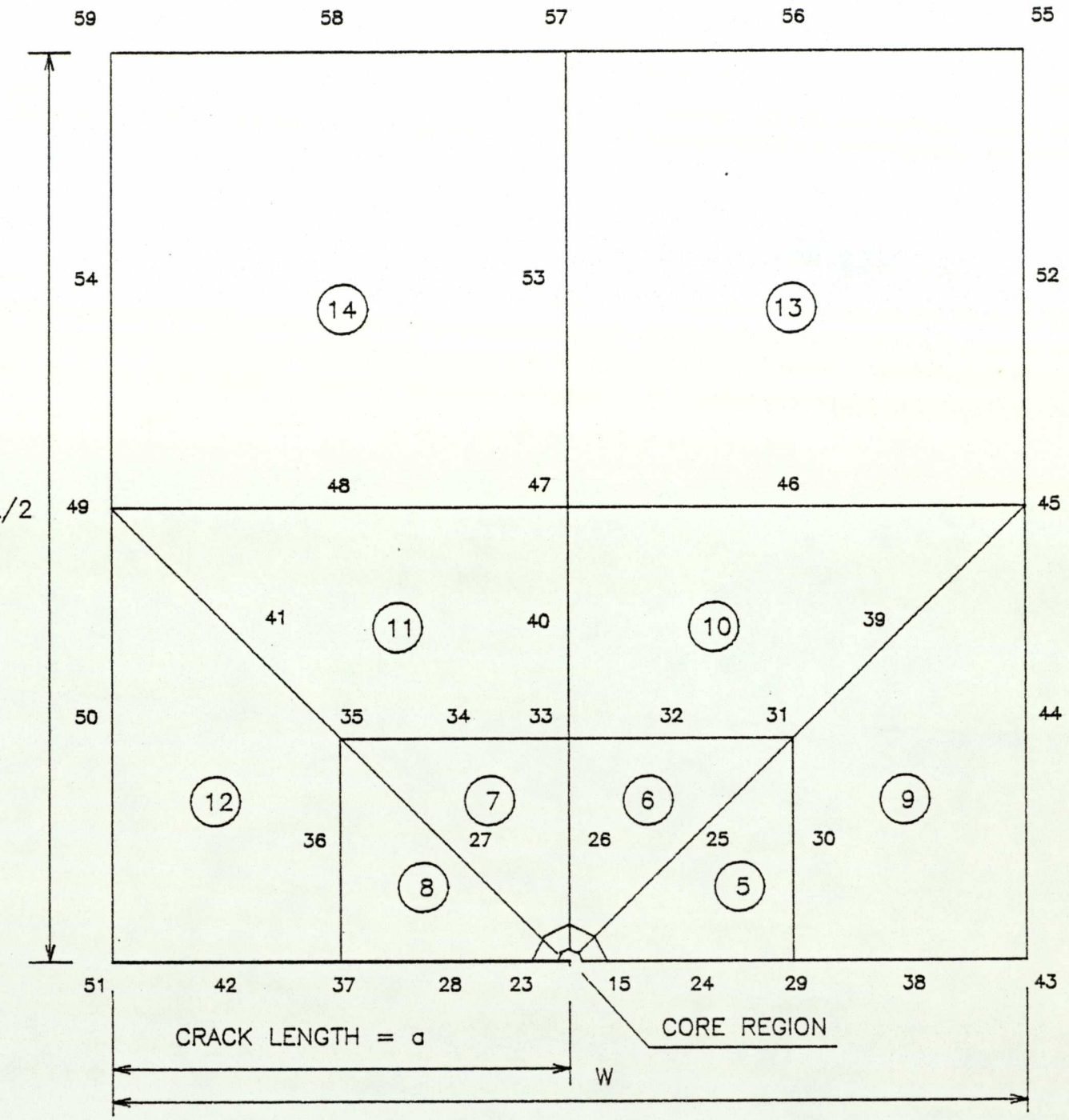

TOTAL NUMBER OF NODES = 59
TOTAL NUMBER OF ELEMENTS = 14

FIGURE (7.3) DISTORTED ELEMENT ARRAY SHOWING ELEMENT AND NODAL NUMBERING OF HALF THE PLATE CONTAINING A 90° SINGLE-EDGE-CRACK, USING QUADRILATERAL ELEMENT.

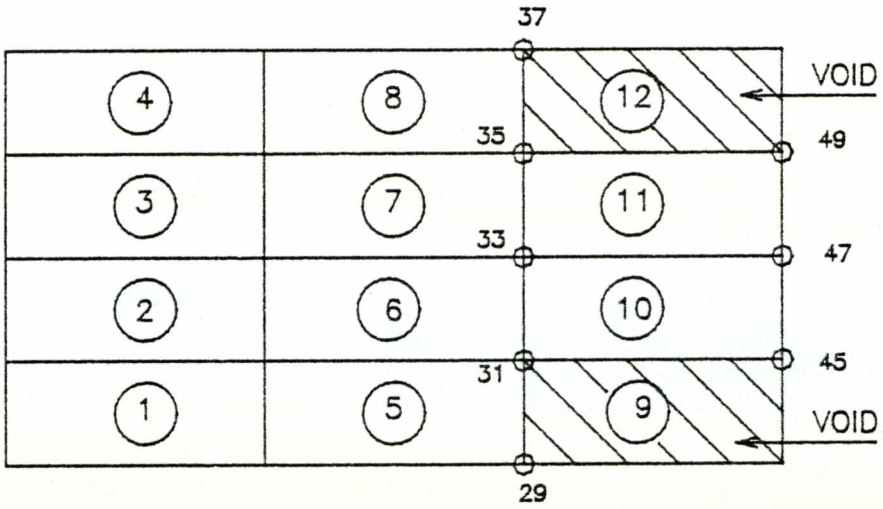

a) ZONE ARRAY SHOWING ZONE AND SUPER NODE NUMBERS.
NOTICE VOID ZONES NUMBER 9 AND 12.

NUMBER OF ZONES BEING USED , NOT INCLUDING VOIDS OR GENERATED ZONES = 6

NUMBER OF DECLARED SUPER NODES , NOT INCLUDING STANDARD GENERATED NODES = 8

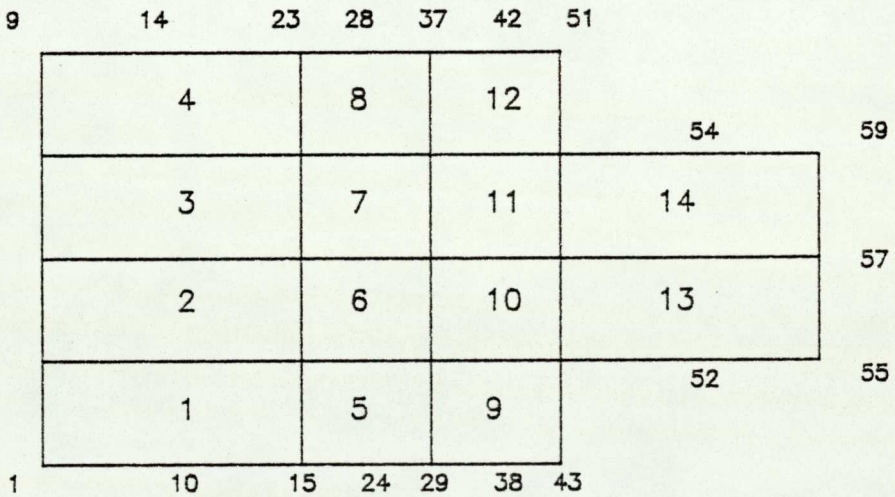

b) ELEMENT ARRAY SHOWING ELEMENT AND NODAL NUMBERING.

TOTAL NUMBER OF ELEMENTS = 14

TOTAL NUMBER OF NODES = 59

FIGURE (7.4) KEY DIAGRAMS FOR ZONE AND ELEMENT ARRAYS .

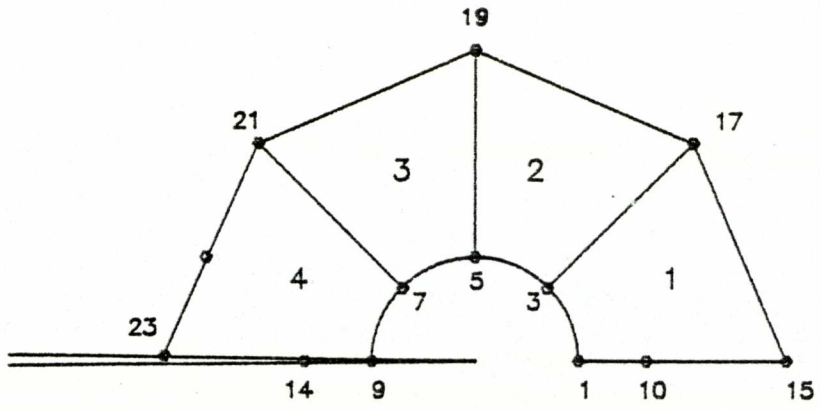

a) CORE REGION FOR MODE I SHOWING ELEMENT AND NODAL NUMBERING. SYMMETRY IS EXPLOITED, ONLY HALF THE CORE IS USED.

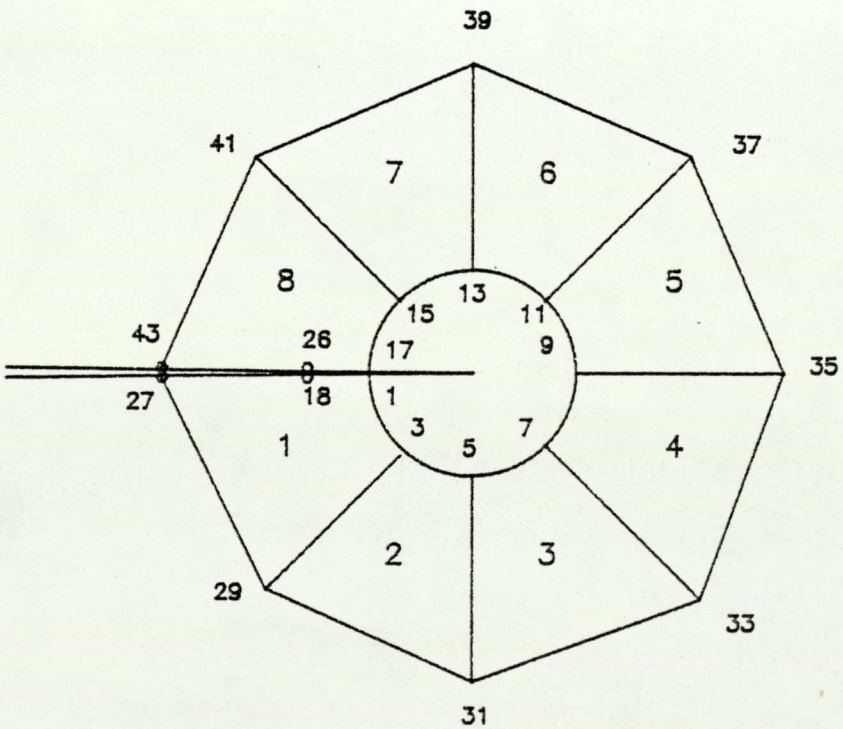

b) CORE REGION FOR MIXED MODE CONFIGURATION, IN THIS CASE THE FULL CORE IS USED, SHOWING A RING OF TRANSITION ELEMENTS.

FIGURE (7.5) CRACK TIP CORE REGION ARRANGEMENT.
(USING ISOPARAMETRIC QUADRILATERAL TRANSITION ELEMENTS).

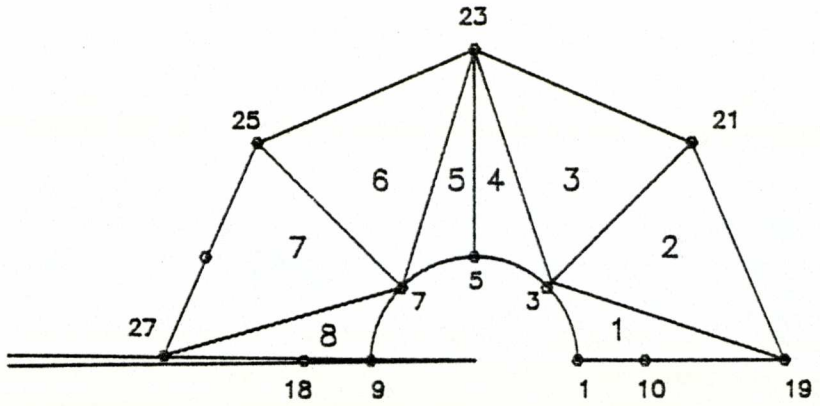

a) CORE REGION FOR MODE I SHOWING ELEMENT AND NODAL NUMBERING. SYMMETRY IS EXPLOITED,ONLY HALF THE CORE IS USED.

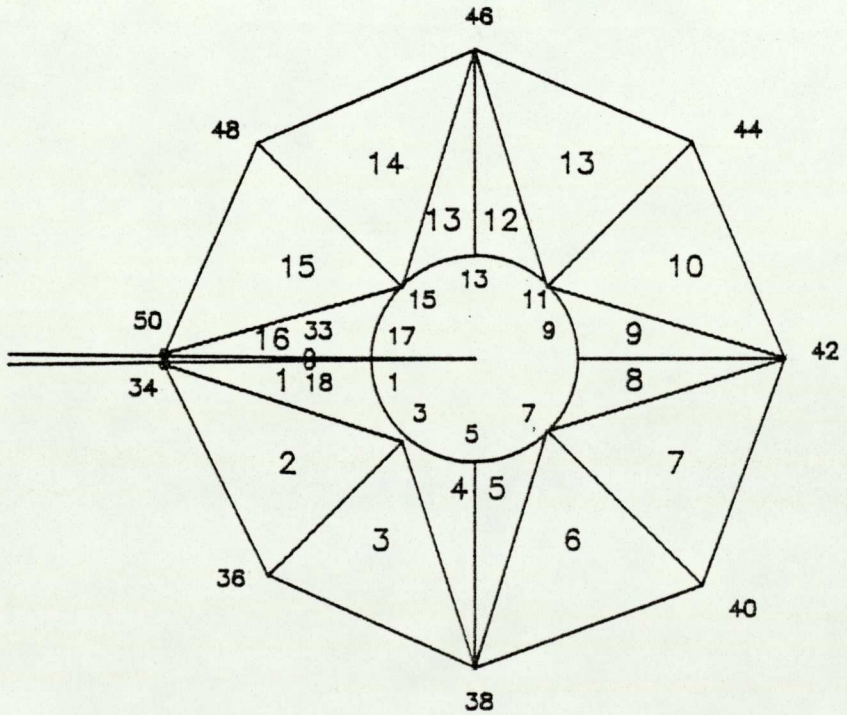

b) CORE REGION FOR MIXED MODE CONFIGURATION, IN THIS CASE THE FULL CORE IS USED, SHOWING A RING OF TRANSITION ELEMENTS.

FIGURE (7.6) CRACK TIP CORE REGION ARRANGEMENT.
(USING ISOPARAMETRIC TRIANGULAR TRANSITION ELEMENTS).

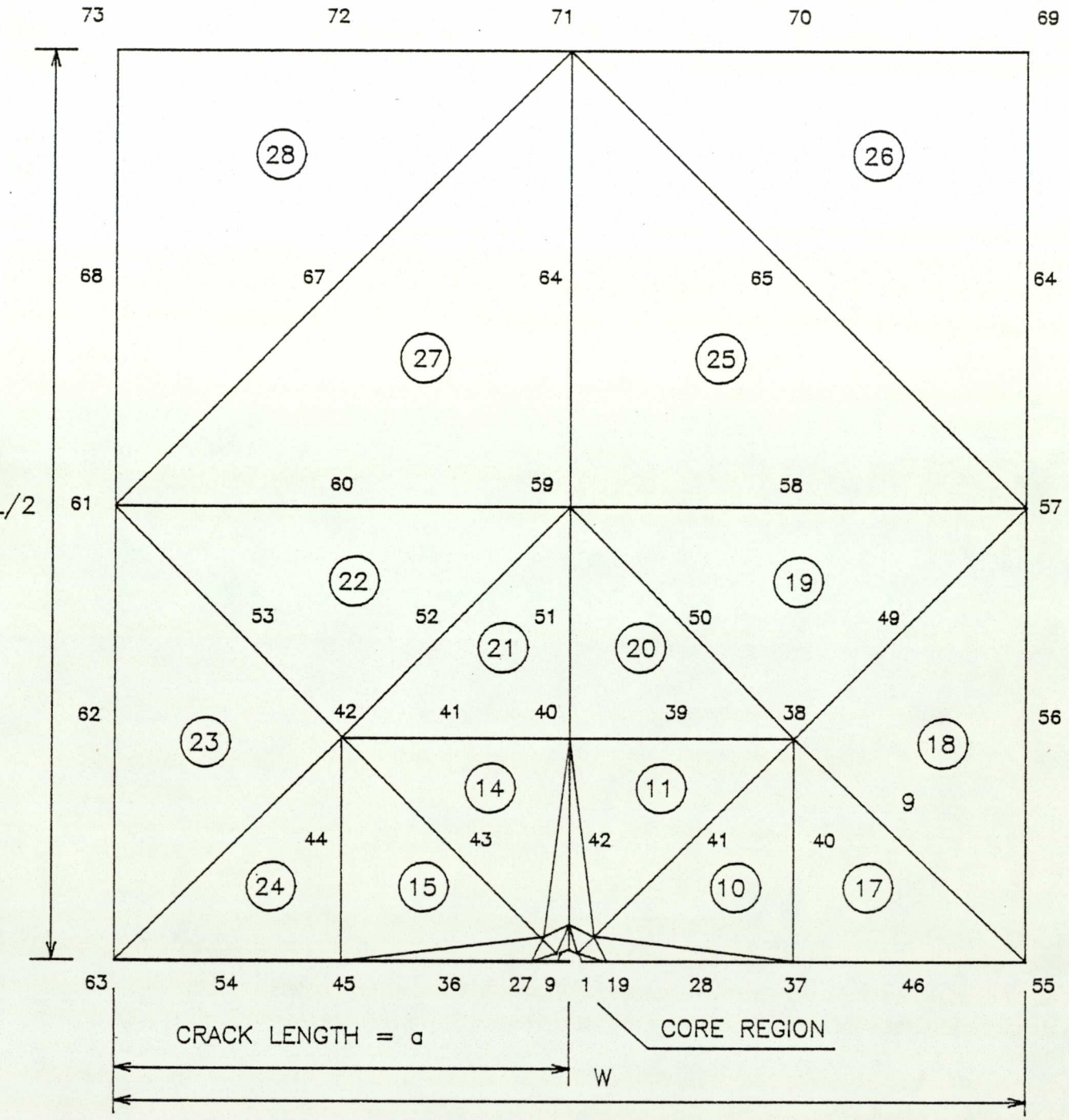

TOTAL NUMBER OF NODES = 73
TOTAL NUMBER OF ELEMENTS = 28

FIGURE (7.7) DISTORTED ELEMENT ARRAY SHOWING ELEMENT AND NODAL NUMBERING OF HALF THE PLATE CONTAINING A 90° SINGLE-EDGE-CRACK, USING TRIANGULAR ELEMENT.

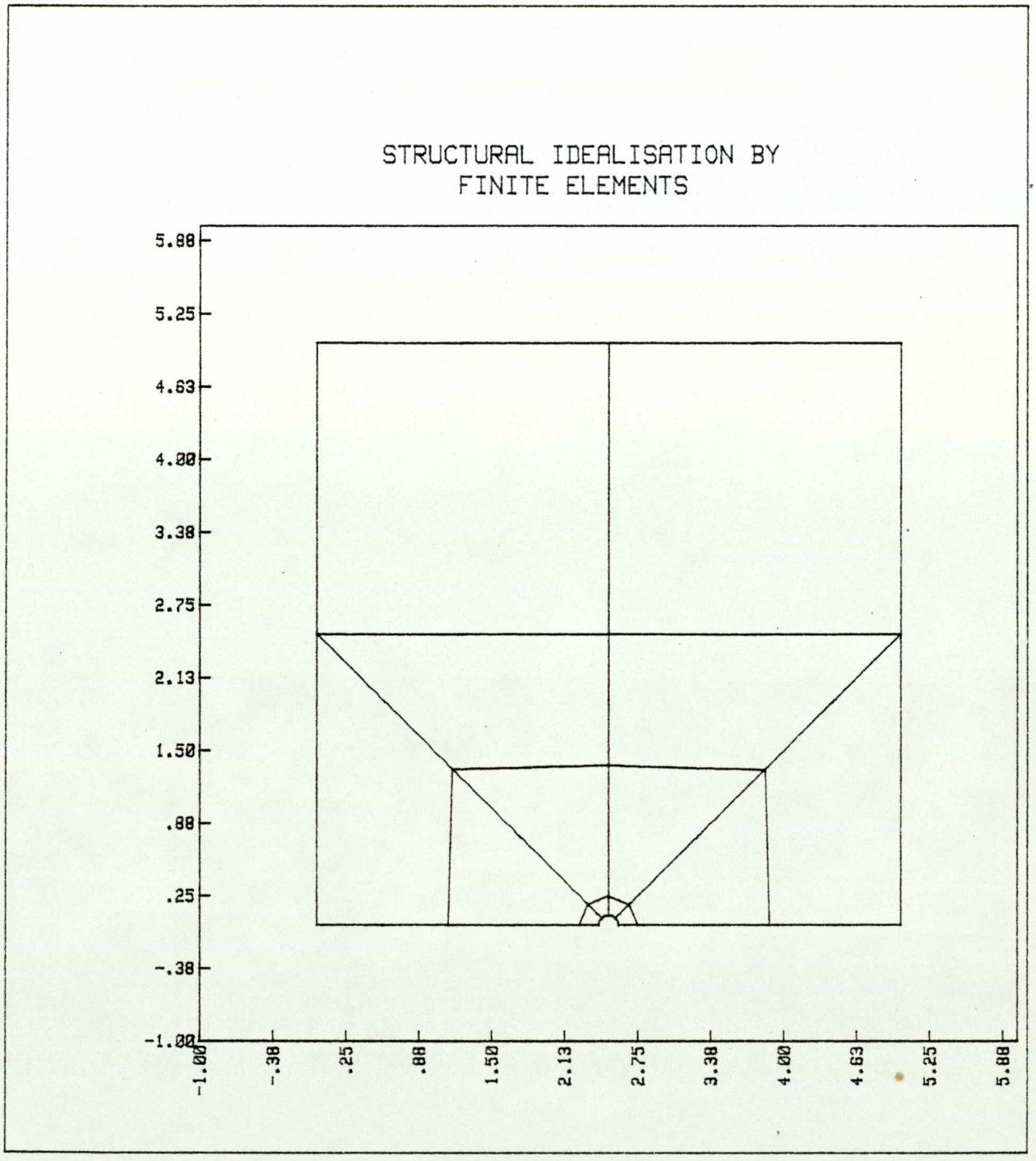

FIGURE (7.8) FINAL STRUCTURAL IDEALISATION DIAGRAM FOR MODE I CRACK PROBLEM IN EXAMPLE 1, OF A PLATE IN TENSION WITH A 90° SINGLE-EDGE-CRACK, EMPLOYING THE ISOPARAMETRIC QUADRILATERAL ELEMENT AROUND THE CORE.

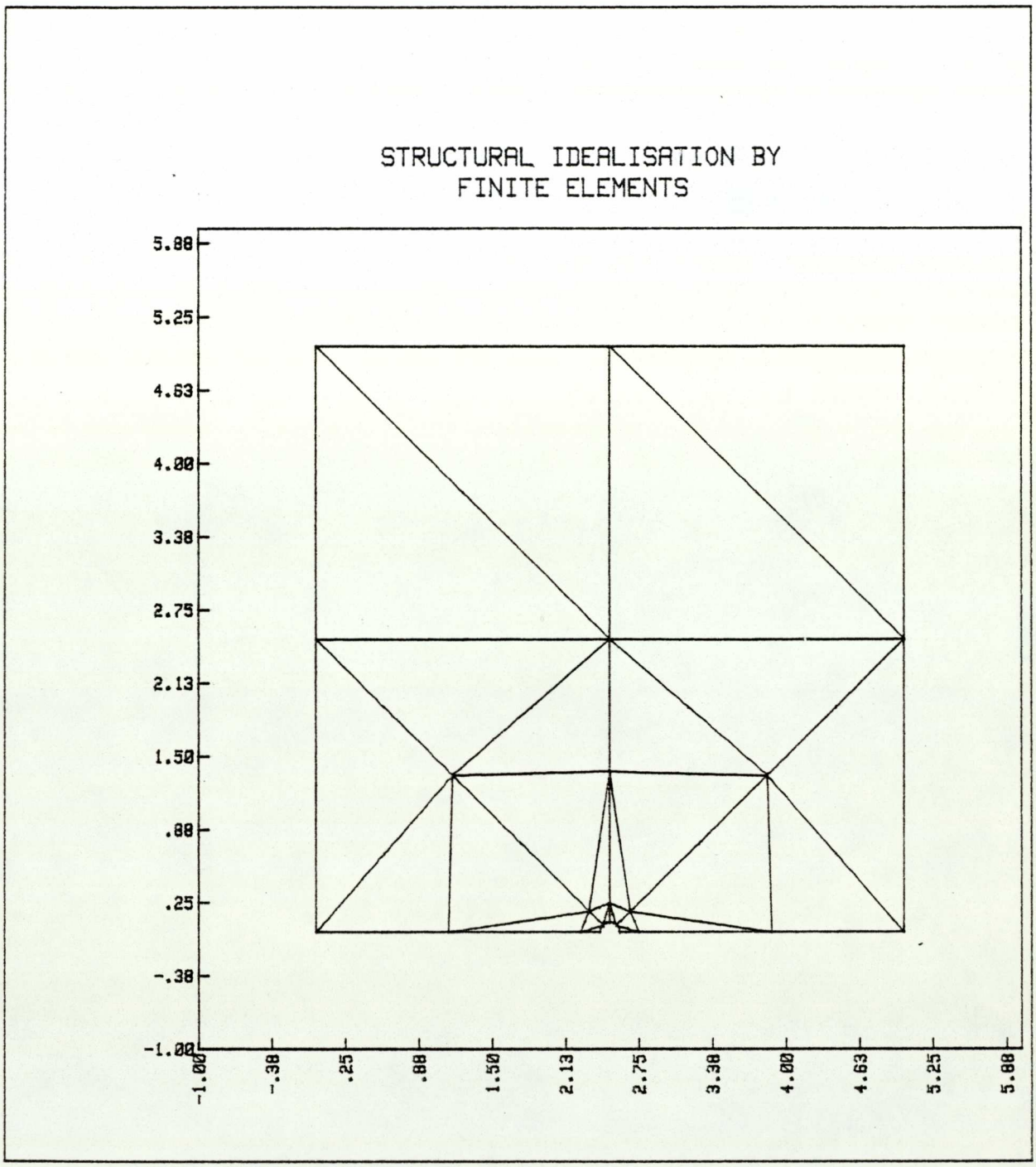

FIGURE (7.9) FINAL STRUCTURAL IDEALISATION DIAGRAM FOR MODE I CRACK PROBLEM IN EXAMPLE 1, OF A PLATE IN TENSION WITH A 90° SINGLE-EDGE-CRACK, EMPLOYING THE ISOPARAMETRIC TRIANGULAR ELEMENT AROUND THE CORE.

DATA INPUT FOR EXAMPLE 1.

QUADRILATERAL ELEMENT.

DATAFILE#1 : DATA1B

DATAFILE#2 : DATA2B

A) Initial control variables

2, 1, 1, 14, 59, 1, 1, 1

B) Control variables

8, 6, 4, 3, 1

C) Standard geometries

1, 1, 1, 9, 2.5, 0, .083, 0, 22.5, 1, 1, 0

D) Specified super-nodes.

1, 5, 0, 29 1, 5, 2.5, 31 1, 2.5, 2.5, 33 1, 0, 2.5, 35

1, 0, 0, 37 1, 5, 5, 45 1, 2.5, 5, 47 1, 0, 5, 49

E) Zone specification

4, 1, 2, 1, 5, 6, 7, 8

2, 1, 1, 1, 10, 11

F) Closing faces

0

G) Boundary conditions, material properties

12

6, 2, 0, 0, 1, 10, 15, 24, 29, 38

1, 3, 0, 0, 43 2, 0, 0, 5E3, 55, 59 1, 0, 0, 1E4 57

2, 0, 0, 2E4, 56, 58

Case : 1

3E7, .3, 1.2E7, 3E7, .3, 1 , 0

DATA INPUT FOR EXAMPLE 1.

TRIANGULAR ELEMENT.

DATAFILE#1 : DATA1T

DATAFILE#2 : DATA2T

A) Initial control variables

2, 0, 1, 28, 73, 1, 1, 1

B) Control variables

8, 6, 4, 3, 1

C) Standard geometries

1, 1, 1, 9, 2.5, 0, .083, 0, 22.5, 1, 1, 0

D) Specified super–nodes.

1, 5, 0, 29 1, 5, 2.5, 31 1, 2.5, 2.5, 33 1, 0, 2.5, 35

1, 0, 0, 37 1, 5, 5, 45 1, 2.5, 5, 47 1, 0, 5, 49

E) Zone specification

4, 1, 2, 1, 5, 6, 7, 8

2, 1, 1, 1, 10, 11

F) Closing faces

0

G) Boundary conditions, material properties

12

6, 2, 0, 0, 1, 10, 19, 28, 37, 46

1, 3, 0, 0, 55 2, 0, 0, 5E3, 69, 73 1, 0, 0, 1E4, 71

2, 0, 0, 2E5, 70, 72

Case : 1

3E7, .3, 1.2E7, 3E7, .3, 1 , 0

non-dimensional K_I is found to be 2.861, while the total number of nodes used in run two using the 6-node triangular element is 73, and the value of the non-dimensional K_I is found to be 2.604.

Paris and Sih, in Reference (13), stated a value of K_I for this problem to be 2.86. So that the result of run one using the 8-node isoparametric quadrilateral element shows no difference if the value obtained is rounded to two decimal places. While there is a difference of 9.1% for K_I if the 6-node isoparametric triangular element is used compared to that of reference (13). This proves that the isoparametric quadrilateral element is more superior to that of the isoparametric triangular element.

Data input for the two meshes used, are given in the same order as that described in Appendix (A).

7.4 EXAMPLE 2 - A PLATE WITH A 90° SINGLE-EDGE-CRACK IN TENSION

Number of nodes on finite element mesh/core interface $N_1 = 17$.

The configuration is the same as that of Example 1. In this example the whole plate is considered as shown in Fig. (7.1), and the mixed-mode fracture program 'PCPOY' is used to solve the problem. So program code input is 3. The full circular core element is used, surrounded by a band of 'Transition' elements, as shown in Fig. (7.5b).

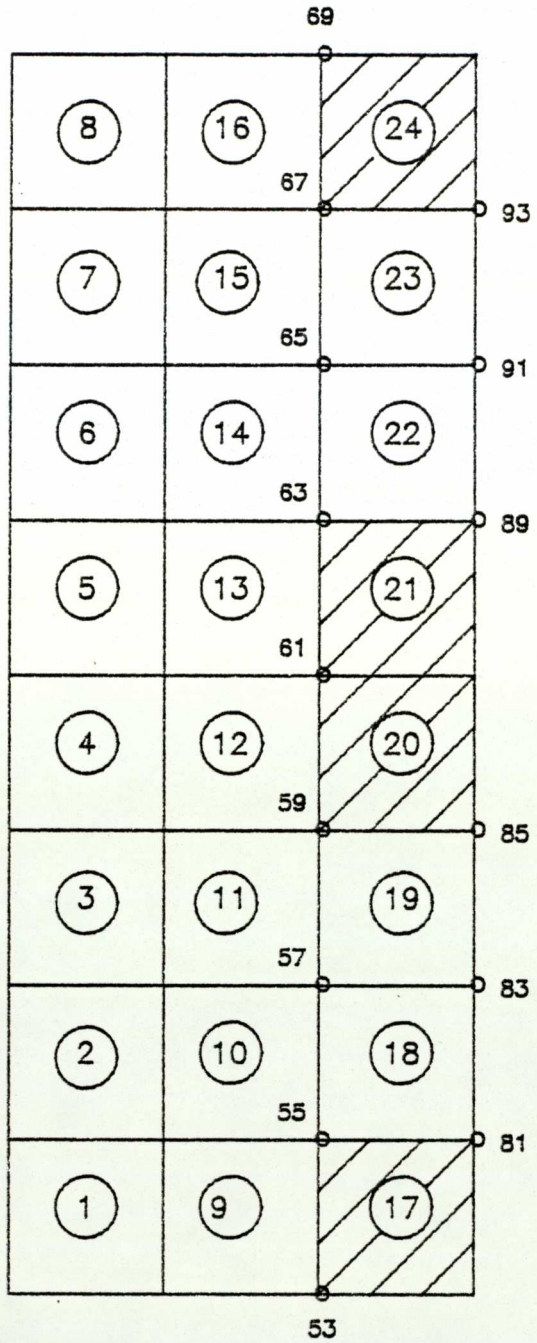

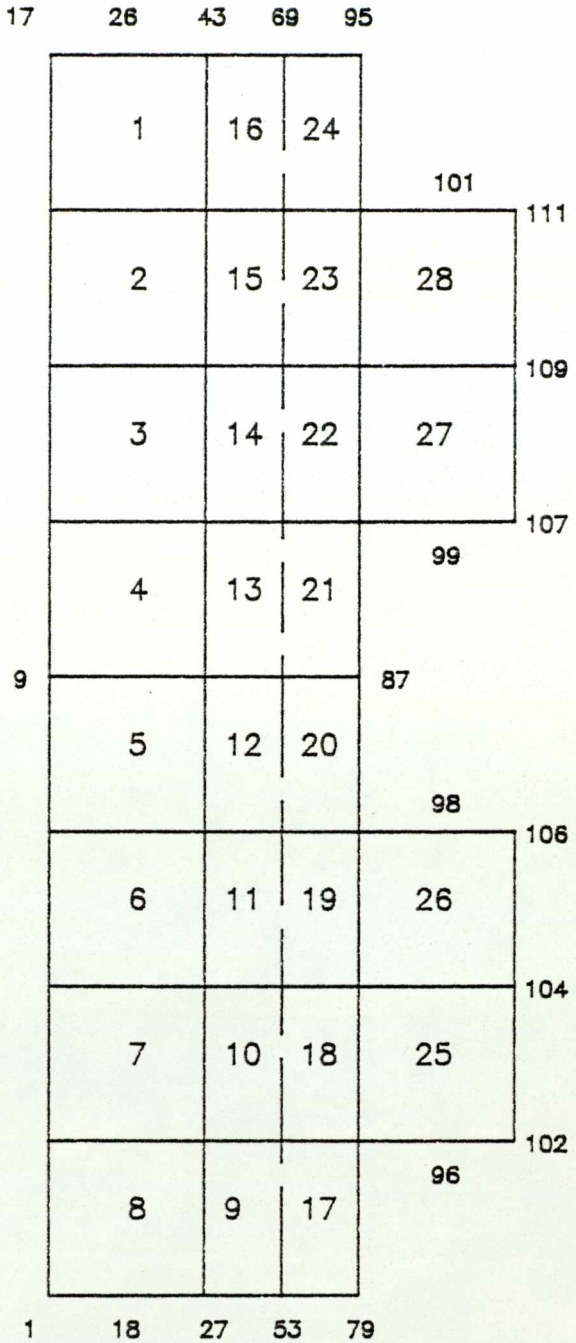

a) ZONE ARRAY DIAGRAM SHOWING ZONE, AND SUPER-NODE NUMBERS. ZONES 17, 20, 21, AND 24 ARE VOID ZONES.

b) ELEMENT ARRAY DIAGRAM, SHOWING ELEMENT AND NODAL NUMBERING.

STANDARD GENERATED ZONES ARE :

1, 2, 3, 4, 5, 6, 7, 8.

NUMBER OF ZONES :

(EXCLUDING VOIDS AND GENERATED ZONES = 12

NUMBER OF SUPER-NODES =14

NUMBER OF ELEMENTS = 28

NUMBER OF NODES =111

FIGURE (7.10) KEY DIAGRAMS FOR ZONE AND ELEMENT ARRAYS, FOR THE MIXED-MODE FRACTURE PROBLEM OF EXAMPLE 2.

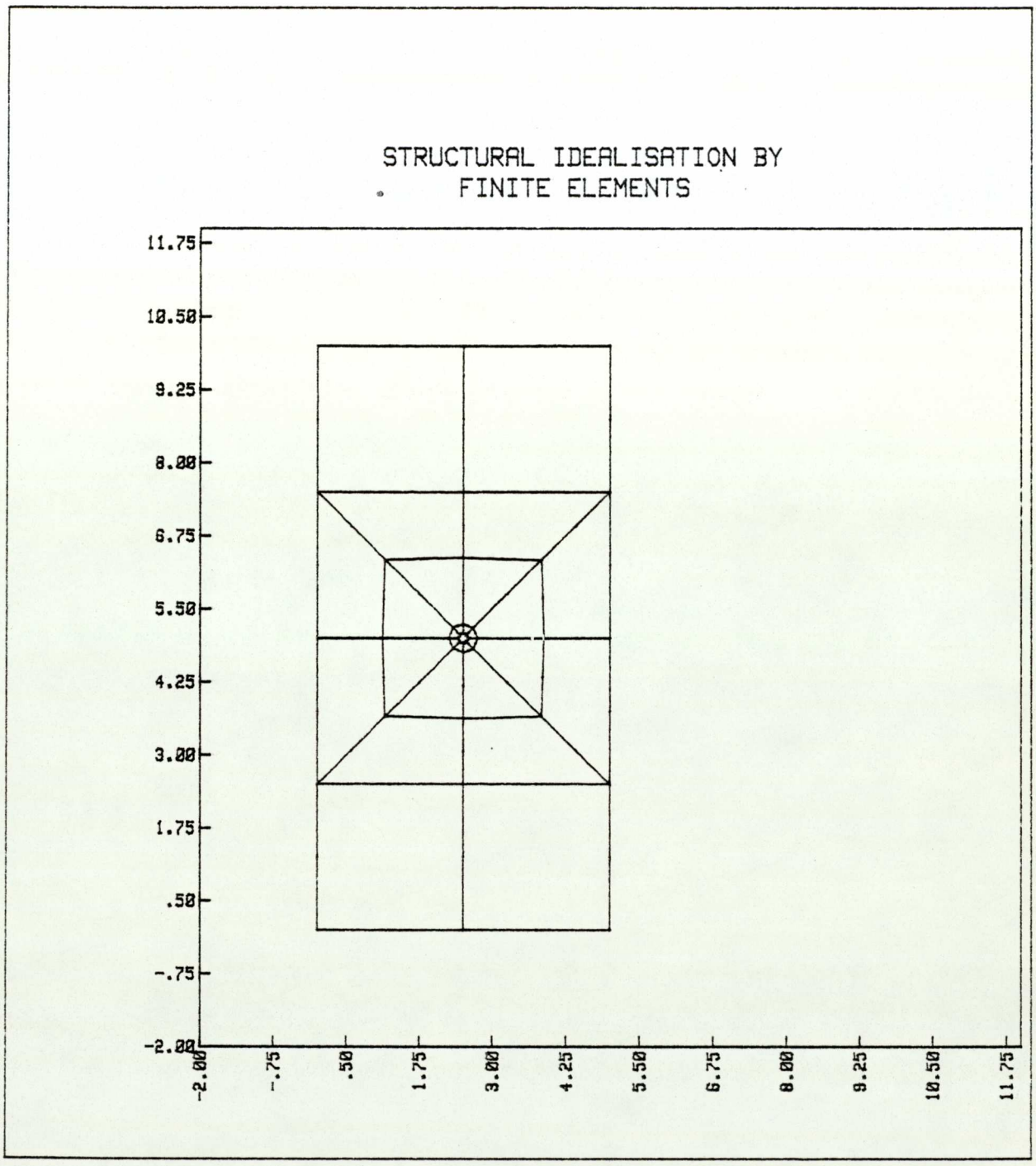

FIGURE (7.11) FINAL STRUCTURAL IDEALISATION DIAGRAM FOR MIXED– MODE CRACK PROBLEM IN EXAMPLE 2, OF A PLATE IN TENSION WITH A 90° SINGLE–EDGE–CRACK, EMPLOYING THE ISOPARAMETRIC QUADRILATERAL ELEMENT AROUND THE CORE.

DATA INPUT FOR EXAMPLE 2.

QUADRILATERAL ELEMENT.

DATAFILE#1 : DATA17

DATAFILE#2 : DATA18

A) Initial control variables

3, 1, 1, 28, 111, 1, 1, 0, 0, 1, 1

B) Control variables

4, 12, 8, 3, 1

C) Standard geometries

1, 1, 17, 2.5, 5.0, .083, −180, 22.5, 1, 1

D) Specified super−nodes.

2, 0, 5, 53, 69 1, 0, 2.5, 55 1, 2.5, 2.5, 57 1, 5, 2.5, 59

1, 5, 5, 61 1, 5, 7.5, 63 1, 2.5, 7.5, 65 1, 0, 7.5, 67

1, 0, 0, 81 1, 2.5, 0, 83 1, 5, 0, 85 1, 5, 10, 89

1, 2.5, 10, 91 1, 0, 10, 93

E) Zone specification

8, 1, 2, 1, 9, 10, 11, 12, 13, 14, 15, 16

4, 1, 1, 1, 18, 19, 22, 23

F) Closing faces

0

G) Boundary conditions, material properties

10, 1, 2, 0, 0, 106

2, 0, 0, 5E3, 107, 111 2, 0, 0, 2E4, 108, 110 1, 0, 0, 1E4, 109

2, 0, 0, −2E4, 103, 105 1, 0, 0, −1E4, 104 1, 3, 0, 0, 102

Case : 1, 3E7, .3, 1.2E7, 3E7, .3, 1 , 0

A zone pattern is established together with element sub-division. The total number of zones being used excluding voids and generated zones are 12. Four void zones are used in generating the mesh, these zones are numbered 17, 20, 21 and 24. The total number of elements are 28, with a total of 111 nodes.

The above problem is treated as a mixed-mode fracture problem in order to verify the values of K_I and K_{II} obtained using the program 'PCPOY'. Normalized values of K_I and K_{II} are computed, K_I is found to be 2.861, as was expected and has no error in comparison to that found in references (13) and (37). The value of normalized K_{II} which ought to be zero is found to be of a very small value of no significance, namely 4.6×10^{-10}.

Data input for this example is given in the same manner as that of the instruction of the user guide in Appendix (A).

7.5 EXAMPLE 3 - A SQUARE PLATE IN UNIFORM TENSION CONTAINING A 45° CENTRAL CRACK.

Dimensions of Plate:

Length L = Width w = 15 a = 2.8

Thickness of plate = 1

Applied Load σ = 120 lbf/in^2

Core radius R_c = 0.1

Number of nodes on the finite element mesh/core interface N_1 = 17

Material properties:

$E = 3 \times 10^7$

$G = 1.2 \times 10^7$

$\nu = 0.3$.

This is a mixed-mode fracture problem involving two crack tips, so program code 3 is used. Two cores are used, one around each crack tip, and each core element is surrouned by a band of 'Transition' elements. Figure (7.5b) shows this configuration. Zones 1-8 and 41-48 are automatically generated by the procedure 'COREGEN' in the mesh generation program.

The total number of zones used excluding voids and generated zones are 42 and the total number of elements in the mesh is 74 with a total number of 262 nodes.

This mesh has been generated using the mesh generation program. A diagram of the structural idealization of the plate with the 45° central crack is shown in Fig. (7.12).

The mixed-mode fracture program 'PCPOY' failed during execution due to the large number of elements in the K matrix array. An error of INTEGER PRECISION OVERFLOW was given by the HP 9845 Desk-TopComputer during the execution of the program. No values of K_I or K_{II} were found, and this is one of the reasons why example 2 has been used in order to verify the program 'PCPOY'.

Data input for this example is given in the next two

DATA INPUT FOR EXAMPLE 3.

DATAFILE#1 : DATA3

DATAFILE#2 : DATA4

A) 3, 1, 1, 74, 262, 1, 1, 0, 0, 1, 1

B) 39, 42, 8, 9, 1

C) 2, 1, 1, 17, 5.5, 5.5, 0.1, 45, 22.5, 1, 1, 131, 41, 17, 9.5, 9.5, 0.1, −135, 22.5, 1, 139, 0

D) 4, 7.5, 7.5, 53, 199, 69, 183

2, 0, 15, 107, 249 2, 5.5, 9.5, 81, 223 2, 5.5, 7.25, 55,225

2, 9.5, 7.75, 95, 135 2, 9.5, 5.5, 93, 211 2, 15, 0, 119, 237

1, 4.5, 6.5, 57 1, 4, 5.5, 59 1, 4.4, 4.4, 61

1, 5.5, 4, 63 1, 6.5, 4.5, 65 1, 7.25, 5.5, 67

1, 3.25, 7.5, 83 1, 2.5, 5.3, 85 1, 3, 3, 87

1, 5.3, 2.5, 89 1, 7.5, 3.25, 91 1, 0, 10, 109

1, 0, 5, 111 1, 0, 0, 113 1, 5, 0, 115

1, 10, 0, 117 1, 10.5, 8.5, 187 1, 11, 9.5, 189

1, 10.6, 10.6, 191 1, 9.5, 11, 193 1, 8.5, 10.5, 195

1, 7.75, 9.5, 197 1, 11.75, 7.5, 213 1, 12.5, 9.7, 215

1, 12, 12, 217 1, 9.7, 12.5, 219 1, 7.5, 11.75, 221

1, 15, 5, 239 1, 15, 10, 241 1, 15, 15, 243

1, 10, 15, 245 1, 5, 15,247

E) 16 ,1 , 2, 1, 9, 10, 11, 12, 13, 14, 15, 16, 49, 50, 51, 52, 53, 54, 55, 56

26 ,1 , 1 , 1, 18, 19, 20, 21, 22, 23, 24, 26, 27, 28, 29, 30, 31 , 58, 59,

60, 61, 62, 63, 64, 66, 67, 68, 69, 70, 71

F) 6,

9, 3, 18, 4, 24, 2, 24, 3, 26, 4, 31, 2,

2, 79, 233, 95, 217

G) 14,

1, 2, 0, 0, 132 1, 0, 0, 100, 126 1, 0, 0, −400, 133

1, 0, 0, 400, 262 1, 0, 0, −200, 134 1, 0, 0, 200, 261

1, 3, 0, 0, 135 1, 0, 0, 400, 260 1, 0, 0, −200, 136

1, 0, 0, 200, 259 1, 0, 0, −400, 137 1, 0, 0, 400, 258

1, 0, 0, −100, 138 1, 0, 0, 100,257

Case : 1

3E7, .3, 1.2E7, 3E7, .3

0

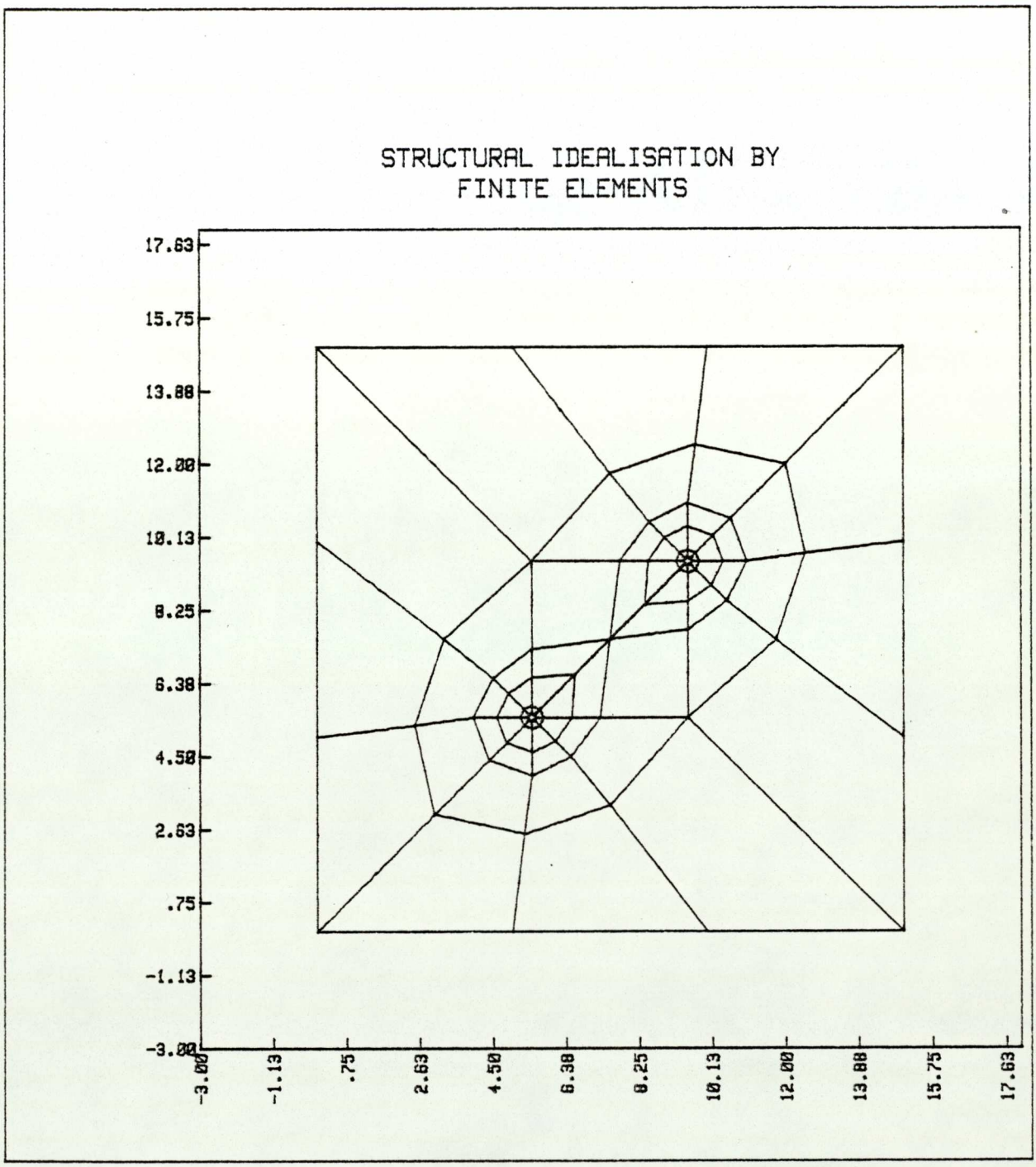

FIGURE (7.12) FINAL STRUCTURAL IDEALISATION DIAGRAM FOR MIXED— MODE CRACK PROBLEM IN EXAMPLE 3, EMPLOYING THE ISOPARAMETRIC QUADRILATERAL ELEMENT AROUND THE CORE REGION AT THE TIPS OF THE CENTRAL SLANTED CRACK.

pages according to instructions given in the user guide in Appendix (A).

7.6 EXAMPLE 4 - A ROUND BAR WITH A CIRCUMFERENTIAL NORMAL-EDGE-CRACK IN TENSION (FIGURE 7.13).

$H/R = 1.4$, $a/R = 0.5$

Core Radius $R_c = 0.1$

Number of nodes on the finite element mesh /core interface $N_1 = 9$

Total number of elements = 56

Total number of nodes = 135

The normalised stress intensity factor is as follows[82]:

$$K_I = \frac{\bar{K}_I}{\sigma_o (2R)^{\frac{1}{2}}} \qquad (7.6)$$

where R is the radius of the round bar

σ_o is the stress in the neck section and equal to 1666 psi in this particular example.

$$\sigma_o = \sigma\left(\frac{D}{D-2a}\right) \qquad (7.7)$$

where D is the diameter of the bar

σ is the applied tensile stress

a is the crack depth.

The above example is a case of an axisymmetric Mode I fracture problem. The program used to find K_I is 'AXYMD1'. The mesh is constructed in a similar manner to that of

Al-Sharqi in Reference (68). Two semi-circular bands of elements surround the core as shown in Fig. (7.14).

Two meshes are constructed in a similar manner to that of Al-Sharqi[68], where the mesh generation is not fully automatic like that used in the other examples. For instruction of data input procedure refer to Appendix (B). Data input for the first mesh is presented as a sample for similar meshes.

Due to symmetry, only half the bar need be considered and hence the core's shape is a semi-circle. An isoparametric triangular ring element is used throughout the mesh around the core region. The mesh is generated for one quarter of the longitudinal section of the bar.

Al-Sharqi, using the same program 'AXYMD1' has generated a mesh of a total number of nodes of 285. The number of nodes employed on the finite element mesh core interface (N_1) was 19. He found the value of the normalised K_I equal to 0.22774 as compared to Hilton and Sih[82] value of 0.235 using 297 nodes and (N_1 = 21), i.e. a difference of 3.1%. The 285 node mesh has failed on the HP 9845 Computer during execution of the program, giving an error of INTEGER PRECISION OVERFLOW, due to the large number of elements in the overall stiffness matrix.

The two meshes used here are within the Computer capacity. The first mesh of a total number of 135 nodes

with (N_1 = 9), and the second mesh with a total number of 255 nodes and (N_1 = 17).

Values of the normalised K_I are shown in Table (7.1) for the two runs. These are compared with those calculated by Hilton and Sih[82] and by Bueckner[81].

The K_I value calculated using the first mesh of a total number of 255 nodes and (N_1 = 17) is closer to Hilton and Sih[82] solution, using a similar configuration of a total number of 297 nodes and (N_1 = 21), than that calculated using 135 nodes and (N_1 = 9). This means that there is a convergence of K_I as the total number of nodes increases.

The total number of nodes which could be used depends on (N_1) and is limited by the computer storage capacity.

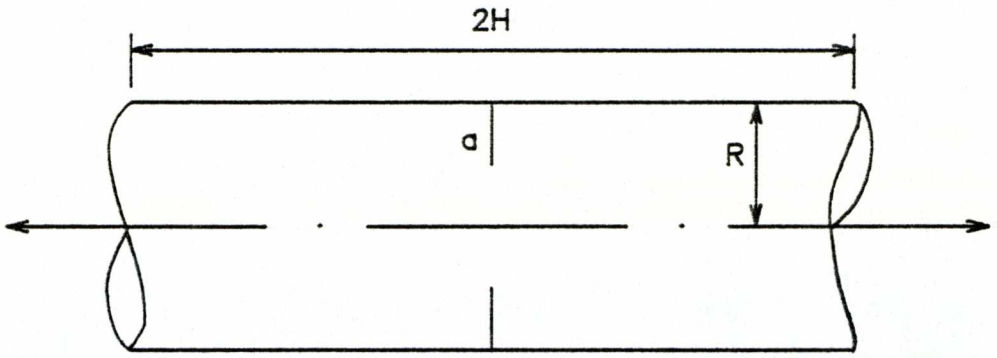

a) LONGITUDINAL SECTION THROUGH ROUND BAR WITH CIRUMFERENTIAL NORMAL EDGE–CRACK IN TENSION.

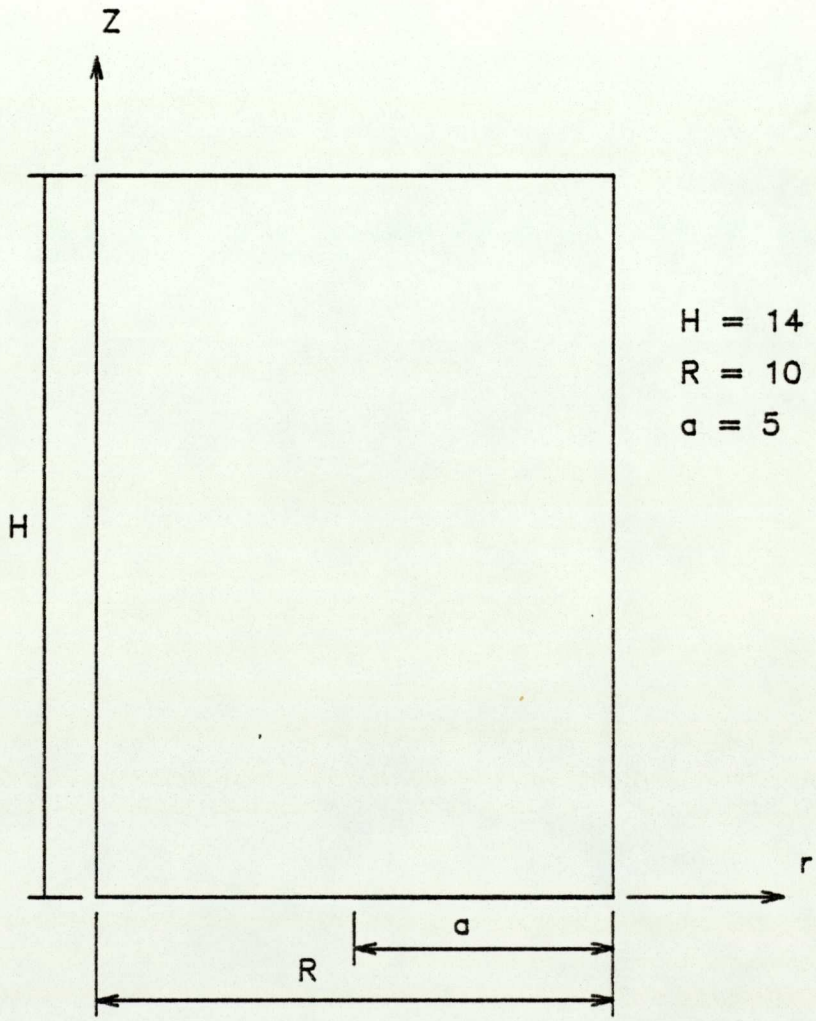

b) ONE QUARTER OF THE ABOVE BAR IS USED IN SOLVING THE PROBLEM. SYMMETRY IS EXPLOITED.

FIGURE (7.13) ROUND BAR WITH A CIRCUMFERENTIAL NORMAL EDGE–CRACK 1N TENSION, OF EXAMPLE 4 FOR AXISYMMETRIC MODE I FRACTURE PROBLEM.

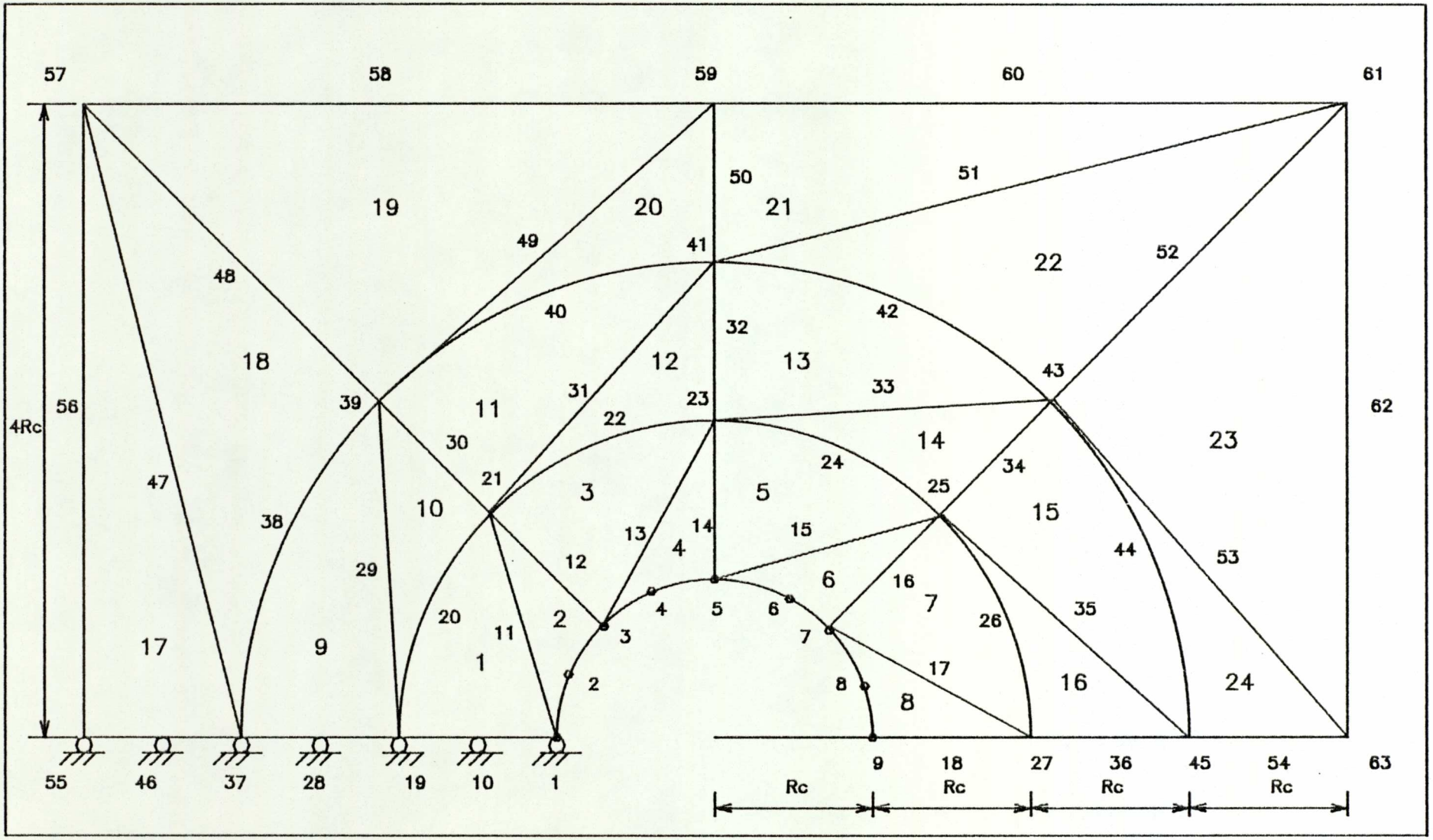

FIGURE (7.14) A DIAGRAM FOR THE CORE REGION WHERE THREE BANDS OF TRIANGULAR ELEMENTS ARE USED ROUND THE CORE ELEMENT, WHERE ELEMENT AND NODAL NUMBERING IS SHOWN FOR EXAMPLE 4.

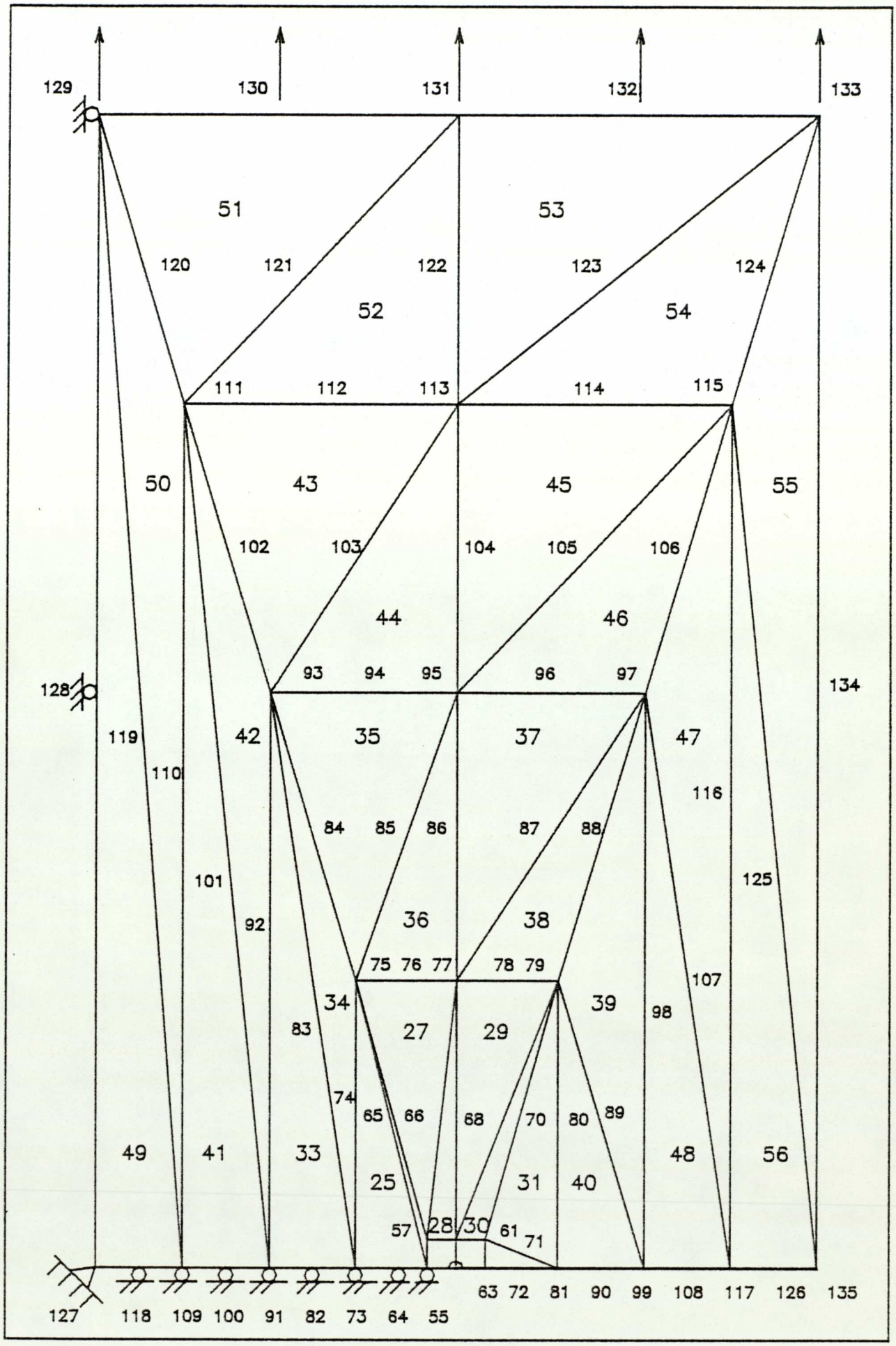

FIGURE (7.15) FINAL STRUCTURAL IDEALISATION OF A ROUND BAR WITH A CIRCUMFERENTIAL NORMAL EDGE–CRACK, OF EXAMPLE 4.

	F.E.PROGRAM "AXYMD1"			F.E.(82)	BUECKNER
	FIRST MESH	SECOND MESH	AL-SHARQI (68)	HILTON AND SIH	(81)
TOTAL NO. OF NODES	135	255	285	297	
N1	9	17	19	21	
NORMALIZED KI	0.2239	0.2274	0.22774	0.235	0.240
% ACCURACY					
FIRST MESH			1.68%	4.7%	6.8%
SECOND MESH			0.15%	3.2%	5.25%

TABLE (7.1) TABULATED VALUES OF KI FOR EXAMPLE 4 .

DATA INPUT FOR EXAMPLE 4

DATAFILE #1 : AXYC4

* NOTE :- REFER TO APPENDIX (B)

DATA INPUT MANUALLY USING AXISYMMETRIC MODE I FRACTURE PROBLEM PROGRAM (AXYMD1).

A) 1, 56, 135, 1, 1, 9, 10, 14, 5, .1, 1, 1

B) 21

Node J	r–Coord Xx(J)	z–Coord Yy(J)	Type Kode	r–Disp or Load Ulx	z–Disp or Load Vly
1	4.90	0	2	0	0
10	4.85	0	2	0	0
19	4.80	0	2	0	0
28	4.75	0	2	0	0
37	4.70	0	2	0	0
46	4.65	0	2	0	0
55	4.60	0	2	0	0
64	4.20	0	2	0	0
73	3.80	0	2	0	0
82	3.30	0	2	0	0
91	2.80	0	2	0	0
100	2.15	0	2	0	0
109	1.50	0	2	0	0
118	0.75	0	2	0	0
127	0	0	3	0	0
128	0	7	1	0	0
129	0	14	1	0	0
130	2.50	14	0	0	21816
131	5.00	14	0	0	21816
132	7.50	14	0	0	65449
133	10.00	14	0	0	21816

3E7, .3, 1.2E7, 3E7, .3

Hnd : 1

CHAPTER 8

8.1 DISCUSSION

The application of the finite element method, as one of the most powerful methods of numerical analysis has been widely used in the second half of this century due to the rapid development of digital computers.

The finite element method has been applied to the solution of problems of cracked bodies, and values for the stress intensity factors within an acceptable engineering accuracy can be calculated.

The programs used in this thesis fall into three major parts. The first is the automatic mesh generation program (MGENUP), which has been written by Wood[15], generates the mesh of any structure under consideration. It divides the domain into sub-regions of quadrilateral or triangular isoparametric element. This program was already in 'BASIC' to suit the HP 9845 desk-top computer. It has been used successfully during the preparation of this thesis. It is necessary to read the instructions in the user guide in Appendix (A) in order to be able to use this program efficiently. The program is not difficult to use, and a minimum number of datas are required to generate the mesh.

The second part of the programs used here are that of the plane stress/strain finite element program 'PLST'. This was written by Robertson[67] using the isoparametric triangular element. It was updated by Wood[15] to suit the automatic mesh generation program, and added the isoparametric quadrilateral element as another choice of element used in the sub-division of the domain. The program was written in Algol language, but has been translated to Basic by a third research student to suit the HP 9845 desk-top computer. Many problems were solved successfully using this program, and samples of the numerical examples to these problems are described in Chapter 3. Fairly accurate results of stresses are calculated and compared with theoretical values available, however, it was found during the course of application of this program on some numerical examples, that values of shear stress specially on stress free boundaries to be spurious, and sometimes values of stresses throughout the domain to be erratic in manner. A method proposed by Hinton et al.[72] using a technique to smooth stresses has been adopted and included in the present plane stress/strain finite element program 'PLST' during the course of this work. In this technique the stresses are sampled at the 4 point Gaussian integration sampling locations to give smoothed stresses at the nodes of the elements. This method is described in Chapter 3, where two examples are given; one of a canitlever with an end load, and the second of a thick cylinder under uniform internal pressure. These

two examples illustrate the validity of this technique. Graphs of calculated stresses with the smoothing technique and without it, show a considerable improvement when using the smoothing technique. Details of the method is described in Section 3.8.

The third part of the programs deals with fracture mechanics problems. All these programs were written in 'Algol' language. They have been translated to 'Basic' to suit the HP 9845 desk-top computer available at the Department of Mechanical Engineering at the University of Aston, as part of the work carried out during the preparation of this thesis.

Two of these programs deal with mode I and mixed-mode I and II plane crack problems, written down originally by Robertson[67]. These are essentially a plane stress/strain program with some modification to include the singularity at the crack tip region. The element used to cater for this singularity is the Hilton and Hutchinson[50] element which has been developed by Richard/Robertson[62], this has already been explained in Chapter 6.

Wood[15] updated the above programs to suit the automatic mesh generation program, and employed the 'transition' element which was introduced by Lynn and Ingraffea[83]. The use of the 'transition' element around the core element allows the number of elements in the crack tip region to be reduced

significantly. This is important in order to reduce the number of degrees of freedom in the idealised component. This has been described fully in section 7.2.

An example of a plate containing a 90° single-edge-crack is used to verify the translated Mode I fracture program (FMODIA). Results of the calcualted stress intensity facotr, K_I, using the isoparametric quadrilateral element, is found to be very accurate compared to that of Paris and Sih[13]. While there was a discrepancy of 9% for the value of K_I, when the isoparametric triangular element is used in the same problem. This is due to the higher order of the quadrilateral element, where it possesses 8 nodes rather than the 6-node triangular element.

For the verification of the translated mixed-mode crack problem program 'pcpoy', an example of a square plate, containing a slanted central crack, was chosen. The program failed during the execution while solving the problem on the computer, due to the size of the overall stiffness matrix. An 'integer precision overflow' error was given by the HP 9845 computer, and no results were obtained. So in order to check the mixed-mode crack program 'pcopy' a simpler example was chosen, which is one of a plate containing a 90° single-edge-crack. Values of K_I and K_{II} were obtained, K_I is found to be identical to that found by using the single mode crack program (FMODTA), while K_{II} has the value of approximately zero as is expected.

The axisymmetric mode I fracture program (AXYMD1) was originally written by Al-Sharqi[68] in Algol language. Again in this program the same core element is used around the crack tip as that for the Mode I and mixed-mode plane fracture problems. This program has been translated to Basic to suit the HP 9845 computer and was run after a minor modification to its input data routine in order to generate the mesh chosen for the idealised problem of a bar with a normal circunferential crack. The mesh employed by Al-Sharqi[68] using 285 nodes could not be executed on the HP 9845 computer, due to 'memory overflow' and 'integer precision overflow'. That happened due to the fact that the overall stiffness matrix has a very large number of elements in it. So, two smaller meshes are develped, one with 135 nodes and the second with 255 nodes. Both of these meshes are used successfully running the (AXYMD1) program and results of K_I is calculated, and compared with that of Hilton and Sih[82], who have used 297 nodes for the mesh of the same problem. The first mesh of 135 nodes gave a difference in the value of K_I of 4.7% and the second mesh of 255 nodes gave a difference in the value of K_I of 3.2%. The mesh employed by Al-Sharqi using 285 nodes gave a difference of 3.1% to that of Hilton and Sih[82].

A review is given also for the most well known methods used for the determination of the stress intensity factors. It categorises these methods into three main classes,

experimental, analytical and approximate methods. The experimental methods are the least accurate of the three, and the approximate methods are the most widely used methods, in particular the finite element method for reasons given in the beginning og the discussion.

8.2 POSSIBLE IMPROVEMENTS AND SUGGESTED FUTURE WORK

(1) The mesh generation program proved to be a very useful package where a minimum number of data input is required in order to generate the desired mesh of the structure. This has been used in conjunction with all the programs mentioned in this thesis, except the axisymmetric program that deals with Mode I crack problems. This needs to be updated in order to be able to use the automatic mesh generation program to generate the mesh rather than using the semi-automatic mesh generation employed in this particular case.

(2) To extend the program mentioned above, from two-dimensional to three-dimensional mesh generation.

(3) To develop the finite element programs from its present two-dimensional to three-dimensional analysis.

(4) To include Mode III stress intensity factor.

(5) To include the plastic effect in the plastic region around the crack tip area. This has been tackled by Hilton and Hutchinson[50], by evaluating elastic-plastic

stress intensity factors for Mode I and III, and also by Wilson[84] for elastic plastic Mode III.

(6) Implementing the existing fracture programs and the proposed one, on a higher capacity version of the desk-top computer, which caters for larger stiffness matrix and have a bigger memory.

(7) Re-organise the program so that it is more compact and more efficient regarding memory available in the computer.

(8) To adopt a more effective solving routine. The frontal solution method could be used where an element by element frontal assembly and elimination procedure is used. Such procedure can utilise a relatively small memory. The advantages of this method is that, at any time only the equations that are currently needed are assembled in the high speed storage[74].

(9) Using the boundary element method in evaluating the stress intensity factors. This method, which is relatively new compared to the finite element method, has been used recently by Rudulphi[78]. One of the features of this method is the reduction in the data input required to solve a problem, particularly in two and three-dimensional problems. This is because the n-dimensional mesh is used for (n+1) dimensional problems[55].

(10) To formulate and analyse non-axisymmetric loading to axisymmetric bodies containing cracks. Here the loading as well as the nodal displacements will be expanded by the standard fourier series. Also the near crack tip displacement function must be expressed as fourier series.

8.3 CONCLUSIONS

The plane stress/strain programs 'PLST' has been implemented successfully on the HP 9845 desk-top computer, a smoothing technique is introduced and improvement on values of the calculated stresses is achieved.

The plane fracture problems have been translated from its original Algol format to Basic successfully. It has been verified through running some numerical examples.

Although the HP 9845 desk-top computer proved to be an excellent choice in solving plane stress/strain problems using the finite element method, it has its limitations in dealing with mixed-mode fracture problems due to firstly, its limited memory,which could be overcome by a suitable organisation of the program structure, so as to use as little memory as possible. Secondly, due to invalid bound on array dimension, where an array is limited by memory size to no more thatn 32767 items, and because of the structure of the stiffness matrix, its size in the mixed mode exceeds this

figure and the program will fail during the execution.

The axisymmetric Mode I fracture problem is translated to Basic and is implemented successfully on this computer, but still the program has to be updated to accept the mesh generation program.

It is found that the finite element method is the most promising method. It has the highest growth rate and with the introduction of special crack tip elements, it will be used more extensively in the future.

CHAPTER 9

9.1 APPENDIX (A)

USER GUIDE FOR THE MESH GENERATION PROGRAM.

The program description, including flow charts and listing in ALGOL is to be found in reference (15), also the program itself is available in BASIC in the department of mechanical engineering stored on a disk.

Here is a step by step user guide of the mesh generation for the following finite element programs.

1) Plane stress/strain.
2) Plane stress/strain modified to accommodate mode I fracture problems.
3) Plane stress/strain modified to accommodate mixed mode I and II fracture problems.
4) Axisymmetric finite element program using axisymmetric loading.
5) Plane stress/strain program–dynamic version.
6) Axisymmetric finite element program modified to accommodate mode I fracture problems.

INPUT DATA PREPARATION.

Input data is required for each individual problem at hand , this data is the minimum amount of information fed into the computer in order to create the mesh required.Care must be taken before the start of running the mesh generation program in order to eliminate any possible error prior to running the program . These data are usually stored in a file on a tape cartridge or a floppy disk , so that information is available if ,and when ,the necessary data are called during the excution of the program . When the program is run sucessfully , a second file is created and the output is again stored on the storage medium to be called again when running a finite element program .

One of the merits of this mesh generation program , beside being versatile , is the graphic plot of the mesh generated ,and that plot could be on the HP 9845 screen or on the Benson plotter if a large plot is required ,or on the 9872A x–y plotter to be fit on any regular paper size.

Numerical examples illustrate the use of the mesh generation program in chapters 3 and 7. It shows how to prepare the input data necessary to create the mesh. But in all problems , the structure is divided into zones , and this could be just a single zone or a multiple zones.Each zone is defined by "super nodes".The minimum number of "super node" are 4 if the sides are straight . A mid–side "super node" is required if any of the sides of the zone is made to fit a curved boundary , so a maximum of 8 "super nodes" is necessary if the four sides of the zone represent curved

boundaries.

Each zone is divided into a number of elements depending on the stress gradient in the actual body when external forces are applied . Areas of steep gradient are fit with more condensly populated number of elements , and those which are not , are fitted with sparsly populated elements. Number of nodes are found and located in their respective places.

The program operates by considering each zone in turn , starting from the left–hand corner of the zone array , and moving vertically up a column and from column to column . the following steps are to be followed:

1) The zone array data is read .
2) The eight super node co–ordinates for the first zone ,are determined ,either from the input data or by direct interpolation.
3) From the zones specified sub–divisions , the element data is generated , determining the node co–ordinates .
4) The element nodal connections are found using the same information as in step 3 .
5) Step 2–4 are repeated for the remaining zones , until the whole array has been scanned .
6) The finite element data is stored in a specified file and the element mesh is plotted .

INPUT DATA PROCEDURE : (for notation see the following section)*

The input data procedure is as follows :

A) PROGRAM CODE.

This consist of a column of input parameters depending on the class of problem dealt with :

PLANE STRESS / STRAIN	FRACTURE MODE I	FRACTURE MODE II	AXISYM	FRACURE MODE I AXISYM	PLANE DYNAMICS
Code (1)	Code (2)	Code (3)	Code (4)	Code (6)	Code (5)
Qort	Qort	Qort	Qort	Qort	Qort
Njob	Njob	Njob	Njob	Njob	Njob
Nelemt	Nelemt	Nelemt	Nelemt	Nelemt	Nelemt
Nnode	Nnode	Nnode	Nnode	Nnode	Nconf
Nsetfs	Thick	Thick	Nsetfs	Nsetfs	Dystrss
Prnt	Nsetfs	Nsetfs	Prnt	Solid	Prnt
Princ	Nsetc	Nskew	Solid	Nmat	Princ
Nskew		Surno	Nmat	Nsetc	Nskew
Nmat		Nsetc	Nsetc	Nsetf	Nmat
Nsetc		Nsetf	Nsetf		
Nsetf					

B) CONTROL VARIABLES

Parameters regarding information about the number of zones and number of super nodes used .

Tnspds :

Number of declared super nodes , i.e not including standard generated nodes. If straight sided zones , only corner nodes are considered .If curved, mid–side nodes should also be included . Also if 2 super nodes coincide , only one is considered .

Pzone :

Number of zones being used , i.e, not including voids or generated zones .

Vzone :

Number of zones along the y–direction .

Hzone :

Number of zones along the x–direction .

Gh :

Graphical output – (1/Yes , 0/No)

C) STANDARD GEOMETRIES

Information is needed if there is standard geometris , i.e , whether there is a crack or not , or if there is a generated section round a core .

Ntip :

Number of crack tips . If > 0 then input the following core parameters :

Nstart – Super node number starting the core .

Zns – Zone number starting the core .

N1 – Number of super nodes on the core face .

X1–Y1 – Cordinates of the crack tip .

Rc — Core radius .

A — Starting angle .

A1 — Incremental angle .

Dy — Zone sub–division in the Y–axis .

Ns — Node number starting the core .

Ngm :

Number of generated sections . If > 0 then input the following parameters :

Nstart — As before.

Zns — As before.

N1 — As before.

X1–Y1 — As before.

R1,R2,R3 — Radii for the inner core , grading node and outer node respectively.

A — As before.

A1 — As before.

Dx ,Dy — Zones sub–division .

D) X AND Y CO–ORDINATES OF SPECIFIED SUPER NODES :

(R AND Z FOR AXISYMMETRIC SOLIDS)

Data sequence entered for each node .

Q — Number of super nodes occupying the position .

Xcod,Ycod — X and Y co–ordinates .

W — String of super nodes occupying the position .

E) DEFINING ZONES

This is information regarding X and Y co–ordinates of the super nodes used in preparing the mesh .

Zone — Number of like zones .

Mn — Material number .

DivX,DivY — Zone sub—divisions in X and Y directions .

P — String of like zone numbers .

F) IDENTIFYING CLOSING SIDES .

Nd — Number of closing faces . If > 0 then input the following parameters for each zone face .

Zn — Zone number .

Side — Side of face to be joined (1, 2, 3, or 4) .

Extra parameters in cases where multiple zone faces are joined .

Coin — Number of coinciding nodes . If > 0 then input the following parameters for each pair of nodes .

Nd — Node number retained .

Cnd — Corresponding node number .

G) BOUNDARY CONDITIONS — MATERIAL PROPERTIES .

Nspec — Number of specified nodes for the first set of constraints.
i.e.,(Nodes where displacements and / or nodal forces are prescribed).

Loop (a)

Q — Number of like nodes .

Kode — Prescription for load or displacement or both .

Ulx — Value of prescibed load or displacement in X—direction .

Vly — Value of prescribed load or displacement in Y—direction .

String of like nodes — The numbers of nodes mentioned in Q .

Sequence of data for each material and depending on the code as

prescribed in (A) .

Code :

1	2	3	4	5	6
Case Ang Thick E V G E V	Case E V G E V	Case E V G E V	Case E V G E V	Case Ang Thick Dens E V G E V	Case E V G E V

Hnd Hnd

→ Data sequence for each skewed node (if Nskew = 0 , pass this section)

Again depending on the Code .

Code :

Loop

1	2	3	4	5	6
Nosk Angsk		Nosk Angsk		Nosk Angsk	

→

Loop (b)

Data sequence for each set of forces .

Nspec — If <> 0 then input as in Loop (a)

Nedges — If <> 0 then input :

Loop (c)

Data sequence for each element edge

Node (I) , Nprees (I) , Zpress (I) ,

NOTE ;

Loop (c) for AXISYM becomes :

Node (I) , Rpress (I) , Zpress (I) ,

Loop (d)

If Nsetc > 1 then repeat loop (b)

Nsetf — Number of set of forces for the new constraints.

Repeat Loop (b)

NOTES for G ;

1) If aproblem has Nsetc = Nsetf = 1 then in Loop (b) nput only the value for Nedges and forget about Nspec.

2) If the loading already has not been considered in loop (a) then input 0 for Nedges.

* NOTATION FOR VARIABLES USED IN PROGRAM .

Code — Finite Element program classification number :

1 — Plane stress / strain .

2 — Fracture mode I .

3 — fracture mode II .

4 — Axisymmetric .

5 — Plane stress / strain free vibration .

6 — Fracture (Axisymmetric) Mode I .

Njob — Number of jobs .

Nelemt — Number of elements .

Nnode — Number of nodes .

Nsetfs — Number of sets of forces.

Nsetf — Number of forces for each set of force input .

Prnt — Type of output :

1 — Stress / Strain at nodes only .

2 — Strees / Strain at element centroids .

3 — Stress / Strain at both locations .

Princ — Principal stresses and strains . (1 / Yes , 0 / No) .

Dystrss — Dynamic stresses and strains . (1 / Yes , 0 / No) .

Nskew — Number of nodes where skewed boundary conditions are applied .

Nmat — Number of materials .

nsetc — Number of sets of constraints .

Thick — Thickness of plate .

Solid — 0 for hollow axisymmetric structure .

1 for solid axisymmetric structure .

Surno — Number of nodes along the crack .

Nspec — Number of points where boundary conditions are prescribed .

i.e .,(point loads and displacements).

Kode — For prescribed loads and displacements .

0 — for prescribed load in X and Y directions .

1 — For prescribed displacement in X , load in Y directions .

2 — For prescribed load in X , and displacement in Y directions .

3 — For prescribed displacement in both X and Y directions .

NOTE : (R and Z for AXISYM instead of X and Y).

Ulx — Value of prescribed load or displacement in X—direction.

Vly — Value of prescribed load or displacement in Y—direction.

Case — Type of problem .

0 — For plane stress .

1 — For plane strain .

Case′ — Type of problem .

0 — For isotropic material .

1 — For orthotropic material .

Ang — Angle of orthotropy .

E — Youngs modulus .

v — Poison ratio .

G — Shear modulus .

Hnd — Direction of crack .

Nosk — Node number where skewed boundary conditions are applied .

Angsk — Corresponding angle of skew .

Qort — Type of element used .

0 — For triangular .

1 — For quadrilateral .

Dens — Material density .

Nod — Node number .

Npress — Normal pressure / unit length .

Tpress — Tangential pressure / unit length .

Nconf — Number of constrained degrees of freedom .

Nedges — Total number of elements edges under distributed loading.

NOTES REGARDING INPUT DATA PROCEDURE

1) In some problems , zone faces are joined , hence it is possible for super nodes to have the same co–ordinates . To reduce the data input , the number of super nodes occupying the same co–ordinates is given , followed by the X and Y co–ordinates and the corresponding super node numbers .

2) A similar situation exists with the zone data , to reduce input the number of like zones is entered , followed by its material type and sub–division , and finally by a string of corresponding zone numbers .

3) The zone faces are numbered :

Side 1 – The left–hand vertical face .

Side 2 – The top horizontal face .

Side 3 – The right–hand vertical face .

Side 4 – The bottom horizontal face .

Nd – Is the number of closing faces – when two sides of two different zones meet each other , one closing face is formed .

Zn – Zone number , from two zones whose sides are going to be closed together , Zn indicates the zone number which is smaller than the other one .

Side – Side number of the face to be joined . It can either be 1,2,3 or 4.

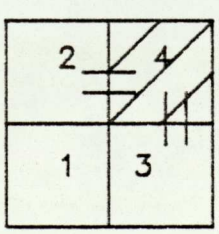

Sides marked by (=) are to be joined .
Zn = 2 , Side = 3

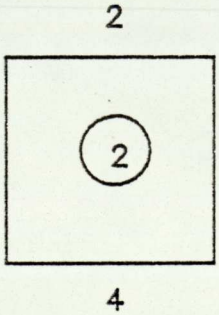

Number of zone faces .

4) PARAMETERS FOR DISTRIBUTED LOADING

When element edges are under distributed loading in a normal and / or tangential direction , the following parameters should be input in order to be able to calculate a set of equivalent point forces to substitute the distributed loading .

The point loads equivalent to the constant distributed loading are calculated manually , using the following equation :

$$\begin{Bmatrix} P1 \\ P2 \\ P3 \end{Bmatrix} = \frac{PL}{6} \begin{Bmatrix} 1 \\ 4 \\ 1 \end{Bmatrix}$$ For plain stress / strain problems .

Wher P1 and P3 are the equivalent loads at corner nodes .

P2 is the equivalent load at mid-side nodes .

P is the load / unit length .

L is the element length .

For Axisymmetric problems the above equation becomes :

$$\begin{Bmatrix} P1 \\ P2 \\ P3 \end{Bmatrix} = \frac{2xPIxLxrxP}{6} \begin{Bmatrix} 1 \\ 4 \\ 1 \end{Bmatrix}$$

Where P1 , P2 , P3 , P , and L as above .

And r is the core radius .

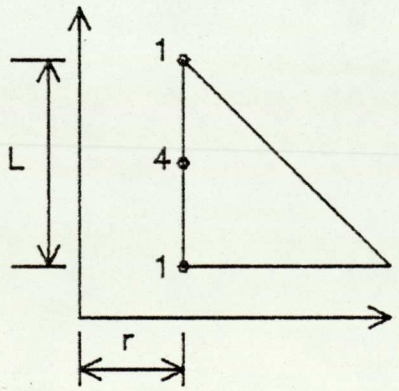

Negdes – Total number of element edges under distributed loading in the discretized structure .

For each edge , there are 3 nodes , and for each node three parameters should be input., Node number , normal pressure , and tangential pressure . Therefore each element edge needs 9 input values to account for the distributed loading on that edge .

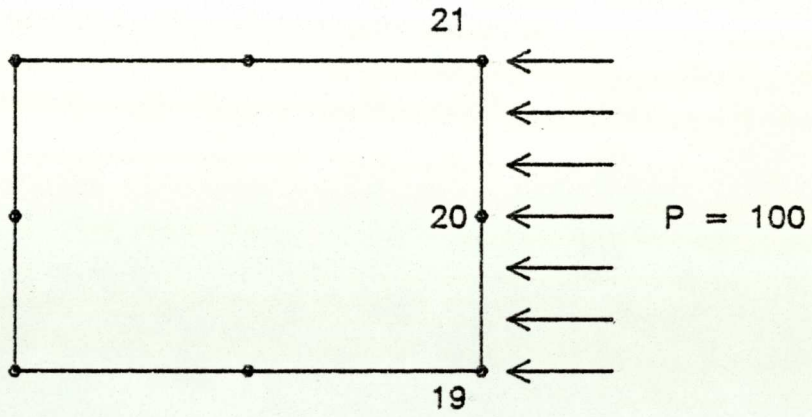

So that for the element shown above with the distributed load of P = 100 :–

NODE	NORMAL PRESSURE	TANGENTIAL PRESSURE
19	100	0
20	100	0
21	100	0

When loading acts on an element edge shared between two elements , depending on which element is considered under loading , numbering sequence and sign conversion differs . Consider the following examples :–

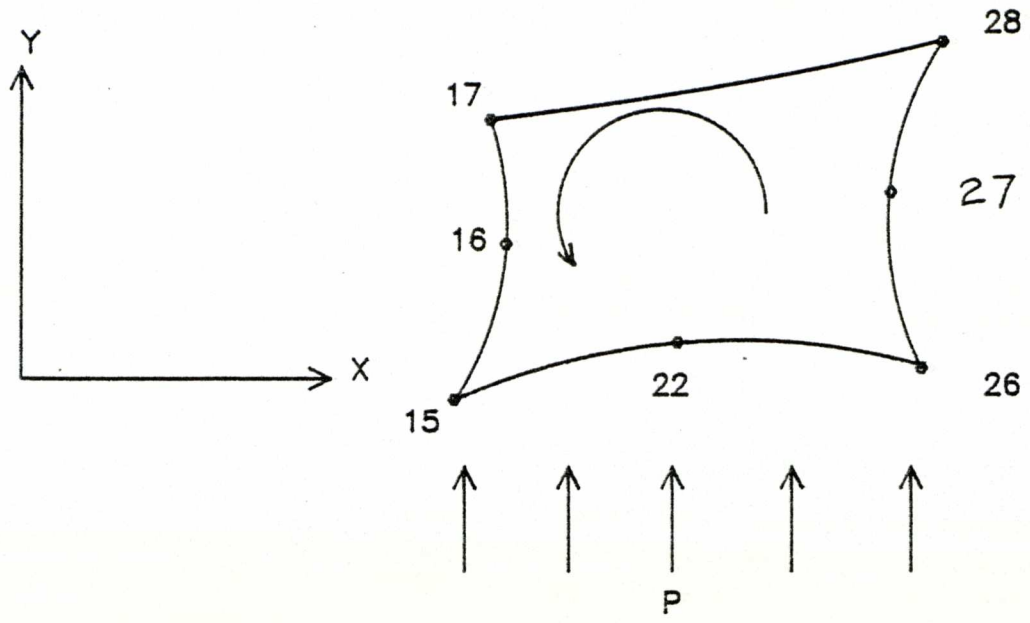

For above element , the nodal numbering sequence is (15 ,22 , 26)

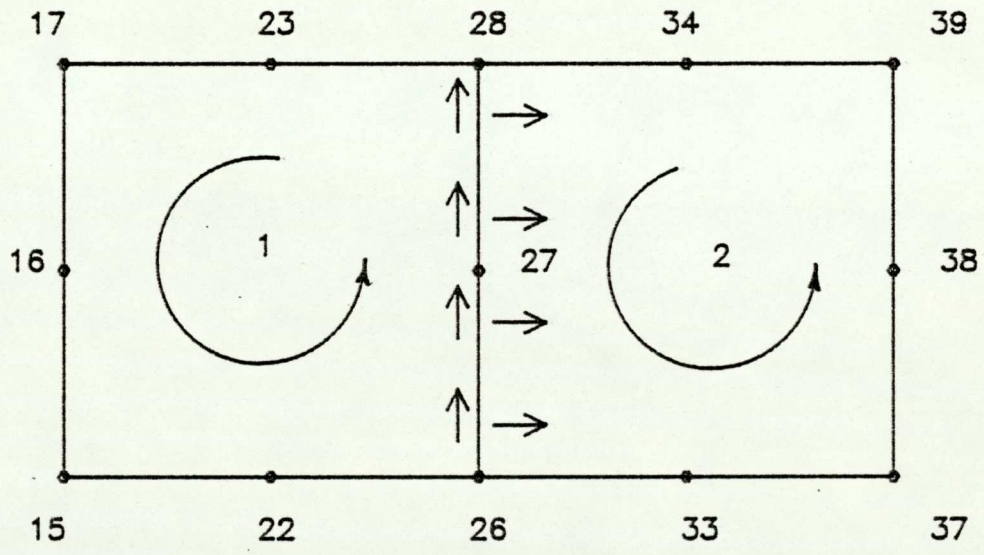

For element (1) nodal numbering is (26 , 27 , 28) , and tangential loading is positive , whereas for element (2) , nodal numbering is (28 , 27 , 26) and the tangential loading is negative .

As for the normal pressure , it is positive for element (2) and negative for element (1) . Tangential pressure is positive if it acts in an anti–clockwise direction with respect to the loaded element .

5) The core radius is usually 1/30 of the crack length .

6) The starting angle (A) can be defined as the angle between the first zone or crack face , and the positive X–axis .i.e.,

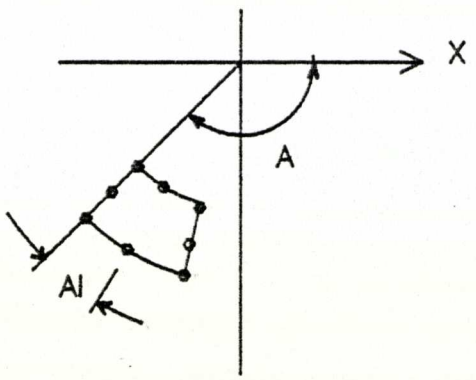

The incremental angle refers to half the angle taken by the zone.

7) If the crack tip faces to the right , then Hnd = 1 . If the crack tip faces to the left then Hnd = 2 .

The core element numbering convention for the Mode I fracture problem , is :

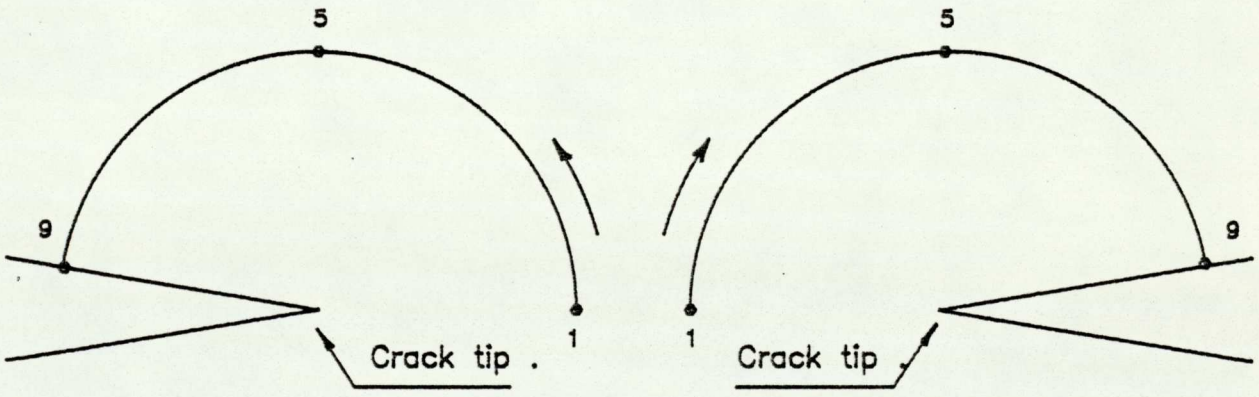

Hnd = 1 Hnd = 2

9.2 APPENDIX (B)

MANUAL INPUT DATA PREPARATION FOR AXISYMMETRIC CRACK PROBLEMS

The following input data are for axisymmetric crack problems fed manually without using the automatic mesh generation program.

A) Program code and initial parameters:

For the first job input the following :–

Njob

Nelemt

Nnode

Nsetf

Nmat

N1 – Number of nodes on core face.

R – Radius of the specimen–Width–r direction.

a – Crack length.

H – Half the length of specimen–Length– z direction.

Rc – Crack tip core radius.

Nsetc – Number of sets of constraints.

Case – 1 in all cases.

B) For first set of constraints:

Nspec – Number of specified nodes.

For each node input :–

J – Node number.

Xx(J) – The r–coordinates.

Yy(J) – The z–coordinates.

Kode(J,1)– Kode ,0 , 1, 2, or 3

Ulx(J,1)– Value of prescribed load or displacement in r–direction

Vly(J,1)– Value of prescribed load or displacement in z–direction

C) IF Nmat>1 THEN :–

For each Nmat input:

Nstel – The number of elements with different material properties for each different material.

Stel – The element numbers of these elements.

*Note :– Bypass section C if Nmat = 1.

For each Matno input :–

D) E , v, G, E, v

E) IF Nsetf>1 THEN

For each Nsetf :–

Nspec

For each Nspec (Number of specified nodes) :–

K – Node number.

Kode(K,I): Kode 0, 1, 2, or 3

Ulx(K,I): Value of prescribed load or displacement in r–direction

Vly(K,I): Value of prescribed load or displacement in z–direction

F) Hnd : Direction of crack

1 : For circumferential crack.

2 : For penny shaped crack.

G) Boundary conditions

IF Nsetc>1 THEN :–

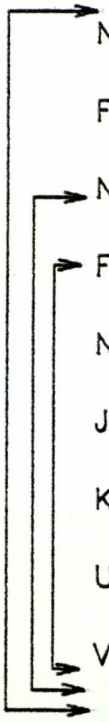

Nnewc — Number of new set of constraints.

For each number of constraints input:—

Nsetf — Number of set of forces for this constraints.

For each Number of Nsetf input:—

Nspec — Number of specified nodes.

J — Node number.

Kode(J,1)— Kode 0, 1, 2, or 3

Ulx(J,1)— Value of prescribed load or displacement in r—direction

Vly(J,1)— Value of prescribed load or displacement in z—direction

* Note: Bypass G if Nsetc = 1

CHAPTER 10

REFERENCES

1. KNOTT, J. F., 'Fundamentals of Fracture Mechanics', Butterworths, London (1975).

2. LIEBOWITZ, H., 'AGARDograph No. 176 on Fracture Mechanics of Aircraft Structure', (1974).

3. BIGGS, W. B., 'Brittle Fracture of Steel', MacDonald and Evans, London (1960).

4. PARKER, A. P., 'The Mechanics of Fracture and Fatigue, An Introduction', E. & F. N. Spon Ltd., London (1981).

5. TIMOSHENKO, S. P., and GOODIER, J. N., 'Theory of Elasticity', McGraw Hill, New York, (1970).

6. GRIFFITH, A. A., 'The Phenomena of Rupture and Flow in Solids', Phil. Trans. R. Soc., Vol. A221, (1921).

7. SIH, G. C., and LIEBOWITZ, H., 'On the Griffith Energy Criteria for Brittle Fracture', Int. J. Solid Struct., Vol. 3, (1967).

8. SIH, G. C., 'Some Basic Problems in Fracture Mechanics and New Concepts', J. Eng. Frac. Mech., Vol. 5, No. 2, pp. 365-377, (1973).

9. SIH, G. C., 'A Special Theory of Crack Propogation, Methods of Analysis and Solutions to Crack Problems', (ed. by. G. C. Sih), p. 21, Noordhoff International Publishing, Holland (1973).

10. OROWAN, E., 'Energy Criteria of Fracture', Weld. Res. Suppl., Vol. 20, (1955).

11. ROOKE, D. P., and BRADSHAW, F. J., 'A Study of Crack Tip Deformation and a Derivation of Fracture Energy', Proc. 2nd Int. Conf. Fracture, Brighton, U.K., (1969).

12. IRWIN, G. R., 'Analysis of Stresses and Strains near the end of a Crack Traversing a Plate', Trans. Am. Soc. Mech. Eng., J. Appli. Mech., Vol. 24, p. 361, (1957).

13. PARIS, P. C., and SIH, G. C., 'Fracture Toughness Testing and its Applications', ASTM.STP. No. 381, Am. Soc. Test. Mater., pp. 30-81, (1965).

14. WILLIAMS, M. L., 'On the Stress Distribution at the Base of a Stationary Crack', Trans. Am. Soc. Mech. Eng., J. Appl. Mech., (1957).

15. WOOD, P. C., 'Application of the Finite Element Method to Problems in Fracture Mechanics', Ph.D., University of Aston, U.K. (1979).

16. IRWIN, G. R., and KIES, J. A., 'Critical Energy Rate Analysis of Fracture Strength', Weld. J. (Res. Suppl.), Vol. 33, pp. 193S-198S (1954).

17. CARTWRIGHT, D. J., and ROOKE, D. P., 'Evaluation of Stress Intensity Factors', The J. Strain. Analysis, Vol. 10, No. 4, October (1975).

18. RAO, A. K., RAJU, I. S., and KRISTNA MURTY, A. V., 'A Powerful Hybrid Method in Finite Element Analysis', Int. J. Num. Meth. in Eng., Vol. 3, pp. 389-403, (1971).

19. SCHROEDL, M. A., McGOWAN, J. J., and SMITH, C. W., 'An Assessment of Factors Influencing Data Obtained by the Photoelastic Stress Freezing Technique for Stress Fields Near Crack Tip', Eng. Fract. Mech., Vol. 4, pp. 801-809, (1972).

20. EMERY, A. F., BARRETT, C. F., and KOBAYASHI, A. S., 'Temperature Distributions and Thermal Stresses in a Partially Filled Annulus', Expl. Mech., Vol. 6, pp. 602-608, (1966).

21. SMITH, D. G., and SMITH, C. W., 'Photoelastic Determination of Mixed Mode Stress Intensity Factors', Eng. Frac. Mech., Vol. 4, pp. 357-366, (1972).

22. PARIS, P. C., 'Fatigue - An Interdisciplinary Approach', pp. 107-127, Eds., J. J. Burke, N. L. Reed and V. Wiess, Syracuse University Press, (1964).

23. JAMES, L. A., and ANDERSON, W. E., 'A Simple Experimental Procedure for Stress Intensity Factor Calibration', Eng. Frac. Mech., Vol. 1, pp.565-568, (1969).

24. DUDDERAR, T. D., and GORMAN, H. J., 'The Determination of Mode I Stress Intensity Factors by Holographic Interferometry', Expl. Mech., Vol. 12, pp. 145-149, (1973).

25. SOMMER, E., 'An Optical Method for Determining the Crack Tip Stress Intensity Factor', Eng. Frac. Mech., Vol. 1, pp. 705-718, (1970).

26. WESTERGAARD, H. M., 'Bearing Pressures and Cracks', J. Appl. Mech., Vol. 61, A49, (1939).

27. TADA, H., 'Westergaard Stress Functions for Several Periodic Crack Problems', Eng. Frac. Mech., Vol. 2, pp. 177-180, (1970).

28. KOBAYASHI, A. S., CHEREPY, R. B., and KINSEL, W.C., 'A Numerical Procedure for Estimating the Stress Intensity Factor of a Crack in a Finite Plate', J. Basic. Eng., Vol. 86, (1964).

29. RICE, J. R., and TRACEY, D. M., 'Computational Fracture Mechanics', in 'Numerical and Computer Methods in Structural Mechanics', by Fenves, S. J., Perrone, N., Robinson, A. R., and Schnobrich, W. C., Academic Press (1973).

30. BOWIE, O. L., and NEAL, D. M., 'Single Edge Crack in Rectangular Tensile Sheet', J. Appl. Mech., Vol. 32, pp. 708-709, (1965).

31. BOWIE, O. L., and NEAL, D. M. 'A Modified Mapping Collocation Technique for Accurate Calculation of Stress Intensity Factors', Int. J. Frac. Mech., Vol. 6, pp. 199-206, (1970).

32. BOWIE, O. L., and FREESE, C. E., 'Central Crack in Plane Orthotropic Rectangular Sheet', Int. J. Frac. Mech., Vol. 8, pp. 49-58, (1972).

33. BOWIE, O. L., FREESE, C. E., and NEAL, D. M., 'Solution of Plane Problems of Elasticity Utilising Partitioning Concepts', J. Appl. Mech., Vol. 40, pp. 767-772, (1973).

34. NEUBER, H., 'Theory of Notch Stresses', Springer, Berlin, (1958).

35. SIH, G. C., and RICE, J. R., 'The Bending of Plates of Dissimilar Materials with Cracks', J. Appl. Mech., Vol. 31, pp. 477-490, (1964).

36. SIH, G. C., and LIEBOWITZ, H., 'Mathematical Theory of Brittle Fracture', Chap. 2, Fracture: An Advanced Treatise, Vol. 2, Ed., H. Liebowitz, Academic Press (1968).

37. ROOKE, D. P., and CARTWRIGHT, D. J., 'Compendium of Stress Intensity Factors', London, HMSO, (1976).

38. SIH, G. C., 'Methods of Analysis and Solution of Crack Problems', Ed., G. C. Sih, Noordhoff, Holland (1973).

39. BLOOM , J. M., and SANDERS, J. L., 'The Effect of a Riveted Stringer on the Stress in Cracked Sheet', J. Appl. Mech., Vol. 33, pp. 561-570, (1966).

40. SMITH, F. W., EMERY, A. F., and KOBAYASHI, A. S., 'Stress Intensity Factors for Semicircular Cracks', J. Appl. Mech., Vol. 34, pp. 953-959, (1967).

41. CHAN, S. K., TUBA, I. S., and WILSON, W. K., 'On the Finite Element Method in Linear Fracture Mechanics', Eng. Frac. Mech., Vol. 2, pp. 1-17, (1970).

42. ANDERSON, G. P., RUGGLES, V. L., and STIBOR, G. S., 'Use of Finite Element Computer Programs in Fracture Mechanics', Int. J. Frac. Mech., Vol. 7, No. 1, pp. 63-76, (1971).

43. WILSON, W. K., and THOMPSON, D. G., 'On the Finite Element Method of Calculating Stress Intensity Factors of Crack Plates in Bending', Eng. Frac. Mech., Vol. 13, pp. 97-102, (1971).

44. WATWOOD, V. B., 'The Finite ELEMENT METHOD for Prediction of Crack Behaviour', Nuc. Eng. and Design, Vol. 4, p. 323, (1969).

45. DIXON, J. R., and POOK, L. P., 'Stress Intensity Factors Calculated Generally by Finite Element Method', Nature, Vol. 224, p. 166, (1969).

46. RICE, J. R., 'A Path Independent Integral and the Approximate Analysis of Strain Concentration by Notches and Cracks', Trans. ASME, SERIES E., J. Appl. Mech., Vol. 35, 2, p. 379 (1968).

47. JERRAM, K., Discussion to a Paper by Smith and Alavi, Int. Conf. on Pressure Vessel Tech., Part III Discussions, ASME, New York, (1970).

48. TRACEY, D. M., 'Finite Elements for Determination of Crack Tip Elastic Stress Intensity Factors', Eng. Frac. Mech., Vol. 3, pp. 255-265, (1971).

49. HENSHELL, R. D., 'Crack Tip Finite Elements are Unnecessary', Int. J. Num. Meth. Eng., Vol. 9, p. 495, (1975).

50. HILTON, P. D., and HUTCHINSON, J. W., 'Plastic Stress Intensity Factors for Cracked Plates', Harvard University Rept., SM-43, May (1969).

51. BENZLEY, S. E. , 'Representation of Singularities with Isoparametric Finite Elements', Int. J. Num. Meth. Eng., Vol. 8, pp. 537-545, (1974).

52. HELLEN, T. K., 'On the Method of Virtual Crack Extensions', Int. J. Num. Meth. Eng., Vol. 9, pp. 182-207, (1975).

53. FAWKES, A. J., 'Finite Elements Applied to Crack Tip Singularities', Ph.D. Thesis, University of Wales, (1976).

54. RAO, S. S., 'The Finite Element Method in Engineering', Pergamon Press, Oxford , (1982).

55. COOK, R. D., 'Concepts and Application of Finite Element Analysis', John Wiley & Sons, New York, (1981).

56. BREBBIA, C. A., 'The Boundary Element Method for Engineers', Pentech Press, London:Plymouth, (1978).

57. SIH, G. C., 'Handbook of Stress Intensity Factors', Lehigh University, Bethlehem, Pensylvania (1973).

58. WILSON, W. K., 'Comparison of the Stress Distribution on the Plane of Symmetry at the WOL Test Specimen obtained by Various Methods and an Interpretation of the Results of a Photoelastic Study of the Specimen', R.T.66-ID7-MEMTL-R2, Westinghouse Res. Lab., Pittsburgh, Pensylvania, (1966).

59. SRWALEY, J. E., JONES, M. H., and GROSS, B., 'Experimental Determination of the Dependence of Crack Extension Force on Crack Length for 4 Single-Edge-Notch Tension Specimen', NASA TND-2396, (1964).

60. RICHARDS, T. H., 'On Using the Finite Element Method in Conjunction with Sub-region Singular Solutions in Fracture Mechanics', Num. Meth. Frac. Mech., Ed., Luxmoore, A.R., and Owen, D. R. J., Proceedings of the 1st Int. Conf., held at University College, Swansea, U.K., 9th-13th January (1978).

61. FAWKES, A. J., OWEN, D. R. J., and LUXMOORE, A. R., 'An Assessment of Crack Tip Singularity Models for use with Isoparametric Elements', Eng. Frac. Mech., Vol. 11, pp. 145-159, (1979).

62. RICHARDS, T. H., and ROBERTSON, 'The Determination of Single and Mixed Mode Stress Intensity Factors for Engineering Components of Practical Interest', Fracture Mechanics in Engineering Practice, Ed. P. Stanley, Applied Science Publishers, Chapter (1), (1976).

63. CARTWRIGHT, D. J., and ROOKE, D. P., 'Methods of Determining Stress Intensity Factors', R. A. E., TR73031, Farnborough, (1973).

64. TADA, H., PARIS, C., and IRWIN, G., 'The Stress Analysis of Cracks Handbook', Del. Research Corp., Pensylvania, (1973).

65. ROOKE, D. P., BARATTA, F. I., and CARTWRIGHT, D. J., 'Simple Methods of Determining Stress Intensity Factors', Eng. Frac. Mech., Vol. 14, pp. 397-426, (1981).

66. SIH, G. C., (Ed.), Mechanics of Fracture (in 6 Volumes), Leyden, Noordhoff, (1973).

67. ROBERTSON, A. W., 'On the Stress Analysis of Cracked Bodies by means of Finite Elements', Ph.D. Thesis, University of Aston in Birmingham, U.K., (1976).

68. AL SHARQI, I. A., 'Finite Element Analysis of Axisymmetric Solids', Ph.D. Thesis, University of Aston in Birmingham U.K. (1977).

69. ZIENKIEWICZ, O. C., and PHILLIPS, D. V., 'An Automatic Mesh Generation Scheme for Plane and Curve Surfaces by Isoparametric Co-ordinates', Int. J. Num. Meth. in Eng., Vol. 3, pp. 519-528, (1971).

70. ZIENKIEWICZ, O. C., IRONS, B. M., ERGATOUDIS, J., and SCOTT, F. C., 'Isoparametric and Associated Element Families for Two and Three Dimensional Analisys', Ed. by I. Holland and K. Bell, Chapter 13, Tapir Press, Trondheim, (1969).

71. HINTON, E., and CAMPBELL, J. S., 'Local and Global Smoothing of Discontinuous Finite Element Functions using a Least Square Method', Int. J. Num. Meth. in Eng., Vol. 8, pp. 461-480, (1974).

72. HINTON, E., SCOTT, F. C., and RICKETTS, R. E., 'Local Least Squares Stress Smoothing for Parabolic Isoparametric Elements', Int. J. Num. Meth. in Eng., Vol. 9, pp. 235-238, (1975).

73. MIRZA, F. A., and OLSON, M. D., 'The Mixed Finite Element Method in Plane Elasticity', Int. J. Num. Meth. in Eng., Vol. 15, pp. 273-289, (1980).

74. AKIN, J. E., 'Application and Implementation of Finite Element Methods', Academic Press, London, New York, (1982).

75. PIN TONG, T. H. H. PIAN, and LARSY, S. J., 'A Hybrid-Element Approach in Crack Problems in Plane Elasticity', Int. J. Num. Meth. in Eng., Vol. 7, pp. 297-308, (1973).

76. WILSON, W. K., 'Fracture Mechanics Technology for Combined Loading and Low-to-Intermediate Strength Materials', Westinghouse Research Labs., Final Tech. Report, No. DAAE-07-67-C-4021, Nov. (1968).

77. ZIENKIEWICZ, O. C., KELLY, D. W., and BETTESS, P., 'The Coupling of the Finite Element Method and Boundary Solution Procedure', Int. J. Num. Meth. in Eng., Vol. 11, No. 2, pp. 355-375, (1977).

78. RUDOLPHI, T., 'A Boundary Element Solution of the Edge Crack Problem', Int. J. Frac., Vol. 18, No. 3, pp. 179-190, (1982).

79. McCLINTOCK, F. A., and IRWIN? G. R., 'Plasticity Aspects of Fracture Mechanics', Fracture Toughness and its Applications, ASTM, STP 381, Am. Soc. Test. Mater., (1965).

80. HILTON, P. D., and SIH, G. C., 'Applications of the Finite Element Method to the Calculation of Stress Intensity Factors', Method and Analysis and Solutions of Crack Problems, (Ed. by G. C. Sih), p. 427, Noordhoff International Publishing, Holland, (1973).

81. BUECKNER, H. F., 'Coefficient for Computation of the Stress Intensity Factor K for a Notched Round Bar', ASTM, STP 381, p. 82, (1965).

82. HILTON, P. D., and SIH, G. C., 'Applications of the Finite Element Mehod to the Calculations of Stress Intensity Factors', Methods of Analysis and Solutions of Crack Problems, (Ed. by G. C. Sih), p. 426, Noordhoff International Publishing, Holland, (1973).

83. LYNN, P. P., and INGRAFFEA, A. R., 'Transition Elements to be used with Quarter-point Crack-tip Elements', Int. J. Num. Meths. in Eng., Vol. 12, pp. 1031-1036, (1978).

84. WILSON, W. K., 'Finite Element Methods for Elastic Bodies Containing Cracks', Methods of Analysis and Solutions of Crack Problems, (Ed. by G. C. Sih), pp. 485-515, Noordhoff International Publishing, Holland, (1973).

85. BYSKOV, E., 'The Calculation of Stress Intensity Factors using the Finite Element Method with Cracked Elements', Int. J. Fract. Mech., Vol. 6, pp. 159-167, (1970).